AM-92-02

An Approximate Solution for Interlaminar Stresses in Laminated Composites

Cheryl A. Rose
Carl T. Herakovich

May 1992

SCHOOL OF ENGINEERING AND
APPLIED SCIENCE

APPLIED MECHANICS PROGRAM

UNIVERSITY OF VIRGINIA
CHARLOTTESVILLE, VIRGINIA 22901

UNIVERSITY OF VIRGINIA
School of Engineering and Applied Science

The University of Virginia's School of Engineering and Applied Science has an undergraduate enrollment of approximately 1,500 students with a graduate enrollment of approximately 600. There are 160 faculty members, a majority of whom conduct research in addition to teaching.

Research is a vital part of the educational program and interests parallel academic specialties. These range from the classical engineering disciplines of Chemical, Civil, Electrical, and Mechanical and Aerospace to newer, more specialized fields of Applied Mechanics, Biomedical Engineering, Systems Engineering, Materials Science, Nuclear Engineering and Engineering Physics, Applied Mathematics and Computer Science. Within these disciplines there are well equipped laboratories for conducting highly specialized research. All departments offer the doctorate; Biomedical and Materials Science grant only graduate degrees. In addition, courses in the humanities are offered within the School.

The University of Virginia (which includes approximately 2,000 faculty and a total of full-time student enrollment of about 17,000), also offers professional degrees under the schools of Architecture, Law, Medicine, Nursing, Commerce, Business Administration, and Education. In addition, the College of Arts and Sciences houses departments of Mathematics, Physics, Chemistry and others relevant to the engineering research program. The School of Engineering and Applied Science is an integral part of this University community which provides opportunities for interdisciplinary work in pursuit of the basic goals of education, research, and public service.

Applied Mechanics Program
School of Engineering and Applied Science
University of Virginia
Charlottesville, Virginia 22903-2442

AM-92-02

May 1992

An Approximate Solution for Interlaminar Stresses in Laminated Composites

Cheryl A. Rose
Carl T. Herakovich

Interim Report

NASA Grant NAG-1-841
NASA Langley Research Center

An Approximate Solution for Interlaminar Stresses in Laminated Composites

ABSTRACT

An approximate solution for interlaminar stresses in finite width, laminated composites subjected to uniform extensional and bending loads is presented. The solution is based upon the principle of minimum complementary energy and an assumed, statically admissible stress state, derived by considering local material mismatch effects and global equilibrium requirements. The stresses in each layer are approximated by polynomial functions of the thickness coordinate, multiplied by combinations of exponential functions of the in-plane coordinate, expressed in terms of fourteen unknown decay parameters. Imposing the stationary condition of the laminate complementary energy with respect to the unknown variables yields a system of fourteen non-linear algebraic equations for the parameters. Newton's method is implemented to solve this system. Once the parameters are known, the stresses can be easily determined at any point in the laminate.

Results are presented for through-thickness and interlaminar stress distributions for angle-ply, cross-ply (symmetric and unsymmetric laminates), and quasi-isotropic laminates subjected to uniform extension and bending. It is shown that the solution compares well with existing finite element solutions and represents an improved approximate solution for interlaminar stresses, primarily at interfaces where global equilibrium is satisfied by the in-plane stresses, but large local mismatch in properties requires the presence of interlaminar stresses. Further, the contributions of both global equilibrium and local material mismatch effects to the stress field are clearly delineated. The results indicate that the significance of local mismatch effects is dependent on lam-

inate stacking sequence. The demonstrated accuracy and efficiency of the solution make it ideally suited for parametric studies.

ACKNOWLEDGEMENT

This work was supported by the NASA Langley Research Center under NASA Grant NAG-1-841. The authors are grateful for this financial support, as well as for the technical advice of the grant monitor, Dr. James H. Starnes, Jr.

TABLE OF CONTENTS

LIST OF FIGURES

LIST OF TABLES

CHAPTER 1

INTRODUCTION

1.1 Introductory Remarks

The high strength-to-weight, and stiffness-to-weight ratios of composite materials and their tailorability to meet strength and stiffness requirements has led to the increased use of composites for structural designs, particularly in aerospace applications. With this increased use has come significant interest in the failure mechanisms of composite materials. Because composite materials are heterogeneous and anisotropic, failure modes occur that are quite different from those seen in more conventional isotropic materials. Laminated composites exhibit two basic failure modes: 1) in-plane fracture, and 2) out of plane delamination [1] failure, matrix failure, fiber/matrix debonding or fiber splitting [2]

Experimental studies have shown that the mode of failure and ultimate failure load of laminates are dependent upon the laminate stacking sequence and the layer thicknesses.[2-8] This phenomenon cannot be explained by classical laminated plate theory (which predicts a planar stress state) combined with in-plane fracture theories, but is attributed to the presence of interlaminar stresses near the free edges of composite laminates.

Interlaminar stresses are caused by the mismatch, or difference, in the material properties between the individual laminae and the laminate and the mismatch in properties between adjacent laminae in the presence of a free edge. Individual layers of a laminate will deform differently, when subjected to the same axial strain, because of differences in their material properties. In a laminate, however, the layers are bonded together, and displacement continuity

at the layer interfaces requires development of interlaminar stresses to equalize the differential deformations and to maintain equilibrium. A detailed discussion of the mechanics of free edge stresses is provided in reference [9].

The interlaminar stresses σ_{33}, σ_{23}, and σ_{13}, shown in Figure 1.1, act upon planes parallel to the interfacial planes between laminae. They exist only within a very local region near the free edges of a laminate and are therefore known as a boundary layer effect or free edge effect. For fiber reinforced composites the interlaminar stresses are transferred between plies through the matrix material that bonds them together. This interfacial region is relatively weak and if the interlaminar stresses are high enough the laminated structure will fail, due to delamination, at loads much lower than those predicted by in-plane failure theories.

A necessary tool to aid in understanding and ultimately preventing delamination type failures is an efficient analytical method which provides reasonably accurate stress predictions in the boundary layer region. The need for such a method is particularly acute in design stages to avoid delamination prone laminates when a large number of possible structural configurations have to be evaluated quickly and economically. Numerous investigators have proposed a variety of methods for calculating interlaminar stresses. The majority of these solutions are numerical in nature and are plagued by computational limitations, particularly with regard to memory requirements. Consequently they become intractable when the number of layers in a laminate becomes even moderately large or when calculations have to be performed repetitively as in an optimization process.

In practical applications composite panels may consist of many layers (100 layers in aircraft structures is not uncommon) of different orientations, thicknesses and material properties. Thus, design of even the simplest composite structural component may involve a large number of

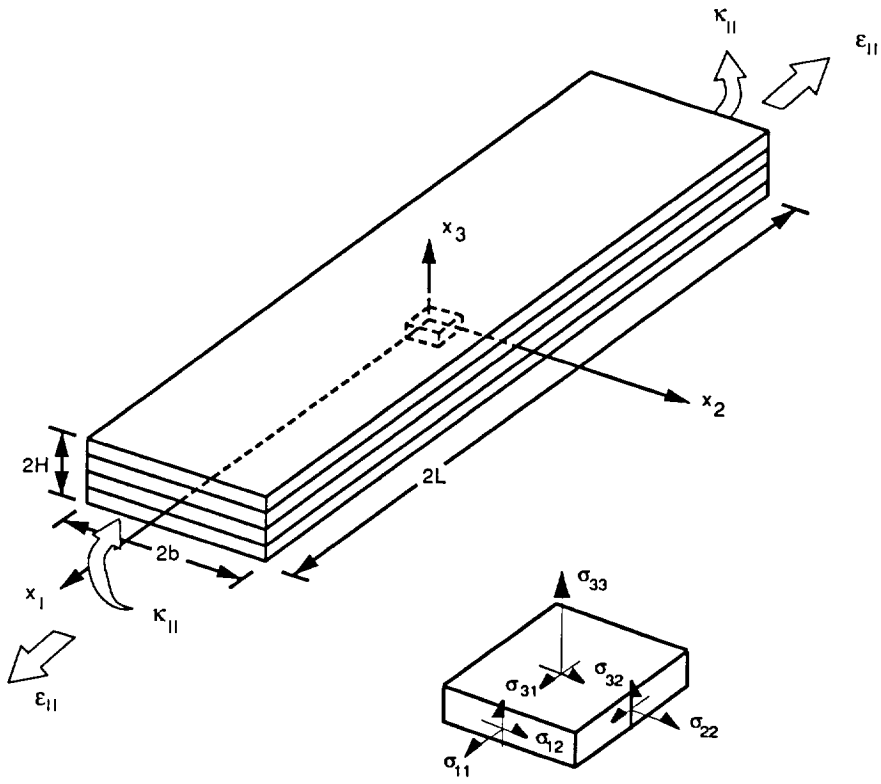

Figure 1.1. Laminate Configuration

design variables in addition to a large number of design constraints. These factors make composite panel design an ideal candidate for numerical optimization.

Several papers, a few of which are listed in the references,[10-18] have been published on the use of numerical optimization for designing composite structures. To the author's knowledge, however, none of the published work on composite design using mathematical optimization techniques considers interlaminar stresses in the problem formulation. This gap in the literature apparently exists because of the complexity and computational inefficiency of the majority of the methods currently available for predicting interlaminar stresses.

1.2 Objective and Scope

The above discussion suggests the need for more efficient approaches for calculating the three dimensional stress field near free edges in laminated composites. An analytical approach is preferred so that the method can be incorporated into a design process which uses numerical optimization techniques. The objective of this research is to provide an approximate analytical model for laminate stress analysis and demonstrate its usefulness. The approximate model is developed for a finite width symmetrically or unsymmetrically laminated coupon with straight free edges subject to uniform extensional or bending loads as shown in Figure 1.1. These loads are considered because they are common in practice. Combined loads can then be analyzed by superposition. The straight, free edge coupon was chosen because it is the simplest configuration to analyze and there are numerous results available in the literature that can be used to verify the model developed. Laminates with many plies as well as hybrid laminates can be analyzed. Also, although the formulation that follows is presented with reference to the simple plate shown in Figure 1.1, more complicated structural configurations can be analyzed using the methodology developed provided the in-plane stress field in the interior can be

obtained from an analytical solution or from some general analysis technique. The methodology can then be employed in a global-local analysis to obtain refined stress solutions in regions of high stress gradients with a coarser global solution used to define the response outside of these regions.

The remainder of this thesis is divided into several sections. Chapter 2 includes a literature review of various methods for predicting interlaminar stresses and a brief discussion of the present method. In Chapter 3 the analytical model is developed. The approach is an extension of previous work by Kassapoglou and Lagace [1,19-21] and is based upon an assumed stress state and the principle of minimum complementary energy. The methodology reduces the stress field determination for a general laminate to the simultaneous solution of 14 non-linear equations. Newton's method is implemented to solve this system. In Chapter 4 the solution is verified and its advantages and limitations are identified by comparison with existing finite element and analytical model results. Comparisons are made for angle-ply, cross-ply and more general laminate configurations. In Chapter 5 additional results are presented demonstrating the utility of the technique and the effect of load conditions and stacking sequence on interlaminar stresses. Finally, Chapter 6 closes with a summary and conclusions of the study. Recommendations for future work are also provided.

CHAPTER 2

LITERATURE REVIEW

Interlaminar stresses have been studied for over twenty years, in hundreds of articles. Only a few are discussed here. For a more complete coverage see the review article by Salamon.[22] The majority of the work has concentrated on the analysis of symmetric laminates with straight free edges subjected to uniform axial extension. A brief review of the more significant contributions to the understanding of interlaminar stresses in these laminates is presented first. This is followed by a review of the literature pertaining to interlaminar stress calculations for laminates in uniform bending. The chapter closes with a summary and discussion of the present solution methodology.

2.1 Laminates in Uniform Axial Extension

The earliest investigations of interlaminar stresses were performed by Hayashi,[23] Hayashi and Sando[24] and Puppo and Evensen.[25] All of these researchers modeled the laminate as a set of anisotropic layers separated by isotropic shear layers. Their analyses neglected the interlaminar normal stress component σ_{33} and predicted a sharp rise in the interlaminar shear stress σ_{23} at the intersection of an interface and the free edge.

In the same year, Pipes and Pagano performed the first numerical study of edge stresses in composite laminates.[26] They studied the elastic response of a $[+45/-45]_s$ laminate subjected to a uniform axial extension (Figure 1.1). Noting St. Venant's principle, they assumed the stresses to be independent of the axial coordinate X_1 in regions away from the areas of load introduction. Under this assumption the general form of the displacement field is

$$u(X_1, X_2, X_3) = X_1 \varepsilon_{11} + U(X_2, X_3) \tag{2.1}$$

$$v(X_1, X_2, X_3) = V(X_2, X_3) \tag{2.2}$$

$$w(X_1, X_2, X_3) = W(X_2, X_3) \tag{2.3}$$

where u, v, and w are displacements in the X_1, X_2, and X_3 coordinate directions respectively, and ε_{11} is the applied axial strain. The reduced elasticity equations governing the laminate behavior were then formulated and solved using the finite difference method.

Their results showed a planar stress field over most of the laminate in agreement with classical lamination theory (CLT). In regions near the laminate free-edge, the lamination theory results were perturbed by the presence of the interlaminar stress components, σ_{13}, σ_{23}, and σ_{33}. The interlaminar stresses were shown to decay rapidly with distance from the free edge and were zero outside of a region of width approximately equal to the laminate thickness. Therefore they concluded that interlaminar stresses are a boundary layer or an edge effect.

Three of the predicted stress components, σ_{23}, σ_{22} and σ_{33} were very small while the interlaminar shear stress σ_{13} was quite large. In addition they noted that the magnitude of σ_{13} at the intersection of the interface and the free edge increased with increasing grid refinement. Based upon these results and those of Bogy[27] and Hess[28,29] for bonded quarter planes of dissimilar materials, they concluded that σ_{13} is singular at this point. The results of this model along with some simplified models for predicting selected interlaminar stress components were used to explain the relationship between interlaminar stresses and the differences in experimentally observed strengths of similar laminates.[4-6,30]

Finite element solutions soon followed. The first finite element solution was provided by Isakson and Levy.[31] They used a displacement based formulation and like Puppo and Evensen modeled the laminate as a combination of anisotropic layers separated by isotropic shear layers,

thus neglecting the interlaminar normal stress. They analyzed a $[+45/-45]_s$ laminate and their predictions for the interlaminar shear stress σ_{13} agreed well with those of Pipes and Pagano. Rybicki[32] used a three-dimensional finite element analysis to obtain approximate solutions for a symmetric laminate subjected to in-plane loading. He used a complementary energy formulation with assumed stress states derived from the three-dimensional Maxwell stress functions. His formulations provided predictions for all three interlaminar stresses and the results showed good agreement with those of Pipes and Pagano.

Later, to improve solution efficiency, several investigators adopted the Pipes-Pagano approach and solved the tensile coupon problem using quasi-three dimensional formulations. The first two-dimensional finite element analysis for the quasi-three dimensional problem was conducted by Herakovich et. al to study mechanical and thermal edge effects in cross-ply and angle-ply laminates.[33,34] Application of this type of formulation to additional laminate configurations soon followed.[35-39] Wang and Crossman[35] analyzed 5 laminate configurations; two cross-ply laminates, an angle-ply laminate, and two quasi-isotropic laminates. By invoking a skyline storage scheme, they were able to use a much finer mesh than had been used in previous analyses and obtained a more accurate description of the stress field in the vicinity of ply interfaces and the free edge. They noted that the interlaminar normal stress σ_{33} is also singular at these points.

The finite element method provided a means for obtaining solutions for a variety of laminate configurations and geometries. Numerous solutions were obtained. These solutions greatly increased the understanding of the free edge problem and the mechanisms contributing to interlaminar stress development. The limitations of numerical procedures for laminate stress analysis, however, also became evident. First, it was quickly realized that the numerical solutions are not economical. Because of the singular nature of the problem, extremely fine

meshes or fine finite difference grids are required in edge regions in order to obtain reasonably accurate predictions of the field variables. Wang and Crossman,[35] for instance, used 192 elements (16 through the thickness) to model each ply in a four ply laminate. Meshing requirements like these and the resulting computer memory and time requirements made analysis of practical laminates prohibitive. Second, it was found that results very near the free edge obtained using different formulations were not consistent. Different researchers not only predicted different magnitudes for interlaminar stress components in this region but also, in some cases, predicted different signs. Some attributed this anomaly to improper satisfaction of the free edge boundary conditions.[37] Others suggested that lack of symmetry in the stress tensor at the singularity[40] may be the cause of the inconsistencies.[38]

In an effort to resolve these inconsistencies and develop more efficient reliable methods for laminate stress analysis, several analytical solution methods were proposed. One of the first fairly sophisticated approaches which was capable of predicting both interlaminar shear stress components as well as the interlaminar normal stress component was provided by Tang[41] and Tang and Levy.[42] They extended the boundary layer theory of plane stress of isotropic elasticity developed by Reiss and Locke[43] to the analysis of laminated composites. Using a zeroth order approximation to the boundary layer problem, the solution in the boundary layer region was separated into a torsion problem and a plane strain problem. The solution exactly satisfied the equilibrium equations and compatibility equations but some of the boundary conditions were not satisfied or were satisfied in an average sense. A similar approach was used by Hsu and Herakovich[44] in the study of angle-ply laminates. Using a perturbation method, they matched an interior solution, where classical lamination plate theory is assumed to be valid, to a boundary layer solution. Their results suggested that both interlaminar shear stress components σ_{13} and σ_{23} are singular in the boundary layer region. Another approach was presented by Wang and

Dickson.[45] They expressed displacements and the interlaminar stresses in each layer in a series of Legendre polynomials, and used Galerkin's method to obtain a system of equations for the unknown constants. Out of plane warping was neglected in the displacement assumptions so their model was only applicable to cross-ply laminates. They stated that the method is capable of handling laminates with a large number of plies but didn't provide any results to support this claim. Also because of convergence difficulties (for larger b/t ratios) in stresses at an interface and the free edge, the solution is limited to very thin laminates.

A similar approach was proposed by Bar-Yoseph and Pian.[46] In their solution, the edge layer stress field is constructed using Legendre Polynomials that exactly satisfy the equilibrium conditions, traction continuity conditions, and the stress free edge conditions. Later they incorporated their assumed stress states into a mixed hybrid finite element formulation.[47] This method was extended by Bar-Yoseph and Siton to include nonlinear material behavior.[48]

Another variational approach was provided by Pagano.[49] He proposed an approximate solution based upon the extension of Reissner's theorem[50] to a laminated body. Requirements for an acceptable laminate field theory were established; all stress components are non-zero, displacement and traction continuity are satisfied at all interfaces, and each layer or sublayer (more than one sublayer per ply is permitted) is in equilibrium. In establishing layer equilibrium, free edge conditions are imposed on force and moment resultants rather than on point-wise tractions. A model which is based upon assumed stress fields in each layer is developed which satisfies these criteria. Explicit functions are assumed for the through thickness variations of stresses. Minimization of Reissner's functional over the entire laminate results in a system of 13N differential equations, where N is the number of sublayers in the laminate, for the in-plane variations of the field variables.

Pagano [51] also delineated the theory for the analysis of an axial coupon. The field equations in this case are constant coefficient, linear differential equations, in the width coordinate y. The homogeneous solution for each independent variable is then a sum of exponential terms of the form

$$f = Fe^{\lambda y} \tag{2.4}$$

The method provides accurate stress distributions in regions near free edges but very large magnitudes of λ, obtained for large N, limited solutions to laminates with $N < 6$ because of computer overflow/underflow violations. Also, although the solution does not include a singularity, the σ_{13} and σ_{33} stress components increased as the number of sublayers used per layer increased. This behavior is similar to that observed with increased mesh refinement when using the finite element method.

Pagano and Soni[52] later took this model and, using a global-local variational formulation, developed a ply/sub-laminate analysis. In regions where a detailed response is required (local region) each ply is represented by the model described above. The remaining areas, e.g. sub-laminates or global regions, are represented by effective elastic properties.[53] The method shows promise but appears to be somewhat sensitive in its predictions to the choice of the global and local domains. Also, if stresses are desired at each interface of an N layered laminate, the global/local analysis must be exercised several times with the local domain containing the interface of interest. Rehfield et. al[54,55] employed a similar approach using their refined theories for the behavior of anisotropic plates for the ply/sublaminate models.[56,57] Their method results in a set of 8N-3 equations, where again N is the number of sublayers.

Most of the solutions described above suggest the presence of a singularity at the intersection of an interface and the free edge. To incorporate the singularity in the formulation, the nature of the singularity must be known before hand. Up to this point Bogy's[27] work on the singularities

on isotropic quarter planes had not been extended to anisotropic materials. Consequently, to better understand the boundary-layer effect in composite laminates, some investigators set out to determine the exactly the singularity at the intersection of the interface of two laminae and the free edge. One such study was presented by Wang and Choi.[58,59] Their formulation is based on the theory of elasticity and Lekhnitskii's[60] complex stress potentials and leads to a pair of coupled governing partial differential equations. The homogeneous solution to the equations is obtained using an eigenfunction expansion. The homogeneous solution showed the existence of a singularity of the form $y^{-\delta}$ at the intersection of an interface and the free edge. They found that the order of the singularity δ is in general very weak and is dependent only on the material constants and fiber orientations of plies adjacent to the interface of interest. Similar studies by Zwiers, Ting and Spilker,[61] and Dempsey and Sinclair[62,63] showed that singularities of the form ln(y), $(\ln(y))^2$, $(\ln(y))^3$, etc. are also present for some combinations of adjacent layers, in addition to the $y^{-\delta}$ singularity. These results, along with numerical studies on the singularities,[39] are significant because they showed that although mathematical singularities exist, they are generally very weak and act over such small distances that approximate solutions that do not incorporate the singularity are accurate except in regions very near the free edge.

2.2 Laminates in Uniform Bending

Few studies have been conducted on laminates in bending. Salamon[64] presented a solution for finite width laminates uniformly bent by end moments applied about the X_2-axis (see Figure 1.1). Using an approach similar to that of Pipes and Pagano[26] the elasticity equations are formulated and solved using the finite difference method. He finds that the interlaminar shear and normal stress distributions are similar for a laminate in uniform bending to those of a laminate in uniform extension.

Finite element studies were conducted by Murthy and Chamis[65] for a variety of load conditions including in-plane and out-of-plane bending, and by Chan and Ochoa[66,67] for laminates under torsion and bending loads. Kassapoglou[68] extended his analysis for extension loading[20] to combined loading cases and bending.

2.3 Summary and Discussion

The above discussion gives an indication of the variety of solutions proposed for obtaining free edge stresses in laminated composites. These solutions have increased the understanding of the mechanics of interlaminar stress development and their effects on the performance of laminated composite structures. Most of these solutions, however, are constrained computationally by the size of laminate system they can handle and therefore have limited practical application. Apparently some tradeoff needs to be made between solution accuracy of the complicated solutions described above and solution efficiency offered by simplified approximate models.

Recently Kassapoglou and Lagace[21] proposed a simplified, approximate technique for determining the stress field in the vicinity of straight free edges of a laminated coupon. A very similar approach was presented by Engrand.[69] Kassapoglou and Lagaces' analysis is based on the principle of minimum complementary energy and an assumed stress state obtained by considering global equilibrium requirements. Generic forms of stress distributions that exactly satisfy the equations of equilibrium, the traction continuity conditions and the free edge stress boundary conditions are assumed within each layer. Explicit polynomial expressions are used for the through-thickness variations of the stresses, while the in-plane variations are taken to be combinations of two decaying exponential functions expressed in terms of two unknown decay parameters. The unknown decay parameters are functions of ply material properties, orientation

and thickness, and laminate stacking sequence, and are determined by minimizing the laminate complementary energy. Once these parameters are determined the stresses can be evaluated at any point in the laminate.

A distinguishing feature of Kassapoglou and Lagaces' model is that run times and computer memory requirements are a linear function of the number of layers in the laminate. This makes for an extremely efficient design tool that can be used to analyze laminates with many layers. The model, however, has trouble predicting interlaminar normal stresses and in some cases interlaminar shear stresses.

Kassapoglou and Lagaces' (KL) method serves as a basis for the approximate solution developed in this investigation. In their stress assumptions only the mismatch between laminae and laminate material properties is considered. The improved solution includes additional terms in the stress assumptions which account for the effect of mismatch in engineering properties between adjacent layers of a laminate. Specifically, the mismatches in coefficient of mutual influence and Poisson's ratio are considered.

CHAPTER 3

SOLUTION FORMULATION

The problem considered is the uniform axial extension or bending of a multi-layered laminated plate. Interest focuses on calculating the stress field in the vicinity of the free edge, i.e. in the boundary layer region. In this chapter, the mathematical boundary value problem for determining the free edge stresses is formulated from the linear theory of elasticity. Because of the analytical complexities of the three dimensional elasticity equations that must be solved within each layer, coupled with the requirement of continuous displacements and stresses at interfaces between layers, an exact elasticity solution for stress analysis in practical laminates is not feasible.[58,59] Hence, an approximate solution is proposed. The approximate solution is based upon the principle of minimum complementary potential energy and stress assumptions constructed in such a manner as to simplify the equations to be solved, while retaining the necessary three dimensional characteristics of the stress field. The stress assumptions exactly satisfy all of the equilibrium requirements. The compatibility equations and displacement continuity conditions are satisfied in an average sense through minimization of the laminate complementary energy.

A singularity is not included in the stress assumptions. As previously mentioned, previous investigators[58,61,62] have shown that a very weak stress singularity is present near the intersection of interfaces and the free edge of composite laminates. However, as Pagano has noted,[49] these singularities are artifacts of the effective modulus approach and do not exist in real materials. Also, the singularity is so weak and acts over such a small portion of the laminate

near the free edge that the assumption of material homogeneity on which the analysis is based breaks down. Further, Pagano suggested that when interpreting stress predictions using an effective modulus approach, average stresses, rather than point stresses, in regions of steep gradients may lead to more realistic conclusions regarding physical behavior.[70] These comments suggest that the stress singularities may be of only academic concern, and a solution that does not include a singularity is equally as valid as one that does, particularly in design applications where a qualitative comparison of the interlaminar stress severity in candidate laminates is the primary interest.

The remainder of the chapter is devoted to development of the approximate solution. In Section 3.1, the elasticity problem is formulated. Section 3.2 summarizes classical lamination theory and the stresses of classical lamination theory are derived in terms of the mismatches in laminate and laminae material properties. These stresses and local mismatch considerations are then used to formulate the refined approximate model as discussed in Section 3.3.

3.1 Problem Statement

The geometry of a long, symmetrically or unsymmetrically laminated plate of finite width is shown in Figure 1.1. The laminate is built up of several layers reinforced by a system of parallel fibers oriented at an angle θ with respect to the laminate longitudinal axis. Perfect bonding between adjacent layers is assumed. The laminate is assumed to be long enough so that away from the ends, where the loads are applied, the stresses and strains are independent of the axial coordinate. Another assumption made is that away from the edges the laminate is in a state of plane stress with the response defined by the classical lamination plate theory model. This assumption places a limitation on the geometry of laminates that can be accurately analyzed using the approximate solution and will be discussed further in Section 3.3.5. Also,

unsymmetric laminates will deflect out-of-plane when subjected to in-plane loads because of the membrane-flexural deformation coupling behavior they exhibit. These out of plane deflections are assumed small, so that geometric coupling effects can be ignored.

An exploded view of the laminate, showing the in-plane and out-of-plane stress components is provided in Figure 3.1. The origin of the global coordinate system (X_1,X_2,X_3) is located at the center of the laminate, with the X_1, X_2, and X_3 axes taken in the axial, transverse, and thickness directions respectively. Local coordinates $x^{(k)}$, $y^{(k)}$, and $z^{(k)}$ are established in each layer, where $y^{(k)} = b - x_2^{(k)}$ is measured from the free edge and $z^{(k)}$ is measured from the bottom of the kth ply. Beginning at the top surface of the laminate, the layers are numbered consecutively from 1 to N. The layers may have different thicknesses and may be different materials. Each layer is represented by a macroscopically homogeneous, linearly elastic, orthotropic material. Since the fiber axes of the individual layers are rotated through an angle θ with respect to the laminate axis, the material behavior of each laminae appears monoclinic in the global coordinate system. The constitutive equations for each layer then have the form

$$\begin{Bmatrix} \varepsilon_{11} \\ \varepsilon_{22} \\ \varepsilon_{33} \\ \gamma_{23} \\ \gamma_{13} \\ \gamma_{12} \end{Bmatrix} = \begin{bmatrix} \bar{S}_{11} & \bar{S}_{12} & \bar{S}_{13} & 0 & 0 & \bar{S}_{16} \\ & \bar{S}_{22} & \bar{S}_{23} & 0 & 0 & \bar{S}_{26} \\ & & \bar{S}_{33} & 0 & 0 & \bar{S}_{36} \\ & \text{SYM} & & \bar{S}_{44} & \bar{S}_{45} & 0 \\ & & & & \bar{S}_{55} & 0 \\ & & & & & \bar{S}_{66} \end{bmatrix} \begin{Bmatrix} \sigma_{11} \\ \sigma_{22} \\ \sigma_{33} \\ \sigma_{23} \\ \sigma_{13} \\ \sigma_{12} \end{Bmatrix} \tag{3.1}$$

where $[\bar{S}_{ij}]$ is the transformed compliance matrix.

3.2 Classical Lamination Theory

3.2.1 Assumptions and Constitutive Relations

According to classical lamination theory, the plate in Figure 1.1 acts as a single integral unit

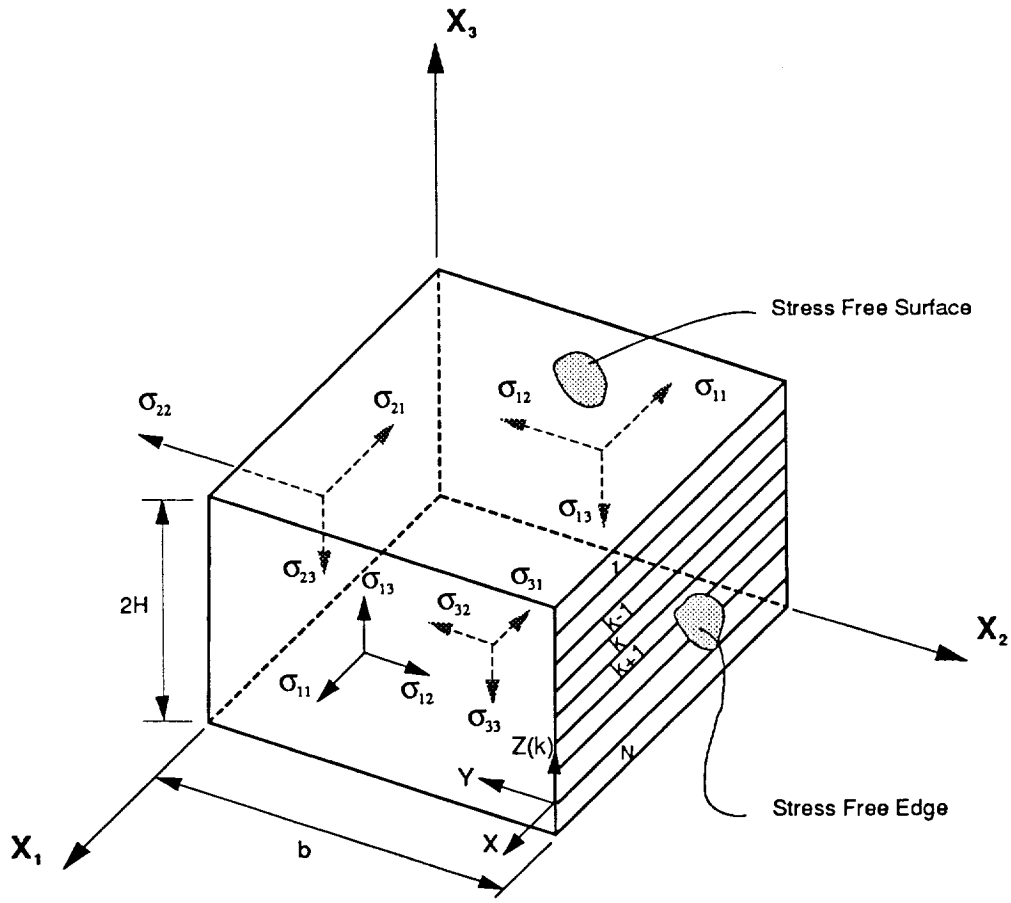

Figure 3.1. Laminate Coordinate System

with smeared elastic properties, and deforms under load in accordance with the Kirchoff deformation assumptions for thin plates. The elastic non-homogeneity of the laminate is taken into account by calculating the stresses in the individual layers using the laminate strains determined with these assumptions. A state of plane stress is assumed in each ply. The plane stress assumption implies

$$\sigma_{33}^{(k)} = \sigma_{23}^{(k)} = \sigma_{13}^{(k)} = 0 \tag{3.2}$$

and the stresses in the k^{th} layer are given by

$$\begin{Bmatrix} \tilde{\sigma}_{11} \\ \tilde{\sigma}_{22} \\ \tilde{\sigma}_{12} \end{Bmatrix}^k = \begin{bmatrix} \bar{Q}_{11} & \bar{Q}_{12} & \bar{Q}_{16} \\ \bar{Q}_{12} & \bar{Q}_{22} & \bar{Q}_{26} \\ \bar{Q}_{16} & \bar{Q}_{26} & \bar{Q}_{66} \end{bmatrix}^k \begin{Bmatrix} \varepsilon_{11} \\ \varepsilon_{22} \\ \gamma_{12} \end{Bmatrix}^k \tag{3.3}$$

where $\bar{Q}_{ij}^{(k)}$ are the reduced stiffnesses in the laminate coordinate system. These relations are used in conjunction with the Kirchoff deformation assumptions to define integrated laminate properties. From the Kirchoff assumptions for thin plates, the laminate strains are

$$\{\varepsilon\}_X = \{\varepsilon^0\}_X + X_3\{\kappa\}_X \tag{3.4}$$

where $\{\varepsilon^0\}_X$ are the laminate middle surface strains and $\{\kappa\}_X$ are the laminate middle surface curvatures. Substituting the through-thickness strain variations (3.4) into the layer constitutive relations (3.3), yields expressions for the stresses in the k^{th} layer in terms of the laminate middle surface strains and curvatures:

$$\begin{Bmatrix} \tilde{\sigma}_{11} \\ \tilde{\sigma}_{22} \\ \tilde{\sigma}_{12} \end{Bmatrix}^k = \begin{bmatrix} \bar{Q}_{11} & \bar{Q}_{12} & \bar{Q}_{16} \\ \bar{Q}_{12} & \bar{Q}_{22} & \bar{Q}_{26} \\ \bar{Q}_{16} & \bar{Q}_{26} & \bar{Q}_{66} \end{bmatrix}^k \left\{ \begin{Bmatrix} \varepsilon_{11}^0 \\ \varepsilon_{22}^0 \\ \gamma_{12}^0 \end{Bmatrix} + X_3 \begin{Bmatrix} \kappa_{11} \\ \kappa_{22} \\ \kappa_{12} \end{Bmatrix} \right\} \tag{3.5}$$

The laminate constitutive relations are then obtained by integrating equation (3.5) through the laminate thickness. This yields

$$\begin{Bmatrix} N \\ M \end{Bmatrix} = \begin{bmatrix} A & B \\ B & D \end{bmatrix} \begin{Bmatrix} \varepsilon^o \\ \kappa \end{Bmatrix} \tag{3.6}$$

where the laminate stiffnesses are

$$[A,B,D] = \int_{-H}^{+H} [\bar{Q}]^k [1, X_3, X_3^2]\, dX_3 \tag{3.7}$$

and the force and moment resultants acting on the laminate are

$$\{N\} = \int_{-H}^{+H} \{\tilde{\sigma}\}^k\, dX_3 \tag{3.8a}$$

$$\{M\} = \int_{-H}^{+H} \{\tilde{\sigma}\}^k\, X_3 dX_3 \tag{3.8b}$$

3.2.2 CLT Stresses from Global Mismatch Considerations

Stresses develop in the classical lamination theory because of the mismatch in material properties between the laminate and the individual layers comprising the laminate. This type of mismatch will be referred to as the global mismatch in material properties. To show the relationship between global mismatch and the classical lamination theory stress components consider a symmetric laminate subjected to in-plane uniaxial extension ε_{11}^0. For this loading and geometry all terms in the [B] matrix are zero, and the extensional response uncouples from the bending response. The laminate constitutive relations are then

$$\{N\} = [A]\{\varepsilon^0\}_X \tag{3.9}$$

and the stresses in the kth ply are

$$\begin{Bmatrix} \tilde{\sigma}_{11} \\ \tilde{\sigma}_{22} \\ \tilde{\sigma}_{12} \end{Bmatrix}^k = \begin{bmatrix} \bar{Q}_{11} & \bar{Q}_{12} & \bar{Q}_{16} \\ \bar{Q}_{12} & \bar{Q}_{22} & \bar{Q}_{26} \\ \bar{Q}_{16} & \bar{Q}_{26} & \bar{Q}_{66} \end{bmatrix}^k \begin{Bmatrix} \varepsilon_{11}^0 \\ \varepsilon_{22}^0 \\ \gamma_{12}^0 \end{Bmatrix} \tag{3.10}$$

where ε_{11}^0, ε_{22}^0, and γ_{12}^0 are the laminate strains and are constant throughout the laminate thickness. The laminate strains ε_{22}^0 and γ_{12}^0 can be related to the applied strain ε_{11}^0 by the

laminate Poisson's ratio, $\bar{\nu}_{12}$, and the laminate coefficient of mutual influence, $\bar{\eta}_{12,1}$, respectively

$$\varepsilon_{22}^0 = -\bar{\nu}_{12}\varepsilon_{11}^0 \qquad (3.11)$$

$$\gamma_{12}^0 = \bar{\eta}_{12,1}\varepsilon_{11}^0$$

where

$$\bar{\nu}_{12} = \frac{A_{12}A_{66} - A_{16}A_{26}}{A_{22}A_{66} - A_{26}^2} \qquad (3.12a)$$

$$\bar{\eta}_{12,1} = \frac{A_{12}A_{26} - A_{16}A_{22}}{A_{22}A_{66} - A_{26}^2} \qquad (3.12b)$$

Now, if the laminate strain ε_{11}^0 is applied to the individual layers, each layer will deform in accordance with its characteristic elastic properties

$$\varepsilon_{11}^{(k)} = \varepsilon_{11}^0$$

$$\varepsilon_{22}^{(k)} = -\nu_{12}^{(k)}\varepsilon_{11}^0 \qquad (3.13)$$

$$\gamma_{12}^{(k)} = \eta_{12,1}^{(k)}\varepsilon_{11}^0$$

where

$$\nu_{12}^{(k)} = \frac{\bar{Q}_{12}^{(k)}\bar{Q}_{66}^{(k)} - \bar{Q}_{16}^{(k)}\bar{Q}_{26}^{(k)}}{\bar{Q}_{22}^{(k)}\bar{Q}_{66}^{(k)} - [\bar{Q}_{26}^{(k)}]^2} \qquad (3.14a)$$

$$\eta_{12,1}^{(k)} = \frac{\bar{Q}_{12}^{(k)}\bar{Q}_{26}^{(k)} - \bar{Q}_{26}^{(k)}\bar{Q}_{22}^{(k)}}{\bar{Q}_{22}^{(k)}\bar{Q}_{66}^{(k)} - [\bar{Q}_{26}^{(k)}]^2} \qquad (3.14b)$$

The stresses $\tilde{\sigma}_{22}^{(k)}$ and $\tilde{\sigma}_{12}^{(k)}$ develop because the strains in equation (3.13) are required to match the strains in equation (3.11). Expressions for the stresses are developed by writing the strain in each layer as a combination of the individual ply strains $\varepsilon_{ii}^{(k)}$, and $\delta\varepsilon_{ii}^{(k)}$ terms, where the $\delta\varepsilon_{ii}^{(k)}$ terms are required to force the total strains in each ply to match the laminate strains

$$\varepsilon_{11}^0 = \varepsilon_{11}^{(k)} \qquad (3.15a)$$

$$\varepsilon_{22}^{0} = \varepsilon_{22}^{(k)} + \delta\varepsilon_{22}^{(k)} \tag{3.15b}$$

$$\gamma_{12}^{0} = \gamma_{12}^{(k)} + \delta\gamma_{12}^{(k)} \tag{3.15c}$$

Substituting into equation (3.10) gives

$$\tilde{\sigma}_{11}^{(k)} = E_{11}^{(k)}\varepsilon_{11}^{0} + \bar{Q}_{12}^{(k)}\delta\varepsilon_{22}^{(k)} + \bar{Q}_{16}^{(k)}\delta\gamma_{12}^{(k)} \tag{3.16a}$$

$$\tilde{\sigma}_{22}^{(k)} = \bar{Q}_{22}^{(k)}\delta\varepsilon_{22}^{(k)} + \bar{Q}_{26}^{(k)}\delta\gamma_{12}^{(k)} \tag{3.16b}$$

$$\tilde{\sigma}_{12}^{(k)} = \bar{Q}_{26}^{(k)}\delta\varepsilon_{22}^{(k)} + \bar{Q}_{66}^{(k)}\delta\gamma_{12}^{(k)} \tag{3.16c}$$

From equations (3.11) and (3.13),

$$\delta\varepsilon_{22}^{(k)} = (\varepsilon_{22}^{0} - \varepsilon_{22}^{(k)}) = \varepsilon_{11}^{0} (-\bar{\nu}_{12} + \nu_{12}^{(k)}) \tag{3.17a}$$

$$\delta\gamma_{xy}^{(k)} = (\gamma_{12}^{0} - \gamma_{12}^{(k)}) = \varepsilon_{11}^{0} (\bar{\eta}_{12,1} - \eta_{12,1}^{(k)}) \tag{3.17b}$$

Combining equations (3.16) and (3.17) then gives the laminae stresses in terms of the laminae stiffnesses, the applied axial strain, and the mismatch in Poisson's ratio and coefficient of mutual influence of the laminae and the laminate:

$$\begin{aligned}
\tilde{\sigma}_{11}^{(k)} &= [E_{11}^{(k)} + \bar{Q}_{12}^{(k)}(\nu_{12}^{(k)} - \bar{\nu}_{12}) + \bar{Q}_{16}^{(k)}(\bar{\eta}_{12,1} - \eta_{12,1}^{(k)})]\varepsilon_{11}^{0} \\
\tilde{\sigma}_{22}^{(k)} &= [\bar{Q}_{22}^{(k)}(\nu_{12}^{(k)} - \bar{\nu}_{12}) + \bar{Q}_{26}^{(k)}(\bar{\eta}_{12,1} - \eta_{12,1}^{(k)})]\varepsilon_{11}^{0} \\
\tilde{\sigma}_{12}^{(k)} &= [\bar{Q}_{26}^{(k)}(\nu_{12}^{(k)} - \bar{\nu}_{12}) + \bar{Q}_{66}^{(k)}(\bar{\eta}_{12,1} - \eta_{12,1}^{(k)})]\varepsilon_{11}^{0}
\end{aligned} \tag{3.18}$$

From these equations it is seen that when the material constants ν_{12} and $\eta_{12,1}$ of the individual plies are identical to those of the laminate, the in-plane stresses $\tilde{\sigma}_{22}^{(k)}$ and $\tilde{\sigma}_{12}^{(k)}$ are zero. On the other hand, when there is a difference in the material constants, the in-plane stresses will in general be non-zero. As shown subsequently in Section 3.3, the magnitudes and signs of the in-plane stresses, and the laminate stacking sequence, have a direct influence on the magnitudes of the interlaminar stress components.

3.2.3 Classical Lamination Theory Summary

The classical lamination theory solution is approximate and in general only satisfies the equilibrium equations and edge boundary conditions in a through-thickness average sense. On a

point by point basis, however, the differential equations of equilibrium are not satisfied by the classical lamination plate theory solution in edge regions where there is a transverse gradient in the in-plane stress field, because the out-of-plane stresses are assumed to be zero. Further the surface tractions are not zero as required by the exact elasticity equations. Thus, the stress field needs to be refined in regions near the boundaries. The next section details the formulation of the refined solution developed in the present investigation.

3.3 Boundary Layer Stress Solution

3.3.1 Problem Formulation

The solution is developed by recalling that the applied loading and hence the stresses and strains are independent of the the axial coordinate. The analysis may then be restricted to any y-z cross section. To take into account warping of the cross section, induced by the presence of off-axis layers, the generalized plane deformation assumption, with orthogonal displacement components u,v, and w is employed.[60] As shown in Figure 3.1, the free edge is defined by y = 0. We assume that the classical lamination theory solution has been obtained and concentrate on calculating stresses in the boundary layer region. The classical lamination theory solution is valid in the interior but predicts non-zero stresses $\tilde{\sigma}_{12}^{(k)}$ and $\tilde{\sigma}_{22}^{(k)}$ at the free edge. This defect in the satisfaction of the free edge boundary conditions is corrected by a refined approximate solution that assumes the total stresses in each layer to be a combination of the classical lamination theory stresses plus an additional contribution to the stress field which is negligible outside the boundary layer region. The in-plane components of the boundary layer terms evaluated at y=0 are taken as the negative of the classical lamination theory values so that the free edge conditions are satisfied. Thus we assume

$$\sigma_{ij}^{(k)}(y,z) = \tilde{\sigma}_{ij}^{(k)}(y,z) + \hat{\sigma}_{ij}^{(k)}(y,z) \tag{3.19}$$

where:

$\sigma_{ij}^{(k)}(y,z)$ is the total stress in the kth ply

$\tilde{\sigma}_{ij}^{(k)}(y,z)$ is the clt stress solution in the kth ply

$\hat{\sigma}_{ij}^{(k)}(y,z)$ is the local solution for the kth ply

Because of the difficulties and inefficiencies encountered with solutions for the free edge stress field based on displacement formulations, a stress formulation is presented. Under the generalized plane deformation assumption, and in the absence of body forces, the equilibrium equations that must be satisfied in each layer have the form

$$-\frac{\partial\sigma_{12}^{(k)}}{\partial y} + \frac{\partial\sigma_{13}^{(k)}}{\partial z} = 0 \tag{3.20a}$$

$$-\frac{\partial\sigma_{22}^{(k)}}{\partial y} + \frac{\partial\sigma_{23}^{(k)}}{\partial z} = 0 \tag{3.20b}$$

$$-\frac{\partial\sigma_{23}^{(k)}}{\partial y} + \frac{\partial\sigma_{33}^{(k)}}{\partial z} = 0 \tag{3.20c}$$

and the associated compatibility equations are,

$$\frac{\partial^2\varepsilon_{11}}{\partial^2 y} = 0 \tag{3.21a}$$

$$\frac{\partial^2\varepsilon_{11}}{\partial y\partial z} = 0 \tag{3.21b}$$

$$\frac{\partial^2\varepsilon_{11}}{\partial^2 z} = 0 \tag{3.21c}$$

$$\frac{\partial^2\varepsilon_{22}}{\partial^2 z} + \frac{\partial^2\varepsilon_{33}}{\partial^2 y} + \frac{2\partial^2\varepsilon_{23}}{\partial y\partial z} = 0 \tag{3.21d}$$

$$\frac{\partial}{\partial y}\left[\frac{\partial\varepsilon_{13}}{\partial y} + \frac{\partial\varepsilon_{12}}{\partial z}\right] = 0 \tag{3.21e}$$

$$\frac{\partial}{\partial z}\left[\frac{\partial\varepsilon_{13}}{\partial y} + \frac{\partial\varepsilon_{12}}{\partial z}\right] = 0 \tag{3.21f}$$

The equilibrium equations (3.20) can be satisfied identically by expressing the stress components

in each layer in terms of the stress functions [60] ϕ and ψ, such that

$$\sigma_{22} = \frac{\partial^2 \phi}{\partial^2 z} \qquad \sigma_{23} = \frac{\partial^2 \phi}{\partial y \partial z} \qquad \sigma_{33} = \frac{\partial^2 \phi}{\partial^2 y} \tag{3.22a}$$

$$\sigma_{12} = \frac{\partial \psi}{\partial z} \qquad \sigma_{13} = \frac{\partial \psi}{\partial y} \tag{3.22b}$$

The sixth stress component σ_{11} is determined from the compatibility equations (3.21a-c) and the strain-stress relations as subsequently described in Section 3.3.5. The stress functions and constitutive relations can then be used in the remaining compatibility equations to yield the following pair of coupled governing partial differential equations for the stress functions.

$$L_3\phi + L_2\psi = -2B_1 - \frac{S_{16}}{S_{11}}B_2 \tag{3.23a}$$

$$L_4\phi + L_3\psi = 0 \tag{3.23b}$$

where, L_2, L_3, and L_4, are linear differential operators defined as:

$$L_2 = R_{55}\frac{\partial^2}{\partial y^2} + R_{66}\frac{\partial^2}{\partial z^2} \tag{3.23c}$$

$$L_3 = R_{26}\frac{\partial^3}{\partial z^3} + R_{36}\frac{\partial^3}{\partial y^2 \partial z} + R_{45}\frac{\partial^3}{\partial y^2 \partial z} \tag{3.23d}$$

$$L_4 = R_{22}\frac{\partial^4}{\partial z^4} + 2R_{23}\frac{\partial^4}{\partial y^2 \partial z^2} + R_{33}\frac{\partial^4}{\partial y^4} + R_{44}\frac{\partial^4}{\partial y^2 \partial z^2} \tag{3.23e}$$

and

$$R_{ij} = \bar{S}_{ij} - \frac{\bar{S}_{i1}\bar{S}_{j1}}{\bar{S}_{11}} \tag{3.24}$$

B_1 and B_2 are determined from the end conditions.

In addition to satisfying equations (3.23) for each layer, the solution must satisfy conditions on the external surfaces of the plate as well as satisfy the conditions of continuous tractions and displacements along interfaces between adjacent layers of the laminate. The traction free conditions at the edges y=0 imply

$$\begin{aligned} \sigma_{12}^{(k)} &= \hat{\sigma}_{12}^{(k)} + \tilde{\sigma}_{12}^{(k)} = 0 \\ \sigma_{22}^{(k)} &= \hat{\sigma}_{22}^{(k)} + \tilde{\sigma}_{22}^{(k)} = 0 \qquad (\text{for } y = 0) \\ \sigma_{23}^{(k)} &= \hat{\sigma}_{23}^{(k)} = 0 \end{aligned} \tag{3.25}$$

The traction free conditions on the top and bottom surfaces require

$$\begin{aligned} \sigma_{13} &= 0 \\ \sigma_{23} &= 0 \qquad (\text{for } X_3 = \pm H) \\ \sigma_{33} &= 0 \end{aligned} \tag{3.26}$$

For perfect bonding between layers, the continuity of displacements and tractions at the layer interfaces impose the six additional conditions on the solution in each layer

$$\sigma_{13}^{(k+1)}(y,t^{(k+1)}) = \sigma_{13}^{(k)}(y,0) \tag{3.27a}$$

$$\sigma_{23}^{(k+1)}(y,t^{(k+1)}) = \sigma_{23}^{(k)}(y,0) \tag{3.27b}$$

$$\sigma_{33}^{(k+1)}(y,t^{(k+1)}) = \sigma_{33}^{(k)}(y,0) \tag{3.27c}$$

$$u^{(k+1)}(y,t^{(k+1)}) = u^{(k)}(y,0) \tag{3.27d}$$

$$v^{(k+1)}(y,t^{(k+1)}) = v^{(k)}(y,0) \tag{3.27e}$$

$$w^{(k+1)}(y,t^{(k+1)}) = w^{(k)}(y,0) \tag{3.27f}$$

where the superscripts k and k+1 designate the ply above and below the interface, respectively. We have also assumed that classical lamination theory stresses are recovered in the interior. This assumption implies the additional conditions

$$\lim_{y \to \infty} \hat{\sigma}_{ij}(y,z)^{(k)} = 0 \tag{3.28}$$

Finally at the ends of the laminate, the kinematic conditions $w = \varepsilon_0 X_1$ or $w = (\kappa_0 X_3) X_1$ are imposed, where ε_0 and κ_0 are applied axial strain and curvature, respectively.

3.3.2 Stress Assumptions

An approximate solution to equations (3.23) subject to the boundary conditions specified in equations (3.25-3.28) is obtained by choosing a stress field that exactly satisfies the differential

equilibrium equations (3.20a-3.20c), and the stress boundary conditions (3.25-3.28). For clarity, explicit expressions for stresses rather than stress functions are presented. Results from previous investigations are used to guide the selection of appropriate stress forms. The previous analyses show large through-thickness gradients as well as large in-plane gradients in the stress field in regions near the free edge and in interfacial regions. In the present investigation, these perturbations in the classical lamination theory stress predictions are approximated by assuming two physical effects contribute to the stress field. The first effect is that represented by the Kassapoglou and Lagace (KL) solution. In this solution, the in-plane stresses predicted by classical lamination theory are used to formulate expressions for the out-of-plane stresses. As previously shown in Section 3.1 the classical lamination theory stresses develop because of the mismatch in engineering properties between the laminate and the individual laminae. The stress field obtained by adding the KL refinement and the classical lamination theory solution exactly satisfies the differential equations of equilibrium, the stress free boundary conditions, and the traction continuity conditions. Thus this contribution is referred to as the global mismatch or global equilibrium effect. The solution obtained from global mismatch considerations, however, assumes the laminate behavior to be qualitatively the same throughout the thickness of the layers, and consequently does not capture the large through thickness gradients in the layer stress fields near the interfacial surfaces. Further, the KL method predicts zero stresses at some interfaces where other analysis methods predict stresses of considerable magnitude. The second effect included in the present formulation is intended to relax some of the constraints imposed by the KL technique and provide an improved approximate theory. This effect is more local in nature than the KL contribution to the stress field, and relates the stresses developing near interfacial planes to the relative displacements of adjacent layers, arising because of the mismatch in engineering properties between these layers. Two material property mismatches are

considered; a coefficient of mutual influence mismatch, and a Poisson's ratio mismatch. Herakovich[8] has shown that these properties are the most important to consider, with regard to interlaminar stress development, for the mechanical loading problem. Poisson's ratio is defined as

$$\nu_{12} = -\frac{\varepsilon_{22}}{\varepsilon_{11}} = -\frac{\bar{S}_{12}}{\bar{S}_{11}} \tag{3.29}$$

and the coefficient of mutual influence is defined as

$$\eta_{12,1} = \frac{\gamma_{12}}{\varepsilon_{11}} = \frac{\bar{S}_{16}}{\bar{S}_{11}} \tag{3.30}$$

where $\bar{S}_{ij}$ are the previously defined compliance coefficients in laminate coordinates. The coefficient of mutual influence mismatch is primarily responsible for the development of σ_{13} and σ_{12}, while the Poisson's ratio mismatch is primarily responsible for development of σ_{22}, σ_{23}, and σ_{33}. Since global equilibrium and the free edge boundary conditions are satisfied by the KL solution, self equilibrating forms are assumed for the local mismatch contributions to the stress field.

The stress components for each layer are chosen as product functions of the thickness variable z, and the in-plane variable y. This leads to the following functional form for each of the effects in the k^{th} ply:

a) global mismatch

$$\hat{\sigma}^{(k)}_{ij_{(E)}}(y,z) = f^{(k)}_{ij}(y)g^{(k)}_{ij}(z) \quad i = 1,2,3, \quad j = 2,3 \tag{3.31}$$

b) mismatch in coefficient of mutual influence

$$\hat{\sigma}^{(k)}_{ij_{(\eta)}}(y,z) = h^{(k)}_{ij}(y)l^{(k)}_{ij}(z) \quad i = 1, \quad j = 2,3 \tag{3.32}$$

c) mismatch in Poisson's ratio

$$\hat{\sigma}^{(k)}_{ij_{(\delta\sigma)}}(y,z) = m^{(k)}_{ij}(y)n^{(k)}_{ij}(z) + m^{(k)}_{ij}(y)p^{(k)}_{ij}(z) \quad i = 2,3, \quad j = 2,3 \tag{3.33}$$

The stress field $\hat{\sigma}(y,z)$ in the kth ply is then the sum of (a), (b) and (c)

$$\hat{\sigma}^{(k)}_{ij}(y,z) = f^{(k)}_{ij}(y)g^{(k)}_{ij}(z) + h^{(k)}_{ij}(y)l^{(k)}_{ij}(z) + m^{(k)}_{ij}(y)n^{(k)}_{ij}(z) + m^{(k)}_{ij}(y)p^{(k)}_{ij}(z) \quad i = 1,2,3, \quad j = 2,3 \tag{3.34}$$

Substituting equation (3.31) into the differential equations of equilibrium yields the following system of ordinary differential equations:

$$\frac{df^{(k)}_{12}(y)}{dy} = f^{(k)}_{13}(y) \tag{3.35}$$

$$\frac{df^{(k)}_{22}(y)}{dy} = f^{(k)}_{23}(y) \qquad \frac{df^{(k)}_{23}(y)}{dy} = f^{(k)}_{33}(y) \tag{3.36}$$

$$g^{(k)}_{12}(z) = \frac{dg^{(k)}_{13}(z)}{dz} \tag{3.37}$$

$$g^{(k)}_{22}(z) = \frac{dg^{(k)}_{23}(z)}{dz} \qquad g^{(k)}_{23}(z) = \frac{dg^{(k)}_{33}(z)}{dz} \tag{3.38}$$

Similar equations are obtained relating the functions in equations (3.32) and (3.34) If equations (3.32) and (3.33) are substituted into the differential equilibrium equations, relationships like equations (3.35) and (3.36) are obtained for the h_{ij}s, and m_{ij}s, and expressions similar to equations (3.37) and (3.38) are obtained relating the l_{ij}s, n_{ij}s, and p_{ij}s. Note that equation (3.35) uncouples from equation (3.36) and equation (3.37) uncouples from equation (3.38). This decoupling was indicated previously in equations (3.22). Thus only four functions have to be assumed for each contribution; two in-plane variations and two through-thickness variations. The remaining functions are determined from the conditions (3.35-3.38).

3.3.3 Global Mismatch (KL Solution)

Following the KL solution, the first refinement to the stress field is made by assuming approximate expressions for the out-of-plane stresses, based upon the in-plane stresses. The in-plane stresses are taken to have the form

$$\hat{\sigma}^{(k)}_{12_{(E)}}(y,z) = f^{(k)}_{12}(y)g^{(k)}_{12}(z) \tag{3.39a}$$

$$\hat{\sigma}^{(k)}_{22_{(E)}}(y,z) = f^{(k)}_{22}(y)g^{(k)}_{22}(z) \tag{3.39b}$$

where $f^{(k)}_{22}(y)$ and $f^{(k)}_{12}(y)$ are unknown functions of y and $g^{(k)}_{12}(z)$ and $g^{(k)}_{22}(z)$ are unknown functions of z. The form of the functions $g^{(k)}_{22}(z)$ and $g^{(k)}_{12}(z)$ is determined by imposing the free edge conditions (3.25) at y = 0

$$\hat{\sigma}^{(k)}_{12_{(E)}}(y=0,z) = -\tilde{\sigma}^{(k)}_{12}(z) \tag{3.40a}$$

$$\hat{\sigma}^{(k)}_{22_{(E)}}(y=0,z) = -\tilde{\sigma}^{(k)}_{22}(z) \tag{3.40b}$$

where $\tilde{\sigma}^{(k)}_{22}(z)$ and $\tilde{\sigma}^{(k)}_{12}(z)$ are the in-plane stress components predicted by classical lamination theory. For a general symmetric or unsymmetric laminate subject to a uniform extension or bending load, classical lamination theory predicts stresses that vary at most linearly through the thickness of each ply. Therefore, we have

$$g^{(k)}_{12}(z) = B^{(k)}_1 z + B^{(k)}_2 \tag{3.41}$$

$$g^{(k)}_{22}(z) = B^{(k)}_3 z + B^{(k)}_4 \tag{3.42}$$

where

$$B^{(k)}_1 = \frac{\tilde{\sigma}^{(k)}_{12_t} - \tilde{\sigma}^{(k)}_{12_b}}{t^{(k)}} \tag{3.43a}$$

$$B^{(k)}_2 = \tilde{\sigma}^{(k)}_{12_b} \tag{3.43b}$$

$$B^{(k)}_3 = \frac{\tilde{\sigma}^{(k)}_{22_t} - \tilde{\sigma}^{(k)}_{22_b}}{t^{(k)}} \tag{3.43c}$$

$$B^{(k)}_4 = \tilde{\sigma}^{(k)}_{22_b} \tag{3.43d}$$

and the t and b subscripts denote the top and bottom of the kth ply, respectively, and $t^{(k)}$ is the thickness of the k^{th} ply. These expressions are then substituted into the equilibrium equations (3.37) and (3.38) and integrated with respect to z to obtain expressions for the through-thickness variations of the interlaminar shear components $\hat{\sigma}^{(k)}_{13_{(E)}}(y,z)$ and $\hat{\sigma}^{(k)}_{23_{(E)}}(y,z)$. After imposing the stress free conditions at the top and bottom surfaces of the laminate, the interlaminar shears may be written as

$$\hat{\sigma}^{(k)}_{13_{(E)}}(y,z) = f^{(k)}_{13}(y)[B^{(k)}_1 z^2/2 + B^{(k)}_2 z + B^{(k)}_5] \tag{3.44}$$

$$\hat{\sigma}^{(k)}_{23_{(E)}}(y,z) = f^{(k)}_{23}(y)[B^{(k)}_3 z^2/2 + B^{(k)}_4 z + B^{(k)}_6] \tag{3.45}$$

In a similar manner, the interlaminar normal stress $\sigma^{(k)}_{33}$ is obtained from equations (3.38) and (3.45)

$$\hat{\sigma}^{(k)}_{33_{(E)}}(y,z) = f^{(k)}_{33}(y)[B^{(k)}_3 z^3/6 + B^{(k)}_4 z^2/2 + B^{(k)}_6 z + B^{(k)}_7] \tag{3.46}$$

Constants $B^{(k)}_5$, $B^{(k)}_6$, and ,$B^{(k)}_7$ are determined from the interfacial traction continuity conditions. Starting at the bottom free surface and working up, they have the form

$$B^{(k)}_5 = \sum_{j=k+1}^{N} \left[B^{(j)}_1 (t^{(j)})^2/2 + B^{(j)}_2 t^{(j)} \right] \qquad k = 1,N-1 \tag{3.47}$$

$$B^{(k)}_6 = \sum_{j=k+1}^{N} \left[B^{(j)}_3 (t^{(j)})^2/2 + B^{(j)}_4 t^{(j)} \right] \qquad k = 1,N-1 \tag{3.48}$$

$$B^{(k)}_7 = \sum_{j=k+1}^{N} \left[B^{(j)}_3 (t^{(j)})^3/6 + B^{(j)}_4 (t^{(j)})^2/2 + \left(B^{(j)}_3 (t^{(j)})^{(2)}/2 + B^{(j)}_4 t^{(j)} \right) \sum_{m=k+1}^{j-1} t^{(m)} \right] \qquad k = 1,N-1 \tag{3.49}$$

and $B^{(N)}_5$, $B^{(N)}_6$ and $B^{(N)}_7$ are all equal to zero.

The stress field $\hat{\sigma}^{(k)}_{ij_{(E)}}(y,z)$ is now expressed in terms of the 2N unknown functions $f^{(k)}_{12}(y)$ and $f^{(k)}_{22}(y)$, where N is the number of layers in the laminate. If $f^{(k)}_{12}(y)$ and $f^{(k)}_{22}(y)$ are expressed in terms of quantities at the interfaces, so that interfacial continuity of tractions is guaranteed, a general solution for these functions may be obtained by invoking the principle of minimum complementary energy. According to this principle, out of all possible stress fields $\sigma^{(k)}_{ij}(y,z)$, that satisfy both equilibrium and the stress boundary conditions, the one that represents the actual equilibrium state, is the one that minimizes the laminate complementary energy.[71] The complementary energy is defined as the strain energy of the laminate minus the external work done on the portion of the laminate where the displacements are prescribed

$$\Pi_c = \sum_{k=1}^{N} \Pi^{(k)}_c = \sum_{k=1}^{N} \iiint_{V_{(k)}} [\,\{\sigma\}^T [\bar{S}] \{\sigma\}\,]^{(k)} dV_k - \iint_{S_u} \{T\}^T \{\bar{u}\} dA \tag{3.50}$$

Using the assumed forms for the stresses in equation (3.50) an expression for the complementary energy in terms of the arbitrary functions $f_{ij}^{(k)}(y)$ is obtained. Since we have assumed stresses to be independent of the axial coordinate X_1, and have assumed explicit functions for the through-thickness variations of the stresses, the z and x integrations can be carried out, reducing the volume integral in equation (3.50) to a line integral in y. Taking the first variation of the simplified integral and equating it to zero yields a system of 2N, constant coefficient, ordinary differential equations for the functions $f_{12}^{(k)}(y)$ and $f_{22}^{(k)}(y)$. These equations and the homogeneous boundary conditions along the free edge define an eigenvalue problem whose solutions are exponential functions of y. The complete solution for any of the functions $f_{12}^{(k)}$ and $f_{22}^{(k)}$ is then obtained as a combination of a particular solution and a linear combination of the eigenfunctions for the homogeneous solution.

A general eigenfunction expansion solution of this type is favorable for a few reasons. First, since separate functions are assumed for each ply, the stresses in individual plies can decay at different rates. Second, as Pagano [51] has shown, the accuracy of the stress field predictions will improve significantly when the number of sublayers used to model a layer increases, just as results improve with finite element models when the mesh is refined. For the same through-thickness discretization, a model of this type will provide more accurate results than finite element models, since continuous functions are used to describe the y variation in the stress field rather than discretized functions as are used in the finite element models. These advantages, however, come at the high cost of solution inefficiency, which is precisely what we are trying to avoid. Run times are a function of the number of layers in the laminate and can become prohibitive for laminates with a large number of plies. Also, as noted earlier, numerical constraints have been shown to limit the number of plies in a laminate that can analyzed by this approach.[51]

Considering the efficiency problems associated with the generalized eigenfunction expansion technique outlined above, KL took a slightly different approach and made some assumptions at the outset on the form of the functions $f_{12}^{(k)}(y)$ and $f_{22}^{(k)}(y)$. These assumptions simplified the energy expression and subsequently reduced the system of equations that had to be solved. First, based upon the fact that the integrals of the in-plane stresses $\sigma_{12}^{(k)}$ and $\sigma_{22}^{(k)}$ through the laminate thickness are zero at any y location, they assumed that $f_{12}^{(k)}(y)$ and $f_{22}^{(k)}(y)$ be the same in all layers

$$\hat{\sigma}_{i2}^{(k)}(y,z) = a(z)^k f_{i2}(y),\ i=1,2 \tag{3.51}$$

By taking in-plane stresses of this form, the analysis greatly simplifies since the number of unknown functions is reduced from 2N to two. The limitation imposed by this technique, however, is that the stresses in all plies are forced to decay at the same rate. KL also went one step further, and assumed explicit sums of exponentials, expressed in terms of unknown decay parameters, for the in-plane variations $f_{12}^{(k)}(y)$ and $f_{22}^{(k)}(y)$. The interlaminar functions were derived from the in-plane functions and the differential equations of equilibrium. Minimization of the laminate complementary energy then resulted in a system of two non-linear algebraic equations for determining the unknown parameters.

KL used exponential functions to describe the in-plane variation in the stresses because they provide for the necessarily rapid decay of the boundary layer stress components with distance from the free edge. Explicit sums of exponential functions are used in this study as well because the KL predictions generally show good trends, and as mentioned above, the Euler Lagrange equations obtained from the more general approach are solved by a series of exponential terms.

KL determined the necessary forms of the in-plane functions by enforcing the requirements of the Force-Balance Method.[19] The Force-Balance method will also be used in deducing the

required forms of the in-plane variations associated with local mismatch effects. The Force-Balance Method is basically a statement of overall force and moment equilibrium, applied to a section of the laminate large enough to satisfy the assumptions of material homogeneity. If a rectangular volume element is taken with its X_2 faces at the laminate center plane and stress free edge, and with the X_{3^+} face corresponding to the top free surface, as shown in Figure 3.1, six equations are derived from the force and moment equilibrium conditions.[20]

Force Equilibrium:

$$\sum F_{X_1}: \quad \int_{3^-} \sigma_{13} dy + \int_{2^-} \sigma_{12} dz = 0 \tag{3.52a}$$

$$\sum F_{X_2}: \quad \int_{2^-} \sigma_{22} dz + \int_{3^-} \sigma_{23} dy = 0 \tag{3.52b}$$

$$\sum F_{X_3}: \quad \int_{3^-} \sigma_{33} dy = 0 \tag{3.52c}$$

Moment Equilibrium:

$$\sum M_{X_1}: \quad \int_{2^-} \sigma_{22} z dz + \int_{Z^-} \sigma_{33} y dy = 0 \tag{3.52d}$$

$$\sum M_{X_2}: \quad \int_{1^+} \sigma_{13} dy dz + \int_{Z^-} \sigma_{12} z dz = 0 \tag{3.52e}$$

$$\sum M_{X_3}: \quad \int_{1^+} \sigma_{12} dy dz + \int_{Z^-} \sigma_{13} (b-y) dy = 0 \tag{3.52f}$$

The subscript on the integral indicates the face over which the integrations are taken.

Equation (3.52c) implies that $\sigma_{33}^{(k)}(y,z)$ is a couple. Therefore, $\sigma_{33}^{(k)}(y,z)$ must cross the y axis at least once, and at least two exponential terms are required to represent this component of stress. KL assumed that one crossing of the y axis represents the lowest energy solution so they used a sum of two exponential functions to represent the transverse variations $f_{22}^{(k)}(y)$, $f_{33}^{(k)}(y)$, and $f_{23}^{(k)}(y)$. Similar considerations were used to determine $f_{12}^{(k)}(y)$ and $f_{22}^{(k)}(y)$.

Considering the above requirements on the form of $f_{ij}(y)$ and the free edge boundary conditions, KL obtained the following final expressions for the stresses in the kth ply:

$$\hat{\sigma}^{(k)}_{22_{(E)}} = \left[-\frac{\lambda_1}{\lambda_1 - 1}\left(e^{-\phi_2 y} - \frac{1}{\lambda_1} e^{-\lambda_1 \phi_2 y} \right) \right] \left[B_3^{(k)} z + B_4^{(k)} \right] \tag{3.53a}$$

$$\hat{\sigma}^{(k)}_{33_{(E)}} = \phi_2^2 \frac{\lambda_1}{\lambda_1 - 1} \left[\lambda_1 e^{-\lambda_1 \phi_2 y} - e^{-\phi_2 y} \right] \left[B_3^{(k)} z^3/6 + B_4^{(k)} z^2/2 + B_6^{(k)} z + B_7^{(k)} \right] \tag{3.53b}$$

$$\hat{\sigma}^{(k)}_{23_{(E)}} = \phi_2 \frac{\lambda_1}{\lambda_1 - 1} \left[e^{-\phi_2 y} - e^{-\lambda_1 \phi_2 y} \right] \left[B_3^{(k)} z^2/2 + B_4^{(k)} z + B_5^{(k)} \right] \tag{3.53c}$$

$$\hat{\sigma}^{(k)}_{12_{(E)}} = -e^{-\phi_1 y} \left[B_1^{(k)} z + B_2^{(k)} \right] \tag{3.53d}$$

$$\hat{\sigma}^{(k)}_{13_{(E)}} = \phi_1 e^{-\phi_1 y} \left[B_1^{(k)} z^2/2 + B_2^{(k)} z + B_5^{(k)} \right] \tag{3.53e}$$

where ϕ_1, ϕ_2, and λ_1 are unknown decay constants determined by minimizing the complementary energy. KL assumed $\phi_1 = \phi_2$ so only two unknown parameters ϕ_1 and λ_1 are used in their solution.

These stress distributions superposed on the classical lamination theory solution satisfy pointwise and global equilibrium, stress free boundary conditions, and interfacial traction continuity conditions. Also equations (3.53) show that for large y all of the $\hat{\sigma}_{ij}$s are zero, so outside the boundary layer region the classical lamination theory solution is recovered. Further, these equations show that the interlaminar stresses predicted by the KL solution at an interface are proportional to $B_5^{(k)}$, $B_6^{(k)}$, and $B_7^{(k)}$. The B's contain stacking sequence information and are basically force ($B_5^{(k)}$, $B_6^{(k)}$) and moment ($B_7^{(k)}$) resultants of the classical lamination theory stresses obtained by carrying out the through-thickness integrations in equations (3.52). Therefore, if the resultant force at an interface, or at any through-thickness location, z, is zero, the KL solution predicts identically zero interlaminar stresses at all points along the interfacial plane having this z-location. This form of assumption, however, is too restrictive. The overall equilibrium equations (3.52) only require that the integral of the interlaminar stresses be zero at any z-location where the through-thickness integration is zero, and not that the stresses

themselves be identically zero at all points along the interfacial plane. In fact, as previously mentioned, results from earlier investigations indicate large interlaminar stresses in interfacial regions where local mismatch of properties is present but interlaminar stresses are not required to satisfy global equilibrium. The next sections outline extension of the KL solution to include additional terms associated with this local property mismatch in the assumed stress field.

3.3.4 Local Material Property Mismatch

Stress assumptions to include local mismatch considerations are developed by defining the interlaminar shear stresses and the interlaminar normal stress at each interface and deriving the remaining stress components from these definitions using the differential equations of equilibrium. This approach has the advantage that the traction continuity conditions are satisfied by the form of the assumptions. The most general form of a definition of this type would have different functions at each interface, as mentioned in the previous section, allowing the stresses in individual plies to decay at different rates. This is a considerable relaxation of the constraint imposed by the KL solution that stresses in all plies decay at the same rate and should lead to increased accuracy in the stress predictions. The drawback of course, is a large reduction in solution efficiency since the number of unknowns is dependent on the number of plies in the laminate. The present formulation is a compromise between the general formulation and that of KL. The same functions are used at all interfaces to define the local mismatch contribution to the stress field. As in the KL solution, using the same function for all interfaces requires the decay of the local mismatch contributions to the stress field to be the same in all plies. However, the decay of the total stress, i.e., equilibrium contribution plus mismatch contribution, may differ in individual plies, if there is a local mismatch contribution in one ply but not in another.

The interlaminar shear stresses arising at an interface are assumed to be proportional to the

mismatch in coefficient of mutual influence or mismatch in Poisson's ratio between the ply above and below the interface of interest. The interlaminar normal stress is assumed to be proportional to the mismatch in Poisson's ratio. The mismatch in coefficient of mutual influence is assumed to affect only the $\sigma_{12}^{(k)}$ and $\sigma_{13}^{(k)}$ components of stress while the Poisson's ratio mismatch is assumed to affect only the $\sigma_{22}^{(k)}$, $\sigma_{23}^{(k)}$, and $\sigma_{33}^{(k)}$ components of stress. This assumption is exact for cross-ply laminates, where only $\sigma_{22}^{(k)}$, $\sigma_{23}^{(k)}$, and $\sigma_{33}^{(k)}$ are present, but is approximate for more general laminates. In angle-ply laminates, for example, the classical lamination theory stresses $\tilde{\sigma}_{22}^{(k)}$ are all zero and there is no Poisson's ratio mismatch between adjacent plies, but interlaminar stress components $\sigma_{23}^{(k)}$ and $\sigma_{33}^{(k)}$, and transverse in-plane stress $\sigma_{22}^{(k)}$ have been shown to develop.[9,26,35,59] These stresses, therefore must result from the coupling between the $\sigma_{12}^{(k)}$, and $\sigma_{13}^{(k)}$ components of stress and the $\sigma_{22}^{(k)}$, $\sigma_{23}^{(k)}$, and $\sigma_{33}^{(k)}$ stress components. This coupling is apparent from the compatibility equations (3.23). For cross-ply laminates, the compatibility equations uncouple and $\sigma_{12}^{(k)}$ and $\sigma_{13}^{(k)}$ are identically zero. The previous predictions, however, have shown $\sigma_{22}^{(k)}$, $\sigma_{23}^{(k)}$, and $\sigma_{33}^{(k)}$ to be an order of magnitude smaller than $\sigma_{13}^{(k)}$ and $\sigma_{12}^{(k)}$ in angle-ply laminates so neglecting this coupling is a felt to be a reasonable assumption.

The in-plane functions, $h_{ij}^{(k)}(y)$, $m_{ij}^{(k)}(y)$, are, as in the KL solution, assumed to be an explicit combination of exponential functions which are chosen such that the interlaminar stress components arising from local mismatch integrate to zero over y. For the $m_{ij}^{(k)}(y)$ functions, the additional restriction that $m_{33}^{(k)}$ (y) has a zero moment about the longitudinal axis is imposed. Thus, the mismatch effect permits non-zero stress contributions, but these stress contributions do not alter the global force and moment equilibrium established through the $f_{ij}^{(k)}(y)$ and $g_{ij}^{(k)}(z)$ functions of the KL solution. The through thickness variations $l_{ij}^{(k)}(z)$, $n_{ij}^{(k)}(z)$, and $p_{ij}^{(k)}(z)$ are polynomial functions chosen so that the stresses resulting from mismatch decay with distance

from an interface. In order to keep the number of unknowns in the solution to a manageable number, the through-thickness decay lengths of the mismatch effects are established a priori and set equal to the thickness $t^{(k)}$ of the individual layers in the laminate. A more general formulation would allow the decay lengths to be variable and left as unknowns to be determined by minimizing the laminate complementary energy, but once again at the expense of increased computational cost. The effect of variable through-thickness decay lengths, obtained by dividing a layer into sublayers, is briefly addressed in Section 4.1.1.

Mismatch in Coefficient of Mutual Influence. The interlaminar shear stress $\sigma_{13}^{(k)}$ at an interface, associated with the mismatch in coefficient of mutual influence, is assumed to be proportional to the mismatch in $\eta_{12,1}$ of the two plies adjacent to that interface. The proportionality constant is a product of an unknown constant A_1, determined by minimizing the laminate complementary energy, and the applied axial strain ε_{11}. The same constant is used for all interfaces.

The mismatch in coefficient of mutual influence at the two interfaces bounding the k^{th} layer are defined

$$\delta\eta_{12,1}(k,1) = \eta_{12,1}(k-1) - \eta_{12,1}(k) \qquad (3.54)$$

$$\delta\eta_{12,1}(k,2) = \eta_{12,1}(k) - \eta_{12,1}(k+1)$$

with $\delta\eta_{12,1}(1,1) = \delta\eta_{12,1}(N,2) = 0$. The layers above and below the kth layer are designated k-1 and k+1, respectively, as indicated below.

k-1
k
k+1

The stresses in a generic layer are influenced by mismatch effects from the two adjoining

interfaces. Two quadratic functions are used to describe the through-thickness variation in shear stress within a layer. One function has the value of the mismatch at the top interface of the kth layer, and a value of zero at the bottom interface, while the other function has the value of the mismatch at the bottom interface of the kth layer, and a value of zero at the top interface. Therefore, the through-thickness function $l_{13}^{(k)}$ is assumed to have the form

$$l_{13}^{(k)}(z) = \left[\delta\eta_{12,1}(k,1)\varepsilon_t^{(k)} z^2/(t^{(k)})^2 + \delta\eta_{12,1}(k,2)\varepsilon_b^{(k)}(1-z/t^{(k)})^2 \right] A_1 \tag{3.55}$$

Equilibrium then requires that the function $l_{12}^{(k)}$ have the form

$$l_{12}^{(k)}(z) = \frac{dl_{13}^{(k)}}{dz}(z) = \left\{ \frac{2z}{[t^{(k)}]^2}\left[\delta\eta_{12,1}(k,1)\varepsilon_t^{(k)} + \delta\eta_{12,1}(k,2)\varepsilon_b^{(k)} \right] - \frac{2}{t^{(k)}}\delta\eta_{12,1}(k,2)\varepsilon_b^{(k)} \right\} A_1 \tag{3.56}$$

where $\varepsilon_t^{(k)}$ and $\varepsilon_b^{(k)}$ are the strains at the top and bottom of the kth layer, respectively, and $t^{(k)}$ is the thickness of the kth layer.

The associated in-plane variation $h_{13}(y)$ is chosen to be the same for all interfaces with the self-equilibrating shape shown in Figure 3.2. As previously mentioned, the same function is used for all interfaces to keep the number of unknowns to a minimum. To obtain the shape shown in Figure 3.2, a combination of two exponential functions is assumed

$$h_{13}(y) = D_1 e^{-\phi_3 y} + D_2 e^{-\lambda_2 \phi_3 y} \tag{3.57}$$

Integrating with respect to y and setting the result to zero, provides a relationship between D_1 and D_2.

$$\frac{D_1}{\phi_3} + \frac{D_2}{\lambda_2 \phi_3} = 0 \tag{3.58}$$

Setting $D_1 = -1$, $h_{13}^{(k)}(y)$ has the self-equilibrating form

$$h_{13}(y) = \lambda_2 e^{-\lambda_2 \phi_3 y} - e^{-\phi_3 y} \tag{3.59}$$

It follows from equilibrium that $h_{12}(y)$ must have the form

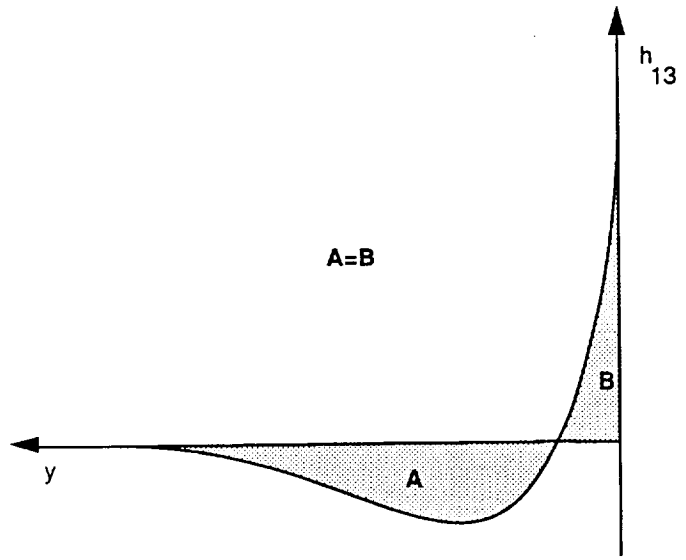

Figure 3.2. Required form for $h_{13}(y)$

$$h_{12}(y) = \int h_{13}(y)\, dy = \frac{1}{\phi_3}\left[-e^{-\lambda_2\phi_3 y} + e^{-\phi_3 y}\right] + D_6 \tag{3.60}$$

where the constant of integration, D_6, must be zero to satisfy the condition that the classical lamination theory solution is recovered in the interior.

Mismatch in Poisson's Ratio. Assumptions for stresses arising from a mismatch in Poisson's ratio are derived in a similar manner to those developed for the coefficient of mutual influence mismatch. The mismatch in Poisson's ratio at an interface results directly in an interlaminar shear stress, $\sigma_{23}^{(k)}$, and an interlaminar normal stress, $\sigma_{33}^{(k)}$. Thus, there are two contributions to the assumed stress state arising from mismatch in Poisson's ratio considerations. The first contribution is in the form of a direct assumption on the interlaminar shear stress at an interface, as was done with the coefficient of mutual influence mismatch. Interlaminar normal stress, $\sigma_{33}^{(k)}$ and transverse in-plane stress, $\sigma_{22}^{(k)}$, are then derived from the differential equations of equilibrium. The second contribution is in the form of an assumption on $\sigma_{33}^{(k)}$, with $\sigma_{23}^{(k)}$ and $\sigma_{22}^{(k)}$

derived from equilibrium considerations. For both contributions, the stress assumed at an interface, either $\sigma_{23}^{(k)}$ or $\sigma_{33}^{(k)}$, is assumed to be proportional to the mismatch in Poisson's ratio, ν_{12}, of the plies adjacent to that interface. As with the coefficient of mutual influence mismatch, the proportionality constants are unknown and are determined by minimizing the laminate complementary energy. The same constants are used for all interfaces.

The definition of the mismatch in Poisson's ratio is similar to the definition for the coefficient of mutual influence mismatch

$$\delta\nu_{12}(k,1) = \nu_{12}(k-1) - \nu_{12}(k) \tag{3.61a}$$

$$\delta\nu_{12}(k,2) = \nu_{12}(k) - \nu_{12}(k+1) \tag{3.61b}$$

with $\delta\nu_{12}(1,1) = \delta\nu_{12}(N,2) = 0$.

Expressions for the through-thickness variations in the stresses in the k^{th} ply are developed by considering a two ply, unsymmetric laminate. Figure 3.3 shows a section of the laminate with the shear stress $\hat{\sigma}_{23}(y,z)$ acting over a face parallel to the free edge and the interlaminar normal stress, $\hat{\sigma}_{33}(y,z)$, acting on the interfacial plane between layer (1) and layer (2). For layer equilibrium the integral

$$\int_0^{t(k)} \hat{\sigma}_{23}(y,z)dz \tag{3.62}$$

evaluated at $y = y_0$ must equal the integral

$$\int_0^{y_0} \hat{\sigma}_{33}(y,z)dy \tag{3.63}$$

over the interface between the two layers. For laminate equilibrium the integral of $\hat{\sigma}_{23}(y,z)$ through the laminate thickness must be zero. (The latter restriction was not imposed when developing the through thickness assumptions for $\hat{\sigma}_{13}(y,z)$ in the previous section because equal

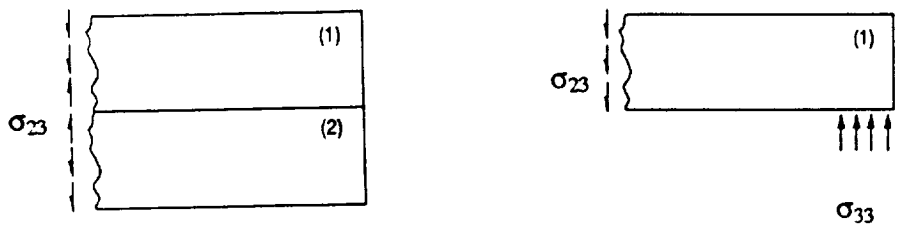

Figure 3.3. Laminate and Sublaminate Equilibrium

and opposite shear stresses act on the ends of the laminate). Possible through-thickness functions for the stress component $\hat{\sigma}_{23}(y,z)$ that satisfy these equilibrium requirements are shown in Figure 3.4.

We begin by formulating the through-thickness functions $n_{ij}^{(k)}(z)$ associated with the assumption on the interlaminar shear stress at an interface. In general there will be a non-zero strain ε_{11} at the (1)-(2) interface, and consequently a non-zero shear stress $\hat{\sigma}_{23}$ there, since we are assuming $\hat{\sigma}_{23}(y,z)$ to be proportional to the axial strain and mismatch in Poisson's ratio at the interface. In order to have a non-zero shear stress at the interface and still satisfy the requirement of overall laminate equilibrium, the through thickness variation of $\hat{\sigma}_{23}(y,z)$ must have the form shown in Case A of Figure 3.4. That is, $n_{23}^{(k)}(z)$ must integrate to zero over each layer thickness. If $\hat{\sigma}_{23}(y,z)$ integrates to zero through the thickness of a layer at any location y, then $\hat{\sigma}_{33}(y,z)$ will be zero at all points y along all interfaces.

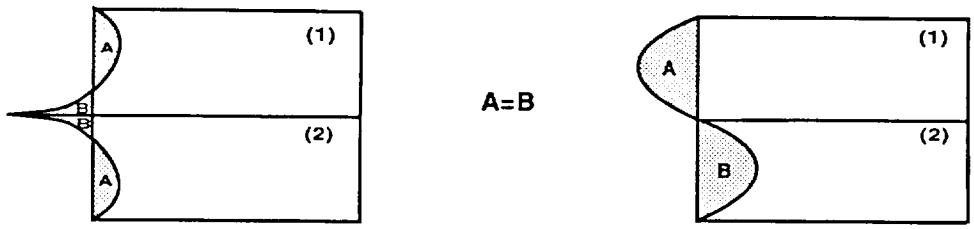

Figure 3.4. Through-thickness distributions of $\hat{\sigma}_{23}(y,z)$

Two quadratic functions are employed to describe the through-thickness variation in shear stress within a layer as was used for the variation in the shear stress $\hat{\sigma}_{13}^{(k)}(y,z)$ in the previous section. An expression for the function associated with the mismatch at the bottom of a ply can be obtained by considering the first ply in Figure 3.4. We assume

$$n_{23}^{(k,2)}(z) = Az^2 + Bz + C \tag{3.64}$$

Imposing the condition that $n_{23}^{(k,2)}$ is proportional to the mismatch $\delta v_{12}(k,2)$ at the bottom interface of the k^{th} layer, and has a value of zero at the top interface gives

$$\hat{\sigma}_{23}(y,z^{(1)}=0) = \delta v_{12}(1,2)\varepsilon_b^{(1)} \tag{3.65a}$$

$$\hat{\sigma}_{23}(y,z^{(1)} = t^{(1)}) = 0 \tag{3.65b}$$

and imposing the requirement that $\hat{\sigma}_{33}^{(k)}$ is zero at all interfaces as outlined above

$$\hat{\sigma}_{33}(y, z^{(1)} = t^{(1)}) = 0 \tag{3.65c}$$

$$\hat{\sigma}_{33}(y, z^{(1)} = 0) = 0 \tag{3.65d}$$

yields

$$n_{23}^{(k,2)} = \delta\nu_{12}(k,2)\varepsilon_b^{(k)}\left[3z^2/(t^{(k)})^2 - 4z/t^{(k)} + 1\right] A_2 \tag{3.66}$$

Similarly, considering ply 2 provides an expression for the function associated with the mismatch at the top of the k^{th} ply

$$n_{23}^{(k,1)} = \delta\nu_{12}(k,1)\varepsilon_t^{(k)}\left[3z^2/(t^{(k)})^2 - 2z/t^{(k)}\right] A_2 \tag{3.67}$$

The through-thickness variation $n_{23}^{(k)}(z)$ in each layer is then the sum of equations (3.66) and (3.67).

$$n_{23}^{(k)}(z) = \left[\delta\nu_{12}(k,1)\varepsilon_t^{(k)}\left[3z^2/(t^{(k)})^2 - 2z/t^{(k)}\right] + \delta\nu_{12}(k,2)\varepsilon_b^{(k)}\left[3z^2(t^{(k)})^2 - 4z/t^{(k)} + 1\right]\right] A_2 \tag{3.68}$$

where A_2 is an unknown constant to be determined by minimizing the laminate complementary energy. Equilibrium then requires that the functions $n_{22}^{(k)}(z)$ and $n_{33}^{(k)}(z)$ have the form

$$n_{22}^{(k)}(z) = \left[\delta\nu_{12}(k,1)\varepsilon_t^{(k)}\left[6z/(t^{(k)})^2 - 2/t^{(k)}\right] + \delta\nu_{12}(k,2)\varepsilon_b^{(k)}\left[6z/(t^{(k)})^2 - 4/t^{(k)}\right]\right] A_2 \tag{3.69}$$

$$n_{33}^{(k)}(z) = \left[\delta\nu_{12}(k,1)\varepsilon_t^{(k)}\left[z^3/(t^{(k)})^2 - z^2/t^{(k)}\right] + \delta\nu_{12}(k,2)\varepsilon_b^{(k)}\left[z^3/(t^{(k)})^2 - 2z^2/t^{(k)} + z\right]\right] A_2 \tag{3.70}$$

The corresponding in-plane function $m_{23}(y)$ is chosen to be self-equilibrating with the shape shown in Figure 3.5 To obtain a shape of this form, a combination of three exponential functions is required

$$m_{23}(y) = D_1 e^{-\phi_4 y} + D_2 e^{-\phi_4\lambda_3 y} + D_3 e^{-\phi_4\lambda_4 y} \tag{3.71}$$

It follows from equilibrium that

$$m_{22}(y) = \int m_{23}(y)dy = -\frac{D_1}{\phi_4}e^{-\phi_4 y} - \frac{D_2}{\phi_4\lambda_3}e^{-\phi_4\lambda_3 y} - \frac{D_3}{\phi_4\lambda_4}e^{-\phi_4\lambda_4 y} + D_4 \tag{3.72}$$

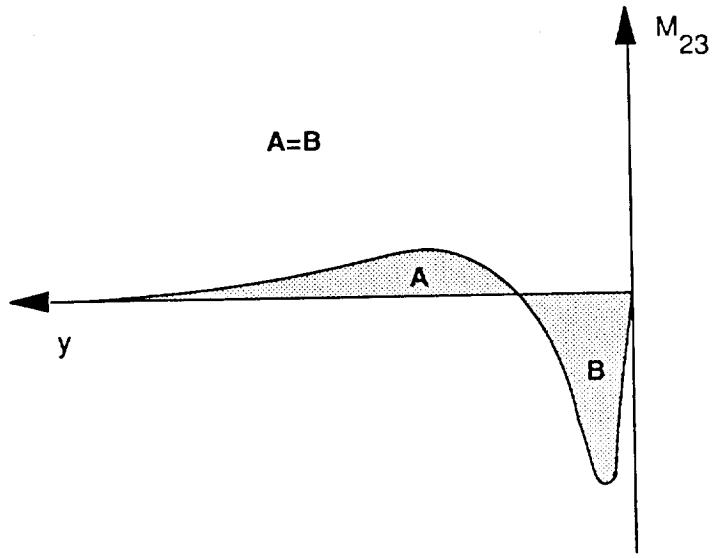

Figure 3.5. Required form for $m_{23}(y)$

$$m_{33}(y) = \frac{dm_{23}(y)}{dy} = -\phi_4 D_1 e^{-\phi_4 y} - \phi_4 \lambda_3 D_2 e^{-\phi_4 \lambda_3 y} - \phi_4 \lambda_4 D_3 e^{-\phi_4 \lambda_4 y} \tag{3.73}$$

where the integration constant D_4 must be zero so that $m_{22}(y)$ is zero for large y. We can now set D_1 to one, without loss of generality, and solve for D_2 and D_3 by imposing the free edge conditions. The free edge condition on $m_{23}(y)$ gives

$$m_{23}(y=0) = 1 + D_2 + D_3 = 0 \tag{3.74}$$

and the free edge condition on m_{22} gives

$$m_{22}(y=0) = -1/\phi_4 - \frac{D_2}{\phi_4 \lambda_3} - \frac{D_3}{\phi_4 \lambda_4} \tag{3.75}$$

D_2 and D_3 are then found to be

$$D_2 = \frac{\lambda_3(1-\lambda_4)}{(\lambda_4 - \lambda_3)} \qquad D_3 = \frac{\lambda_4(\lambda_3 - 1)}{(\lambda_4 - \lambda_3)} \tag{3.76}$$

The through-width functions associated with the Poisson's ratio mismatch and the direct

assumption on the interlaminar shear stress then have the form

$$m_{22} = \frac{-1}{\phi_4}\left[e^{-\phi_4 y} + \frac{(1-\lambda_4)}{(\lambda_4-\lambda_3)}e^{-\phi_4\lambda_3 y} + \frac{(\lambda_3-1)}{(\lambda_4-\lambda_3)}e^{-\phi_4\lambda_4 y}\right] \tag{3.77}$$

$$m_{23} = \left[e^{-\phi_4 y} + \frac{\lambda_3(1-\lambda_4)}{(\lambda_4-\lambda_3)}e^{-\phi_4\lambda_3 y} + \frac{\lambda_4(\lambda_3-1)}{(\lambda_4-\lambda_3)}e^{-\phi_4\lambda_4 y}\right] \tag{3.78}$$

$$m_{33} = -\phi_4\left[e^{-\phi_4 y} + \frac{\lambda_3^2(1-\lambda_4)}{(\lambda_4-\lambda_3)}e^{-\phi_4\lambda_3 y} + \frac{\lambda_4^2(\lambda_3-1)}{(\lambda_4-\lambda_3)}e^{-\phi_4\lambda_4 y}\right] \tag{3.79}$$

Note these forms satisfy the self-equilibrating requirements outlined in the introduction to this section, provided classical lamination theory stresses are recovered in the interior region, i.e. provided the laminate is wide enough for the exponential terms to be zero in regions removed from the edge. Under these conditions, the self equilibrating requirements are identically met as a result of satisfying the boundary conditions.

$$\int_{y=0}^{y=b} m_{23}(y)dy = m_{22}(b) - m_{22}(0) = 0 \tag{3.80}$$

$$\int_{y=0}^{y=b} m_{33}(y)dy = m_{23}(b) - m_{23}(0) = 0 \tag{3.81}$$

$$\int_{y=0}^{y=b} m_{33}(y)dy = m_{22}(b) - m_{22}(0) = 0 \tag{3.82}$$

To develop expressions for the direct assumption on interlaminar normal stress we again consider a two layer unsymmetric laminate. We assume $\hat{\sigma}_{33}(y,z)$ varies cubically through a layer thickness so the interlaminar shear stress $\hat{\sigma}_{23}(y,z)$ will again vary quadratically. Recall that for laminate equilibrium and layer equilibrium to be satisfied, $\hat{\sigma}_{23}(y,z)$ must be distributed through the laminate thickness with a form like that shown in either Figure 3.4a or 3.4b. Since it is desired to have a non-zero interlaminar normal stress at the interfaces and since we have

already explicitly assumed $\hat{\sigma}_{23}(y,z)$ at the interfaces, $\hat{\sigma}_{23}(y,z)$ associated with the normal stress assumption will have the form shown in Figure 3.4b. Using this requirement, and proceeding as was done for the $n_{23}^{(k)}$ function, the following through thickness variation $p_{33}^{(k)}$ for the interlaminar normal stress in the k^{th} layer is obtained

$$p_{33}^{(k)}(z) = \left[\delta v_{12_n}(k,1)\varepsilon_t^{(k)}\left[-2z^3/(t^{(k)})^3 + 3z^2/(t^{(k)})^2 \right] + \delta v_{12_n}(k,2)\varepsilon_b^{(k)}\left[2z^3/(t^{(k)})^3 - 3z^2/(t^{(k)})^2 + 1 \right] \right] A_3 \quad (3.83)$$

Equilibrium then requires the functions $p_{23}^{(k)}(z)$ and $p_{22}^{(k)}(z)$ have the form

$$p_{23}^{(k)}(z) = \left[\delta v_{12_n}(k,1)\varepsilon_t^{(k)}\left[-6z^2/(t^{(k)})^3 + 6z/(t^{(k)})^2 \right] + \delta v_{12_n}(k,2)\varepsilon_b^{(k)}\left[6z^2/(t^{(k)})^3 - 6z/(t^{(k)})^2 + 1 \right] \right] A_3 \quad (3.84)$$

$$p_{22}^{(k)}(z) = \left[\delta v_{12_n}(k,1)\varepsilon_t^{(k)}\left[-12z/(t^{(k)})^3 + 6/(t^{(k)})^2 \right] + \delta v_{12_n}(k,2)\varepsilon_b^{(k)}\left[12z/(t^{(k)})^3 - 6/(t^{(k)})^2 \right] \right] A_3 \quad (3.85)$$

The δv_{12_n} in equations (3.83-3.85) are the equal to the δv_{12} in equations (3.68-3.70) for layers above the midplane and equal to their negative for layers below the midplane, since the interlaminar normal stresses are symmetric with respect to the midplane for the case of uniform axial extension of a symmetric laminate, and are antisymmetric for the case of uniform bending. The through-width assumptions associated with equations (3.83-3.85) are of the same form as equations (3.77-3.79) but divided by ϕ to give dimensionally consistent stress expressions.

3.3.5 Total Stress Assumptions

The final form of the stress assumptions in each layer of the laminate can now be obtained by combining the classical lamination theory solution and the stress field refinements obtained from global and local material mismatch considerations in accordance with equation (3.34). The final forms of the stress assumptions including all contributions are then

$$\sigma_{12}^{(k)} = \left[1 - e^{-\phi_1 y}\right]\left[B_1^{(k)} z + B_2^{(k)}\right] \tag{3.86}$$

$$- \frac{A_1}{\phi_3}\left[e^{-\lambda_2\phi_3 y} - e^{-\phi_3 y}\right]\left[\frac{2z}{[t^{(k)}]^2}\left[\delta\eta_{12,1}(k,1)\varepsilon_t^{(k)} + \delta\eta_{12,1}(k,2)\varepsilon_b^{(k)}\right] - \frac{2}{t^{(k)}}\delta\eta_{12,1}(k,2)\varepsilon_b^{(k)}\right]$$

$$\sigma_{13}^{(k)} = \phi_1\, e^{-\phi_1 y}\left[B_1^{(k)} z^2/2 + B_2^{(k)} z + B_5^{(k)}\right] \tag{3.87}$$

$$+ A_1\left[\lambda_2 e^{-\lambda_2\phi_3 y} - e^{-\phi_3 y}\right]\left[\delta\eta_{12,1}(k,1)\varepsilon_t^{(k)} z^2/(t^{(k)})^2 + \delta\eta_{12,1}(k,2)\varepsilon_b^{(k)}(1 - z/(t^{(k)})^2)\right]$$

$$\sigma_{22}^{(k)} = \left[1 - \frac{\lambda_1}{\lambda_1 - 1}\left[e^{-\phi_2 y} - \frac{1}{\lambda_1}e^{-\lambda_1\phi_2 y}\right]\right]\left[B_3^{(k)} z + B_4^{(k)}\right] \tag{3.88}$$

$$- \frac{A_2}{\phi_4}\left[e^{-\phi_4 y} + \frac{(1-\lambda_4)}{(\lambda_4 - \lambda_3)}e^{-\phi_4\lambda_3 y} + \frac{(\lambda_3 - 1)}{(\lambda_4 - \lambda_3)}e^{-\phi_4\lambda_4 y}\right]\left[\delta v_{12}(k,1)\varepsilon_t^{(k)}\left[6z/(t^{(k)})^2 - 2/t^{(k)}\right]\right.$$

$$\left. + \delta v_{12}(k,2)\varepsilon_b^{(k)}\left[6z/(t^{(k)})^2 - 4/t^{(k)}\right]\right]$$

$$- \frac{A_3}{\phi_5^2}\left[e^{-\phi_5 y} + \frac{(1-\lambda_6)}{(\lambda_6 - \lambda_5)}e^{-\phi_5\lambda_5 y} + \frac{(\lambda_5 - 1)}{(\lambda_6 - \lambda_5)}e^{-\phi_5\lambda_6 y}\right]\left[\delta v_{12_a}(k,1)\varepsilon_t^{(k)}\left[-12z/(t^{(k)})^3 + 6/(t^{(k)})^2\right]\right.$$

$$\left. + \delta v_{12_a}(k,2)\varepsilon_b^{(k)}\left[12z/(t^{(k)})^3 - 6/(t^{(k)})^2\right]\right]$$

$$\sigma_{23}^{(k)} = \phi_2\frac{\lambda_1}{\lambda_1 - 1}\left[e^{-\phi_2 y} - e^{-\lambda_1\phi_2 y}\right]\left[B_3^{(k)} z^2/2 + B_4^{(k)} z + B_6^{(k)}\right] \tag{3.89}$$

$$+ A_2\left[e^{-\phi_4 y} + \lambda_3\frac{(1-\lambda_4)}{(\lambda_4 - \lambda_3)}e^{-\phi_4\lambda_3 y} + \lambda_4\frac{(\lambda_3 - 1)}{(\lambda_4 - \lambda_3)}e^{-\phi_4\lambda_4 y}\right]\left[\delta v_{12}(k,1)\varepsilon_t^{(k)}\left[3z^2/(t^{(k)})^2 - 2z/t^{(k)}\right]\right.$$

$$\left. + \delta v_{12}(k,2)\varepsilon_b^{(k)}\left[3z^2/(t^{(k)})^2 - 4z/t^{(k)} + 1\right]\right]$$

$$- \frac{A_3}{\phi_5}\left[e^{-\phi_5 y} + \lambda_5\frac{(1-\lambda_6)}{(\lambda_6 - \lambda_5)}e^{-\phi_5\lambda_5 y} + \lambda_6\frac{(\lambda_5 - 1)}{(\lambda_6 - \lambda_5)}e^{-\phi_5\lambda_6 y}\right]\left[\delta v_{12_a}(k,1)\varepsilon_t^{(k)}\left[-6z^2/(t^{(k)})^3 + 6z/(t^{(k)})^2\right]\right.$$

$$\left. + \delta v_{12_a}(k,2)\varepsilon_b^{(k)}\left[6z^2/(t^{(k)})^3 - 6z/(t^{(k)})^2\right]\right]$$

$$\sigma_{33}^{(k)} = \phi_2^2\frac{\lambda_1}{\lambda_1 - 1}\left[\lambda_1 e^{-\lambda_1\phi_2 y} - e^{-\phi_2 y}\right]\left[B_3^{(k)} z^3/6 + B_4^{(k)} z^2/2 + B_6^{(k)} z + B_7^{(k)}\right] \tag{3.90}$$

$$- A_2\phi_4\left[e^{-\phi_4 y} + \lambda_3^2\frac{(1-\lambda_4)}{(\lambda_4-\lambda_3)}e^{-\phi_4\lambda_3 y} + \lambda_4^2\frac{(\lambda_3-1)}{(\lambda_4-\lambda_3)}e^{-\phi_4\lambda_4 y}\right]\left[\delta\nu_{12}(k,1)\varepsilon_t^{(k)}\left[z^3/(t^{(k)})^2 - z^2/t^{(k)}\right]\right.$$

$$\left. + \delta\nu_{12}(k,2)\varepsilon_b^{(k)}\left[z^3/(t^{(k)})^2 - 2z^2/t^{(k)} + z\right]\right]$$

$$- A_3\left[e^{-\phi_5 y} + \lambda_5^2\frac{(1-\lambda_6)}{(\lambda_6-\lambda_5)}e^{-\phi_5\lambda_5 y} + \lambda_6^2\frac{(\lambda_5-1)}{(\lambda_6-\lambda_5)}e^{-\phi_5\lambda_6 y}\right]\left[\delta\nu_{12_n}(k,1)\varepsilon_t^{(k)}\left[-2z^3/(t^{(k)})^3 + 3z^2/t^{(k)^2}\right]\right.$$

$$\left. + \delta\nu_{12_n}(k,2)\varepsilon_b^{(k)}\left[2z^3/(t^{(k)})^3 - 3z^2/(t^{(k)})^2 + 1\right]\right]$$

The assumption that stresses are not dependent on the longitudinal coordinate X_1 caused $\sigma_{11}^{(k)}$ to drop out of the equilibrium equations. The strain compatibility equations and strain-stress equations are used to determine $\sigma_{11}^{(k)}$, as suggested in Reference [68]. It follows from equations (3.21a-c) that $\varepsilon_{11}^{(k)}$ is a linear function of y and z:

$$\varepsilon_{11}^{(k)} = A^{(k)}y + B^{(k)}z + C^{(k)} \tag{3.91}$$

Now $\varepsilon_{11}^{(k)}$ can be expressed in terms of the stress field using the constitutive equations (3.1):

$$\varepsilon_{11}^{(k)} = \bar{S}_{11}^{(k)}\sigma_{11}^{(k)} + \bar{S}_{12}^{(k)}\sigma_{22}^{(k)} + \bar{S}_{13}^{(k)}\sigma_{33}^{(k)} + \bar{S}_{16}^{(k)}\sigma_{12}^{(k)} = A^{(k)}y + B^{(k)}z + C^{(k)} \tag{3.92}$$

For large y, the left hand side of equation (3.92) is independent of y because the classical lamination theory solution is recovered away from the free edge. This implies $A^{(k)} = 0$. Solving for $\sigma_{11}^{(k)}$ then gives:

$$\sigma_{11}^{(k)} = K_1^{(k)}z + K_2^{(k)} - \frac{1}{\bar{S}_{11}^{(k)}}\left[\bar{S}_{12}^{(k)}\sigma_{22}^{(k)} + \bar{S}_{13}^{(k)}\sigma_{33}^{(k)} + \bar{S}_{16}^{(k)}\sigma_{12}^{(k)}\right] \tag{3.93}$$

The constants $K_1^{(k)}$ and $K_2^{(k)}$ are obtained by matching the solution at large y with the solution given by classical lamination theory.

$$\lim_{y\to\infty}\sigma_{11}^{(k)} = B_9^{(k)}z + B_{10}^{(k)} = K_1^{(k)}z + K_2^{(k)} - \frac{1}{\bar{S}_{11}^{(k)}}\left[S_{12}^{(k)}(B_3^{(k)}z + B_4^{(k)}) + \bar{S}_{16}^{(k)}(B_1^{(k)}z + B_2^{(k)})\right] \tag{3.94}$$

We therefore obtain

$$\sigma_{11}^{(k)} = \left[B_9^{(k)} + \frac{\bar{S}_{12}^{(k)}}{\bar{S}_{11}^{(k)}} B_3^{(k)} + \frac{\bar{S}_{16}^{(k)}}{\bar{S}_{11}^{(k)}} B_1^{(k)} \right] z + \left[B_{10}^{(k)} + \frac{\bar{S}_{12}^{(k)}}{\bar{S}_{11}^{(k)}} B_4^{(k)} + \frac{\bar{S}_{16}^{(k)}}{\bar{S}_{11}^{(k)}} B_2^{(k)} \right] - \frac{1}{\bar{S}_{11}^{(k)}} \left\{ \bar{S}_{12}^{(k)} \sigma_{22}^{(k)} + \bar{S}_{13}^{(k)} \sigma_{33}^{(k)} + \bar{S}_{16}^{(k)} \sigma_{12}^{(k)} \right\} \tag{3.95}$$

or more simply

$$\sigma_{11}^{(k)} = \frac{1}{\bar{S}_{11}^{(k)}} \left[\left\{ \bar{S}_{11}^{(k)} \tilde{\sigma}_{11}^{(k)} + \bar{S}_{12}^{(k)} \tilde{\sigma}_{22}^{(k)} + \bar{S}_{16}^{(k)} \tilde{\sigma}_{12}^{(k)} \right\} - \left\{ \bar{S}_{12}^{(k)} \sigma_{22}^{(k)} + \bar{S}_{13}^{(k)} \sigma_{33}^{(k)} + \bar{S}_{16}^{(k)} \sigma_{12}^{(k)} \right\} \right] \tag{3.96a}$$

where

$$\tilde{\sigma}_{11}^{(k)} = B_9^{(k)} z + B_{10}^{(k)} \tag{3.96b}$$

$$\tilde{\sigma}_{22}^{(k)} = B_3^{(k)} z + B_4^{(k)} \tag{3.96c}$$

$$\tilde{\sigma}_{12}^{(k)} = B_1^{(k)} z + B_2^{(k)} \tag{3.96d}$$

The stresses are now expressed in terms of the unknown decay parameters ϕ_i and λ_j and the proportionality constants A_k, through equations (3.86-3.90) and equation 3.96. The condition of minimum complementary energy is used to determine these constants.

3.3.6 Complementary Energy Minimization

The complementary energy can be expressed as a summation over the individual plies as

$$\Pi_c = \sum_{k=1}^{N} \Pi_c^{(k)} = \sum_{k=1}^{N} \iiint_{V_{(k)}} [\, \{\sigma\}^T [\bar{S}] \{\sigma\} \,]^{(k)} dV_k - \iint_{S_u} \{T\}^T \{\bar{u}\} dA \tag{3.97}$$

where V_k is the volume of the k^{th} ply, S_u is the portion of the boundary over which displacements are prescribed, $\{\bar{u}\}$ are the prescribed displacements, $\{T\}^T$ are the associated tractions on the displacement boundary S_u and $[\bar{S}]^{(k)}$ is the compliance matrix of the k^{th} layer with respect to the laminate coordinate system.

In order to evaluate the energy expression in equation (3.97) the prescribed displacement $\{\bar{u}\}$

must be determined. Since the displacement u_{11} in the laminate does not vary with y over the ends where the displacements are prescribed, u_{11} may be obtained by integrating the strain ε_{11} at the center of the laminate. That is

$$u_{11} = \int \varepsilon_{11} dX_1 = \int [\bar{S}_{11}\tilde{\sigma}_{11}^{(k)} + \bar{S}_{12}\tilde{\sigma}_{22}^{(k)} + \bar{S}_{16}\tilde{\sigma}_{12}^{(k)}] dX_1 \tag{3.98}$$

By symmetry, $u_{11} = 0$, at $X_1 = 0$, so at $X_1 = L$, the prescribed displacement $\bar{u}_{11}$ is given by

$$\bar{u}_{11} = (\bar{S}_{11}\tilde{\sigma}_{11}^{(k)} + \bar{S}_{12}\tilde{\sigma}_{22}^{(k)} + \bar{S}_{16}\tilde{\sigma}_{12}^{(k)})L \tag{3.99}$$

The volume integration with respect to X_1 will yield a factor of 2L multiplying that term, since the stresses and compliances are not dependent on the longitudinal coordinate X_1 and, therefore, it is only necessary to compute the complementary energy per unit length of the laminate. Additionally, for thin laminates[72] only half of the laminate, ($0<X_2<b$), needs to be considered. Further, since explicit piecewise continuous functions have been assumed for the through-thickness variations, the z integration is performed by summing the individual integrals in $z^{(k)}$. Making these simplifications and substituting for $[\bar{S}]$, $\{\bar{u}\}$, and $\sigma_{11}^{(k)}$ we obtain the following expanded expression for the complementary energy in the laminate

$$\Pi_c = \sum_{k=1}^{N} \iiint_{V_{(k)}} \left[R_{22}\frac{\sigma_{22}^{(k)^2}}{2} + R_{33}\frac{\sigma_{33}^{(k)^2}}{2} + R_{66}\frac{\sigma_{12}^{(k)^2}}{2} + R_{44}\frac{\sigma_{23}^{(k)^2}}{2} + R_{55}\frac{\sigma_{13}^{(k)^2}}{2} \right. \tag{3.100}$$

$$+ R_{23}\sigma_{33}^{(k)}\sigma_{22}^{(k)} + R_{45}\sigma_{13}^{(k)}\sigma_{23}^{(k)} + R_{26}\sigma_{22}^{(k)}\sigma_{12}^{(k)} + R_{36}\sigma_{12}^{(k)}\sigma_{33}^{(k)}$$

$$\left. + \frac{1}{\bar{S}_{11}}\left(\bar{S}_{12}\sigma_{22}^{(k)} + \bar{S}_{16}\sigma_{12}^{(k)}\right)\left(\bar{S}_{11}\tilde{\sigma}_{11}^{(k)} + \bar{S}_{12}\tilde{\sigma}_{22}^{(k)} + \bar{S}_{16}\tilde{\sigma}_{12}^{(k)}\right) \right] dV_{(k)}$$

where the R_{ij} are as previously defined in equation (3.24), and terms that are not functions of the unknown parameters have been omitted. Once the integrations have been performed, the complementary energy Π_c may be written as

$$\Pi_c = C_1(\phi_i,\lambda_i) + A_1C_2(\phi_i,\lambda_i) + A_2C_3(\phi_i,\lambda_i) + A_3C_4(\phi_i,\lambda_i) + A_1A_2C_5(\phi_i,\lambda_i) + A_2A_3C_6(\phi_i,\lambda_i) + A_1A_3C_7(\phi_i,\lambda_i) + A_1^2C_8(\phi_i,\lambda_i) + A_2^2C_9(\phi_i,\lambda_i) + A_3^2C_{10}(\phi_i,\lambda_i) \quad (3.101)$$

where the C_m, (m = 1,10) are polynomial functions of ϕ_i and λ_j multiplied by constants d_k, and are expanded in Appendix A. The polynomials represent the result of the integration in the transverse direction y, and the d_k represent the integration through the thickness of the z variations of the stresses. Note, that the expressions for the transverse integrations presented in Appendix A, are not exact expressions for the definite integrals in equation (3.100), but are based on the assumption that

$$e^{-\phi_i b} = e^{-\phi_i\lambda_j b} = 0 \quad (3.102)$$

This assumption implies that $\phi_i b$ is very large, that is the laminate is wide relative to its thickness. This places a restriction on the geometry of laminates that can be analyzed using the present formulation, but the severity of this restriction cannot be ascertained until the parameters ϕ_i and λ_j have been determined.

The variation of Π_c with respect to the unknown parameters ϕ_i, λ_j, and A_k can now be taken and set equal to zero. This results in a system of fourteen coupled, non-linear algebraic equations for the unknowns written symbolically as

$$\frac{\partial \Pi_c}{\partial \phi_i} = 0 \qquad (i=1,5) \quad (3.103a)$$

$$\frac{\partial \Pi_c}{\partial \lambda_j} = 0 \qquad (j=1,6) \quad (3.103b)$$

$$\frac{\partial \Pi_c}{\partial A_k} = 0 \qquad (k=1,3) \quad (3.103c)$$

The form of these equations is shown in Appendix A.

3.3.7 Solution of System of Equations

The problem has now been reduced to solution of the systems of equations (3.103). Since these equations are non-linear, root finding proceeds by iteration. Basically, two numerical

approaches can be employed for finding the roots. Since the equations represent the gradient of the complementary energy, one approach is to find the minimum of the energy function (objective function) using a general numerical unconstrained optimization technique. Another approach that can be taken is to solve the simultaneous system using Newton's Method. Theoretically, the minimization technique should be more efficient, since the search for a minimum can basically be reduced to a one dimensional problem, that is, a minimum can be found by moving "downhill" on a single surface.[73] There is not an analogous procedure for finding a multi-dimensional root. However, both methods were tried in the present investigation, and greater success was experienced using Newton's method.

Both Newton's method and numerical optimization techniques are started by providing the iterative algorithm with an initial approximate guess to the solution. One difficulty with Newton's method is that the solution may not converge from a given initial guess. Convergence is only guaranteed if the initial approximate solution is in the neighborhood of the solution. Another problem associated with the solution of non-linear equations is the possibility of multiple solutions, in our case corresponding to local minima of the energy function, requiring the iterative procedure to be initiated from several different starting values of the independent variables to ensure that the "best" solution is obtained. The "best" solution is the one corresponding to the lowest energy. In the present study, the initial approximate solutions were generated based upon the results of the KL solution. The KL solution can be solved very quickly and gives an indication of the magnitudes of the decay parameters ϕ_i and λ_i. Several starting points were generated by bracketing the KL solution and then incrementing the independent variables, ϕ_i and λ_i within the "brackets". Initial approximations for the proportionality constants A_k were obtained by simultaneously solving the three equations (3.103c), at the starting values of ϕ_i and λ_j. With the decay parameters known, the constants

$C_{m,}$ (m=1,10) can be evaluated, and equations (3.103c) are linear in the unknowns A_k. Negative values of ϕ_i and λ_j were discarded because they physically correspond to growing stresses with distance from the free edge, and complex roots were discarded because they in general lead to complex energy.

3.3.8 Solution Implementation

The equations presented in the previous section are incorporated in a FORTRAN program AAIS. The laminate configuration, i.e stacking sequence, and ply thicknesses, ply orientations, ply material properties, and loading conditions are required input. With this information, the classical lamination theory solution is obtained.

Once the classical lamination theory solution has been obtained, the energy expressions may be formulated and solved for the unknown constants. As mentioned in the previous section, two approaches were used to obtain the constants. IMSL[74] routines were called to implement both approaches. For the optimization, IMSL routine DBCODH was used. DBCODH minimizes a function of N variables with simple bounds using a modified Newton method and a finite difference approximation to the Hessian. To solve equations (3.103) as a non-linear system, IMSL routine DNEQNF was used. DNEQNF uses a variation of Newton's method and the finite-difference method to estimate the Jacobian. There are also IMSL routines available that require the user to provide an exact Jacobian. These methods were not used because of the length of calculations necessary to obtain the Jacobian matrix.

The program output includes the classical lamination theory stresses, values for the unknown constants, the laminate strain energy, complementary energy and compliance constants. This information is then input to a postprocessor that can be used to calculate through thickness and interlaminar stress distributions at any desired location. Contributions from all effects are

delineated in the output files.

CHAPTER 4

COMPARISON WITH PREVIOUS RESULTS

In this chapter and in Chapter 5, the approximate theory presented in the previous sections is applied to the stress analysis of several finite width, straight free edge laminates subjected to uniform extension and bending. Because of the general nature of the formulation and its simplicity in terms of the number of unknown parameters, the applications are straight forward. Recall from the previous discussion, that for general laminates, the stresses in individual layers are expressed in terms of fourteen unspecified parameters, ϕ_i (i=1,5), λ_j (j=1,6), and A_k (k=1,3) that are determined by minimizing the laminate complementary energy. For cross-ply and angle-ply laminates, in which some of the stress components are zero, or are assumed to be zero, fewer parameters must be determined. For cross-ply laminates the number of parameters reduces to ten, since σ_{12} and σ_{13} are identically zero, and in symmetric angle-ply laminates subjected to uniform extension the number reduces to three. The reduced number of unknown parameters for the angle-ply laminates is a reflection of the assumption made in the present formulation that σ_{13} is the only non-zero interlaminar stress. In unsymmetric angle-ply laminates and angle-ply laminates subjected to bending load, the number reduces to six. For a particular type of laminate, however, the number of unknown parameters is independent of the number of layers in the laminate, their material properties, and orientations. Obtaining classical lamination theory stresses in the plate interior is the only laminate dependent calculation which must be performed prior to determination of the interlaminar stresses. Consequently, computation times are linearly proportional to the number of layers in the laminate, and the

analysis can be applied to laminates with a large number of layers.

As indicated in the previous chapter several simplying assumptions were made in formulating the present approximate theory in order to obtain a methodology with the efficiency characteristics outlined above. These assumptions will, to some extent, result in a decrease in accuracy of the response predicted by the present theory as related to that given by more complicated models. Therefore, to gain some confidence in the model, this chapter presents comparisons between predictions of the present theory and well known solutions available in the literature. First comparisons are presented for laminates subjected to extension loading. These comparisons are followed by results for laminates in uniform bending.

4.1 Laminates in Uniform Extension

In this section we compare the response predicted by the present method of analysis with that given by other investigators[35,59,74] for finite width symmetric laminates subjected to uniform axial strain, ε_{11} = 0.1%. Specifically, four laminates are examined; $[90_{50}/0_{50}]_s$, $[0_{50}/90_{50}]_s$, $[\pm 45_{50}]_s$, and $[45_{50}/-45_{50}/0_{50}/90_{50}]_s$. In all laminates, the layers have equal thickness h = 0.25 in., and the thickness to width ratio of the laminate is taken to be one to four. Thus for the cross-ply and angle-ply laminates we have $H = 2h$ and $b = 8h$, where a quasi-isotropic laminate has $H = 4h$, $b = 16h$. The elastic properties of each graphite-epoxy laminae are taken to be equal to those given in the early studies of interlaminar stresses[26] and are provided in Table 4.1.

TABLE 4.1. Lamina Material Properties for Typical Graphite-Epoxy

Typical Graphite-Epoxy Material Properties					
E_1 (msi)	E_2 (msi)	G_{12} (msi)	G_{23} (msi)	ν_{12}	ν_{23}
20.0	2.1	0.85	0.85	0.21	0.21

4.1.1 Angle-Ply Laminates

The $[\pm 45_{50}]_s$ laminate has been studied by numerous investigators. In this section predictions given by the present theory for various stress components are compared with solutions obtained by Wang and Choi,[59] using an eigenfunction expansion solution, and by Wang and Crossman,[35] using a finite element analysis based upon constant strain, triangular elements. In all analyses the quasi-three dimensional assumption is made, that is, stresses and strains are assumed independent of the axial coordinate X_1. Before presenting results the issue of variable through-thickness decay of the local mismatch effects discussed in Section 3.3.4 is briefly addressed. The terminology and notations introduced in the following discussion will be used throughout the remainder of this text.

Recall from Section 3.3.4, that in order to keep the number of unknowns in the present solution to a manageable number, the through-thickness decay lengths of the local mismatch effects were established a priori and set equal to the thicknesses $h^{(k)}$ and $h^{(k+1)}$ of the layers adjacent to an interface where there is a mismatch in material properties. This specification of decay length is evident upon examination of equations (3.86-3.90). The extent in the thickness

direction of the local mismatch contributions can, however, be varied by representing each physical layer in the body as an assemblage of sublayers. For $[\theta_1/\theta_2]_s$ or $[\theta_1/\theta_2]_t$ laminates in which there is only one interfacial plane where there is a discontinuity in material properties, two sublayers in each layer with thicknesses t_1 and t_2, as shown in Figure 4.1, are all that is required to assess the influence of the through-thickness decay length of local mismatch effects on the stress field predictions. For more general laminate configurations, where the stresses in a generic layer are influenced by mismatch effects from two adjoining interfaces, at most three sublayers are required. The results presented throughout this thesis were generated by either modeling each layer as one unit, i.e., no sublayers, or by dividing each layer into two sublayers with thicknesses t_1 and t_2, as shown in Figure 4.1. Predictions obtained by representing each physical layer in the body as one unit are denoted by N=1, and results obtained by representing each layer as two sublayers are denoted N=2.

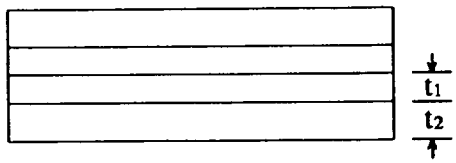

Figure 4.1. Through Thickness Discretization

The influence of the through-thickness discretization on the stress field predictions and laminate complementary energy has been studied for the $[\pm 45]_s$ laminate. As shown in Figure 4.1, the decay length of the local mismatch effects will be equal to t_1 when two sublayers are used to model a layer. The "optimum" values for t_1 and t_2 can be determined, for a particular laminate, by allowing them to vary in several applications of the AAIS program, and then selecting the set that corresponds to the minimum complementary energy. For the $[\pm 45]_s$

laminate considered here, the values t_1 = 0.11 in., and t_2 = 0.14 in. were obtained. The magnitude of σ_{13} at the intersection of the ±45 interface and the free edge has also been determined. Values are provided in Table 4.2 which shows the increase in the maximum magnitude σ_{13}, with decreasing decay length, down to the length corresponding to the minimum complementary energy.

The through-thickness decay length not only affects the stress magnitudes, but also the distribution of stress. In order to illustrate this effect, two curves are presented in the subsequent figures (Figures 4.2 and 4.4) for the present theory predictions. The curves N = 1, as previously mentioned, correspond to modeling each layer as one unit, and the curves N = 2 were generated using the "optimum" thicknesses given above.

The width distribution of the interlaminar shear stress σ_{13} at the ±45 interface predicted by the present technique and the analytical solution in [59] are shown in Figure 4.2. As can be seen, the present solution predictions for both N = 1 and N = 2 agree well with the previous solution. There is a small difference in the predictions at the intersection of the interface and the free edge. The elasticity solution of Wang and Choi[59] predicts a stress singularity at this point. Similar behavior is displayed by displacement based finite element formulations, which predict increasing stresses in elements adjacent to the singular point, as the size of the elements near this location decreases. The present solution does not include a singularity in the formulation, but as previously discussed, the magnitude of σ_{13} at the intersection of the interface and the free edge is a function of the through-thickness decay length of the local mismatch effect.

Interlaminar stress distributions along the 45/-45 interface for σ_{23} and σ_{33} are provided in Figure 4.3. For an angle-ply laminate, Poisson's ratio mismatch between adjacent plies is zero, and the in-plane stress $\tilde{\sigma}_{22}$ is zero, so the present theory predicts identically zero stresses σ_{23} and

TABLE 4.2. Increase in σ_{13} with Decrease in Decay Length

t_2 (in)	$-\sigma_{13}$ (ksi)
0.25	1.43
0.20	1.52
0.15	1.64
0.14	1.67
0.13	1.70
0.12	1.74
0.11	1.78

σ_{33} (see equations 3.89,3.90). The most pertinent observation to be made from this figure is that although the other solutions predict non-zero stresses σ_{23} and σ_{33} they are small compared with σ_{13}. The normal stress is less than 20% of σ_{13} and the shear stress σ_{23} is less than 5%. Note also that the σ_{23} distribution predicted by Wang and Crossman[35] does not satisfy the traction free edge condition. Wang and Choi[59], on the other hand, predict σ_{23} to be zero at the free edge, but their distribution for σ_{23} does not satisfy the transverse integral force equilibrium equation (3.52b), since σ_{23} obviously does not integrate to zero over X_2. Differences are also noted in the interlaminar normal stress predictions. Wang and Crossman's finite element solution predicts tensile stress at the free edge, but Wang and Choi's elasticity solution predicts compressive stresses.

Comparisons of through-thickness distributions of the interlaminar shear stress σ_{13} are also

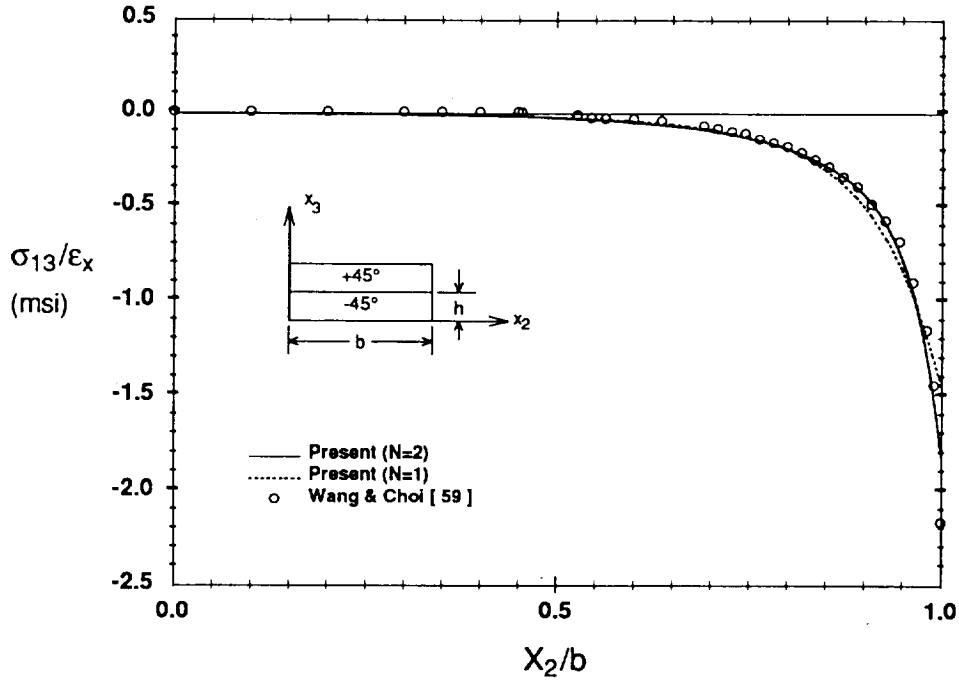

Figure 4.2. Comparison With Previous Results [59] for σ_{13} at 45/-45 Interface in $[+45_{50}/-45_{50}]_s$ Laminate ($\varepsilon_{11} = 0.1\%$)

made. In Figure 4.4, distributions at $X_2/b = 1$, and $X_2/b = 0.89$ calculated by the present approach and Wang and Choi's eigenfunction expansion solution, are shown. The present solution for N=2 agrees fairly well with the elasticity solution at $X_2/b = 1$. The major discrepancy in the results occurs at the intersection of the interface and the free edge, where the present analysis predicts finite maximum stress and the eigenfunction expansion solution becomes unbounded as $X_2 \rightarrow b$, and $X_3 \rightarrow h$. Away from the free edge, at $X_2/b = 0.89$, generally good agreement between the two solutions is observed throughout the laminate thickness for both N=1 and N=2 of the present theory.

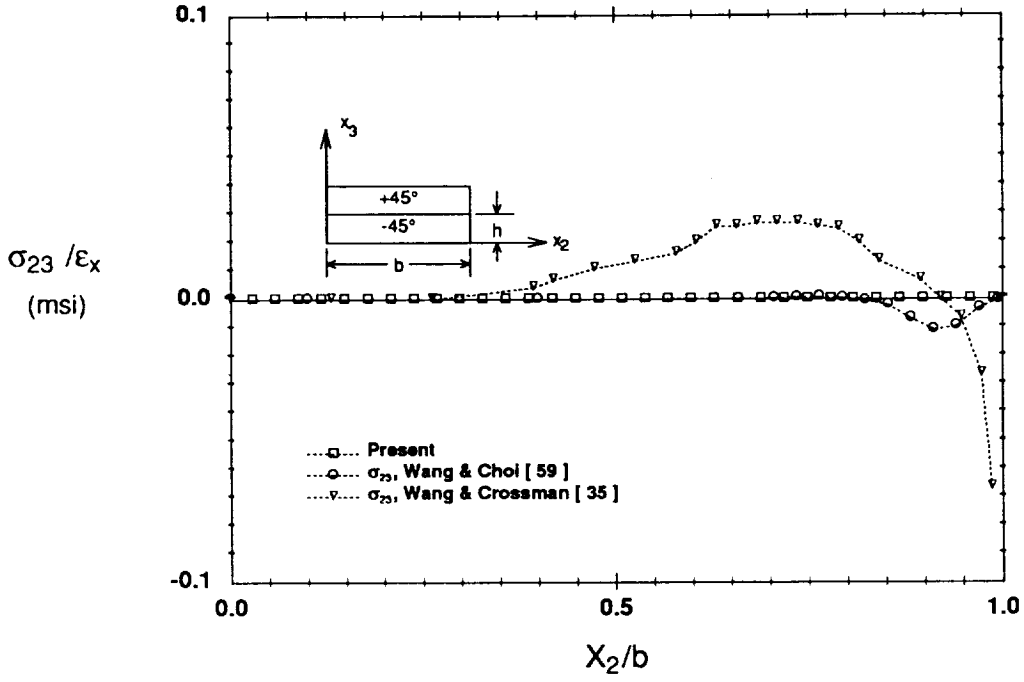

(a) σ_{23} Comparison

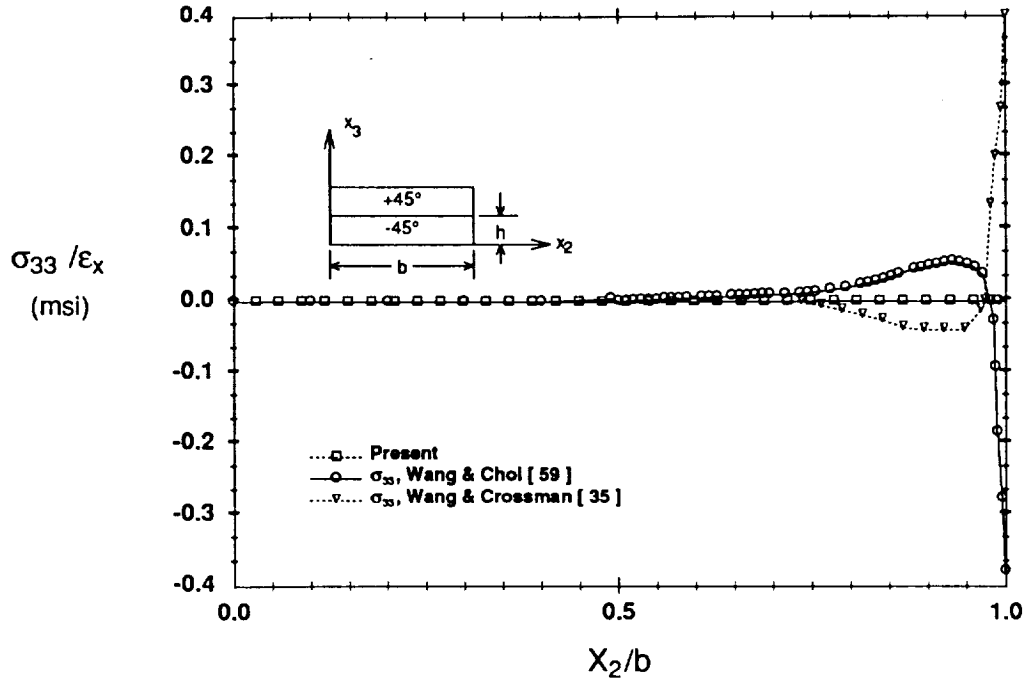

(b) σ_{33} Comparison

Figure 4.3. Comparison With Previous Results [35],[59] for σ_{23} and σ_{33} at 45/-45 Interface in $[+45_{50}/-45_{50}]_s$ Laminate ($\varepsilon_{11} = 0.1\%$)

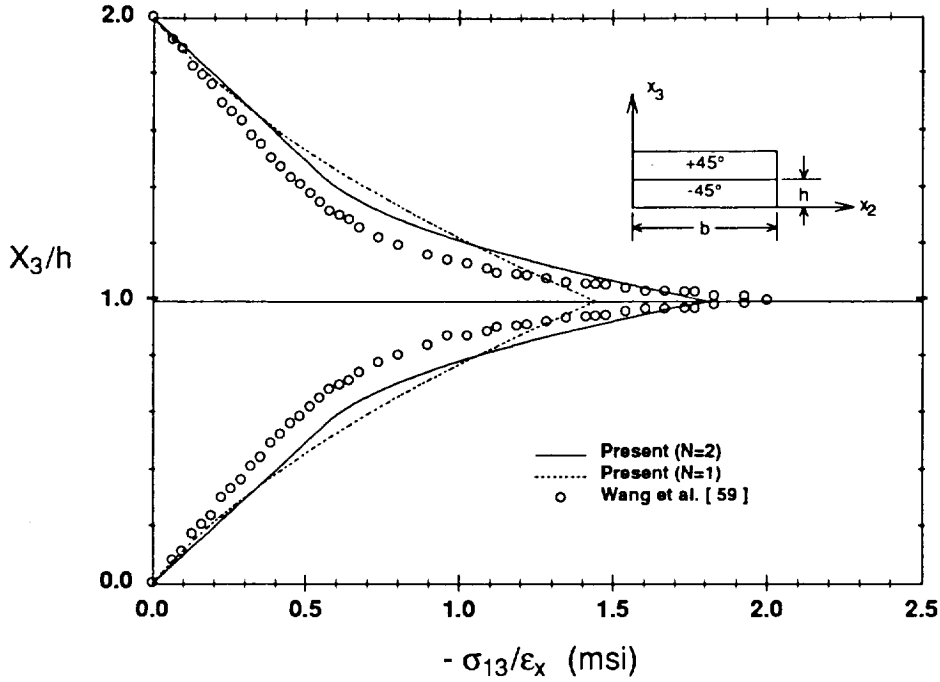

(a) X_2 / b = 1.0

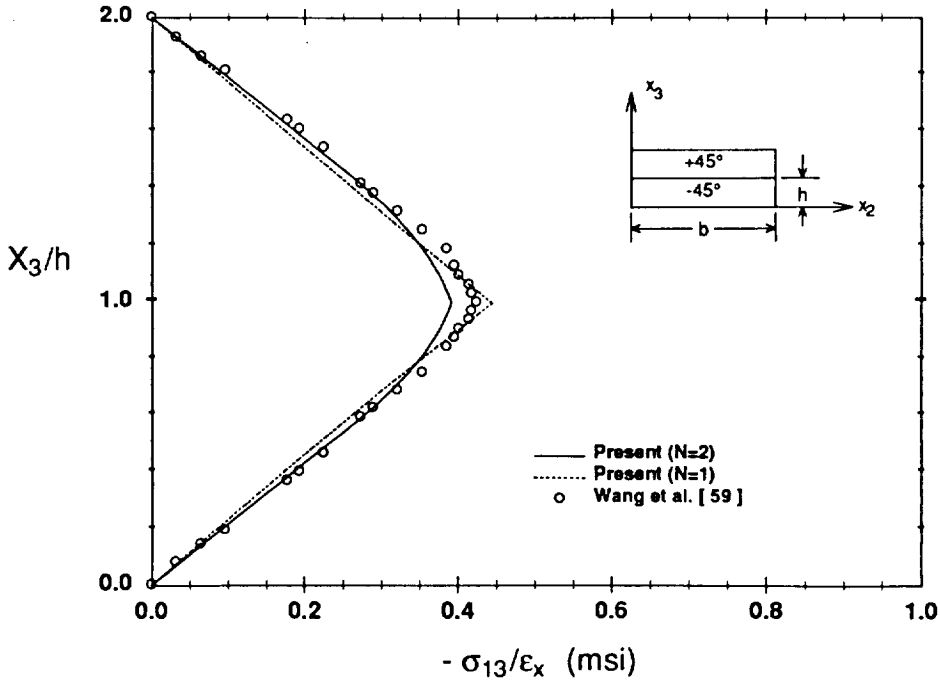

(b) X_2 / b = 0.89

Figure 4.4. Comparison With Previous Results [59] for Through-Thickness σ_{13} in $[+45_{50}/-45_{50}]_s$ Laminate ($\varepsilon_{11} = 0.1\%$)

4.1.2 Cross-Ply Laminates

Interlaminar stress comparisons between results predicted by the present theory and finite element analysis of Herakovich et al.,[75] for $[0_{50}/90_{50}]_s$ and $[90_{50}/0_{50}]_s$ laminates are presented in this section. For these laminates, the in-plane shear stresses σ_{12} and interlaminar shear stresses σ_{13} are zero. The present solution results were obtained using N=1.

Figure 4.5 shows the width dependence of the interlaminar shear stress σ_{23} and normal stress σ_{33}, at the 0/90 interface of the two laminates. The present predictions compare fairly well with the finite element results, again differing mainly right at the intersection of the interface and the free edge. Note, the present theory satisfies the traction-free boundary condition exactly, and classical lamination theory stresses are recovered in the interior. The finite element results satisfy the traction-free boundary condition only approximately. There are also differences in the predictions of σ_{33} at the free edge with the most noteworthy being that the finite element method predicts tensile σ_{33} in the $[90_4/0_4]_s$ laminate where the present solution predicts a small compressive stress. The gradient of the σ_{33} distribution is very steep near the free edge and the two solutions predict similar slopes.

4.1.3 Quasi-Isotropic Laminates

Quasi-isotropic laminates have been studied by a number of investigators using the finite element method. Here we consider specifically the laminate stacking sequence $[45_{50}/-45_{50}/0_{50}/90_{50}]_s$. Illustrative results for this laminate predicted by the present theory are compared with Wang and Crossman's[35] finite element predictions. Each layer was represented as one unit (N=1) in obtaining the present results.

Distributions of interlaminar normal stress σ_{33} along the laminate midplane and the 45/-45

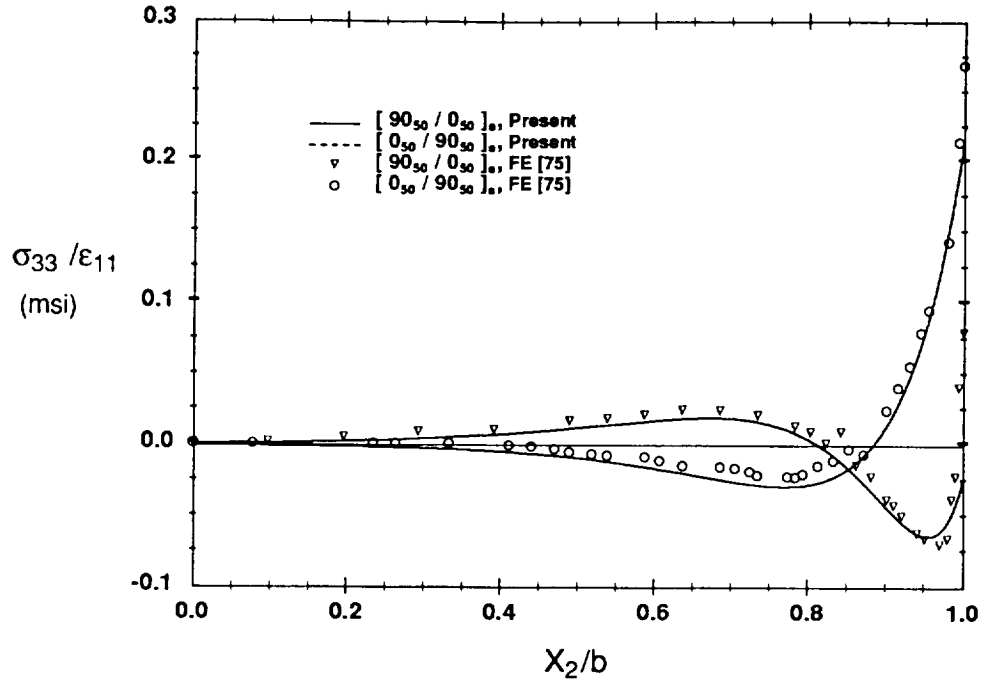

(a) σ_{33} Comparison

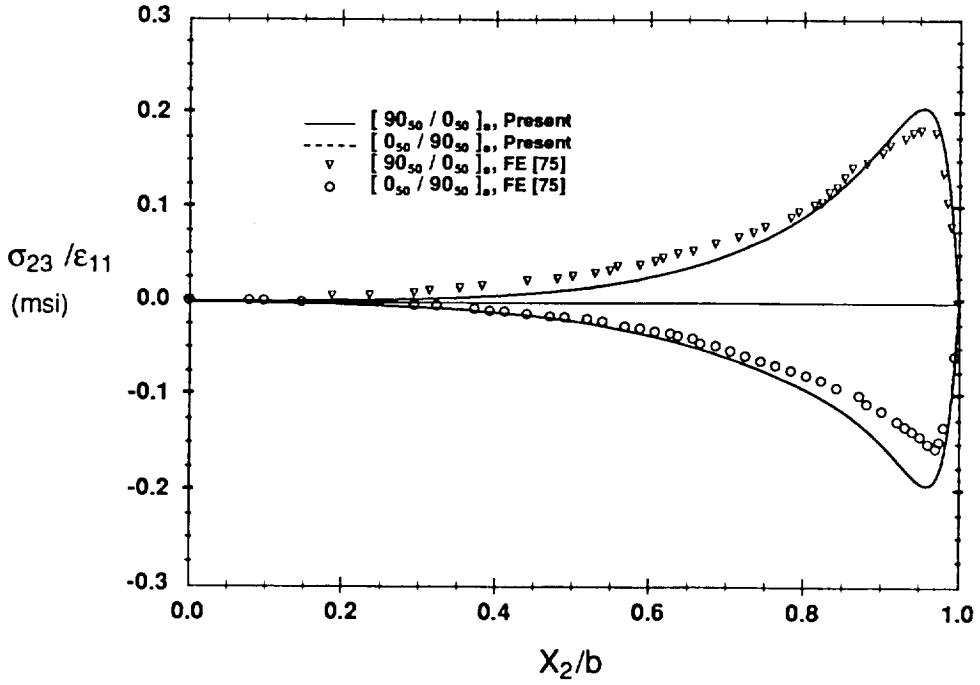

(b) σ_{23} Comparison

Figure 4.5. Comparison With Previous Results [75] for σ_{23} and σ_{33} at 90/0 Interface in $[90_4/0_4]_s$ and $[0_4/90_4]_s$ Laminates ($\varepsilon_{11} = 0.1\%$)

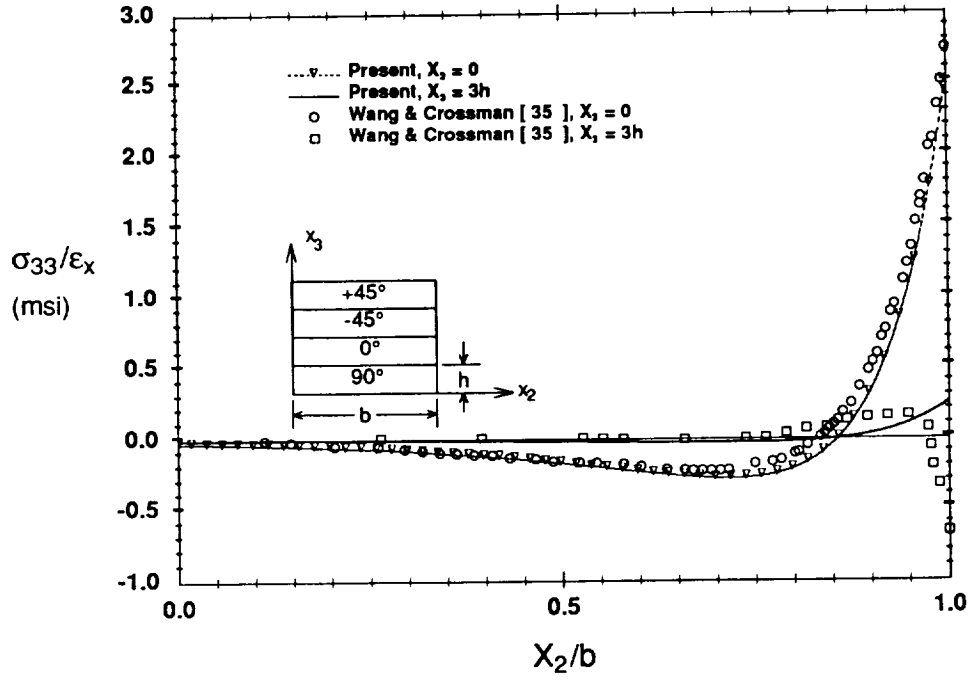

Figure 4.6. Comparison With Previous Results [35] for σ_{33} at Various Interfaces in $[45_{50}/-45_{50}/0_{50}/90_{50}]_s$ Laminate ($\varepsilon_{11} = 0.1\%$)

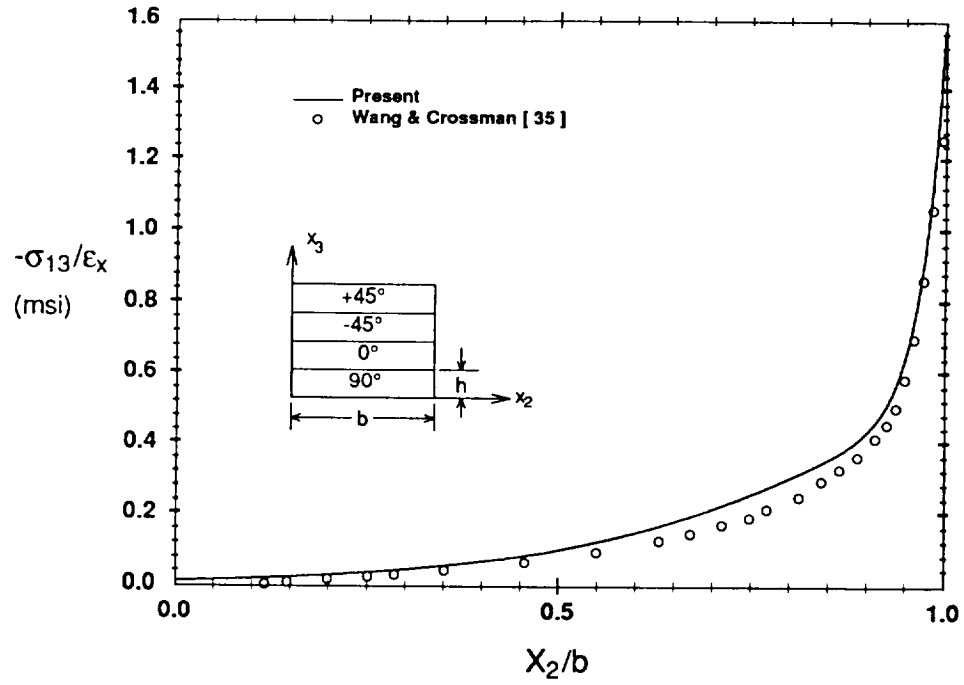

Figure 4.7. Comparison With Previous Results [35] for σ_{13} at 45/-45 Interface in $[45_{50}/-45_{50}/0_{50}/90_{50}]_s$ Laminate ($\varepsilon_{11} = 0.1\%$)

interface are shown in Figure 4.6. Clearly, both methods agree quite well at the midplane. Similar results were obtained at the interfaces $X_3 = h$, and $X_3 = 2h$. The predictions of the two methods at the 45/-45 interface ($X_3 = 3h$), however, differ significantly. The present analysis only shows the normal stress crossing the X_2 axis once, while the analysis in [35] predicts two crossings, with the stress reversing sign and becoming compressive near the free edge. Possible causes for this difference are discussed in the next chapter.

Figures 4.7 and 4.8 show comparisons of the interlaminar shear stress predictions, at the 45/-45 (σ_{13}) and 0/90 (σ_{23}) interfaces, respectively. Again, for both cases, the present theory agrees quite well with the finite element results.

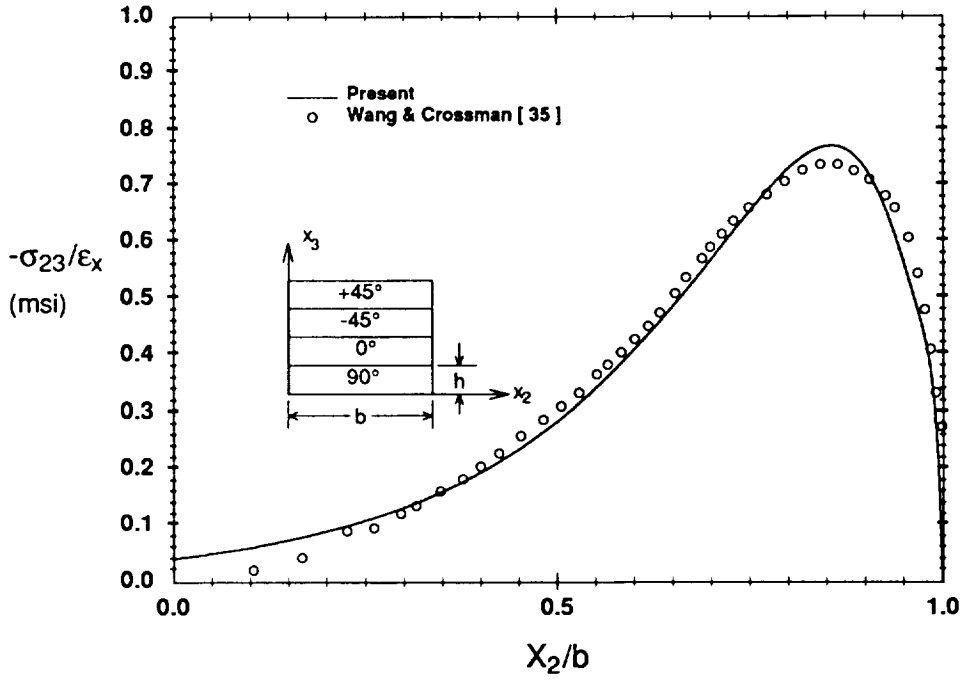

Figure 4.8. Comparison With Previous Results [35] for σ_{23} at 0/90 Interface in $[45_{50}/-45_{50}/0_{50}/90_{50}]_s$ Laminate ($\varepsilon_{11} = 0.1\%$)

4.2 Laminates in Bending

As previously discussed, interlaminar stress calculations for laminates in bending have received relatively little attention in the literature. However, bending loads are common in practical applications. Salamon[64] has presented results based upon a finite difference solution similar to that presented by Pipes and Pagano,[26] for a $[0_{50}/90_{50}]_s$ laminate with the material properties given in Table 4.1 and subjected to end moments about the transverse (X_2) axis. Chan and Ochoa [66] have presented results for several $[0_2/\theta_2]_s$ laminates under the same moment loading. Comparison is made here with the solution in [64].

Comparison of the interlaminar normal stress along the 0/90 interface is shown in Figure 4.9. The laminate is loaded such that the maximum bending strain $\varepsilon_{11} = -0.1\%$ is developed at the

top surface. Stresses are normalized, as in [64], by the elementary bending stress ($\bar{\sigma}_{11}$) that would develop in a undirectional laminate (θ=0) at the X_3 location corresponding to the 0/90 interface ($\bar{\sigma}_{11}$ = 10 ksi). As the figure shows, the agreement between solutions is not as good as in the axial extension case, but the trends are similar. The major discrepancy occurs at the free edge, where the finite difference solution predicts tensile stress about 1-1/2 times larger than the present solution.

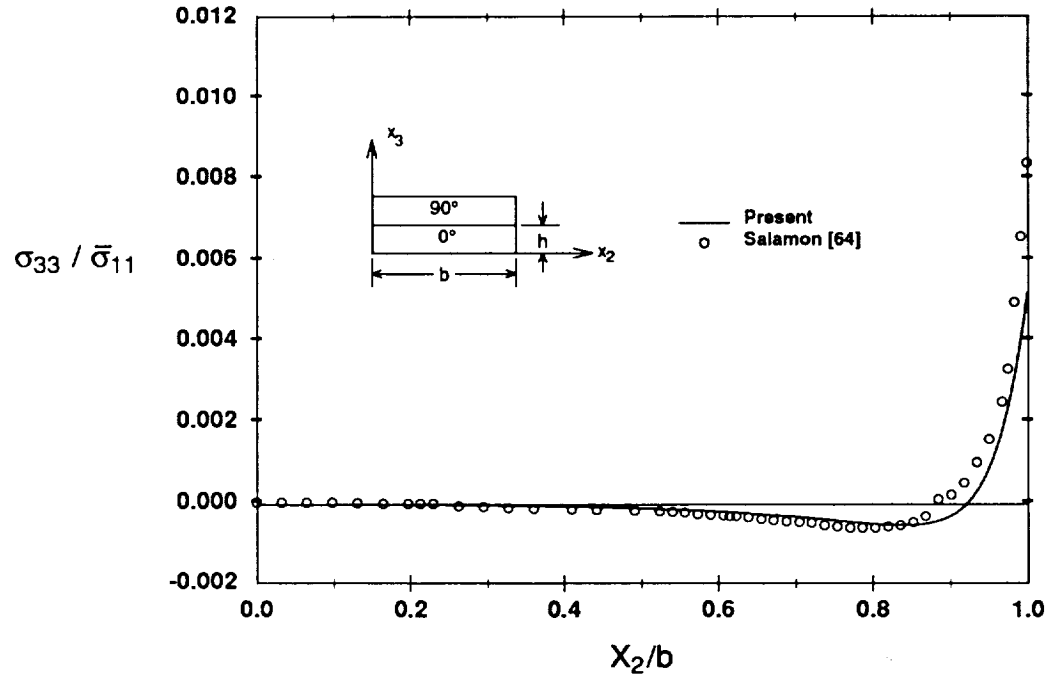

Figure 4.9. Comparison With Previous Results [64] for σ_{33} at 90/0 Interface in $[90_4/0_4]_s$ Laminate in Bending

CHAPTER 5

APPLICATIONS AND DISCUSSION

The comparisons presented in the previous chapter showed that the predictions of the present solution are, generally, in good agreement with predictions obtained from a variety of other solution methods for extension and bending loads in a variety of laminates. In this chapter, the analysis is applied to additional laminates to demonstrate the utility of the method as a design tool and to provide a brief study of the influence of laminate configuration and loading on the interlaminar stress state. Also, as was discussed in Chapter 3, the total stresses in the laminate arise from two physical mechanisms - local and global mismatch in material properties. In the subsequent discussion the relative significance of these contributions to the stress field is examined.

Results in the form of through-thickness and interfacial stress distributions are presented for symmetric and unsymmetric cross-ply laminates and for symmetric angle-ply and quasi-isotropic laminates subjected to bending and extension loads. Through-width distributions are presented only at ply interfaces. Distributions for other locations, however, can be obtained easily. Comparisons are presented for results obtained using the present formulation, the KL solution, and finite element solutions, where available. As subsequently shown, the current solution predicts interlaminar stresses which are generally in close agreement with finite element results, and improves the KL solution primarily at interfaces where global equilibrium is satisfied by the lamination theory stresses, but local mismatch in material properties induces large interlaminar stresses. When studying the figures, recall that the magnitudes of stresses

predicted by the finite element models at the intersection of layer interfaces and the free edge (singular point) are a function of the fineness of the mesh near this point. Thus emphasis should be placed on comparison of entire stress distributions away from these points where finite element results are more accurate.

Unless otherwise noted, the finite element results for extension of cross-ply laminates were generated using a program previously developed by Norwood[76] and the finite element results for the angle-ply and quasi-isotropic laminates were generated using the program CLFE2D.[77] Norwood's program is based upon a full three-dimensional formulation, while CLFE2D makes the quasi-three dimensional assumption. Quarter symmetry models (i.e. one quarter of cross section modeled) were used in all analyses.

For the symmetric laminates the axial strain loading was $\varepsilon_x = 0.1\%$, and the axial curvature loading was $\kappa_x = 0.1$. For the unsymmetric laminates, it was more convenient to apply end loads rather than end strains and curvatures to obtain the classical lamination theory results. For these cases axial extension load N_x and uniform bending load M_x were applied. The material properties of a T300-5208 graphite epoxy used in the analyses are provided in Table 5.1. All plies were taken to have thickness t = 0.005 in.

5.1 Cross-ply Laminates

Cross-ply laminates are the simplest of the laminate configurations because there are no off axis plies. Consequently, the coefficient of mutual influence is zero in all plies and the interlaminar shear stress, σ_{13}, is identically zero throughout the laminate. These laminates are therefore studied to isolate the influence of Poisson's ratio mismatch on the development of interlaminar shear stress σ_{23} and interlaminar normal stress σ_{33}.

TABLE 5.1. T300-5208 Graphite-Epoxy Material Properties

T300-5208 Graphite-Epoxy Material Properties					
E_1 (msi)	E_2 (msi)	G_{12} (msi)	G_{23} (msi)	ν_{12}	ν_{23}
19.2	1.56	0.82	0.52	0.24	0.49

Results are presented for three laminates: $[0_4/90_4]_s$, $[90_4/0_4]_s$, and $[0_4/90_4]_t$, subjected to bending and extension loads. Classical lamination theory stresses for the symmetric and unsymmetric laminates for these two load cases are provided in Appendix C (Tables C.1 and C.2). With the lamination theory stresses given, the unknown parameters in the assumed stress expressions have been determined by minimizing the laminate complementary energy. The values obtained for the present theory, along with the parameters ϕ_2 and λ_1 required in the KL solution are given in Tables 5.2 (symmetric laminates) and 5.3 (unsymmetric laminates). The KL solution parameters are shown within parenthesis. Note, ϕ_1, ϕ_3, λ_2 and A_1 do not appear in the tables since σ_{12} and σ_{13} are zero for these laminates. All results presented for the current method were obtained by representing each layer as one unit (N=1). The layers were all of equal thickness, h = 0.020 in. Analyses made with N=2, where each layer was divided into two sublayers of equal thickness, resulted in higher energies. The through-thickness decay length for N=1 then corresponds to the number of plies in the individual layers of the laminate. The decay lengths, denoted by h, are also presented in Tables 5.2 and 5.3.

The symmetric and unsymmetric laminates respond very differently to applied loads. In symmetric laminates the membrane-flexural coupling terms, B_{ij} are all zero, so that when these

TABLE 5.2. Solution Parameters for Symmetric Cross-Ply Laminates

Solution Parameters For Symmetric Cross Ply Laminates				
Constant	Extension		Bending	
	$[0_4/90_4]_s$	$[90_4/0_4]_s$	$[0_4/90_4]_s$	$[90_4/0_4]_s$
ϕ_2 (1/in)	47.32 (71.66)	52.59 (58.63)	39.10 (39.49)	71.73 (115.7)
ϕ_4 (1/in)	28.30	37.36	33.13	45.15
ϕ_5 (1/in)	33.42	36.39	42.92	45.73
λ_1	0.972 (0.655)	0.952 (3.952)	1.979 (1.000)	1.758 (1.000)
λ_3	3.817	1.754	8.025	4.422
λ_4	11.49	9.406	4.564	4.307
λ_5	2.175	3.341	3.326	3.291
λ_6	1.905	1.817	1.543	1.313
A_2X10^{-5} (psi)	-4.151	-1.311	-4.705	-4.381
A_3X10^{-5} (psi)	-2.919	3.988	-6.104	3.870
h (in)	.020	.020	.020	.020

TABLE 5.3. Solution Parameters for Unsymmetric Cross-Ply Laminates

Solution Parameters For Unsymmetric Cross Ply Laminate		
Constant	Extension	Bending
ϕ_2 (1/in)	68.72 (201.4)	70.33 108.2
ϕ_4 (1/in)	52.79	54.73
ϕ_5 (1/in)	89.25	60.69
λ_1	0.915 (1.000)	2.660 (1.000)
λ_3	3.448	2.831
λ_4	3.632	3.712
λ_5	1.312	5.911
λ_6	0.862	0.726
A_2X10^{-5} (psi)	-7.158	-7.493
A_3X10^{-5} (psi)	5.074	-3.685
h (in)	.020	.020

laminates are subjected to extensional loads they remain plane. The unsymmetric laminate, on the other hand, has non-zero B_{11} and B_{22} and will deflect out of plane when extended. Comparison of stress distributions in symmetric and unsymmetric laminates then provides an indication of the effect of out-of-plane deflections on the interlaminar stresses. Norwood[76] has shown that when the out of plane deflections are large - on the order of the laminate thickness - a nonlinear analysis which accounts for geometric coupling effects is required to accurately characterize the interlaminar stress response. In the present analysis, all out of plane deflections are assumed small so that a linear analysis is valid.

5.1.1 Symmetric Laminates - Extensional Load

Stress distributions for $[0_4/90_4]_s$ and $[90_4/0_4]_s$ laminates are provided in Figures 5.1-5.8. Stresses determined by the finite element analysis, the KL solution, and the present solution, equations (3.88-3.90), are shown. Through-thickness distributions are provided for the top half of the laminate, with stresses plotted as a function of the normalized distance $\bar{X}_3 = X_3/h$ from the laminate midplane, where h denotes one layer thickness. Interlaminar shear stress is anti-symmetric about the midplane and interlaminar normal stress is symmetric. Interfacial distributions are also shown, with stresses plotted as a function of the normalized distance X_2/b from the laminate center, where b is the laminate half width. In all plots, stresses are normalized by the average far field stress $N_{11}/2H$ where N_{11} is the far field load obtained from lamination theory, and H is the laminate half thickness. The normalized stresses are denoted $\bar{\sigma}_{33}$ and $\bar{\sigma}_{23}$.

Figure 5.1 shows comparison of finite element results, the KL predictions and the present solution for the through-thickness distributions of the interlaminar normal stress σ_{33} at $X_2 = 0.999b$ for the two laminates. Evident from these figures is the significant improvement of the present theory over the KL solution, with the present solution predicting trends similar to

those displayed by the finite element results. In particular, note the asymmetry in response of the 0/90 and 90/0 laminates predicted by both the finite element analysis and the current model, while the KL solution, which is based entirely upon global equilibrium predicts close to symmetric response of these two laminates. That is the KL solution predicts the stress response in the two laminates to be basically mirror images of each other. Also significant from a design point of view, is failure of the KL solution to predict tensile interlaminar normal stress, at any location in the $[90_4/0_4]_s$ laminate, since tensile interlaminar normal stresses are more detrimental to the integrity of laminated composite structures than compressive interlaminar normal stresses.

The difference in the stress response of the two laminates and the predictions of the three methods is further illustrated in Figure 5.2 which presents σ_{33} distributions along the 0/90 interface. Clearly, the present theory agrees quite well with the finite element results for both laminates, but the KL solution diverges near the free edge in the case of the $[90_4/0_4]_s$ laminate. Consistent results from all three solutions are obtained for this laminate only at sufficiently large distance from the free edge (e.g. $X_2 \approx 0.95b$).

Similar comparative through-thickness and interfacial distributions for the interlaminar shear stress σ_{23} are shown in Figures 5.3 and 5.4. Again, the results of the present solution compare more favorably with the finite element results than do the KL results. The most noticeable discrepancies are observed in the through-thickness distributions. The relative difference in the maximum value of the shear stress obtained by finite elements and the present solution is 10%, for the 90/0 laminate, while the relative difference between finite elements and the KL solution is approximately 38%. Also note that the stress gradients in the thickness and width directions predicted by the present theory and finite element method are more severe than estimated by the KL solution.

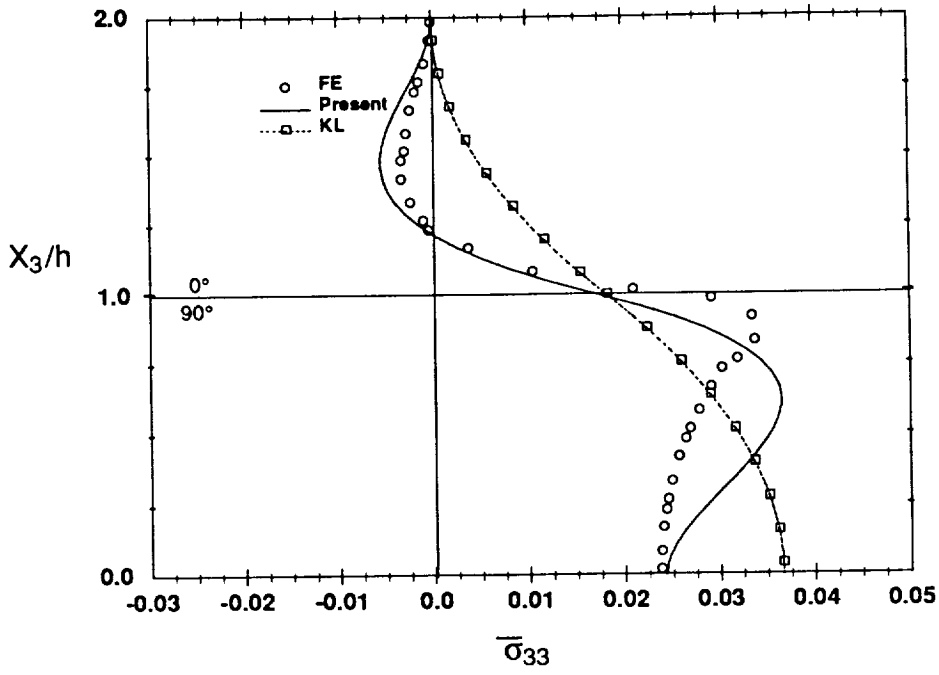

a) $[0_4/90_4]_s$ Laminate

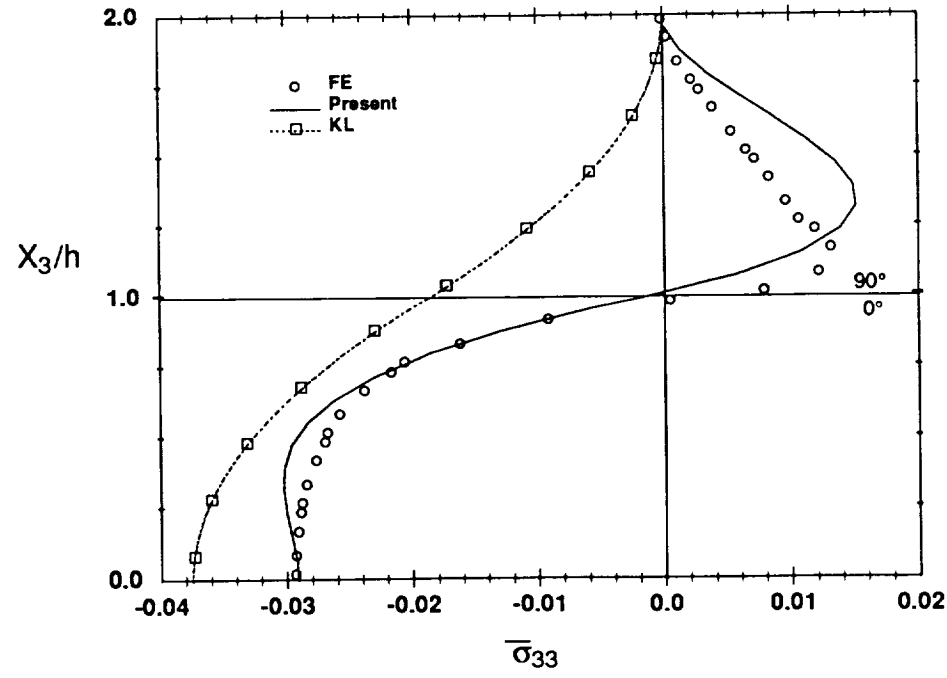

(b) $[90_4/0_4]_s$ Laminate

Figure 5.1. Comparisons for σ_{33} at $X_2/b = 0.999$ in $[0_4/90_4]_s$ and $[90_4/0_4]_s$ Laminates - Extension

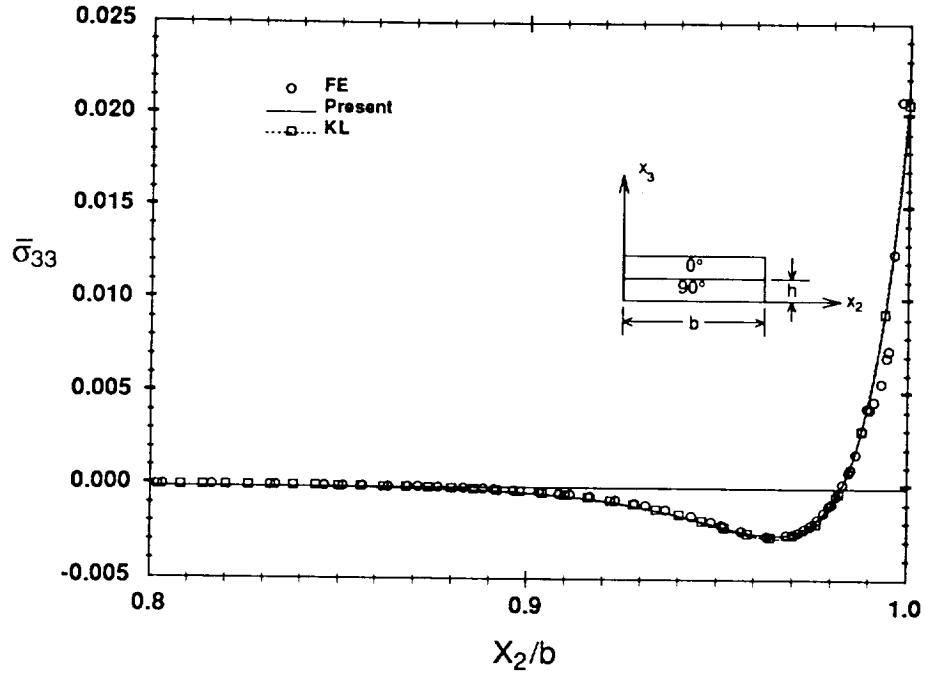

(a) $[0_4/90_4]_s$ Laminate

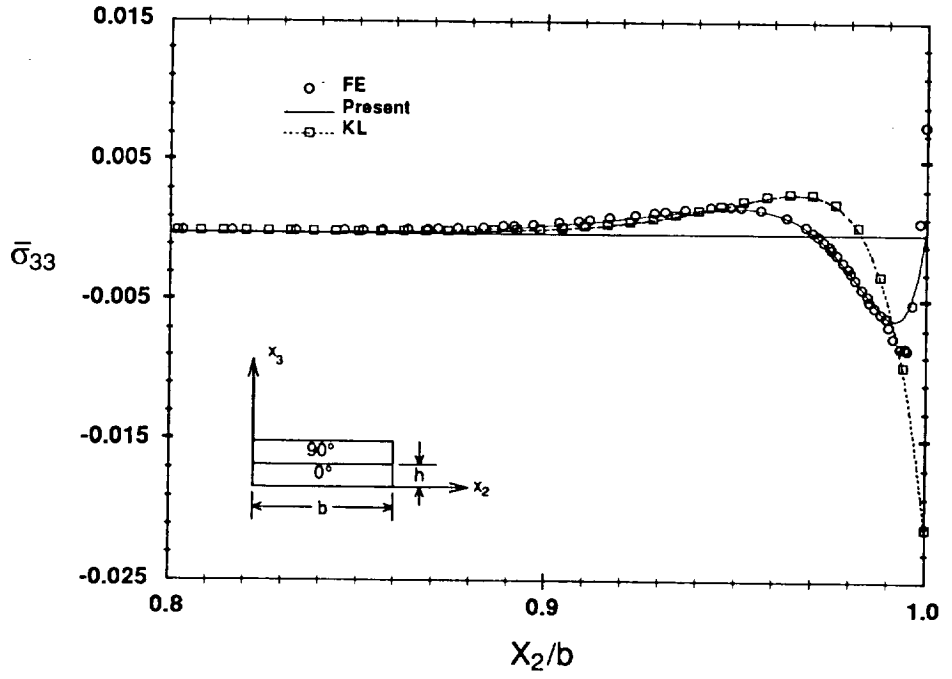

(b) $[90_4/0_4]_s$ Laminate

Figure 5.2. Comparisons for σ_{33} at 0/90 Interface in $[0_4/90_4]_s$ and $[90_4/0_4]_s$ Laminates - Extension

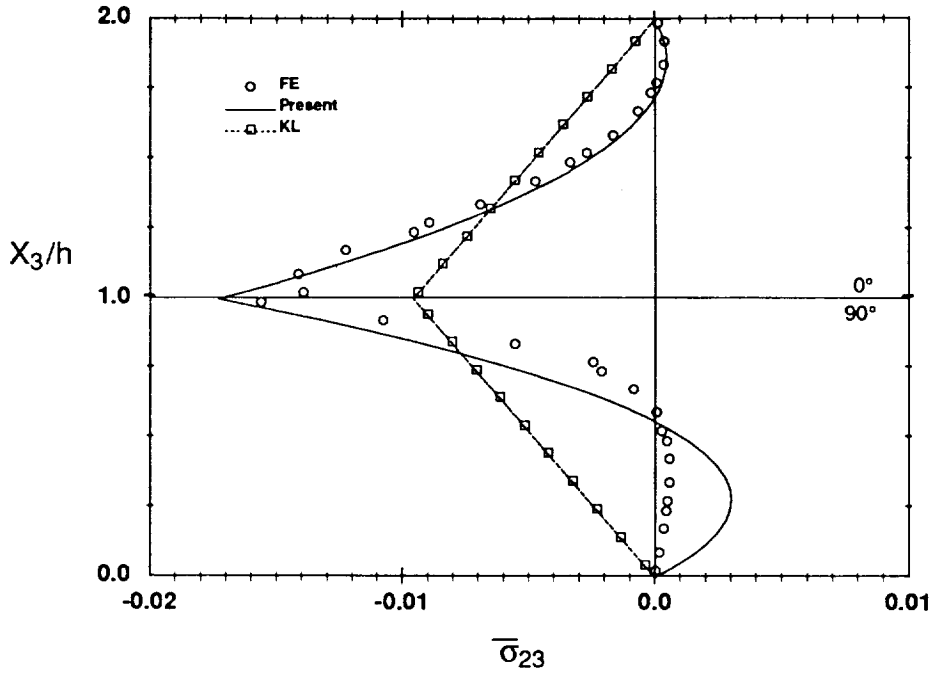

(a) $[0_4/90_4]_s$ Laminate

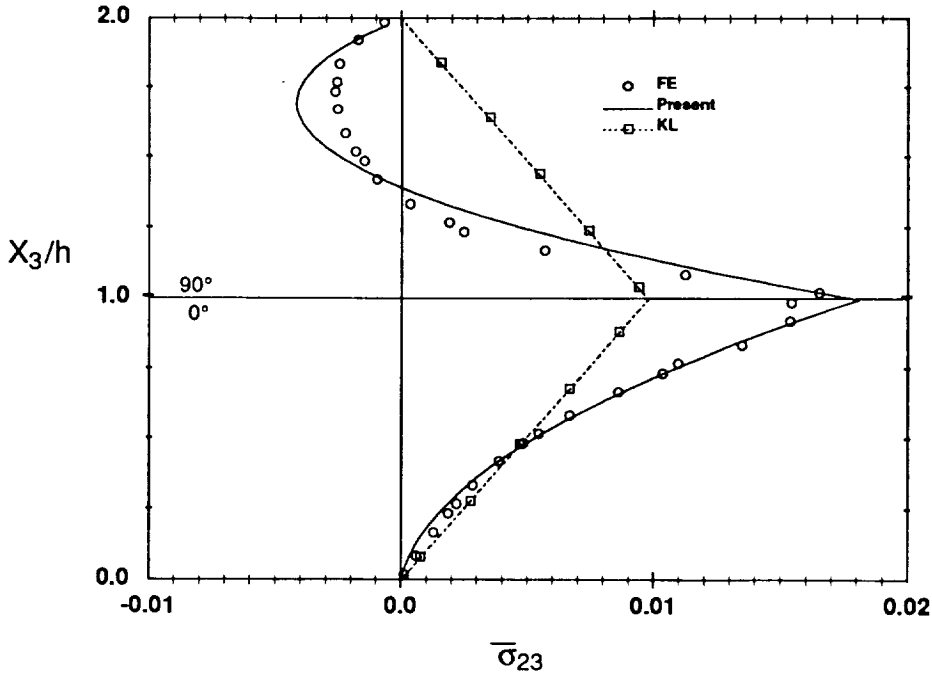

(b) $[90_4/0_4]_s$ Laminate

Figure 5.3. Comparisons for σ_{23} at $X_2/b = 0.993$ in $[0_4/90_4]_s$ and $[90_4/0_4]_s$ Laminates - Extension

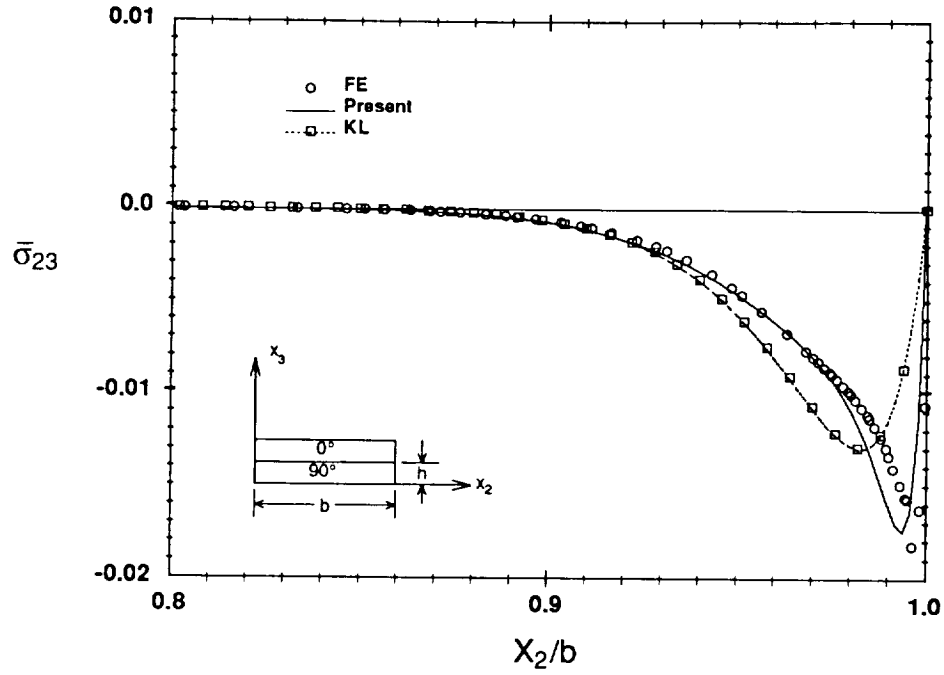

(a) $[0_4/90_4]_s$ Laminate

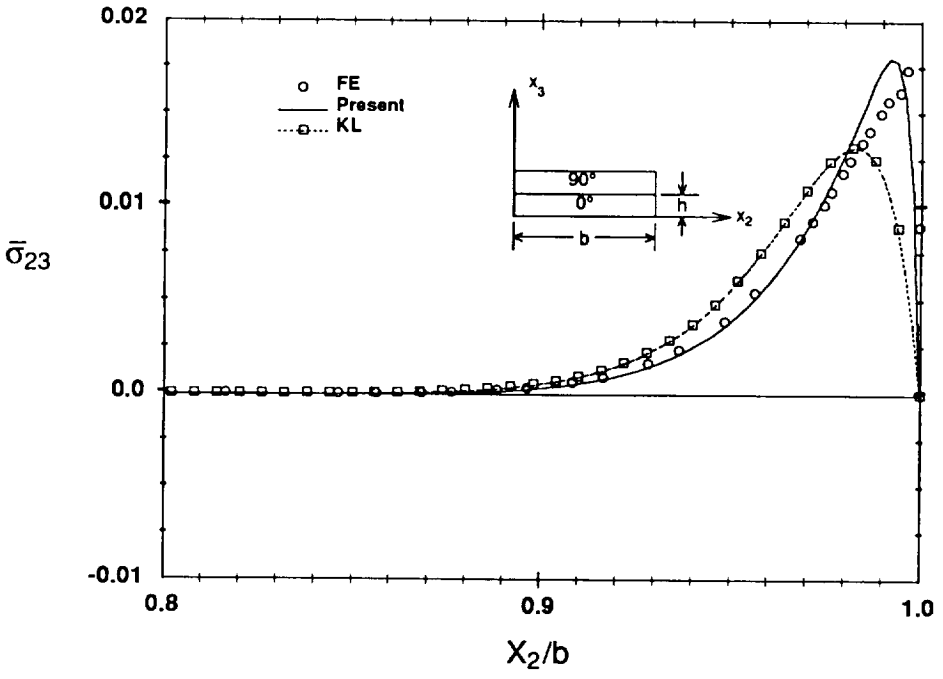

(b) $[90_4/0_4]_s$ Laminate

Figure 5.4. Comparisons for σ_{23} at 0/90 Interface in $[0_4/90_4]_s$ and $[90_4/0_4]_s$ Laminates - Extension

The inability of the KL solution to predict the difference in behavior of the 0/90 and 90/0 laminates described above suggests that this solution does not include enough degrees of freedom in the assumed stresses to accurately define the stress response, in some cases, and that "local effects" might be the cause of the asymmetry in stresses observed in these laminates. The relative influence of the local and global effects is illustrated in Figures 5.5 and 5.6, which delineate all of the contributions to the stress field incorporated in the present theory. The equilibrium contribution represents the first term in equations (3.89,3.90), the shear mismatch is the second term (multiplying A_2) and the normal mismatch is the third term (multiplying A_3). Note that although the KL solution and the equilibrium solution are identical in form, the KL solution curves in Figures 5.1 and 5.2 are not coincident with the equilibrium contribution plots in Figures 5.5 and 5.6 since different ϕ's and λ's were employed to obtain the two distributions (see Table 5.2).

Figure 5.5 provides through-thickness distributions for the interlaminar normal stress σ_{33} near the free edge. Equilibrium and mismatch effects contribute throughout both laminate thicknesses, except at the midplane, where the stresses result solely from the equilibrium contribution. There is no local mismatch in material properties at the midplane. As discussed earlier, the through-thickness extent of the mismatch contribution is controlled by the level of discretization used to model each layer and would decrease if the 0° and 90° layers were divided into sublayers. The most significant observation made from this figure is that the normal mismatch contribution is the component primarily responsible for the differences in the stress predictions provided by the present solution for the two laminates. The equilibrium and shear mismatch contributions have similar influences on the total distribution in both laminates, but the normal mismatch contribution has opposite effects.

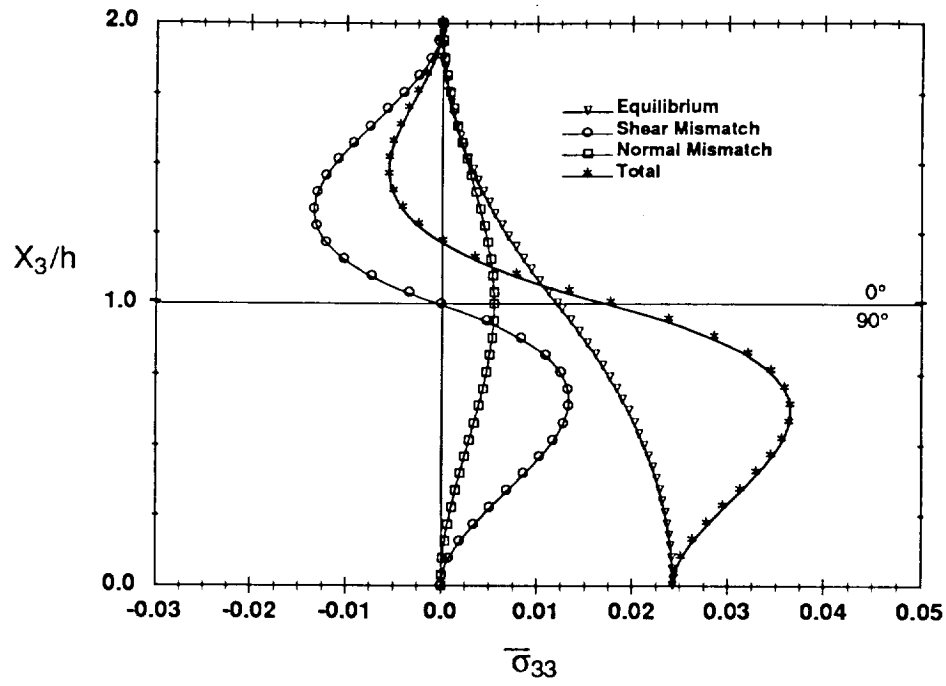

(a) $[0_4/90_4]_s$ Laminate

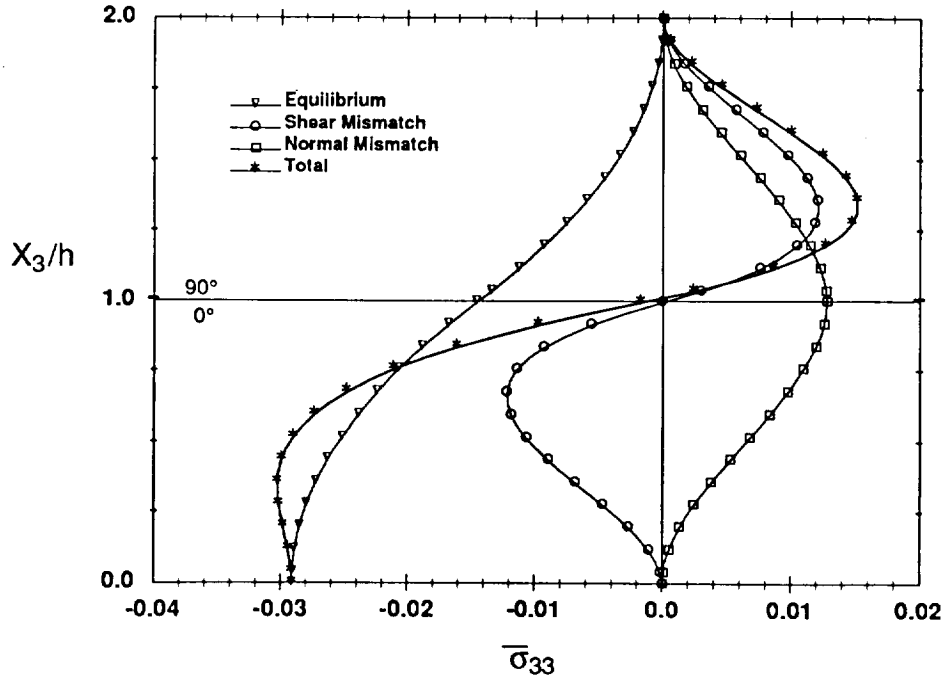

(b) $[90_4/0_4]_s$ Laminate

Figure 5.5. Contributions to σ_{33} at $X_2/b = 0.999$ in $[0_4/90_4]_s$ and $[90_4/0_4]_s$ Laminates - Extension

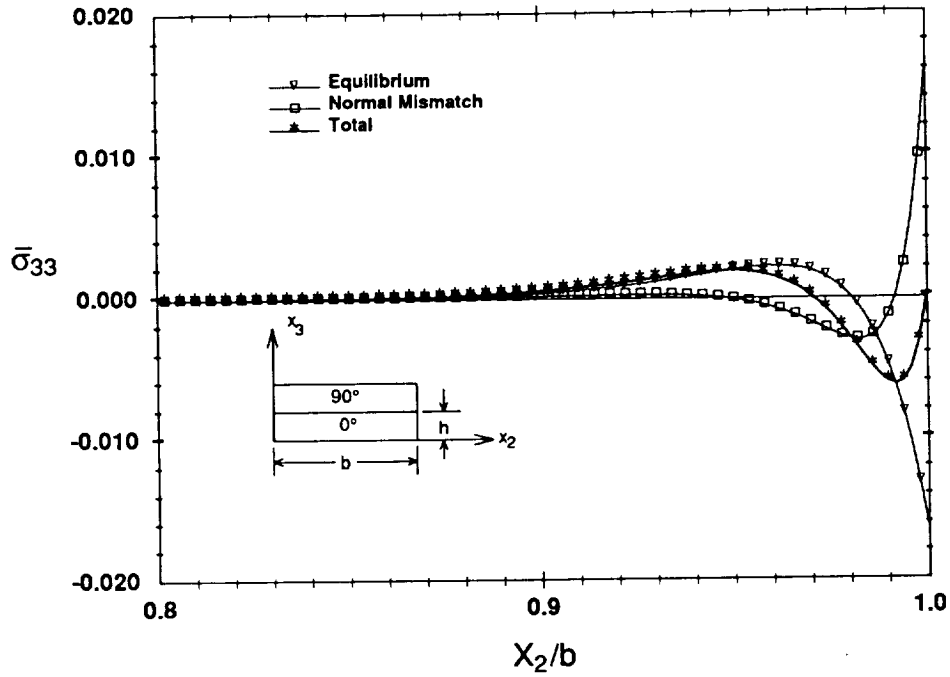

Figure 5.6. Contributions to σ_{33} at 0/90 Interface in $[90_4/0_4]_s$ Laminate - Extension

The influence of the normal mismatch effect on the total interlaminar normal stress is more vividly illustrated in Figure 5.6 which presents individual contributions to the σ_{33} stress component along the 0/90 interface of the $[90_4/0_4]_s$ laminate. The mismatch effects are not as significant for the $[0_4/90_4]_s$ laminate and are not discussed here. Distributions for this laminate are provided in Appendix C (Figure C.1) for completeness. Recall, the shear mismatch contribution to the normal stress is zero at *all* interfaces and therefore is not shown in the figure. Near the free edge, the normal mismatch component has magnitude approximately equal to the equilibrium contribution but of opposite sign; the mismatch contribution totally changes the character of the interfacial stress distribution and causes a reversal in stress near the free edge, tending toward positive stress as the free edge is approached. This type of behavior cannot be predicted by the KL solution, because of the constraint imposed by the their solution that stresses in all layers decay at the same rate. At the midplane, the mismatch terms are zero, and the stresses result solely from equilibrium. The current theory, the finite element method and the KL solution all predict the normal stress to be distributed over the interfacial plane $X_3 = 0$ (midplane) as shown in Figure 5.7. The KL solution requires the through width stresses at the 0/90 interface to have the same form, as displayed in Figure 5.2b.

Similar distributions for the interlaminar shear stress σ_{23} are provided in Appendix C (Figures C.2-C.3). As was the case for the interlaminar normal stress the normal mismatch contribution is responsible for the asymmetry in the through-thickness distributions σ_{23} observed in Figure 5.3. The influence of the mismatch contribution on the shear stresses is directly evident from Figure 5.4, resulting in an intensification of the stress in both magnitude and gradient.

Another issue briefly addressed is that of solution accuracy as related to the number of eigenfunctions employed in the stress expressions. Several solutions have been developed

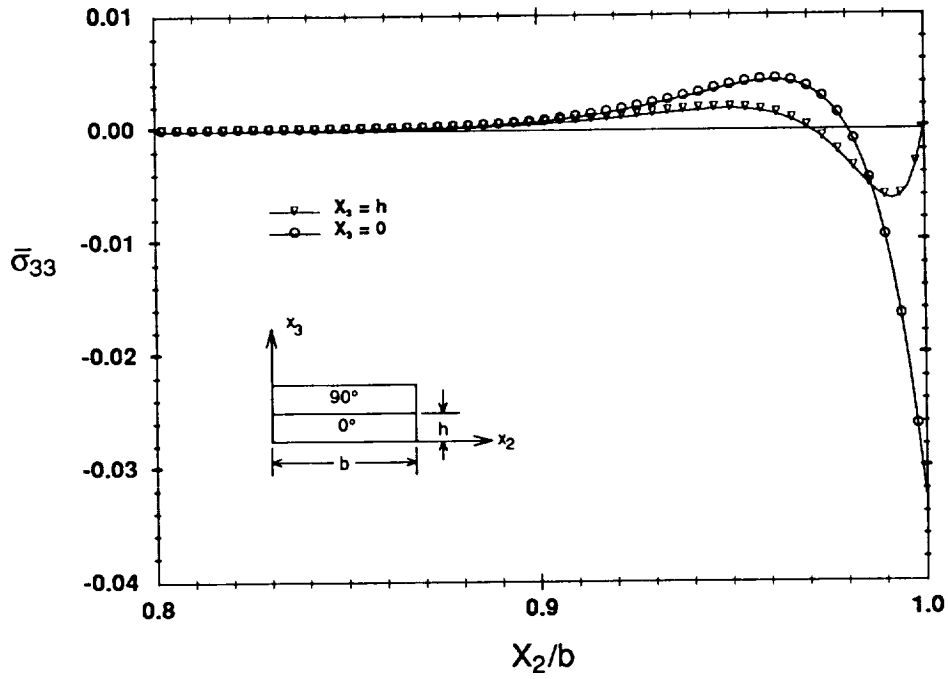

Figure 5.7. σ_{33} Stress at the 0/90 Interface and Midplane for $[90_4/0_4]_s$ Laminate - Extension

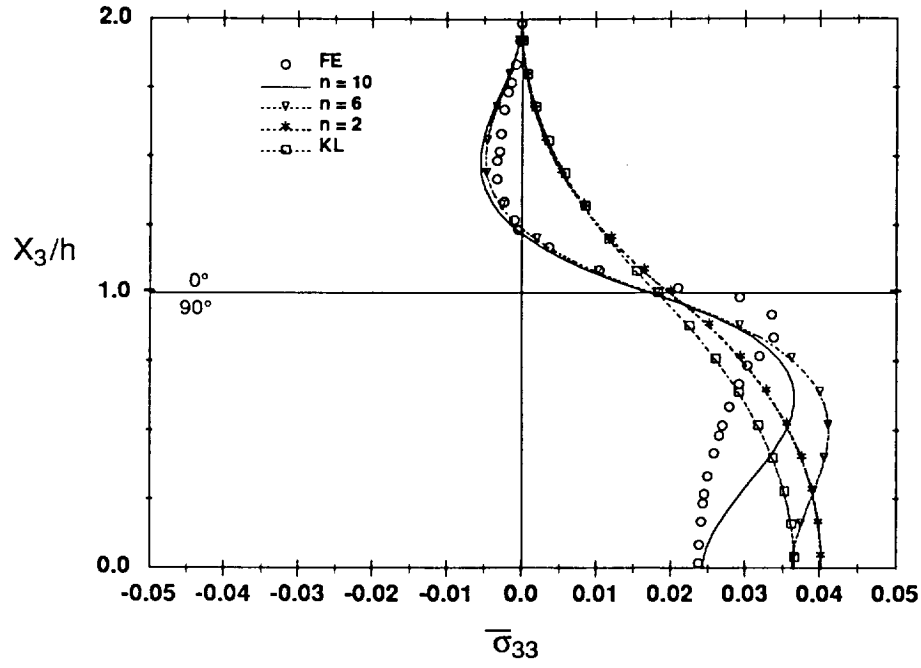

a) $[0_4/90_4]_s$ Laminate

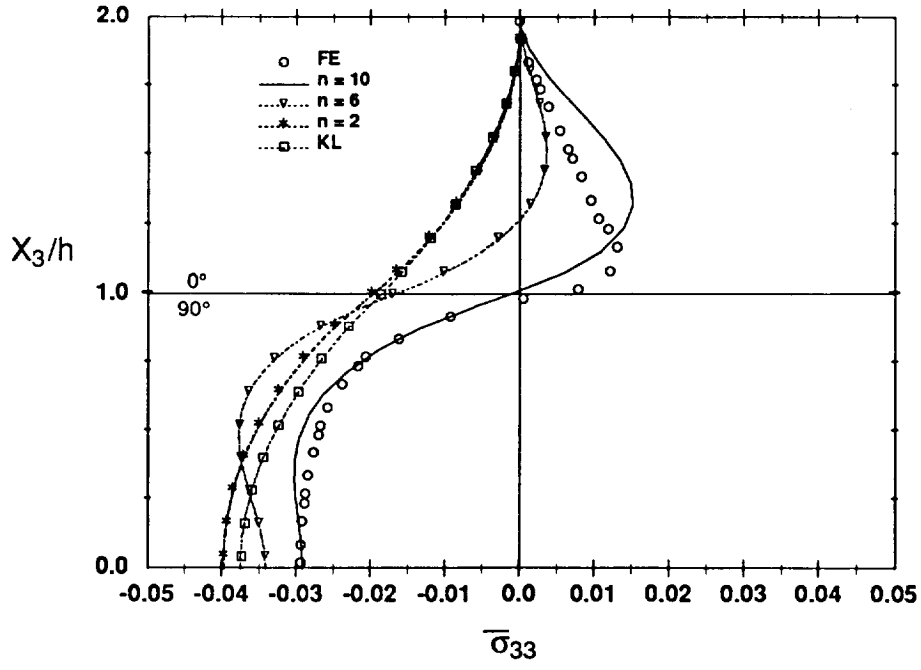

b) $[90_4/0_4]_s$ Laminate

Figure 5.8. σ_{33} Stress at $X_2/b = 0.999$ in $[0_4/90_4]_s$ and $[90_4/0_4]_s$ Laminates for n=2,6,10 - Extension

TABLE 5.4. Complementary Energy for Different Orders of Approximation

Complementary Energy for Different Orders of Approximation			
$[0_4/90_4]_s$		$[90_4/0_4]_s$	
N	$\phi_{i_c} X10^3$(lb–in.)	N	$\phi_{i_c} X10^3$(lb–in.)
n=2 (KL)	4.9696	n=2 (KL)	4.4233
2	4.8185	2	4.3325
6	4.5743	6	4.0304
10	4.429022	10	3.711539

throughout the course of this investigation, with each modification increasing the number of terms incorporated in the assumed stress states. Recall that the latest modification includes fourteen parameters in the stress expressions for the most general laminate configurations. As previously indicated, this number reduces to ten for cross-ply laminates. Figure 5.8 illustrates the variation of the interlaminar normal stress σ_{33} with $\overline{X}_3$ as computed by solutions employing two parameters (2 term solution, n=2), six parameters (n=6), and the full ten term solution (n=10). The KL solution and finite element solutions are also presented for reference. Stress expressions for the two term solution are provided in Appendix B. The stress expressions for the six term solution are identical to those given in equations (3.89-3.90) without the last terms (terms multiplying A_3). As the figure shows, the predictions of the two term solution are nearly coincident with the KL solution. The six term solution provides improved results, relative to the

finite element predictions, but still hasn't captured the differences in response of the 0/90 and 90/0 laminates. The ten term solution, as previously mentioned, captures this asymmetry.

Laminate complementary energy values have also been evaluated for the various degrees of approximation. These values are provided in Table 5.4. As the table shows, the n=10 solution gives the lowest energy of the solutions considered. No statement can be made at this point regarding solution convergence.

5.1.2 Symmetric Laminates - Bending Load

In this section distributions obtained from the present methodology and the KL solution for $[0_4/90_4]_s$ and $[90_4/0_4]_s$ laminates subjected to uniform bending loads are presented. Through-thickness and interlaminar stress distributions are provided. As was done in the previous section, through-thickness plots are presented only for the top half of the laminate, but the stress symmetry conditions about the laminate midplane are different for bending than they were for extension. In the case of uniform bending, interlaminar normal stress is antisymmetric about the midplane, and interlaminar shear stress is symmetric. Interfacial distributions are again plotted as a function of the normalized distance X_2/b from the laminate center, where b is the laminate half width. Unless otherwise noted, all stress components are normalized by $M_{11}H/2I$, where M_{11} is the far field moment, given from classical lamination theory, H is the laminate half thickness, and I is the moment of inertia of a unit width section of the laminate. The normalized stresses are denoted by $\bar{\sigma}_{33}$ and $\bar{\sigma}_{23}$.

Figures 5.9 and 5.10 show comparisons between the present solution and KL predictions for through-thickness distributions of the interlaminar normal and shear stresses at two locations near the laminate free edge. The most significant observation to be made from these figures is that both solutions predict more severe interlaminar normal and shear stresses in the $[90_4/0_4]_s$

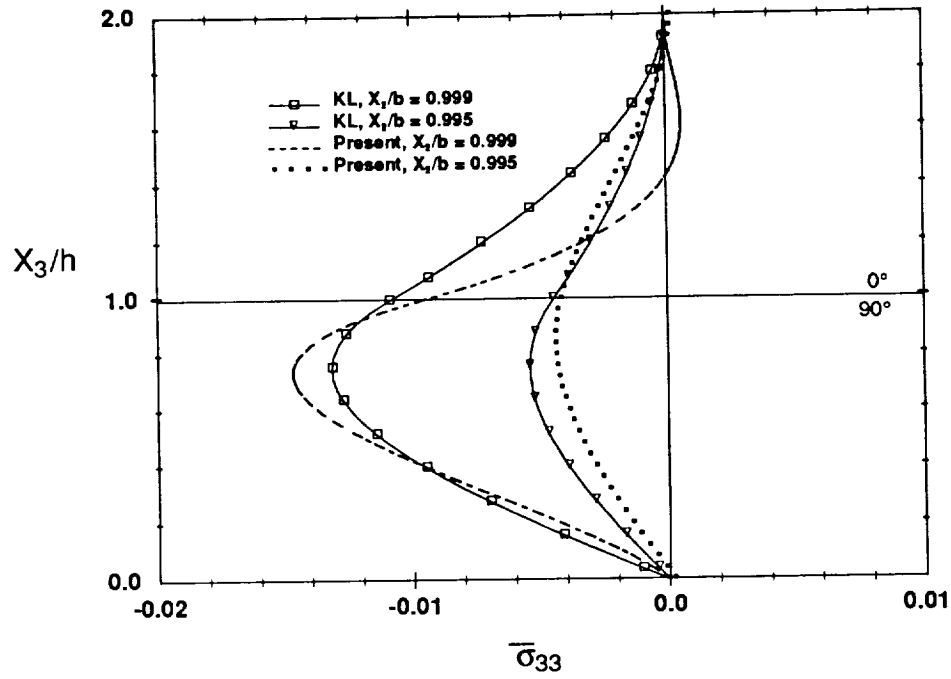

(a) $[0_4/90_4]_s$ Laminate

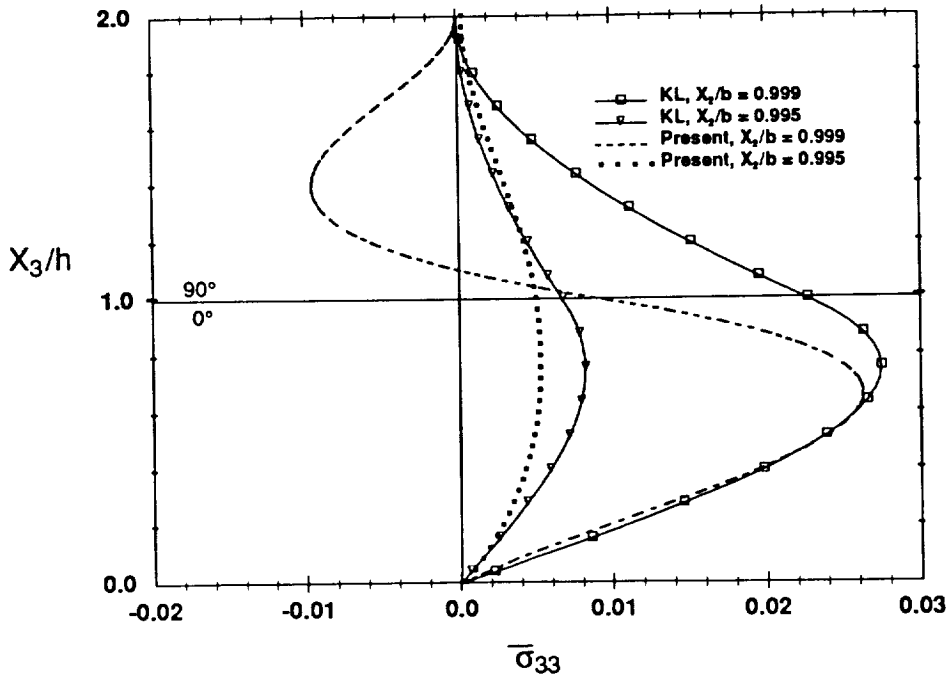

(b) $[90_4/0_4]_s$ Laminate

Figure 5.9. σ_{33} Near Free Edge in $[0_4/90_4]_s$ and $[90_4/0_4]_s$ Laminates in Bending

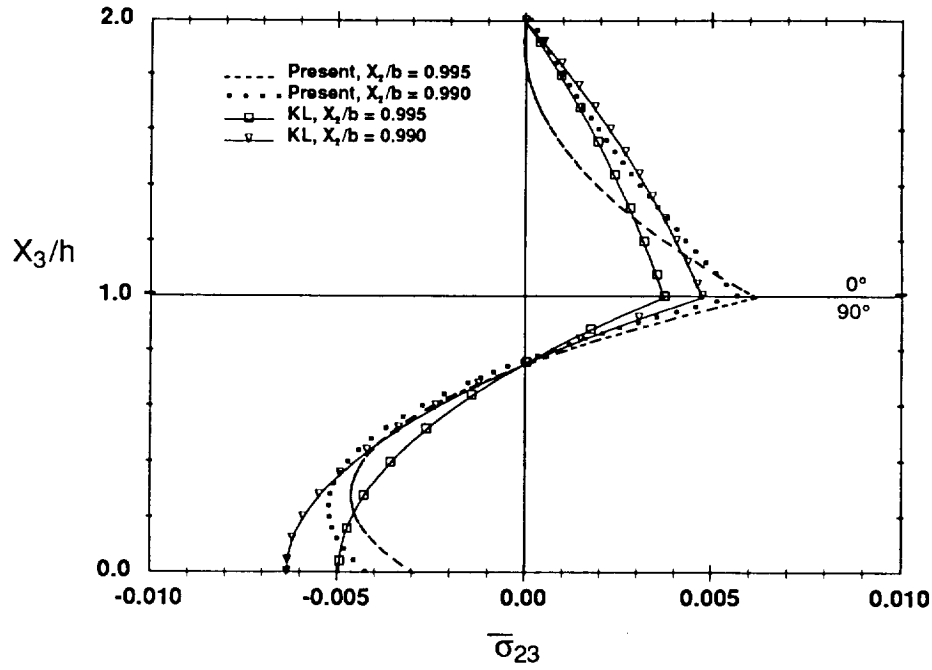

(a) $[0_4/90_4]_s$ Laminate

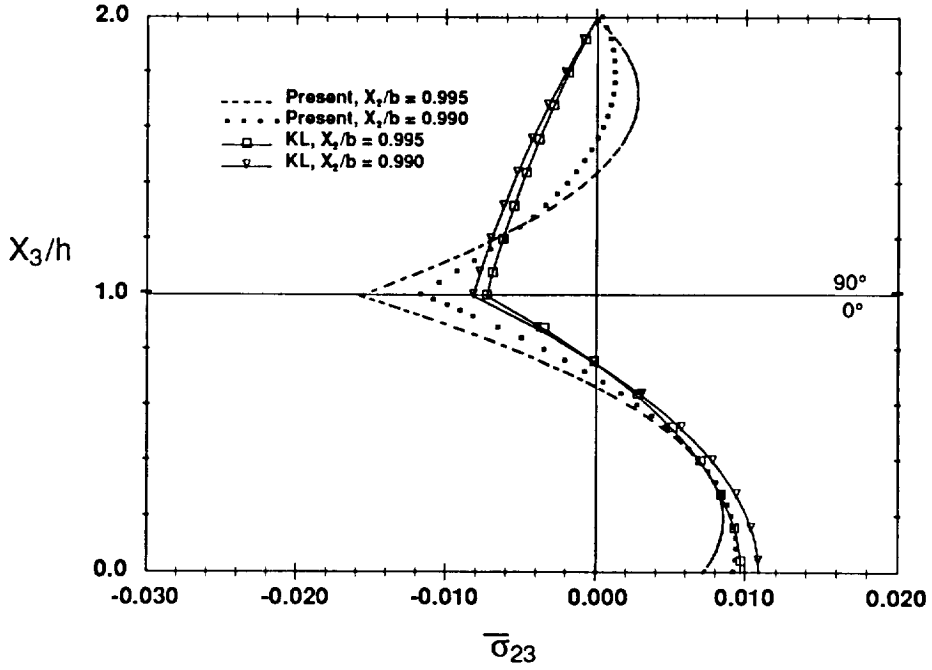

(b) $[90_4/0_4]_s$ Laminate

Figure 5.10. σ_{23} Near Free Edge in $[0_4/90_4]_s$ and $[90_4/0_4]_s$ Laminates in in Bending

laminate than in the $[0_4/90_4]_s$ laminate for the same loading, with the maximum stresses in the 90/0 configuration being nearly twice as large as those in the 0/90 layup. Physically this is expected and is fortunate, since the 0/90 laminate is much stiffer in bending and therefore preferred for such applications. The forms of the through-thickness distributions obtained by the two approaches are however different. The most noticeable differences are in the interlaminar normal stress predictions for the $[90_4/0_4]_s$ laminate at $X_2/b = 0.999$, as shown in Figure 5.9b. The present solution predicts much larger through thickness gradients than the KL solution, but the KL results show interlaminar normal stress twice as large as the present theory at the 90/0 interface. Much smaller differences are observed in the predictions of the two methods for the interlaminar normal stress in the 0/90 laminate at the same X_2 location (Figure 5.9a). In both laminates, the solutions are in much closer agreement slightly away from the edge at $X_2/b = 0.995$. The interlaminar shear stress predictions of the two methods, on the other hand, still have different forms at $X_2/b = 0.990$, as displayed in Figure 5.10.

The distributions presented in Figures 5.9 and 5.10 suggest that the mismatch effects have a stronger influence on the stress distributions in the $[90_4/0_4]_s$ laminate than in the $[0_4/90_4]_s$ laminate. This is more clearly illustrated in Figures 5.11 and 5.12 which show width distributions of both interlaminar stresses at the 0/90 interface. Figure 5.11 shows the interfacial distribution of σ_{33} for both laminates. The two methods predict essentially the same results in the $[0_4/90_4]_s$ laminate. However, the results are quite different for the $[90_4/0_4]_s$ laminate. The KL solution predicts a much steeper stress gradient, a maximum stress approximately three times larger than the present theory, and a larger stress reversal away from the free edge. The mismatch component reduces the stress at the free edge and flattens the distribution as the distance from the free edge becomes larger. Differences are also exhibited in the shear stress σ_{23} (Figure 5.12). For the $[90_4/0_4]_s$ laminate the current solution predicts maximum stress twice as

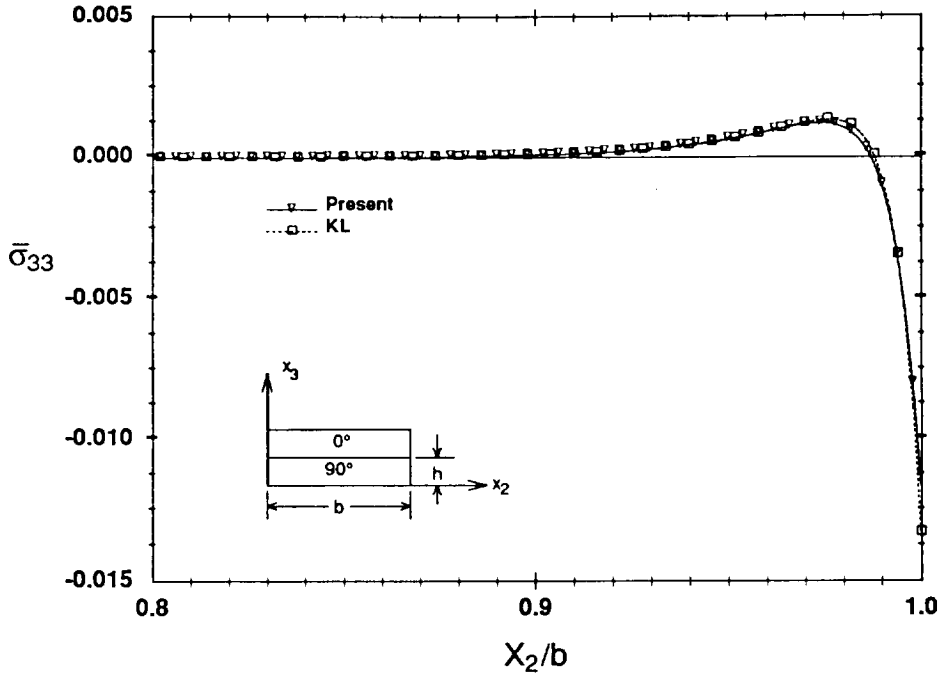

(a) $[0_4/90_4]_s$ Laminate

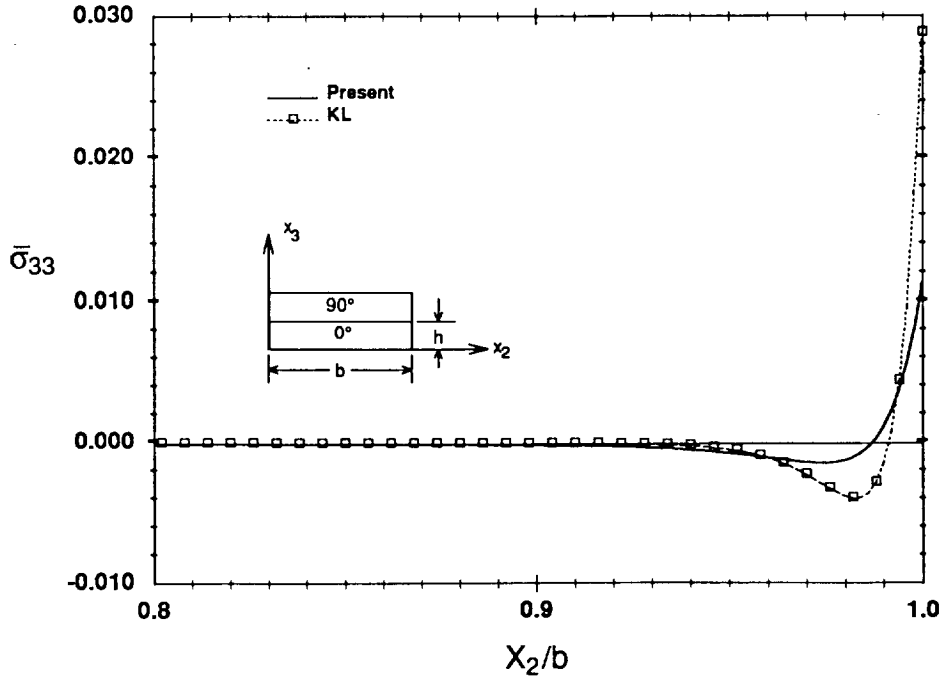

(b) $[90_4/0_4]_s$ Laminate

Figure 5.11. σ_{33} at 0/90 Interface for $[0_4/90_4]_s$ and $[90_4/0_4]_s$ Laminates in Bending

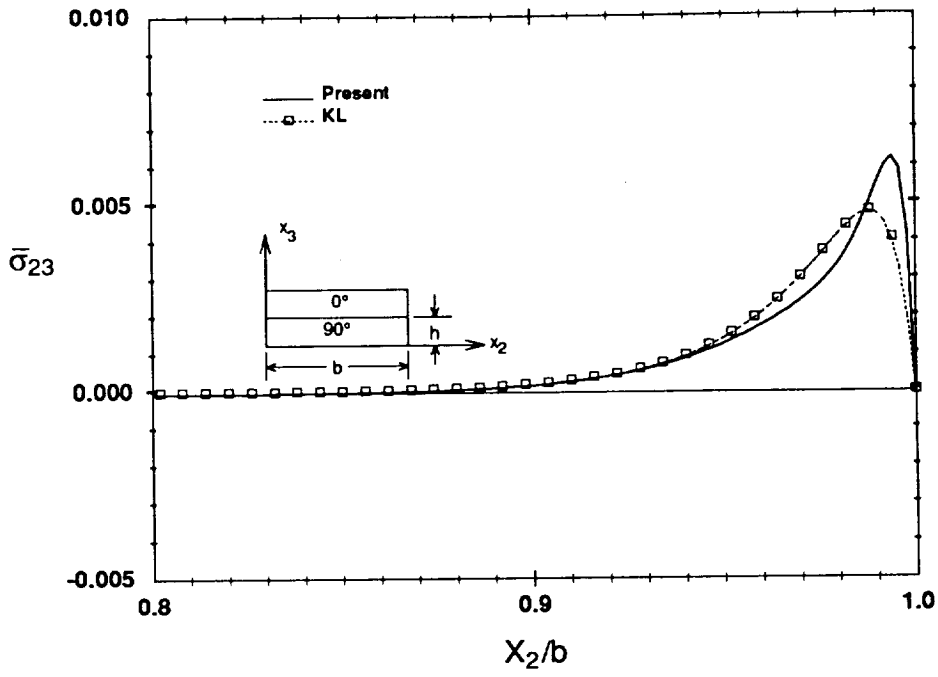

(a) $[0_4/90_4]_s$ Laminate

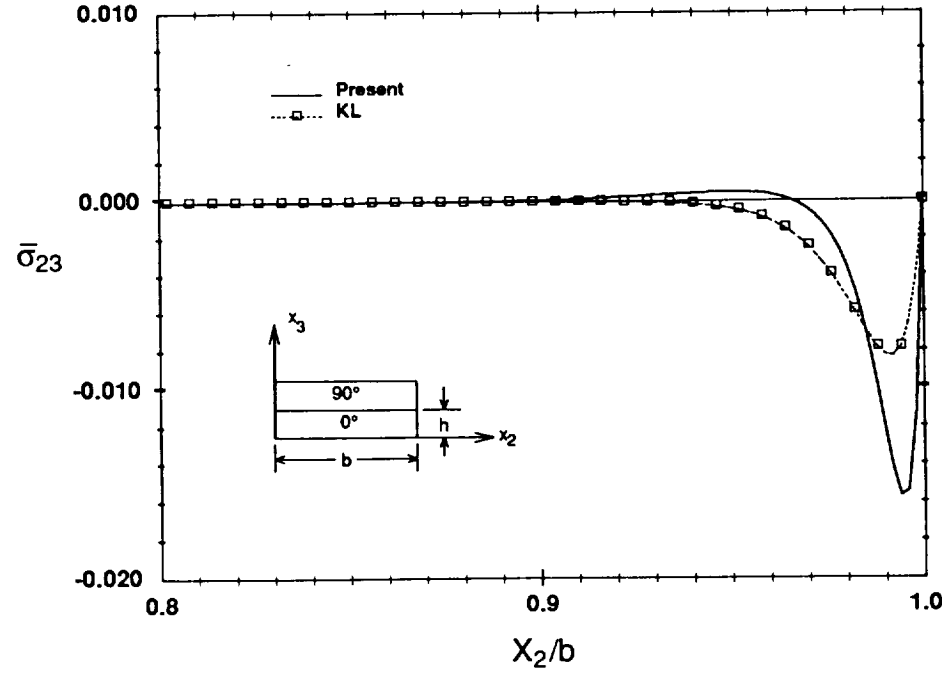

(b) $[90_4/0_4]_s$ Laminate

Figure 5.12. σ_{23} at 0/90 Interface for $[0_4/90_4]_s$ and $[90_4/0_4]_s$ Laminates in Bending

large as KL.

The above discussion in conjunction with results obtained for the extension case suggest that the additional mismatch terms included in the present theory, over those included in the KL formulation, are required for accurate analysis in some cross-ply laminates subjected to bending loads. Additional analyses and comparison with other solutions and experimental results, as they become available, are necessary to support or refute this claim.

The contributions of the various physical effects for this problem are similar to the extension case and are not discussed. Total through-thickness and interfacial distributions of stresses along with the individual contributions of global and local mismatch components are provided in Appendix C (Figures C.4 - C.7)

It is also of interest to compare the stresses developed in laminates when subjected to extension load with those that develop when the laminate is subjected to uniform bending. Here, a comparison is made between the stresses at the 0/90 interface in the $[0_4/90_4]_s$ laminate. In order to do so, a slightly different normalization scheme is used for the bending stresses than was used in the previous figures. In the following figures the bending stresses at the 0/90 interface are normalized by the average of the longitudinal stress $\tilde{\sigma}_{11}$ in the 0° and 90° plies obtained from classical lamination theory at that interface. A similar normalization was used for the axial extension load case and provides an indication of the severity of the interlaminar stresses relative to the in-plane far field stress $\tilde{\sigma}_{11}$.

Figure 5.13 shows comparisons of the 0/90 interface interlaminar normal and shear stresses for the two load cases. The shear stress distribution is very similar for both load conditions, but the character of the normal stress distribution is somewhat changed. In the bending analysis, a larger maximum normal stress is noted, and a larger stress gradient shifted toward the free edge

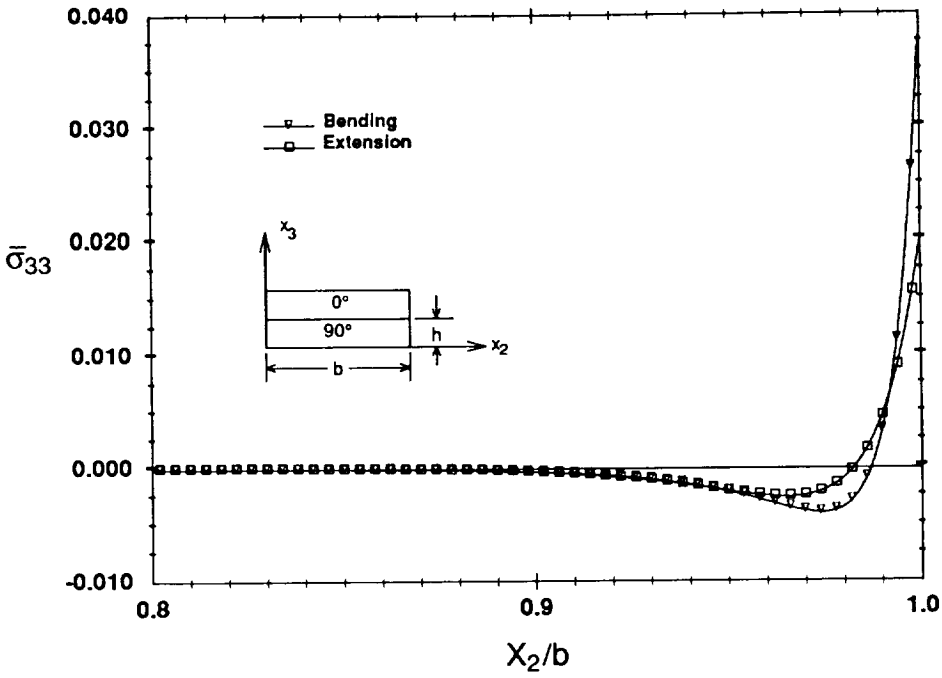

(a) Interlaminar Normal Stress

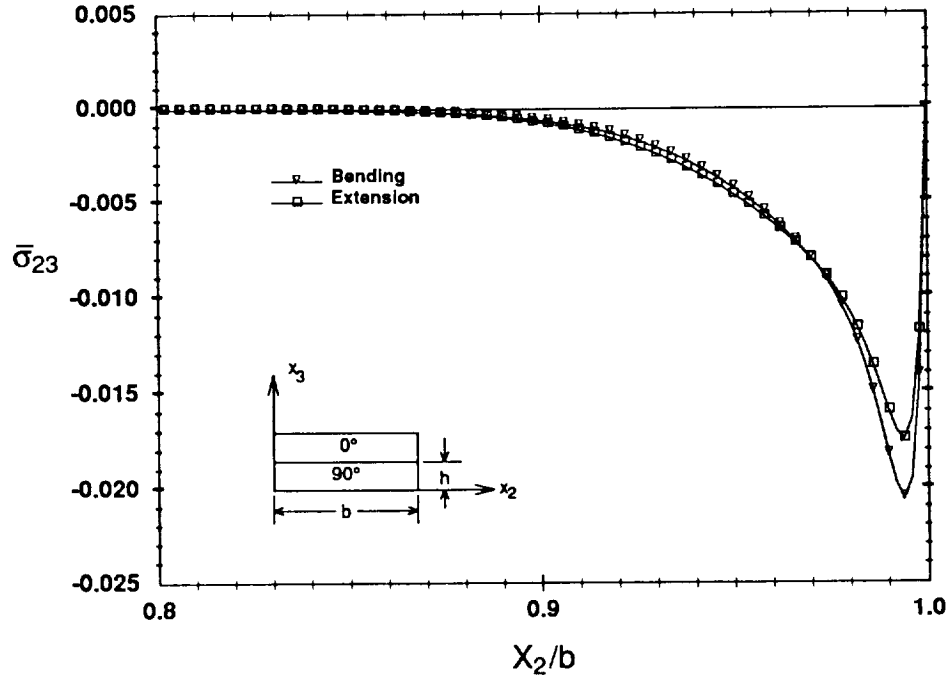

(b) Interlaminar Shear Stress

Figure 5.13. Comparison of Bending and Extension Stresses σ_{33} and σ_{23} at 0/90 Interface for $[0_4/90_4]_s$ Laminates

is observed. Further, the normal stress does not experience as large of a reversal away from the free edge in the extension case as in the bending case. The boundary layer width is approximately the same for the two load conditions. The maximum magnitude of both the interlaminar shear stress and the interlaminar normal stress occurs for the bending case.

5.1.3 Unsymmetric Laminates - Extensional Load

This section discusses results predicted by the present theory for extensional loading (N_{11}) of an unsymmetric $[0_4/90_4]_t$ laminate. Through-thickness distributions of normalized classical lamination theory in-plane stress $\bar{\sigma}_{22}$, for extensional and bending loads (to be discussed in the next section) are provided in Figure 5.14. The stresses for extensional loading are normalized by $N_{11}/2H$, and the stresses for bending loads are normalized by $M_{11}H/2I$. The linear variation of the in-plane stresses through the thickness for the extension loading results from a positive κ_{11} curvature which develops in the plate because of the laminate-membrane flexural coupling. For the bending load, the laminate develops both curvatures κ_{11} and κ_{22}.

Through-thickness distributions (for the entire laminate thickness) of the normalized stresses $\bar{\sigma}_{33}$ and $\bar{\sigma}_{23}$ near the free edge are shown in Figure 5.15. The bottom surface of the laminate is denoted by $X_3/h = -1$ and the top surface corresponds to $X_3/h = 1$. As the figure shows, shear stresses are nearly symmetric about the 90/0 interface and the normal stress is close to antisymmetric. Changing the stacking sequence from $[0_4/90_4]_t$ to $[90_4/0_4]_t$ simply results in a change in sign of the shear stress distribution. The maximum tensile normal stress occurs at $X_{3/H} \simeq 0.35$, and the maximum shear stress develops at the 90/0 interface.

Figure 5.16 illustrates the character of the interfacial distributions of normal and shear stress along the 0/90 interface. Note that a solution based entirely upon overall equilibrium, predicts zero interlaminar normal stress at this interface. Recall that the interfacial normal stress, or the

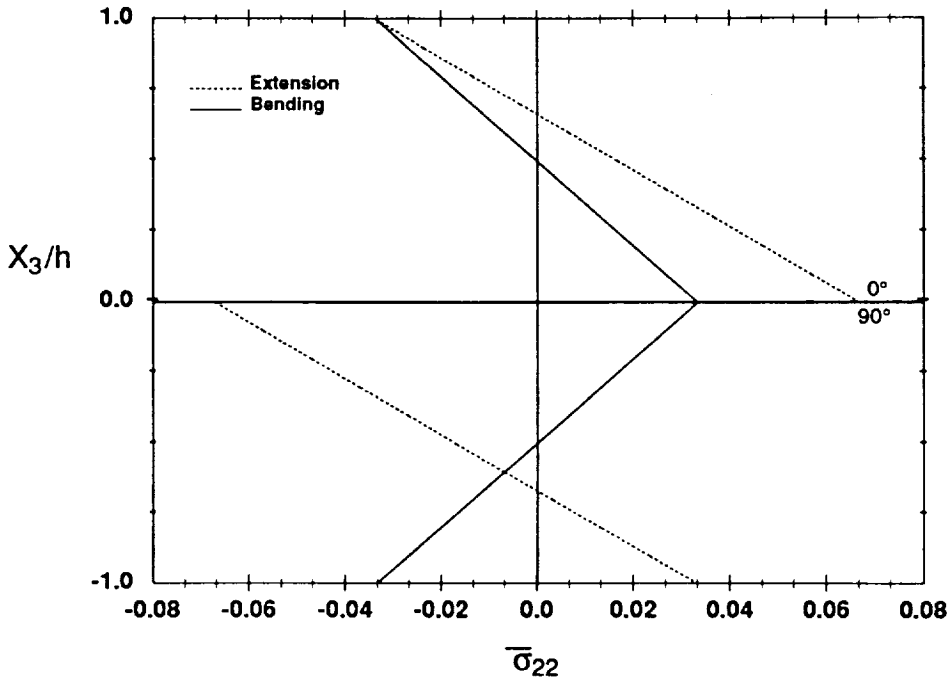

Figure 5.14. Through-Thickness $\tilde{\sigma}_{22}$ for $[0_4/90_4]_t$ Laminate for Bending and Extension Loads

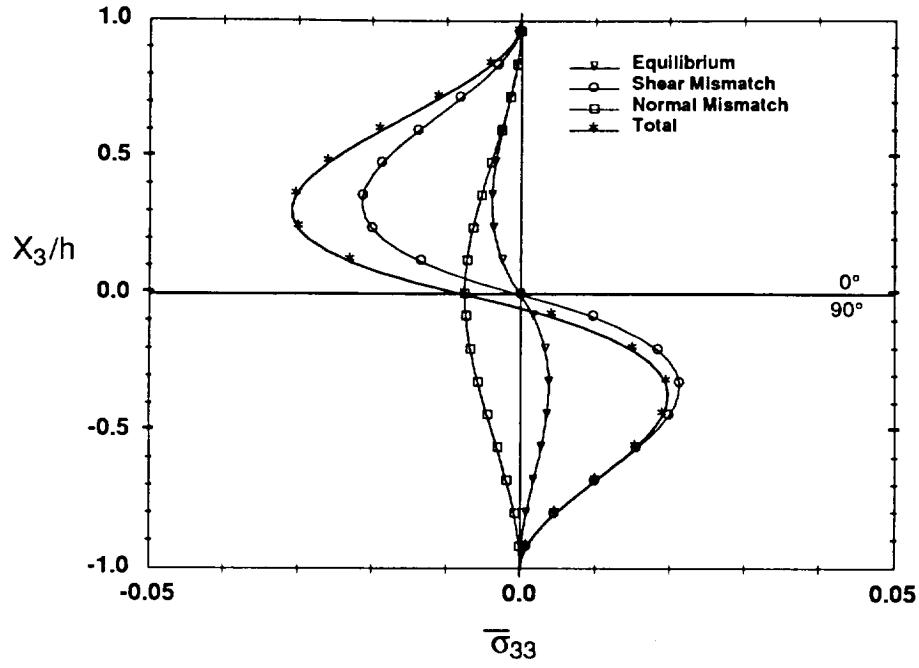

(a) σ_{33} at $X_2/b = 0.999$

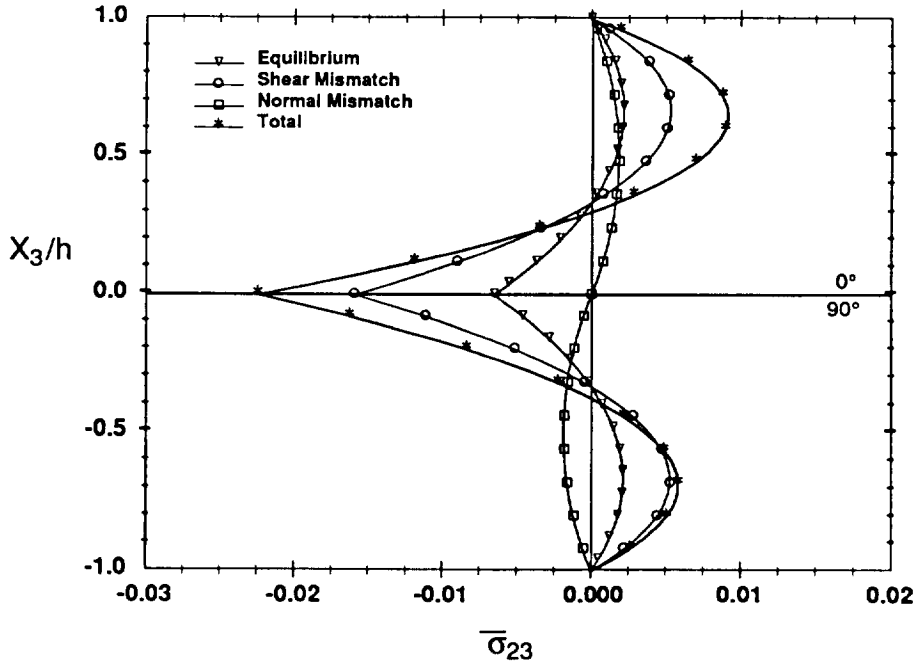

(b) σ_{23} at $X_2/b = 0.993$

Figure 5.15. σ_{33} and σ_{23} Near Free Edge for $[0_4/90_4]_t$ Laminate - Extension Load

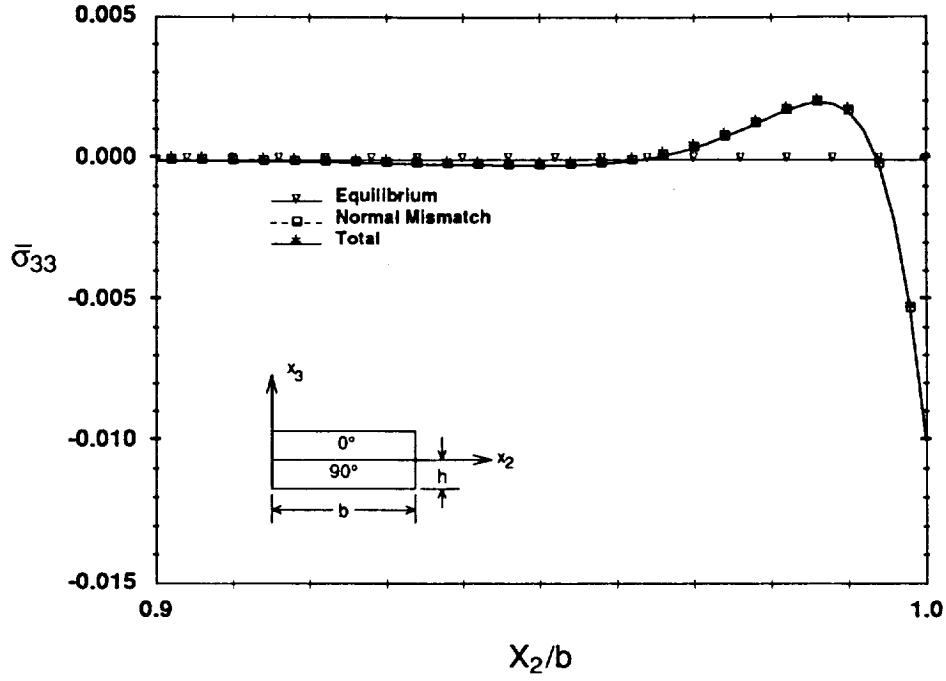

(a) Interlaminar Normal Stress

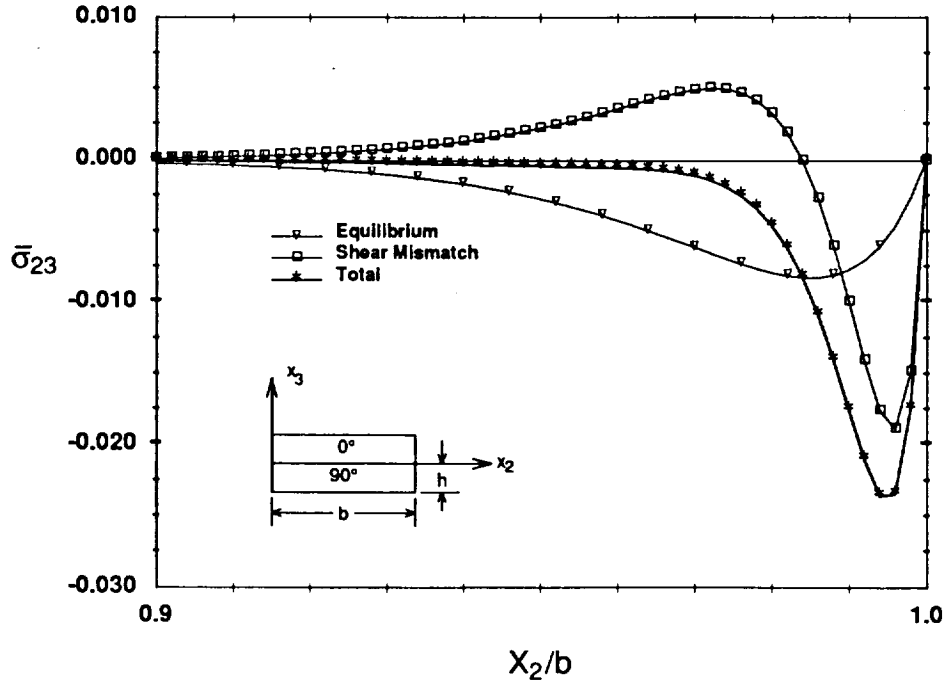

(b) Interlaminar Shear Stress

Figure 5.16. σ_{33} and σ_{23} at 0/90 Interface for $[0_4/90_4]_t$ Laminate - Extension Load

normal stress at any z-location predicted by the equilibrium solution, is proportional to the moment of the in-plane transverse stresses $\tilde{\sigma}_{22}$ about an axis parallel to the longitudinal axis X_1, lying in the X_1-X_3 plane of interest. This moment is represented by the term $B_7(k)$ in equation (3.90). As can be seen from Figure 5.14, moment equilibrium is satisfied by the lamination theory stresses at the 0/90 interface; that is $B_7(k)$ is zero there. Interlaminar normal stresses are therefore not required at this interface for sublaminate equilibrium, but arise solely from local mismatch effects. As it turns out, the mismatch contribution is not critical for the load case considered, but it may be significant for compression loading, or in a combined loading situation. For the interlaminar shear stress (Figure 5.16b), mismatch and equilibrium effects both contribute at the 0/90 interface. The mismatch contribution shifts the peak total shear stress toward the free edge and results in larger maximum stress and steeper gradient than predicted by a solution based on equilibrium considerations alone. As a result, shear stresses predicted by the present theory are distributed over a smaller portion of the 0/90 interface than an equilibrium solution would indicate.

5.1.4 Unsymmetric Laminates - Bending Load

In order to illustrate the influence of load conditions on the interlaminar stress state, an analysis has also been conducted for uniform bending of the unsymmetric $[0_4/90_4]_t$ laminate. Comparison of through-thickness distributions for the extensional (Figure 5.15) and bending (Figure 5.17) load cases indicates larger through-thickness gradients and larger normalized interlaminar stresses for extensional loading. However, for the bending load case, the maximum normalized interlaminar normal stress occurs near the 0/90 interface, and is larger at the 0/90 interface than in the extension case. This stress is tensile if the stacking sequence is reversed, or equivalently, if the direction of the applied moment is changed. Consequently, bending may

represent the more severe loading case, in terms of delamination, for this laminate configuration.

Interfacial distributions for the contributions of the various physical effects are clearly delineated in Figure 5.18. In contrast to the extensional loading case, mismatch and equilibrium effects contribute to the normal stress at the 0/90 interface, but the equilibrium contribution to the shear stress is zero. The interlaminar shear stress at this interface results from mismatch considerations alone, and is distributed over the laminate width with the self-equilibrating form shown in Figure 5.18b. The mismatch contribution to the normal stress tends to flatten the total distribution and reduces the maximum stress at the free edge from that predicted by the equilibrium contribution.

5.1.5 Unsymmetric Laminates - Combined Load

The results of the previous two sections can be superposed to obtain results for a variety of combined load conditions, and examination of the figures together provides some insight into the types and combinations of loading that will magnify the interlaminar stresses or make them less severe. One loading condition of interest is that which produces constant strain ε_{11} and zero curvature κ_{11} in the laminate, since this type of condition allows for direct comparison with symmetric laminates subjected to uniform end extension. Under such a loading, the laminate will assume a pure cylindrical shape, with curvature K_{22}. As Norwood[76] has discussed, the upper half of a $[0/90]_s$ laminate is equivalent to an unsymmetric $[0/90]_t$ laminate constrained from deflecting out of plane by the restraint $u_3(X_1, X_2, 0) = 0$ applied to its lower surface when uniformly extended. Comparison of the interlaminar stress distributions for these two laminates then gives an indication, within the limits of linear theory, of the influence of the out-of-plane deflections on the severity of the interlaminar stresses.

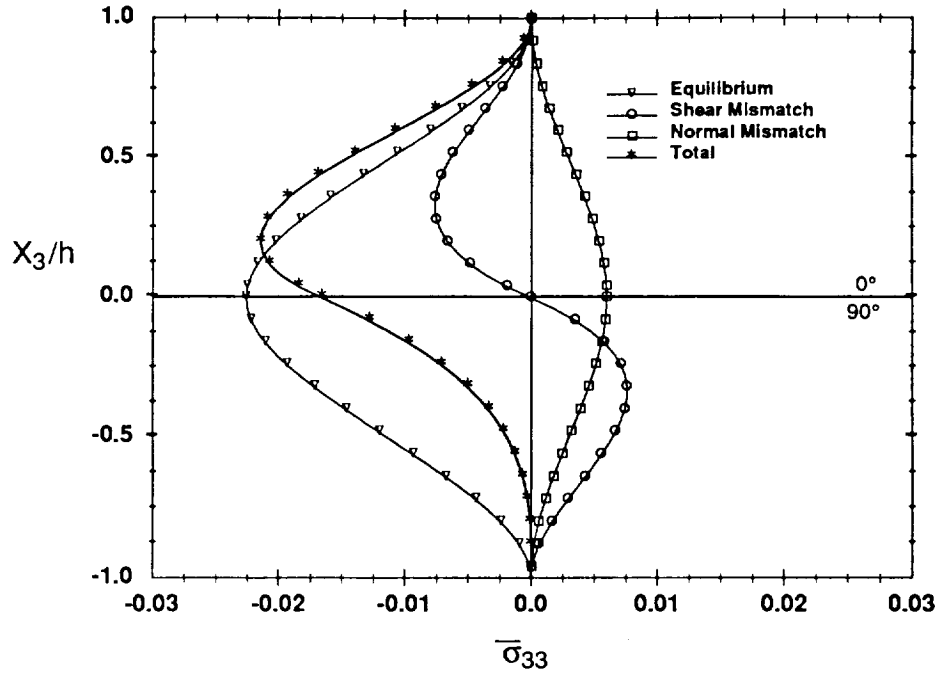

(a) σ_{33} at $X_2/b = 0.999$

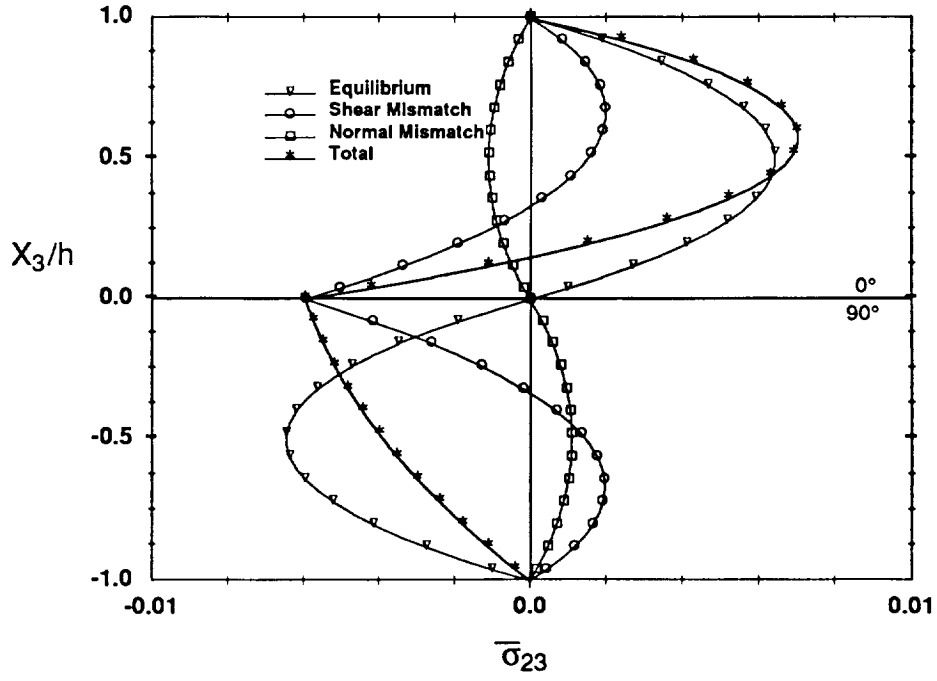

(b) σ_{23} at $X_2/b = 0.993$

Figure 5.17. σ_{33} and σ_{23} Near Free Edge for $[0_4/90_4]_t$ Laminate - Bending Load

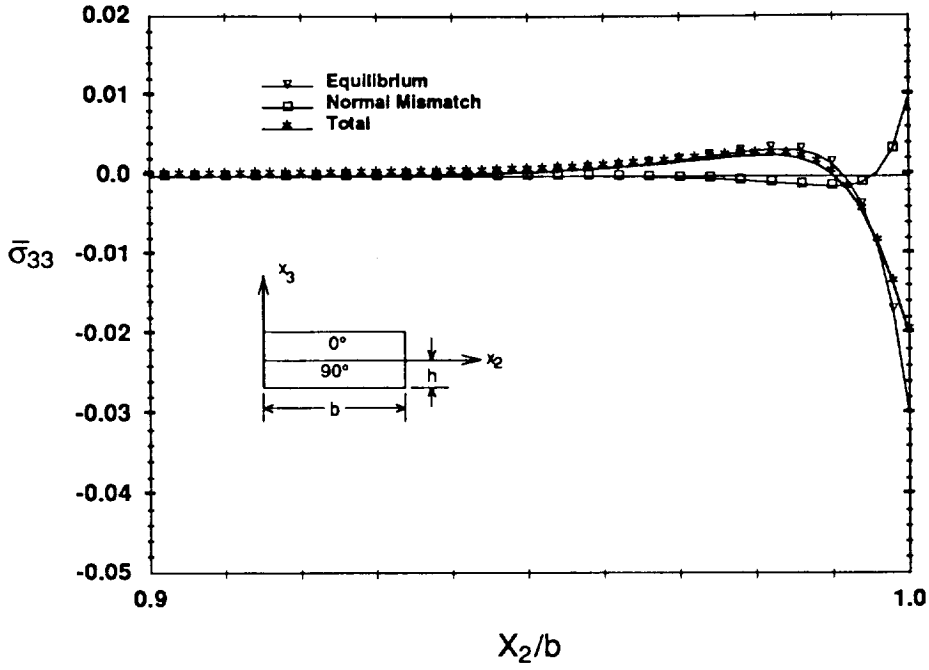

(a) Interlaminar Normal Stress

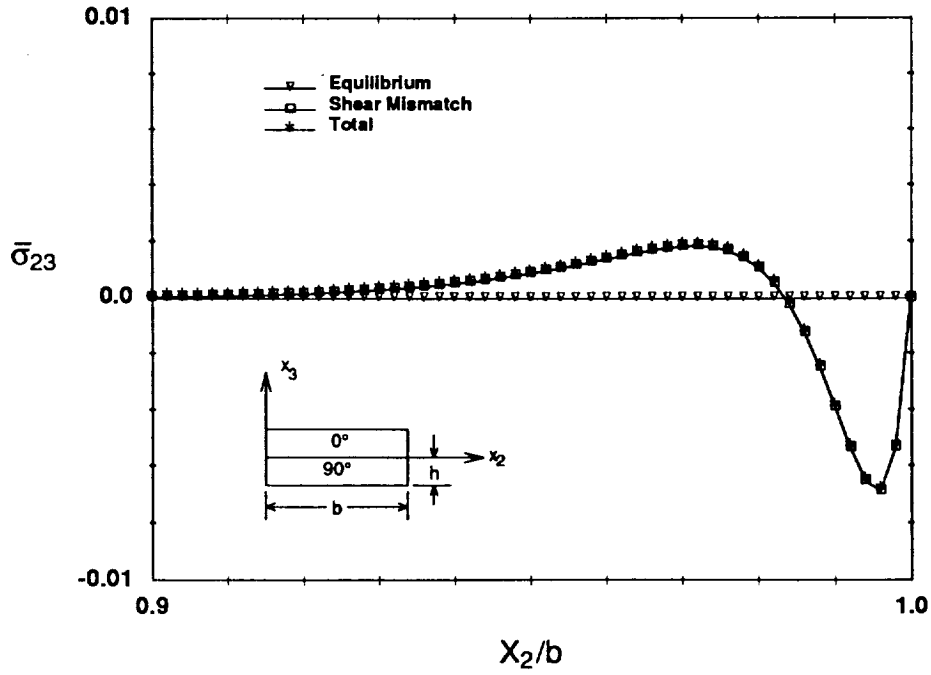

(b) Interlaminar Shear Stress

Figure 5.18. σ_{33} and σ_{23} at 0/90 Interface for $[0_4/90_4]_t$ Laminate - Bending Load

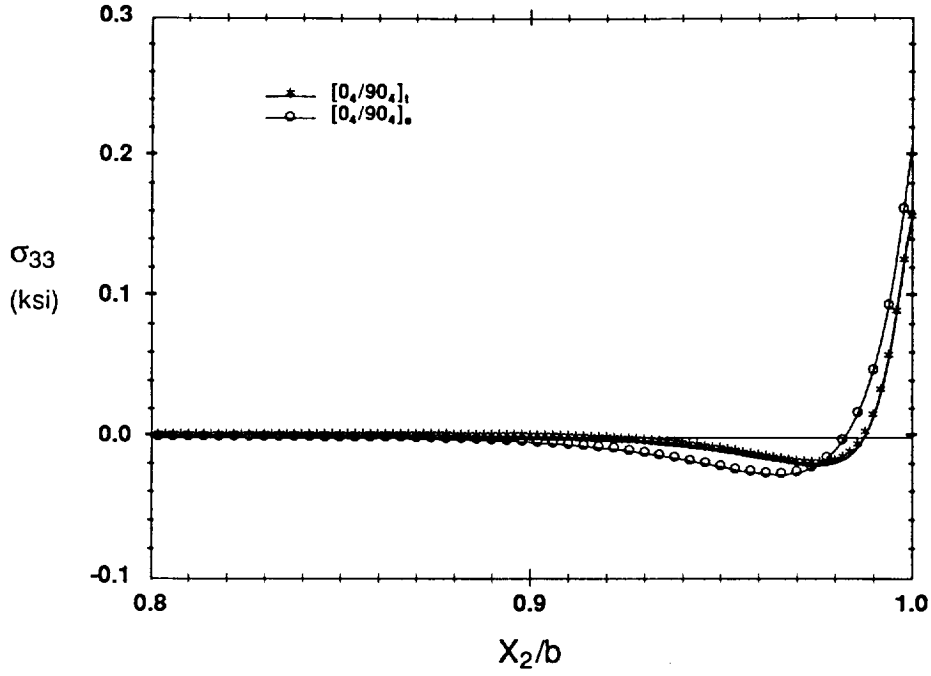

(a) Interlaminar Normal Stress

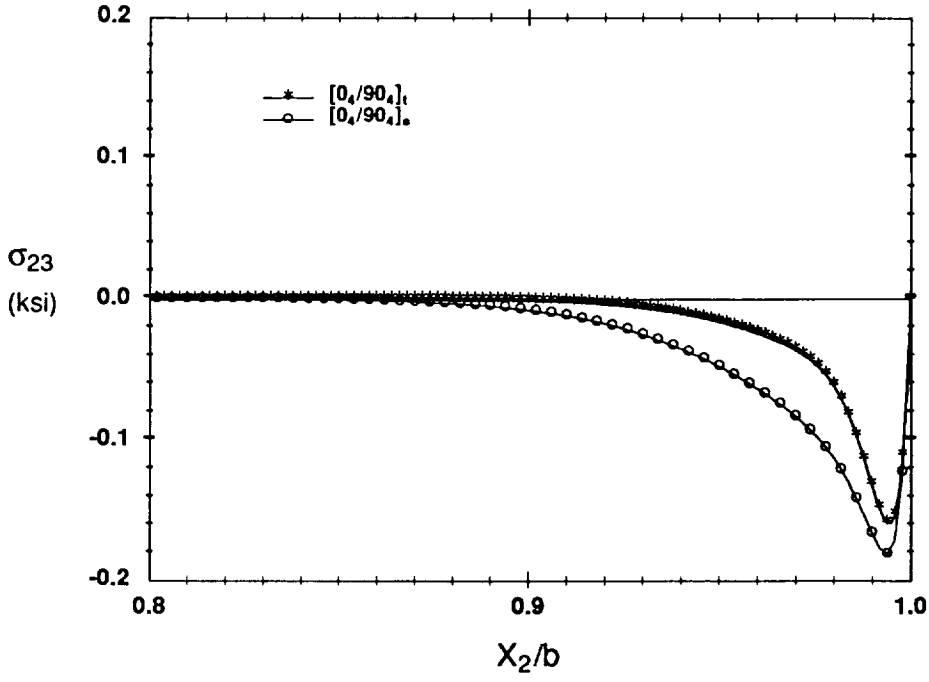

(b) Interlaminar Shear Stress

Figure 5.19. σ_{33} and σ_{23} Stress at 0/90 Interface for $[0_4/90_4]_s$ and $[0_4/90_4]_t$ Laminates ($\varepsilon_{11} = 0.1\%$)

Stress distributions along the 0/90 interface of $[0_4/90_4]_s$ and $[0_4/90_4]_t$ laminates are provided in Figure 5.19. The maximum interlaminar normal stress at the free edge is tensile in both laminates (Figure 5.19a). The distribution for the unsymmetric laminate is, however, flatter away from the free edge than in the symmetric laminate, and attains a lower peak value. The maximum σ_{33} predicted by the present theory in the unsymmetric laminate is 24% smaller than that obtained for the symmetric laminate. Similar observations are made for the interlaminar shear stress σ_{23} (Figure 5.19b). In both laminates the shear stress rises sharply as the free edge is approached and then decreases rapidly to satisfy the traction free boundary condition. The stress gradient in the unsymmetric laminate is seen to be slightly larger than in the symmetric laminate, but as was the case for the normal stress, the maximum shear stress is smaller in the unsymmetric laminate. The largest σ_{23} predicted by the present theory is approximately 12% percent smaller in the unsymmetric laminate than in the symmetric laminate. The predicted trends are in agreement with those predicted by Norwood,[76] using a finite element analysis, and with his conclusion that interlaminar normal stress and shear stress "in the unsymmetric $[0_4/90_4]_t$ laminate are relieved by out of plane deflections"[76].

5.2 Angle-Ply Laminates

In contrast to cross-ply laminates, angle-ply laminates, with individual laminae oriented at angles $+\theta$ and $-\theta$ to the global axis isolate the influence of local mismatch in coefficient of mutual influence on the interlaminar stresses, since Poisson's ratios are identical for the $+\theta$ and $-\theta$ layers. Results are presented only for the extension of symmetric angle-ply laminates because of difficulties encountered when analyzing some angle-ply laminates subjected to bending load, and unsymmetric angle-ply laminates subjected to extension loads. Before presenting the results for the symmetric laminates a brief discussion of the nature of this problem

is provided.

In laminates where there is large local mismatch in coefficient of mutual influence between adjacent layers, in combination with a curvature κ_{12} the numerical solution of the non-linear system of equations became unstable, and jumped back and forth between two widely spaced solutions. One of the solutions made sense physically, but the other led to extremely small decay rates. This was found to be the case for both symmetric laminates subjected to bending loads and unsymmetric laminates under uniform extension. Incidentally, this problem was not restricted to angle-ply laminates. The solution for a $[0/30]_s$ laminate subjected to uniform bending, for instance would not converge, while no problems were encountered with a $[0/75]_s$ laminate. The difference in these laminates is the magnitude of the local mismatch in coefficient of mutual influence and the curvature κ_{12}.

Unfortunately, the source of the problem is still unknown, but a few possible explanations are proposed. First, it is possible that some inconsistencies may have been introduced into the analysis by the manner in which the end conditions are being applied. Currently, displacements in the axial direction (u_1) are prescribed and the other displacements are taken to be zero, simulating the conditions that would be present in an end gripped specimen. This is in effect introducing an axial dependence on the stresses that might be more severe for cases where κ_{12} is large. Another approximation made, that may loose validity when large curvatures are present, is the assumption that only half of the laminate width needs to be modeled. However, the KL solution runs for all of these laminates. This suggests that if the above mentioned approximations are the source of the problem, the errors introduced by making them are magnified by the additional terms associated with coefficient of mutual influence mismatch that are incorporated in the current solution. Or there may be an error in the computer program associated with terms involving the product of the coefficient of mutual influence mismatch and

linearly varying stresses due to κ_{12}. Finally, there is the possibility that the problem is purely numerical.

5.2.1 Symmetric Laminates - Uniform Extension

For the uniform extension of symmetric angle-ply laminates, the transverse in-plane stresses $\bar{\sigma}_{22}$ from classical lamination theory are zero. Thus, interlaminar normal stress σ_{33} and shear stress σ_{23} are not required for equilibrium, and have been shown to be small compared with σ_{13}. The present theory and KL solution predict identically zero σ_{23} and σ_{33}, so the discussion that follows will focus on the effects of fiber orientation and stacking sequence on interlaminar shear stress σ_{13}. Results are presented for two different stacking sequences - clustered $[+\theta_2/-\theta_2]_s$ and alternating $[(\pm\theta)_2]_s$ - of angle-ply laminates with $\theta = 10°$. To achieve the same level of local mismatch contribution for all laminates, a through-thickness decay length of one ply thickness ($h = 0.005$) was used. For the clustered laminate this decay length corresponds to representing each layer as two sublayers of equal thickness. The decay lengths and remaining constants in the assumed stress states are provided in Table 5.5. For the angle-ply laminates, the only constants of interest are ϕ_1, ϕ_3, λ_2, and A_1, and the results of the study indicate $\phi_1 = \phi_3$. As previously discussed, this reduced number of constants is a reflection of the fact that the approximate solution predicts σ_{13} to be the only non-zero interlaminar stress component for angle-ply laminates subjected to extensional load. Classical lamination theory stresses for the two laminates are provided in Table C.3.

Through-thickness distributions of the interlaminar shear stress σ_{13} at $X_2/b = 0.999$ for the two different stacking sequences are provided in Figure 5.20. In this figure, and subsequent figures, stresses are normalized by the average applied far field stress, $N_{11}/2H$. Normalized stresses are denoted with an overbar. The results in Figure 5.20a for a $[(+10)_2/(-10)_2]_s$ show

TABLE 5.5. Solution Parameters for Angle-Ply Laminates

Solution Parameters For Angle-Ply Laminates		
Constant	$[(\pm 10)_2]_s$	$[10_2/-10_2]_s$
ϕ_2 (1/in)	120.7	109.3
λ_2	4.135	3.727
$A_1 X 10^{-5}$	2.145	2.060
h (in)	0.020	0.020

reasonably good correlation between all three methods. Similar results were obtained for other "clustered" angle-ply laminates with stacking sequence of the type $[(+\theta)_2/(-\theta)_2]_s$. Recall that the interfacial shear stress σ_{13} predicted by the KL solution is proportional to the through-thickness integral of the in-plane shear stresses $\tilde{\sigma}_{12}$ above or below the interface of interest. This integral is represented by the force sum $B_5^{(k)}$ in equation (3.87). For the clustered family of laminates this force sum is non-zero at all locations X_3, and sub-laminate equilibrium requires the interlaminar shear stresses be non-zero throughout the laminate thickness.

On the other hand, in "alternating" angle-ply laminates (Figure 5.20b) equilibrium is satisfied at the second interface by the lamination theory stresses, that is $B_5^{(k)}$ is zero there. Consequently, interlaminar stresses are not required for equilibrium and the KL solution predicts identically zero shear stress σ_{13} at this interface, while the modified solution of the present study and finite element model predict shear stress of considerable magnitude. These large local interlaminar shear stresses can be attributed to the large mismatch in $\eta_{xy,x}$ at the $-\theta/\theta$ interface. Also note

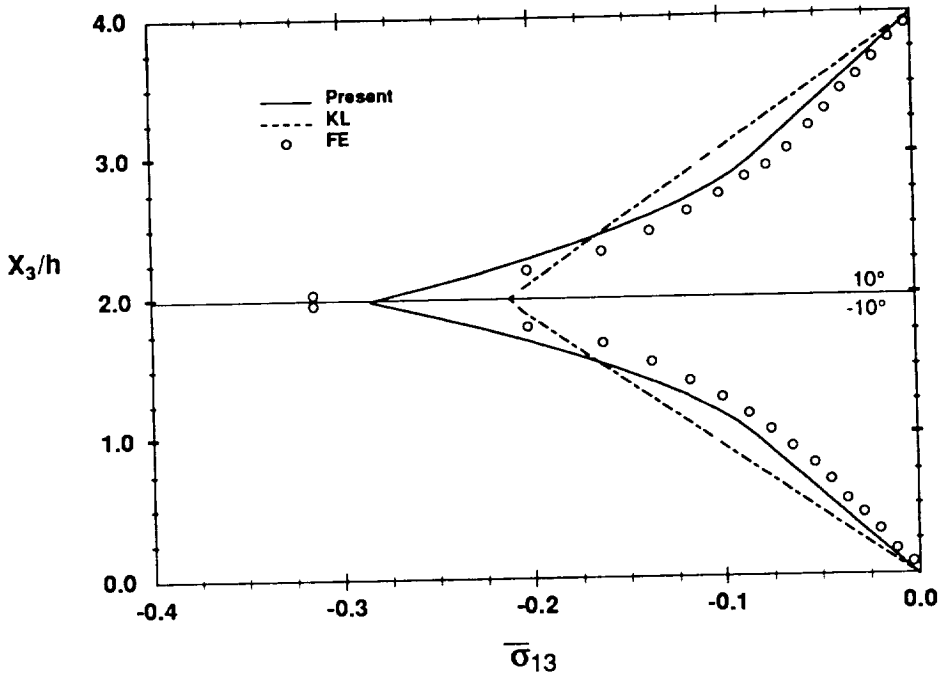

(a) Clustered Layers

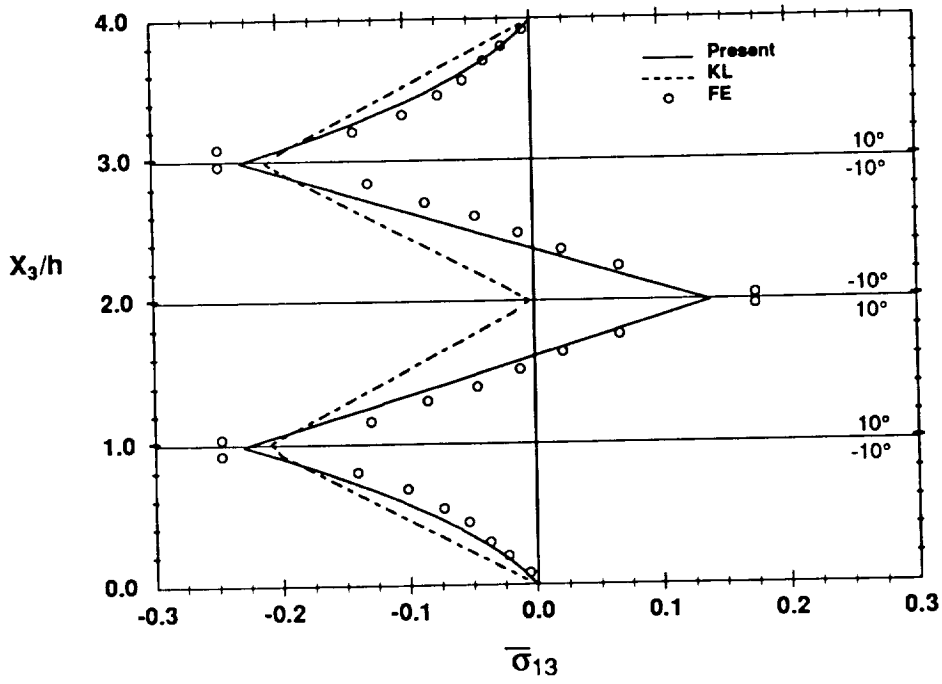

(b) Alternating Layers

Figure 5.20. σ_{13} at $X_2/b = 0.999$ for $[(+10)_2/(-10)_2]_s$ and $[(\pm 10)_2]_s$ Laminates - Extension

that σ_{13} is large at the 10/-10 interface, having a magnitude of 0.25 times the average applied stress. The stress is large because the the mismatch in $\eta_{xy,x}$ is large. As shown subsequently, the shear stresses decrease for larger fiber angles as the mismatch in $\eta_{xy,x}$ decreases.

The relative contributions of the two physical effects for this problem are depicted in Figure 5.21 where the total through-thickness distributions of σ_{13} are presented along with distributions of the global and local mismatch contributions to the stress field. It is clear from Figure 5.21 that for the layer discretization used to obtain these results, i.e. representing each layer as two sublayers with thicknesses equal to one ply thickness, there is no local mismatch contribution in the top and bottom halves of the first and second layers, respectively, whereas global mismatch or equilibrium contributes throughout. As discussed previously, the through-thickness extent of the local mismatch contribution to the stress field is governed by the thickness of the sublayers adjacent to interfaces where a mismatch in material properties is present. In contrast to the clustered configuration, both equilibrium and mismatch contribute throughout all layers of the $[(\pm 10)_2]_s$ laminate (Figure 5.21b). Again, the extent of the mismatch contribution would be changed if different "sublayer" thicknesses were used.

Interlaminar distributions of σ_{13} along interfaces in the $[(\pm 10)_2]_s$ laminate are presented in Figures 5.22 and 5.23. Figure 5.22 shows the predictions of the present solution, the KL solution and finite element analysis along the first and second interfaces of the laminate. The three methods compare quite well at the first interface (Figure 5.22a), but only the present solution and finite element results agree along the second interface. As discussed above, the KL solution predicts zero shear stress σ_{13} along the entire second interface, and the total stress results solely from local mismatch effects. In Figure 5.23 the distributions of the total shear stress and the individual mismatch contributions along the first interface are delineated. The local mismatch distribution is self-equilibrating, integrating to zero over X_2, while the

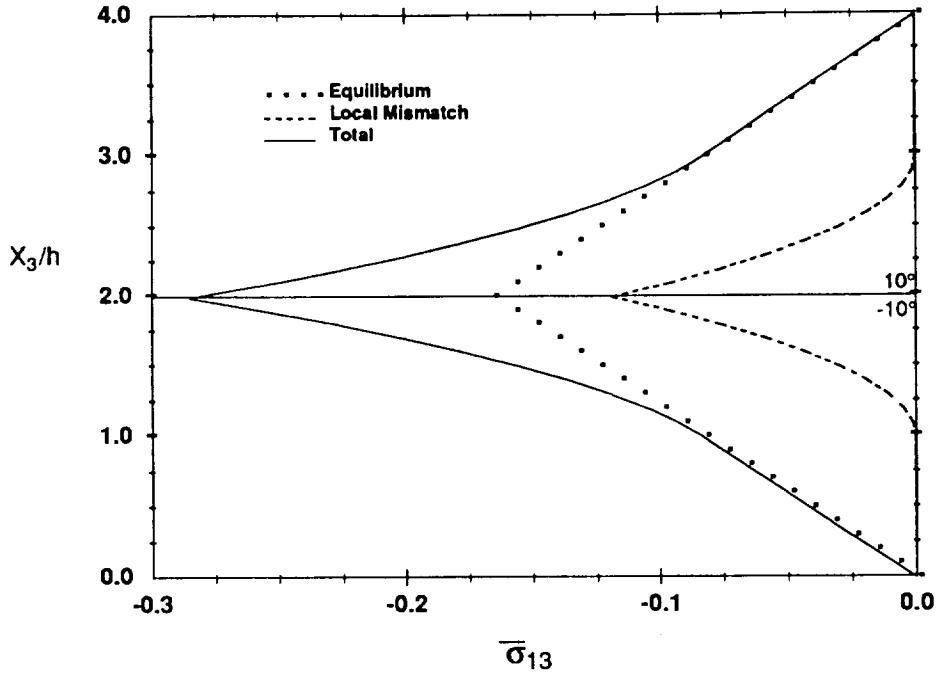

(a) Clustered Layers

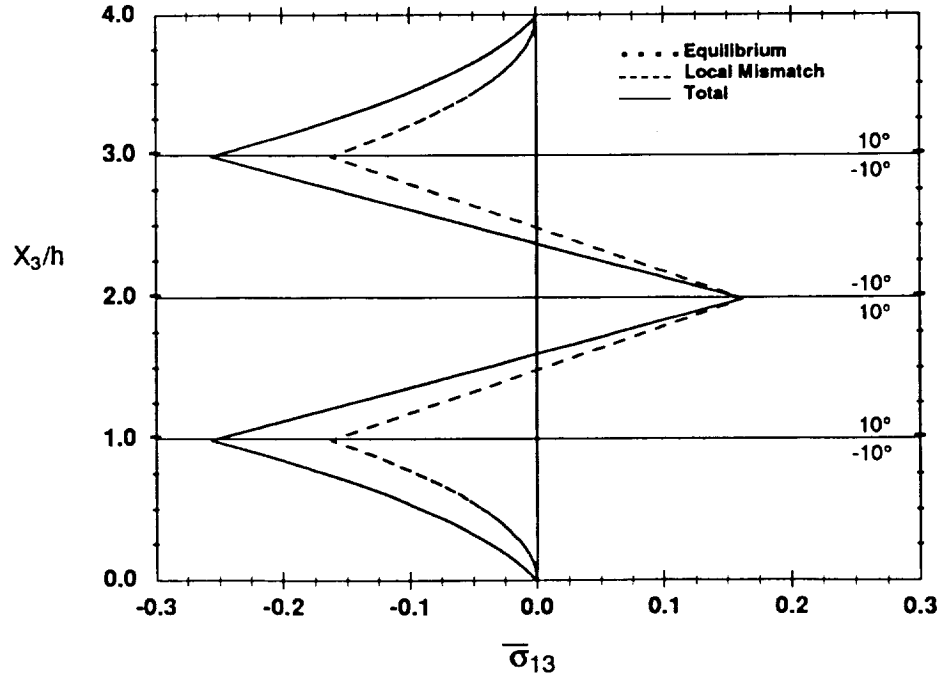

(b) Alternating Layers

Figure 5.21. Contributions to σ_{13} in $[(+10)_2/(-10)_2]_s$ and $[(\pm 10)_2]_s$ Laminates - Extension

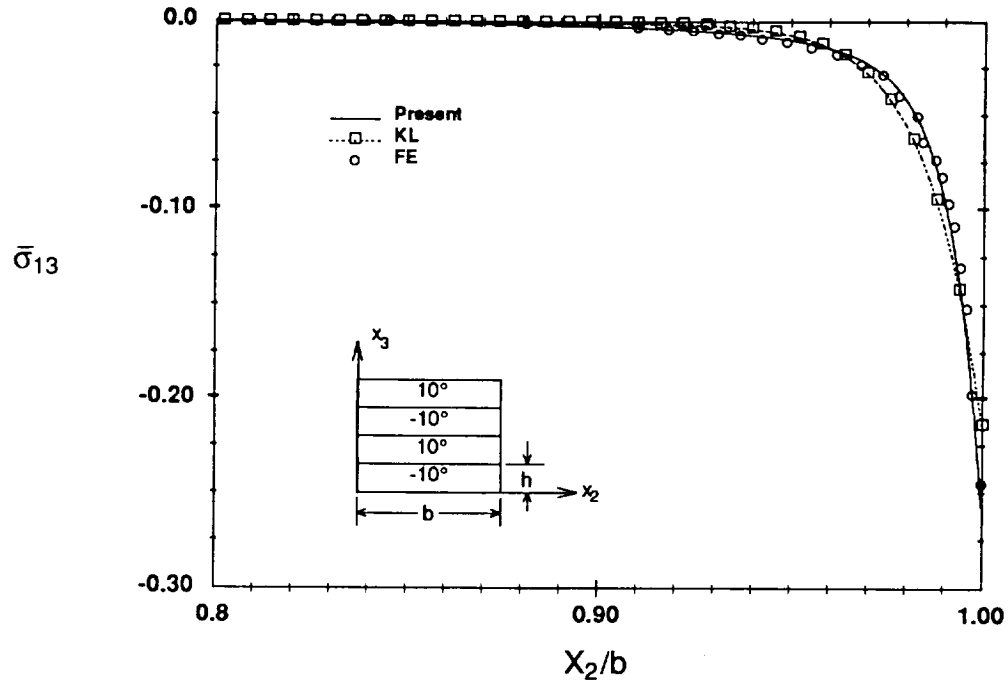

(a) First (10/-10) Interface

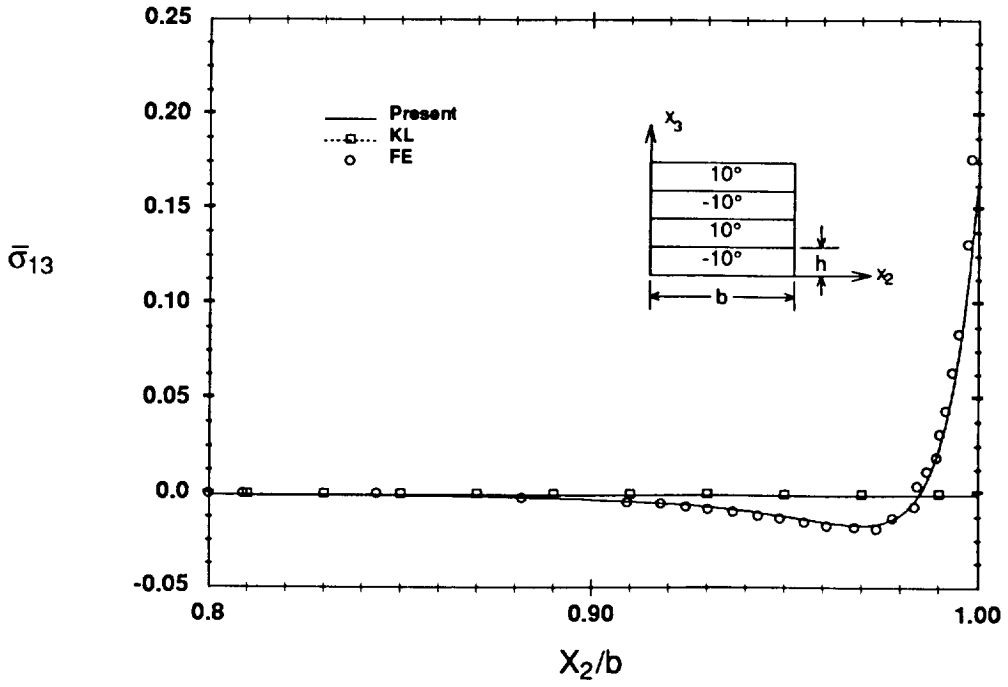

(b) Second (-10/10) Interface

Figure 5.22. σ_{13} at First and Second Interfaces for $[(\pm 10)_2]_s$ Laminate - Extension

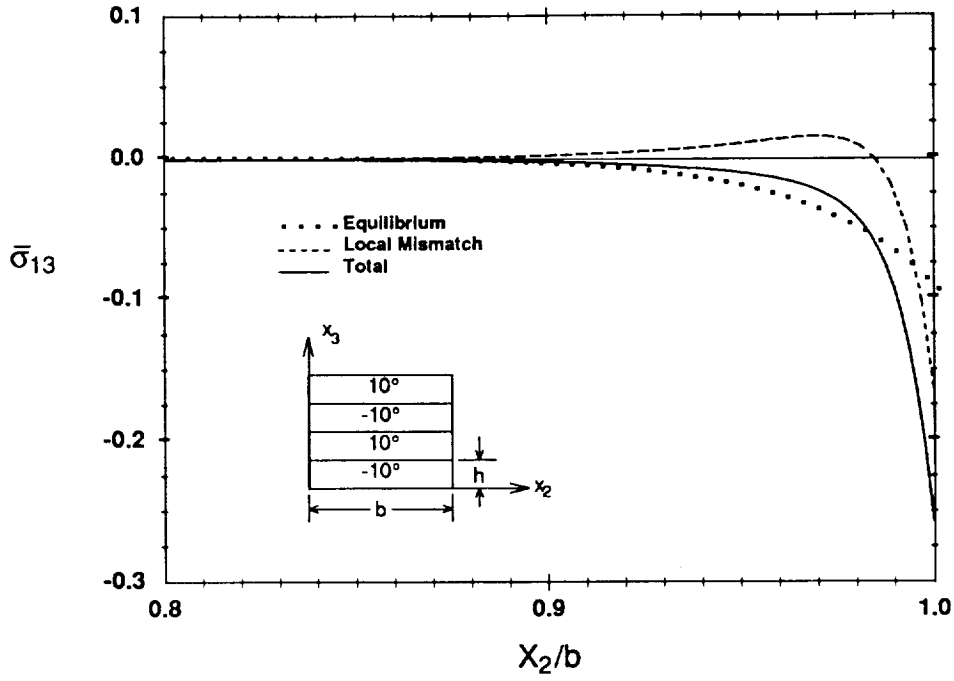

Figure 5.23. Contributions to σ_{13} at First Interface in $[(\pm 10)_2]_s$ Laminate - Extension

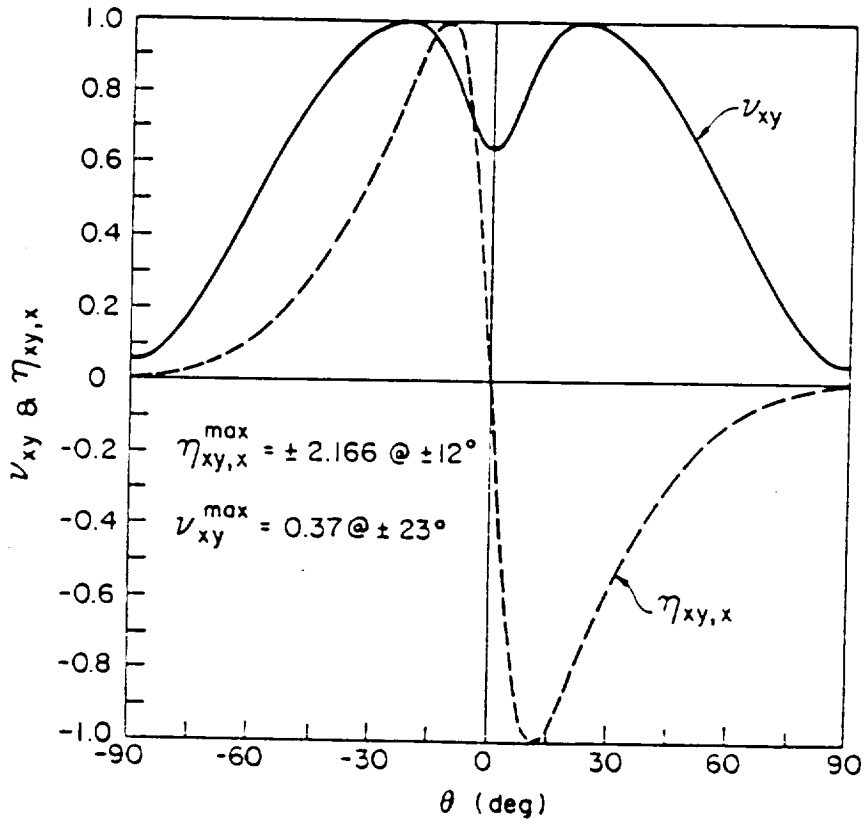

Figure 5.24. Coefficient of Mutual Influence and Poisson's Ratio

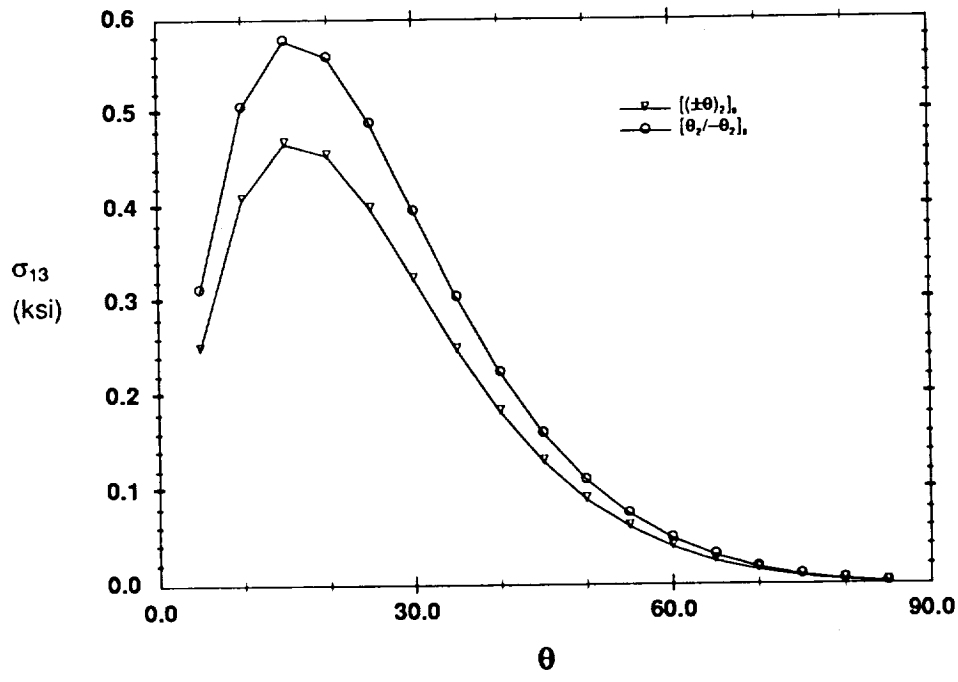

Figure 5.25. Maximum σ_{13} for $[(\pm 10)_2]_s$ and $[(+10)_2/(-10)_2]_s$ Laminates - Extension

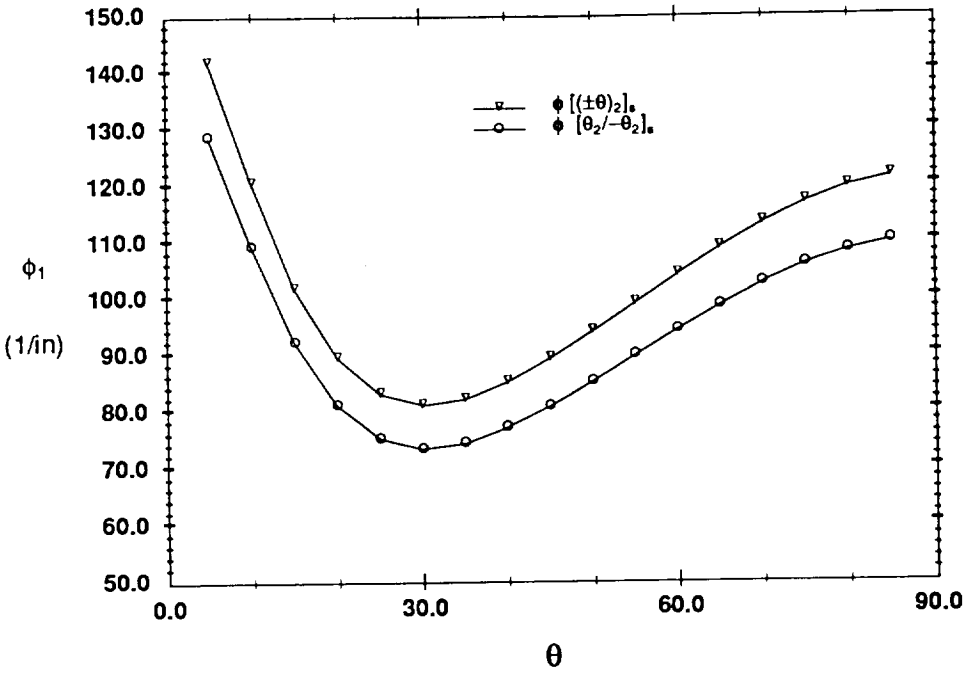

(a) Variation of ϕ_1 with θ

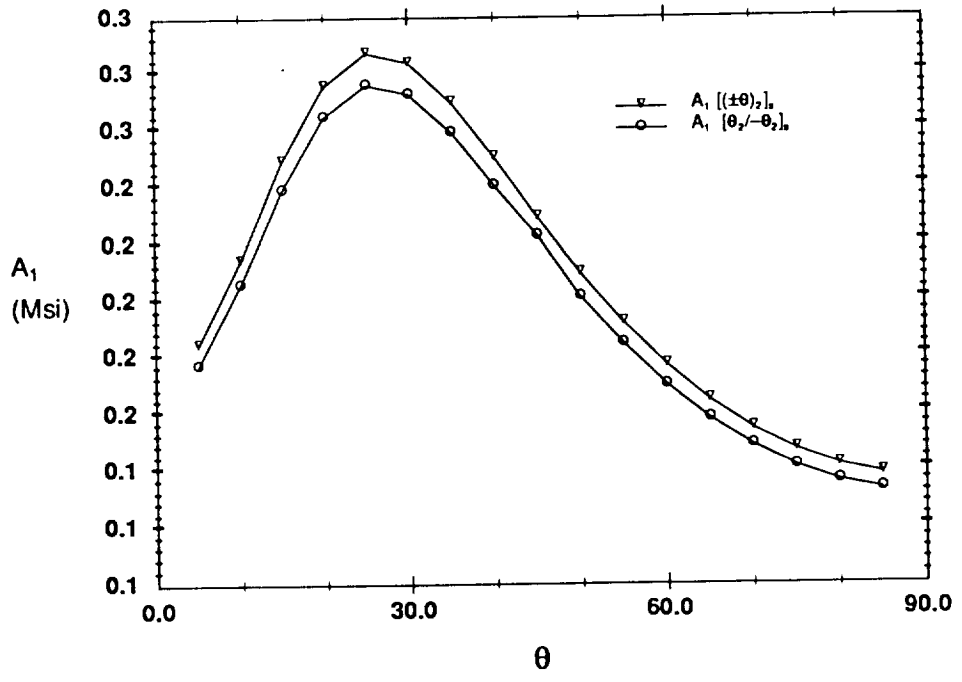

(b) Variation of A_1 with θ

Figure 5.26. ϕ_1 and A_1 vs. θ for $[(\pm 10)_2]_s$ and $[(+10)_2/(-10)_2]_s$ Laminates

equilibrium contribution is equivalent to a non-zero interfacial force. The results indicate a larger contribution from local mismatch at the intersection of the interface and free edge than from global mismatch (equilibrium). However, the boundary layer width is approximately the same for both effects.

The influence of fiber orientation on the stress field characteristics is illustrated in Figures 5.24-5.26 for both "clustered" and "alternating" stacking sequences. Figure 5.24 shows the variation in coefficient of mutual influence and Poisson's ratio as a function of θ for a T300-5208 graphite epoxy with the material properties given in Table 5.1. As can be seen, $\eta_{12,1}$ attains a maximum value at $\theta \approx 15°$. Thus, the interlaminar shear stresses are expected to be maximum in angle ply laminates with adjacent +15/−15 layers. Figure 5.25, which shows the variation in the maximum intensity of σ_{13} with θ, for both stacking sequences, demonstrates that this is in fact the case. The parameters in the assumed stress expressions are also functions of θ. The variation of ϕ_1 with θ for the two stacking configurations is depicted in Figure 5.26a where it is evident that ϕ_1 attains a minimum at $\theta = 30°$ for both stacking sequences. The constant A_1 on the other hand reaches a maximum at $\theta = 25°$ (Figure 5.26b). The constant λ_2 is independent of θ,but does depend on stacking sequence. As indicated in Table 5.5 $\lambda_2 = 4.135$ for the alternating sequence and $\lambda_2 = 3.727$ for the clustered sequence.

5.3 Quasi-Isotropic Laminates

Quasi-isotropic laminates are currently used extensively in practice because of their isotropic in-plane elastic properties. Symmetric quasi-isotropic laminates made with equal percentages of 0, 90, +45, and -45 degree laminae orientations are examined here. There are twelve unique configurations of this type, as shown in Table 5.6, if it is assumed that the +45 and -45 layers can be interchanged. In the table, the laminates are divided into two groups; those with adjacent ±45

layers and those with interspersed ±45 layers. This terminology will be used throughout the subsequent discussion.

In quasi-isotropic laminates, in contrast to the special cases of angle-ply laminates and cross-ply laminates discussed in the previous sections, both a mismatch in ν_{12} and $\eta_{12,1}$ may exist between adjacent layers. Consequently, all stresses are in general non-zero, and the total fourteen parameters ϕ_i (i = 1,5), λ_j (j = 1,6), and A_k (k = 1,2,3), in the assumed stress expressions must be determined in order to evaluate the stresses in the individual plies.

5.3.1 Extensional Load

Analyses have been conducted for the uniform extension of all twelve laminates listed in Table 5.6, but because of the large number of plots necessary to characterize the stress field near the free edge in each laminate, results in the form of through-thickness and interfacial stress distributions are provided for only three of these: $[90/45/0/-45]_s$, $[45/90/0/-45]_s$ and $[0/45/-45/90]_s$. These laminates were chosen to illustrate the influence of adjacent ±45 layers and interspersed ±45 layers on the interlaminar stress state and to study the relative magnitudes of the mismatch and equilibrium contributions to the stress field for different stacking sequences.

Stress distributions for the interspersed $[90/45/0/-45]_s$ and $[45/90/0/-45]_s$ laminates and the $[0/45/-45/90]_s$ laminate with adjacent ±45 layers are provided in Figures 5.27-5.31. Stresses determined by finite element analysis, the KL solution, and the present theory (equations (3.86-3.89)) are shown. The finite element results for the $[90/45/0/-45]_s$ and $[0/45/-45/90]_s$ laminates were generated previously by Herakovich[9] using the program CLFE2D, and the finite element results for the $[45/90/0/-45]_s$ were obtained by the author using Norwood's[76] program. The present theory results were generated using a through-thickness decay length of one layer thickness. All layers were of equal thickness, $t^{(k)} = h = 0.005$ in. The parameters ϕ_i , λ_j, and A_k

TABLE 5.6. Quasi-Isotropic Laminates

Interspersed ±45 Laminates	Adjacent ±45 Laminates (ksi)
$[90/45/0/-45]_s$	$[90/0/\pm45]_s$
$[0/-45/90/45]_s$	$[90/\pm45/0]_s$
$[45/90/0/-45]_s$	$[0/90/\pm45]_s$
$[45/90/-45/0]_s$	$[0/\pm45/90]_s$
$[45/0/90/-45]_s$	$[\pm45/90/0]_s$
$[45/0/-45/90]_s$	$[\pm45/0/90]_s$

for the laminates considered in this section are provided in Table 5.7. Solution parameters for the remaining quasi-isotropic laminates listed in Table 5.6 are provided in Appendix D (Tables D.2-D.5). In all figures, stresses are normalized by the average far field stress $\bar{\sigma}_{11} = N_{11}/2H$ where N_{11} is the far field load, and 2H is the laminate thickness. Classical lamination theory stresses for the three laminates subjected to uniform extension are provided in Table D.1.

Figures 5.27-5.29 display through-thickness distributions of the interlaminar stress components for the two interspersed stacking sequences. The results in Figure 5.27 and 5.28 for the interlaminar stresses in the $[45/90/0/-45]_s$ laminate show similar trends in the predictions of all three methods. The results of the present theory for the interlaminar shear stress σ_{13}, shown in Figure 5.27a, and the interlaminar shear stress σ_{23}, presented in Figure 5.28, however, show better correlation with the finite element solution than exhibited by the KL solution. The present solution more accurately predicts stress magnitudes, and more closely approximates the through-thickness variations in the stresses than does the KL solution.

TABLE 5.7. Solution Parameters for Quasi-Isotropic Laminates

Solution Parameters For Quasi-Isotropic Laminates $\varepsilon_{11} = 0.1\%$			
Constant	$[45/90/0/-45]_s$	$[90/45/0/-45]_s$	$[0/\pm45/90]_s$
ϕ_1 (1/in)	54.85	50.02	61.75
ϕ_2 (1/in)	59.82	61.75	58.81
ϕ_3 (1/in)	47.06	99.81	97.46
ϕ_4 (1/in)	70.08	56.23	56.04
ϕ_5 (1/in)	95.28	174.5	62.39
λ_1	6.725	1.386	3.530
λ_2	7.801	3.189	4.302
λ_3	12.31	3.661	8.821
λ_4	11.90	21.11	19.86
λ_5	1.490	5.047	5.189
λ_6	1.572	0.352	5.082
$A_1 X10^{-5}$ (psi)	6.203	3.703	1.565
$A_2 X10^{-5}$ (psi)	-10.57	-3.801	-1.505
$A_3 X10^{-5}$ (psi)	-38.81	-1.002	-1.068
h (in)	.020	.020	.020

Similar observations are made with regard to the normal stress predictions, depicted in Figure 5.27b. All methods correlate fairly well, except at the laminate midplane. At the midplane, the present solution and KL solution predict larger compressive interlaminar normal stress than finite elements. A possible cause for the difference between the finite element predictions and the present solution is discussed later in this section.

The similarities in the predictions of the three methods for stresses in the $[45/90/0/-45]_s$ laminate discussed above suggests that, for this laminate, mismatch effects do not have much of an effect on the overall distribution of stress in the laminate; that is, global equilibrium dominates the development of the interlaminar stresses.

In the remaining interspersed laminates, where the 90 degree laminae is positioned at the top or bottom of the stack, $[90/45/0/-45]_s$ and $[45/0/-45/90]_s$, mismatch effects have a significant influence on the total stress distributions. This is clearly illustrated for the $[90/45/0/-45]_s$ laminate in Figures 5.29 and 5.30. These figures show comparisons of the three methods for through-thickness distributions of σ_{13} (Figure 5.29a) and interlaminar normal stress (Figure 5.29b), and for interfacial distributions of σ_{23} (Figure 5.30). Evident from Figures 5.29a and 5.29b is the significant improvement of the present theory over the KL solution, with the present theory predicting trends more similar to those displayed by the finite element results. The modified solution of the present study and the finite element model predict more severe through-thickness gradients for the interlaminar normal stress, and generally larger shear stresses σ_{13} than the KL solution. At the first interface (90/45), for instance, the present theory and finite elements predict interlaminar shear stress σ_{13} (Figure 5.29b) to be approximately 6% of the average far field stress, where the KL solution predicts identically zero stress. At this interface, equilibrium is satisfied by the KL solution, due to the in-plane shear stress $\tilde{\sigma}_{12}$ being zero in the 90 degree layer. The non-zero stress σ_{13} at this interface then results solely from the mismatch

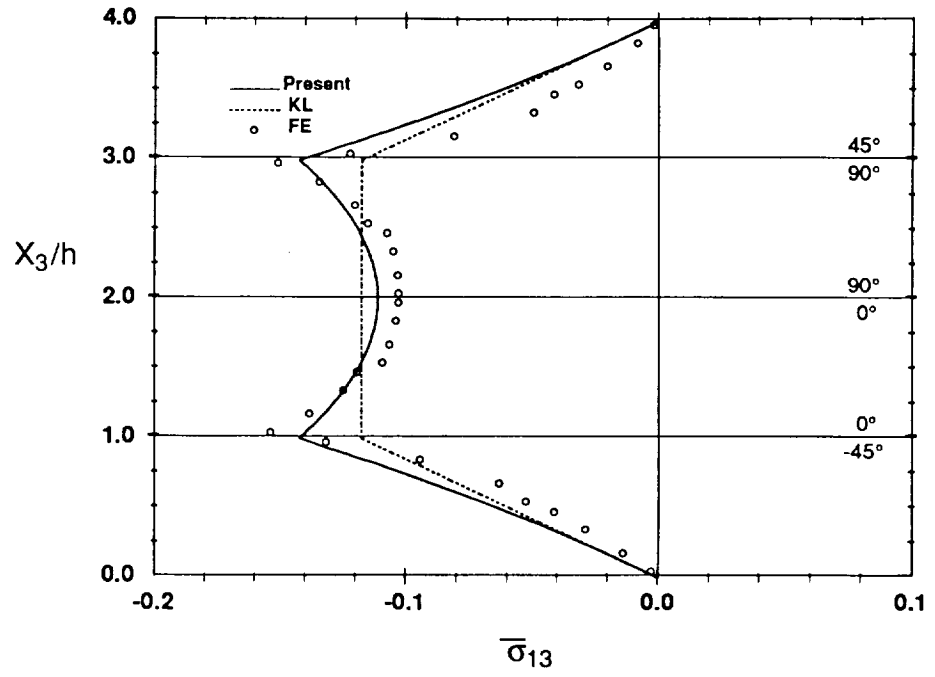

(a) $\bar{\sigma}_{13}$ at $X_2/b = 0.999$

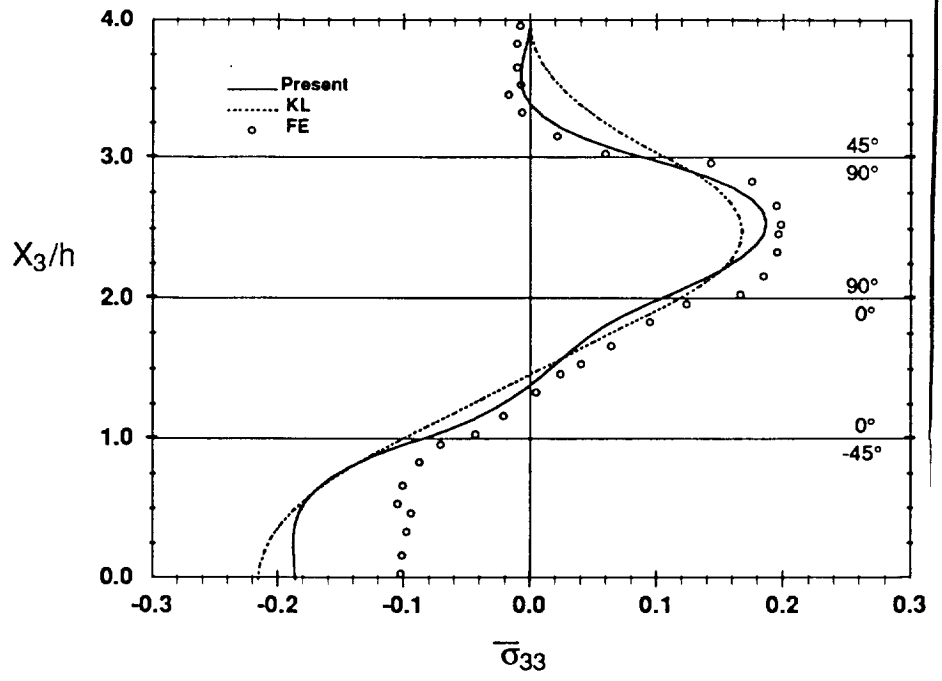

(b) $\bar{\sigma}_{33}$ at $X_2/b = 0.999$

Figure 5.27. σ_{13} and σ_{33} at $X_2/b = 0.999$ in $[45/90/0/-45]_s$ Laminate - Extension

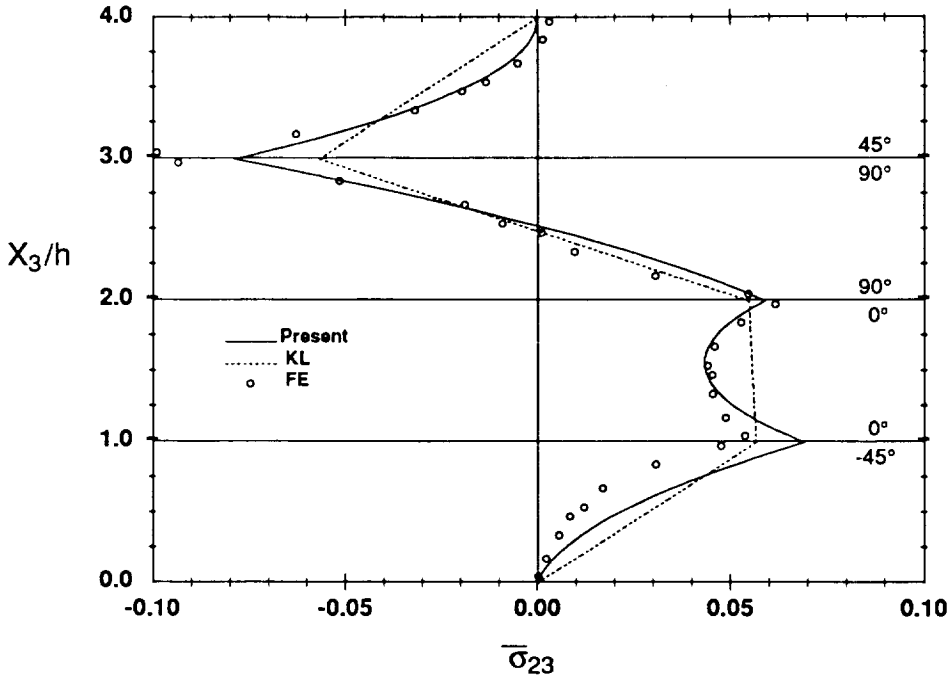

Figure 5.28. σ_{23} at $X_2/b = 0.993$ in $[45/90/0/-45]_s$ Laminate - Extension

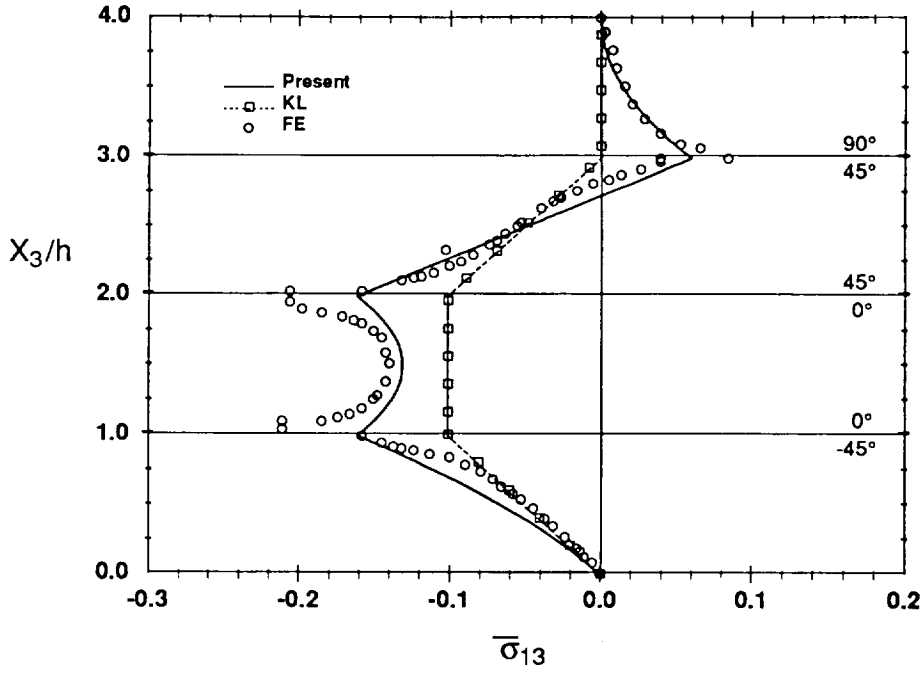

(a) $\bar{\sigma}_{13}$ at $X_2/b = 0.999$

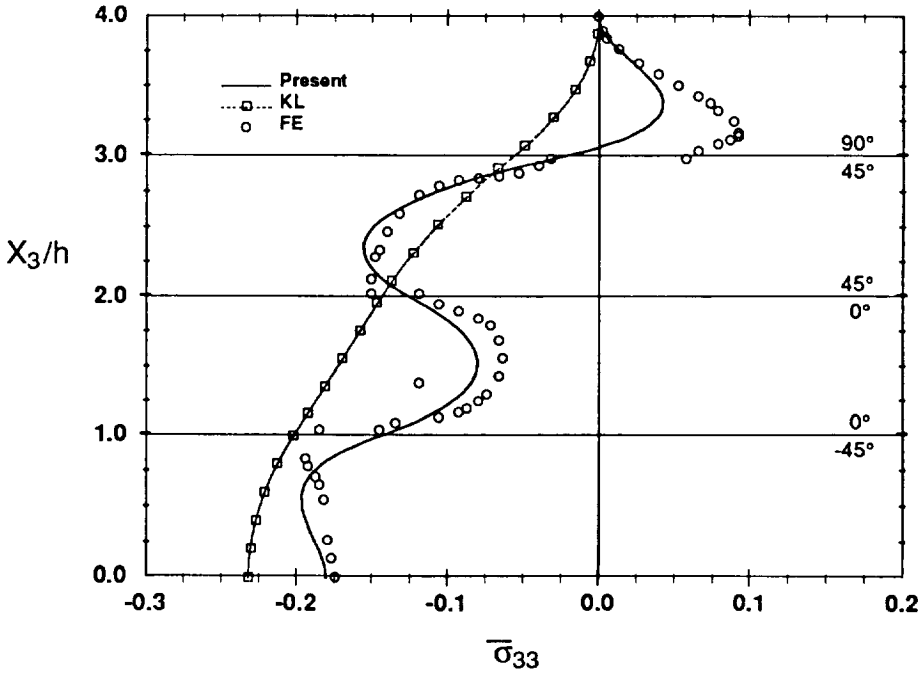

(b) $\bar{\sigma}_{33}$ at $X_2/b = 0.999$

Figure 5.29. σ_{13} and σ_{33} at $X_2/b = 0.999$ in $[90/45/0/-45]_s$ Laminate - Extension

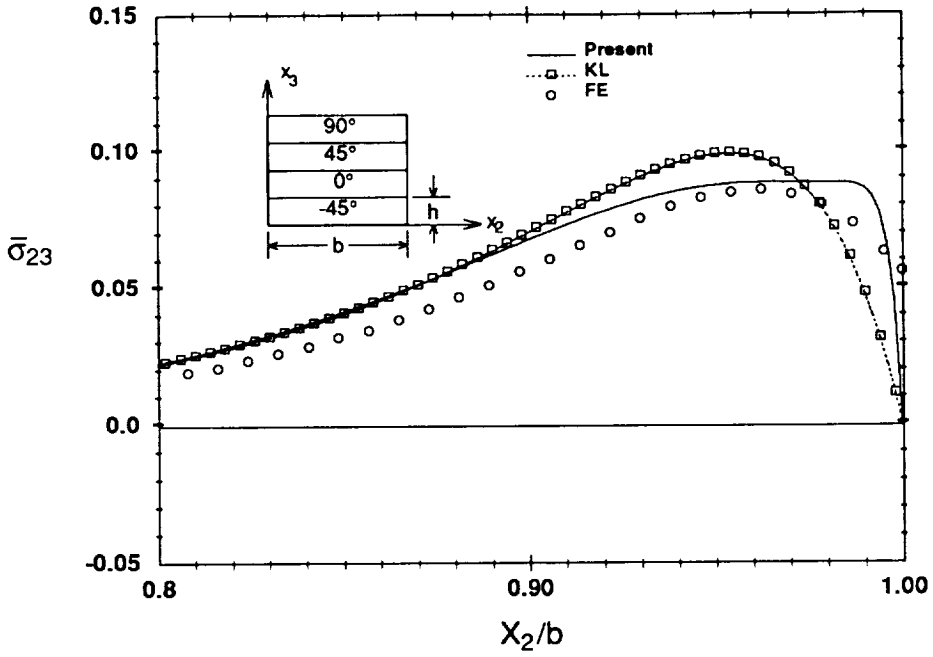

(a) First (90/45) Interface

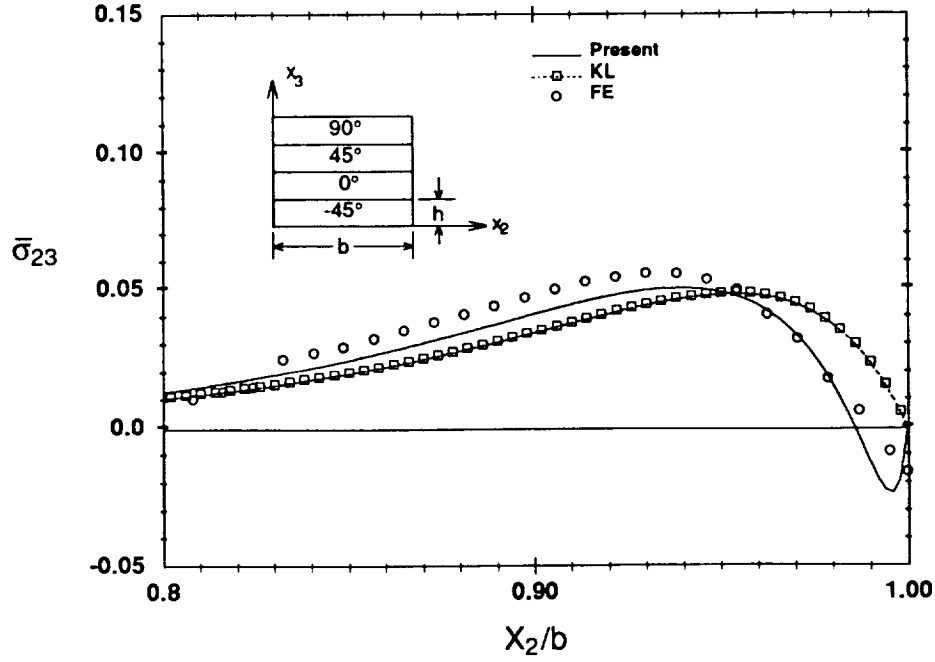

(b) Second (45/0) Interface

Figure 5.30. σ_{23} at First and Second Interfaces in $[90/45/0/-45]_s$ Laminate - Extension

in $\eta_{12,1}$ between the 90 degree and 45 degree layers.

There are also differences in the predictions of the three methods for the interlaminar shear stress σ_{23}. Through-thickness finite element data is not available for σ_{23}, but interfacial results (first and second interfaces), presented in Figure 5.30, indicate that the present solution compares more favorably with finite element results than do the KL results. Recall, that the KL solution requires the stress distributions at these interfaces to be of the same form, since stresses are constrained to decay at the same rate in all plies. The present theory and the finite element method, on the other hand, exhibit variations in the character of the interfacial distributions for these two interfaces. The most significant difference in the interfacial predictions for σ_{23} observed is at the second interface where the local mismatch contribution causes a reversal in stress near the free edge (Figure 5.30b). These differences and the differences discussed above in the σ_{13} and σ_{33} predictions could be significant when evaluating the structural response of candidate laminates to an applied load, and are clear evidence of the influence of local mismatch effects on the total stresses and the necessity for including these effects in the stress analysis.

Similar conclusions can be drawn for the quasi-isotropic laminates with adjacent ±45 layers; that is, in these laminates local mismatch effects are significant and a design or analysis based upon stress predictions obtained from global equilibrium considerations alone can be misleading. This observation is illustrated in Figure 5.31, which shows predictions for interlaminar shear stress σ_{13} and σ_{33} in a $[0/45/-45/90]_s$ laminate which are typical of results obtained for laminates having adjacent ±45 degree layers. Note from Figure 5.31a that the maximum shear stress develops at the 45/-45 interface, where the mismatch in $\eta_{12,1}$ is the largest. The present theory predicts σ_{13} at the 45/-45 interface 5% smaller than predicted by finite elements, while KL underpredicts the finite element stresses by 38%. Similar trends were observed in the predictions of the three methods for the other quasi-isotropic laminates with

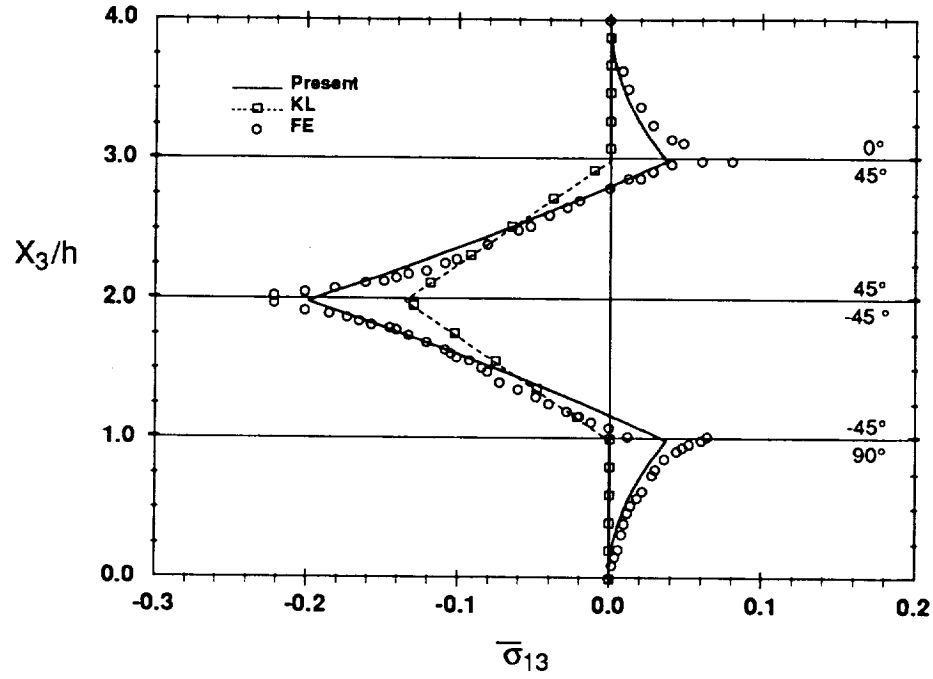

(a) $\bar{\sigma}_{13}$ at $X_2/b = 0.999$

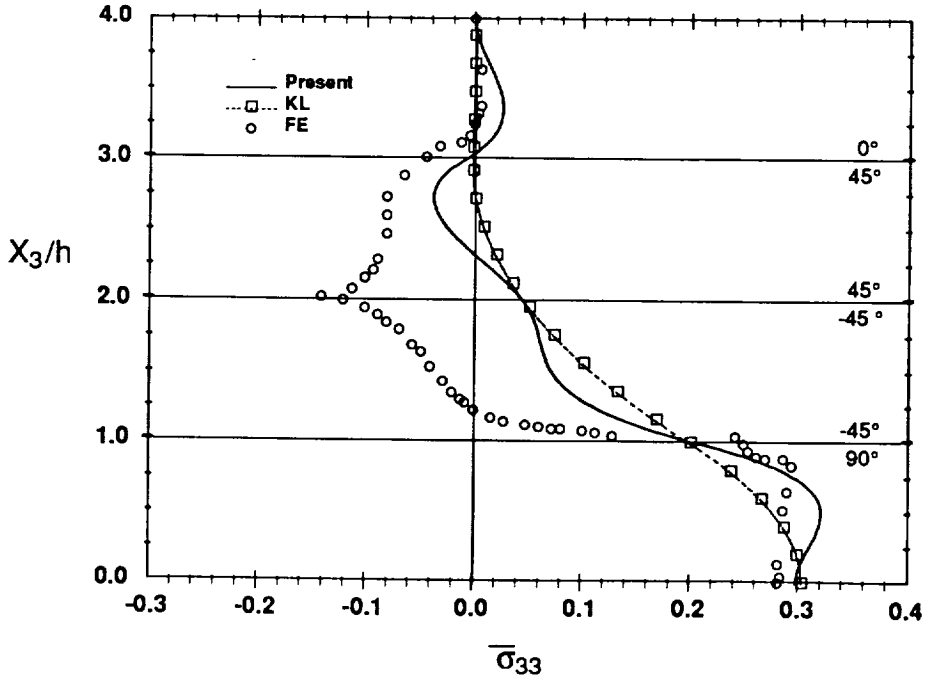

(b) $\bar{\sigma}_{33}$ at $X_2/b = 0.999$

Figure 5.31. σ_{13} and σ_{33} at $X_2/b = 0.999$ in $[0/45/-45/90]_s$ Laminate - Extension

adjacent ±45 layers. In the other laminates, the shear stress predicted at the +45/-45 interface by the present solution and the finite element method was as much as 50% to 100% larger than predicted by the KL solution.

Results are also provided in Figure 5.31b for the interlaminar normal stress in the $[0/+45/-45/90]_s$ laminate. Again, these results are typical of those obtained for the group of adjacent quasi-isotropic laminates. Note that the finite element solution predicts larger through-thickness gradients in the normal stress than predicted by either the KL solution or the present solution. The present theory appears to be starting to pick up the trends displayed by the finite element results, but does not predict the large compressive stress at the 45/-45 interface.

One possible cause for the differences in normal stress predictions of the present theory and finite element methods at the 45/-45 interface of the laminate shown in Figure 5.31b is the assumed lack of coupling, in the present analysis, between the coefficient of mutual influence mismatch and the interlaminar stresses σ_{23} and σ_{33}, and between Poisson's ratio mismatch and interlaminar shear stress σ_{13}. This lack of coupling is also thought to be the reason for the poor correlation in the normal stress predictions of the present solution and the finite element results at the midplane of the $[45/90/0/-45]_s$ laminate discussed at the beginning of this section, and for the differences in the normal stress predictions of the present theory and finite elements at the first interface of the $[45/-45/0/90]_s$ discussed in Section 4.1.3 (Figure 4.6).

Recall from the development in Chapter 3, that the coefficient of mutual influence mismatch was assumed to affect only the σ_{12} and σ_{13} components of stress while the Poisson's ratio mismatch was assumed to affect only the σ_{22}, σ_{23} and σ_{33} stress components. This assumption could be made for the problem studied since the assumption that stresses are independent of the longitudinal coordinate X_1 led to a reduced system of equilibrium equations, where the stresses

σ_{12} and σ_{13} uncoupled from σ_{22}, σ_{23} and σ_{33}. However, as briefly discussed in Chapter 3, the stresses are coupled by the compatibility equations, and would be in the equilibrium equations for more general problems where the longitudinal independence could not be assumed. Therefore, an improved stress field assumption would include the same eigenfunctions in the expressions for all of the stresses, and would relate interlaminar stresses σ_{22}, σ_{23}, and σ_{33} to the mismatch in coefficient of mutual influence and interlaminar shear stress σ_{13} to Poisson's ratio mismatch.

To summarize the results of this section, the above discussion indicates that stacking sequence has a significant influence on the relative magnitudes of the mismatch and equilibrium contributions to the stress field. In the laminates with interspersed ±45 layers, the factor having the largest effect on the magnitude of the different contributions is the location of the 90 degree laminae in the stacking sequence. This is explained by considering Poisson's ratio mismatch. The variation in Poisson's ratio with fiber orientation θ for a T300-5208 graphite-epoxy, is shown in Figure 5.24. As can be seen from the figure, the mismatch in Poisson's ratio between a +45 degree or -45 degree layer and a 0 degree layer is much larger than the mismatch between a 45 degree layer and a 90 degree layer. In the interspersed laminates with the 90 degree laminae as a middle layer, there is only one occurrence of adjacent 0 degree and 45 degree layers. In the interspersed laminates with the 90 degree laminae placed at the top or bottom of the stack, on the other hand, there are two occurrences of adjacent 45 degree and 0 degree layers, and the mismatch contribution to the total stress state is more significant. In the laminates with ±45 layers, the coefficient of mutual influence mismatch is large, and the local mismatch effects again contribute significantly to the total stress. These observations are made clear by examining Figures 5.28, 5.29 and 5.31 together and comparing the relatives differences in the predictions of the present method and KL solution for the different stacking sequences.

5.3.2 Bending Load

In order to illustrate the influence of load condition on the interlaminar stress, quasi-isotropic laminates subjected to bending load (negative curvature κ_{11}) have also been analyzed. In this section, comparisons of the through-thickness distributions of the interlaminar normal stress and shear stresses for a $[45/-45/90/0]_s$ laminate subjected to bending ($-\kappa_{11}$) and extension loads are presented (Figures 5.32-5.34). As usual, distributions are presented for the top half of the laminate. In the case of bending, interlaminar normal stress is antisymmetric about the midplane, and interlaminar shear stress is symmetric. For the extensional load case, interlaminar shear stress is antisymmetric about the midplane and interlaminar normal stress is symmetric. As has been done in the previous sections, bending stresses are normalized by $M_{11}H/2I$, and extensional stresses are normalized with respect to $N_{11}/2H$ where M_{11} and N_{11} are the applied far field loads. All results were generated using a through thickness decay length of one layer thickness (h = 0.005 in.), and the solution parameters ϕ_i, λ_j, and A_k given in Table 5.8.

Comparison of the through-thickness stress plots in Figures 5.32-5.34 shows similar distributions for all interlaminar stress components for bending and extension load. In both cases, the maximum interlaminar normal stress is tensile and develops at $X_3/h \simeq 1.6$. The maximum shear stresses also occur at the same through-thickness location in both load cases. The maximum interlaminar shear stress σ_{13} develops at the first interface ($X_3/h = 3$), and the interlaminar shear stress σ_{23} attains a maximum at the second interface. The combined load case would then represent a more severe condition in terms of delamination potential, with bending and extension stresses combining above the laminate midplane.

TABLE 5.8. Solution Parameters for $[45/-45/90/0]_s$ Laminate

Solution Parameters For $[45/-45/90/0]_s$ Laminate		
Constant	Extension	Bending
ϕ_1 (1/in)	57.07	72.03
ϕ_2 (1/in)	63.25	58.37
ϕ_3 (1/in)	99.07	69.22
ϕ_4 (1/in)	66.82	46.96
ϕ_5 (1/in)	95.58	48.99
λ_1	1.966	4.744
λ_2	4.034	5.372
λ_3	5.070	10.71
λ_4	18.02	11.80
λ_5	1.565	4.816
λ_6	6.062	7.777
A_2X10^{-5} (psi)	1.773	1.388
A_2X10^{-5} (psi)	-3.741	-2.372
A_3X10^{-5} (psi)	-1.892	-2.857
h (in)	.020	.020

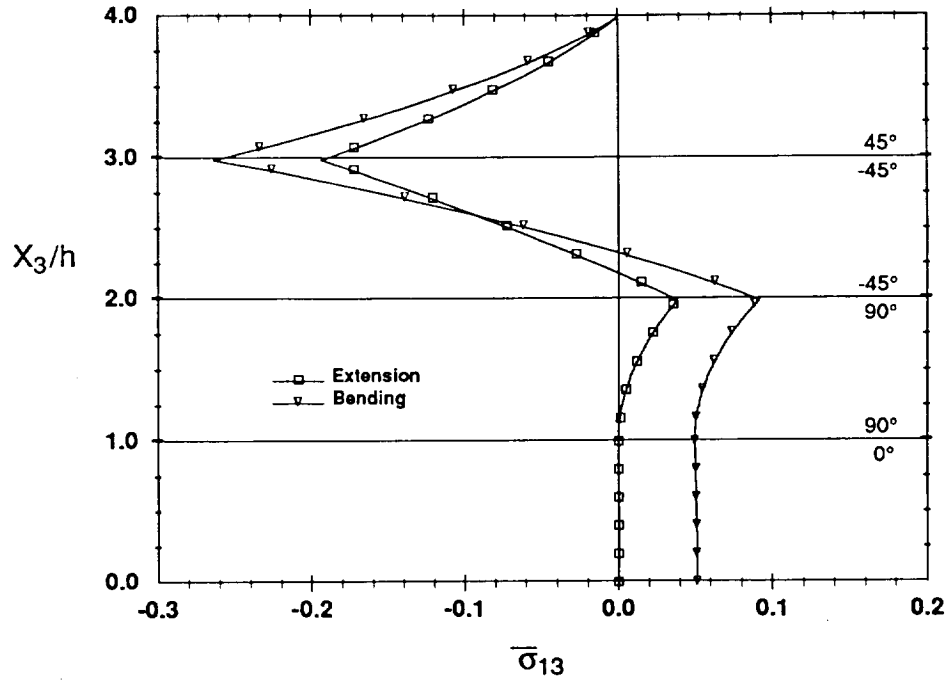

Figure 5.32. σ_{13} at $X_2/b = 0.999$ in $[45/-45/90/0]_s$ Laminate, Bending and Extension

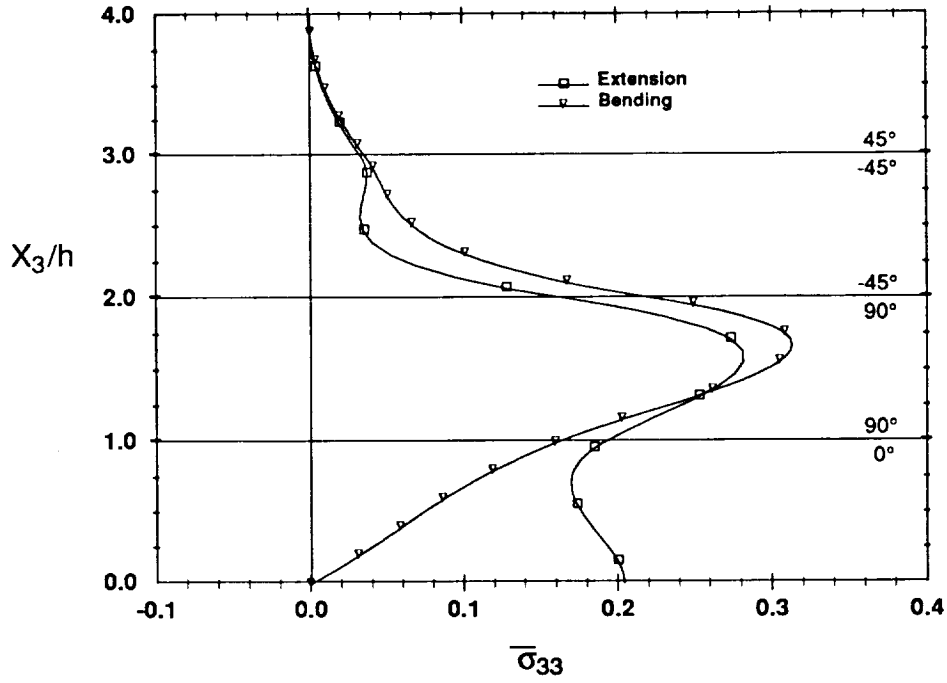

Figure 5.33. σ_{33} at $X_2/b = 0.999$ in $[45/-45/90/0]_s$ Laminate, Bending and Extension

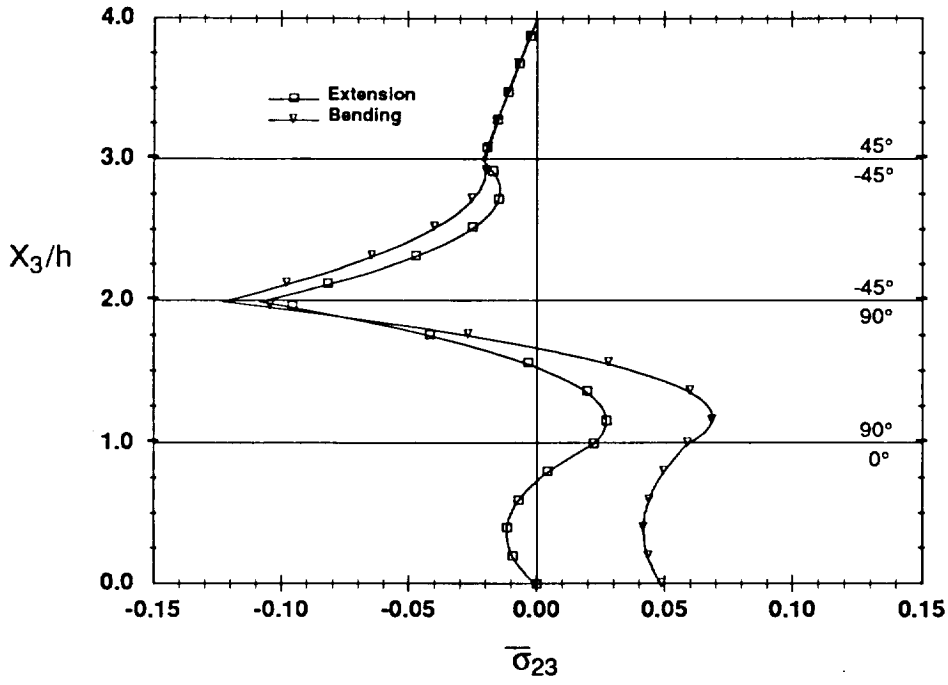

Figure 5.34. σ_{23} at $X_2/b = 0.993$ in $[45/-45/90/0]_s$ Laminate, Bending and Extension

CHAPTER 6

CONCLUSIONS AND RECOMMENDATIONS

6.1 Summary of Method

The purpose of this study was to develop an efficient approximate solution for interlaminar stresses near free edges of finite width, laminated composites subjected to bending and extension loads and to demonstrate the utility of the methodology. The analysis developed is an extension of a method recently presented by Kassapaglou and Lagace,[20] and is based upon the principle of minimum complementary energy and an assumed stress state, derived by considering material mismatch considerations and global equilibrium requirements. In the KL solution only the mismatch between laminae and laminate material properties was considered. The present solution extended their technique by including additional terms in the stress assumptions, which account for the local material property mismatch in coefficient of mutual influence and Poisson's ratio between adjacent layers in the laminate. The differential equations of equilibrium, the interfacial traction continuity and boundary conditions of stress were identically satisfied by the assumed stresses. The strain compatibility equations and interfacial displacement continuity conditions were satisfied approximately by imposing the stationary condition of laminate complementary energy.

The developed methodology is general, and in theory, can be extended for the analysis of other load cases, such as in-plane bending and torsion, or to more general structural configurations, provided a plane stress state is recovered in the member's interior region, and the stress components do not vary with the longitudinal coordinate. The plane stress solution can be

obtained from an analytical solution, if available, or from a numerical technique, such as the finite element method. The methodology could then be employed in a global-local analysis to obtain stress solutions in regions of high stress gradients with a coarser solution used to define the response outside of these regions.

As the previous paragraph indicates, a major advantage of the method presented is the fact that in-plane stresses, obtained from classical lamination theory, are the only required input to the solution. Other advantages, as compared with numerical solutions, or some of the complicated analytical models that have appeared in the literature, include the relative simplicity of the theory, in terms of the number of parameters that must be determined in order to obtain stress distributions, solution efficiency, output readability, and the ease of application for the simple geometry considered. For the most general laminate, only fourteen parameters must be determined prior to calculating stresses. This number reduces to ten for cross-ply laminates and to three for symmetric angle-ply laminates subjected to extensional load. For bending of angle-ply laminates, or extension of unsymmetric angle-ply laminates, the number reduces to six. In any case, the number of parameters is independent of the number of layers in the laminate, their material properties, and orientations. Consequently, the analysis can be applied to laminates with a large number of plies. Finally, a major asset of the solution is the insight it provides into the fundamental physical mechanisms, global equilibrium and local mismatch effects, that contribute to interlaminar stress development. Contributions from each of these effects are clearly delineated in the solution output. This type of information cannot be obtained from a finite element analysis.

6.2 Conclusions

The development of the solution methodology has been accompanied by application of the

stress analysis to several finite width laminates subjected to uniform extension and bending load. Symmetric and unsymmetric cross-ply laminates, symmetric angle-ply laminates, and symmetric quasi-isotropic laminates have been studied. Comparisons in stress predictions were presented for results obtained using the present solution, the KL solution, and finite element solutions, where available. Several conclusions can be drawn based upon the results of these studies:

(1) The present method compares well with finite element methods and provides significantly improved stress predictions as compared with the KL solution which is based entirely upon global equilibrium considerations. In particular, the present solution more accurately predicts stress magnitudes and interlaminar stress gradients near interfaces where there is a large material property mismatch between adjacent layers. Further, the present method accurately characterizes the through-thickness gradients in the layer stress fields near the interfacial surfaces, while the KL solution predicts the laminate behavior to be qualitatively the same throughout the thickness of the layers.

(2) The relative importance of local mismatch and equilibrium considerations was found to be a function of stacking sequence. This was the case for all of the laminate families analyzed. Specifically, the following observations were made:

(a) In angle-ply laminates subjected to axial loading large mismatches in the coefficient of mutual influence induced large interlaminar shear stress σ_{13}. In alternating stacking sequences, $[(+\theta/-\theta)_2]_s$, local mismatch resulted in stresses of considerable magnitude at interfaces where the KL solution predicted zero stresses. These results were in agreement with finite element results.

(b) In symmetric cross-ply laminates, subjected to both bending and extension loads, local mismatch effects had a more pronounced effect on the stress predictions in

$[90/0]_s$ laminates than in $[0/90]_s$ laminates, and were the cause of the asymmetry in stresses observed in these laminates. More specifically, the mismatch contribution associated with Poisson's ratio mismatch and the direct assumption on interlaminar normal stress (referred to as normal mismatch contribution) was found to be the component primarily responsible for differences in the stress predictions provided by the present solution for the two laminates.

(c) In the quasi-isotropic laminates considered (laminates with equal percentages of 0, 45, -45, and 90 degree layers) the degree of local mismatch contribution was also found to be dependent on stacking sequence. Specifically, in interspersed configurations, with the 90 degree layer separating the 45 and -45 degree layers, the mismatch contribution to all interlaminar stress components was small compared with the equilibrium contribution. For these laminates it was concluded that the magnitude of the stresses was primarily dependent on the force and moment developed at any through-thickness location by the intralaminar stresses σ_{22}. This was physically explained by the fact that the Poisson's ratio mismatch and mismatch in coefficient of mutual influence between adjacent layers in this laminate are smaller than in interspersed laminates with the 45 and -45 degree layers separated by zero degree layers and in laminates with adjacent +45 and -45 degree layers. These results clearly indicated the influence of local mismatch effects on the stresses and the necessity for including mismatch considerations in laminate design.

(3) For the laminates considered, bending and extension loads resulted in similar interlaminar stress distributions in terms of magnitude and boundary layers widths.

(4) Comparison of results for an unsymmetric cross-ply $[0/90]_t$ and a symmetric cross ply

$[0/90]_s$ subjected to extension load showed that the out of plane deflections of the unsymmetric laminate relieved both interlaminar shear stress and interlaminar normal stress.

(5) Difficulties were encountered in the analysis of laminates having large local mismatch in coefficient of mutual influence in combination with curvature κ_{12}. This was true for both symmetric laminates subjected to bending loads and unsymmetric laminates under uniform extension. Thus, at the present time, there is a limitation on the general applicability of the developed solution. The source of the problem has not been identified but may be attributed to some possible inconsistencies introduced by the manner in which end conditions are currently applied, or possibly with the assumption that only half of the laminate width needs to be analyzed. The assumption of modeling half of the laminate width is recognized to be an approximation for laminates with off-axis plies. This approximation may loose validity when large curvatures κ_{12} are developed. It is also possible that the problem is purely numerical or is the result of a coding error. This topic was discussed in more detail in Section 5.2 and is an area requiring additional study.

6.3 Recommendations for Future Work

The solution method developed has been shown to generally produce accurate predictions for interlaminar stresses near straight free edges of laminated plates. Although the model was developed for specific load conditions, and was based upon some assumptions that limit its application, it can be extended to more general analyses. Some recommendations for extension of the method and additional possible applications are presented in this section. First, however, some suggestions are provided for solution modifications that might lead to increased accuracy in the stress predictions. Recommendations related to solution efficiency are also provided.

The results of the previous chapter showed that the least accurate results were obtained for

the interlaminar normal stress. It was suggested that improvements in the stress predictions might be achieved by incorporating additional exponential terms in the assumed stress expressions which account for the coupling between coefficient of mutual influence mismatch and interlaminar stresses σ_{23} and σ_{33}, and the coupling between Poisson's ratio and interlaminar shear stress σ_{13}. This could be accomplished by including an additional term in Equation (3.87) for the interlaminar shear stress σ_{13} with the same form as that multiplying A_1 but proportional to the mismatch in Poisson's ratio. Similarly, additional terms in the expressions for σ_{23} and σ_{33} with the same forms as the mismatch terms incorporated presently, but proportional to mismatch in coefficient of mutual influence could be included. The remaining stress components would then by determined from the differential equations of equilibrium.

Another possible improvement to the stress assumptions would allow for a priori unspecified through-thickness decay rates for the local mismatch effects. One way in which this could be incorporated into the present theory would be to assume exponential functions for the through-thickness variations of the local mismatch, expressed in terms of unknown through-thickness decay parameters as was done for the width variations in the present solution. The σ_{13} variation would require one exponential function, while σ_{23} and σ_{33} would require a combination of two functions.

The above recommended modifications should lead to improved accuracy, however, the additional level of complexity introduced, may not be worth the effort. Further, solution efficiency will decline as the number of terms is increased. In this connection, the issue of computational efficiency of the current solution is addressed. The current solution generally executes in less than 15 CPU seconds on an IBM RS6000, for twenty different initial approximations to the solution. This run time, is of course dependent on the convergence tolerance used when solving the non-linear system and how good the initial guess is. In

generating the results presented in this thesis, as many as 500 initial guesses were employed for the most general laminates. This large number of starting points was felt necessary because of the difficulty with the present method of determining a good initial guess. Additional work is necessary to improve this aspect of the solution.

Other areas of possible future work include extension to additional load cases such as in-plane bending and torsion, and to problems where stresses are a function of the longitudinal coordinate X_1. The method could also be extended to analyze more general structural configurations. One configuration of particular interest, is a stiffened panel. Extension of the method to analyze skin-stiffener interface stresses, or stresses in the tip of a stiffener blade is an area recommended for future work.

Coupling of the stress analysis with an experimental program and some type of failure analysis or delamination initiation predictions is also recommended. Analytical failure predictions or delamination initiation predictions, based upon the stress analysis of the present work, could then be correlated with experimentally observed behavior.

Finally, the methodology should be linked with a numerical optimization program to develop a design capability for laminated composites in which interlaminar stresses are considered. This capability will provide engineers with an efficient methodology for designing delamination resistant structures.

REFERENCES

1. Kassapoglou, C., "Interlaminar Stresses at Straight Free Edges of Composite Laminates", Master's Thesis, Massachusetts Institute of Technology, 1984.

2. Herakovich, C.T., "Failure Modes and Damage Accumulation in Laminated Composites with Free Edges", *Composites Science and Technology*, Vol. 36, 1989, pp. 105-119.

3. Foye, R. L., and Baker, D. J., "Design of Orthotropic Laminates", presented at the 11th Annual AIAA Structures, Structural Dynamics, and Materials Conference, Denver, Colorado, April 1970.

4. Pagano, N.J., "The Influence of Stacking Sequence on Laminate Strength", *Journal of Composite Materials*, Vol. 5, January 1971, pp. 50-57.

5. Pagano, N.J., and Pipes, R. B., "Some Observations on the Interlaminar Strength of Composite Laminates", *"International Journal of Mechanical Sciences"*, Vol. 15, 1973, pp. 679-688.

6. Pagano, N.J., "On the Calculation of Interlaminar Normal Stress in Composite Laminate", *Journal of Composite Materials*, Vol. 8, January 1974, pp. 65-81.

7. Herakovich, C. T., "Influence of Layer Thickness on the Strength of Angle-Ply Laminates", *Journal of Composite Materials*, Vol. 16, May 1982, pp. 216-227.

8. Herakovich, C.T., "On the Relationship Between Engineering Properties and Delamination in Composite Materials", *Journal of Composite Materials*, Vol. 15, July 1981, pp. 336-348.

9. Herakovich, C. T., "Free Edge Effects in Laminated Composites", *Handbook of Composites, Vol. 2 - Structures and Design*, C. T. Herakovich and Y. M. Tarnopol'skii, eds., Elsevier Science Publishers, 1988, pp. 187-230.

10. Watkins, R.I., and Morris, A.J., "A Multicriteria Objective Function Optimization Scheme for Laminated Composites for Use in Multilevel Structural Optimization Schemes", *Computer Methods in Applied Mechanics and Engineering*, Vol. 60, 1987, pp. 233-251.

11. Schmit, L.A., Jnr, and Farchi, B., "Optimum Laminate Design for Strength and Stiffness", *International Journal for Numerical Methods in Engineering"*, Vol. 7, 1973, pp. 519-536.

12. Hiron, Yoichi, "Optimum Design of Laminated Plates Under Axial Compression", *AIAA Journal*, Vol. 17, 1979, pp. 1017-1019.

13. Park, Won J., "An Optimal Design of Simple Symmetric Laminates Under the First Ply Failure Criterion", *Journal of Composite Materials*, vol 16, 1982, pp. 341-353.

14. Tauchert, T.R., and Adibhatla, " Design of Laminated Plates for Maximum Stiffness", *Journal of Composite Materials*, Vol. 18, 1984, pp. 58-69.

15. Knot, H.S., Venkaya, V.B., Johnson, C. D., and Tischler, V. A., "Optimization of Composite Laminates", *International Journal of Solids and Structures*, Vol. 9, 1973, pp. 1225-1236.

16. Krishnamachari, O. I., and Broutman, L. J., "Structural Design Optimization of Composite Laminates", *Journal of Reinforced Plastics and Composites*, Vol. 7, 1988, pp. 459-474.

17. Kam, T. Y., Lai, M. D., "Multilevel Optimal Design of Laminated Composite Plate Structures", *Computers and Structures*, Vol. 31, 1989, pp. 197-202.

18. Schmit, L. A., and Mchrinfar, Massood, "Multilevel Optimum Design of Structures with Fiber-Composite Stiffened-Panel Components", *AIAA Journal*, Vol. 20, 1982, pp 138-147.

19. Lagace, P. A., and Kassapoglou, C., 1985, "An Efficient Method for the Calculation of Interlaminar Stresses in Composite Materials: Part 1 - The Force Balance Method," Technology Laboratory for Advanced Composites Report 85-5, Massachusetts Institute of Technology, Cambridge, MA.

20. Kassapoglou, C., and Lagace, P. A., "An Efficient Method for the Calculation of Interlaminar Stresses in Composite Materials", *Journal of Applied Mechanics*, Vol. 53, December, 1986, pp. 744-750.

21. Kassapoglou, C., and Lagace, P. A., "Closed Form Solutions for the Interlaminar Stress Field in Angle-Ply and Cross-Ply Laminates", *Journal of Composite Materials*, Vol. 21, April 1987, pp. 292- 307.

22. Salamon, N. J., "An Assessment of the Interlaminar Stress Problem in Laminated Composites", *Journal of Composite Materials Supplement*, Vol. 14, 1980, pp. 177-193.

23. Hayashi, Tsuyoshi, "Analytical Study of Interlaminar Shear Stresses in a Laminated Composite Plate, Transactions of Japan Society for Aeronautics and Space Science, Vol. 10, No. 17, 1967, pp. 49-58.

24. Hayashi, Tsuyoshi, Sando, Shinsuke, and Takagishi, Toshio, "Interlaminar Shear Stresses in Composite Laminates", Proceedings of 2nd Symposium on Composite Materials, Japan, 1969, pp. 173-214.

25. Puppo, A. H., and Evensen, H. A., "Interlaminar Shear in Laminated Composites Under Generalized Plane Stress", *Journal of Composite Materials*, Vol. 4, April 1970, pp. 204-220.

26. Pipes, R. B., and Pagano, N. J., "Interlaminar Stresses in Composite Laminates Under Uniform Axial Extension", *Journal of Composite Materials*, Vol. 4, October 1970, pp. 538-548.

27. Bogy, David B., "Edge-bonded Dissimilar Orthogonal Elastic Wedges Under Normal and Shear Loading", *Journal of Applied Mechanics*, September 1968, pp. 460-466.

28. Hess, M. S., "The End Problem for a Laminated Elastic Strip-I. The General Solution", *Journal of Composite Materials*, Vol. 3, 1969, pp. 262-280.

29. Hess, M. S., "The End Problem for a Laminated Elastic Strip-II. Differential Expansion Stresses", *Journal of Composite Materials*, Vol. 3, 1969, pp. 630-641.

30. Pipes, R. B., and Pagano, N. J., "Interlaminar Stresses in Composite Laminates-An Approximate Elasticity Solution", *Journal of Applied Mechanics*, September 1974, pp 668-672.

31. Isakson, G. and Levy, A., "Finite Element Analysis of Interlaminar Shear in Fibrous Composites", *Journal of Composite Materials*, Vol. 5, 1971, pp. 273-276.

32. Rybicki, E. F., "Approximate Three-Dimensional Solutions for Symmetric Laminates Under In-plane Loading", *Journal of Composite Materials*, Vol. 5, 1971, pp. 354-360.

33. Herakovich, C. T., "On Thermal Edge Effects in Composite Laminates", *International Journal of Mechanical Sciences*, Vol. 18, 1976, pp. 129-134.

34. Herakovich, C. T., Renieri, G. D., and Brinson, H. F., "Finite Element Analysis of Mechanical and Thermal Edge Effects in Composite Laminates", Proceedings of the Army Symposium on Solid Mechanics, Composite Materials: The Influence of Mechanics of Failure on Design, September 1976, pp. 237-247.

35. Wang, A. S. D. and Crossman, F. W., "Some New Results on Edge Effects in Symmetric Composite Laminates", *Journal of Composite Materials*, Vol. 11, 1977, pp. 92-107.

36. Whitcomb, J. D. and Raju, I. S., "Superposition Method for Analysis of Free-Edge Stresses", *Journal of Composite Materials*, Vol. 17, 1983, pp. 492-507.

37. Spilker, R. L., "Edge Effects in Symmetric Composite Laminates: Importance of Satisfying the Traction-Free-Edge Condition", *Journal of Composite Materials*, Vol. 14, 1980, pp. 2-19.

38. Whitcomb, J. D., Raju, I. S., and Goree, J. G., "Reliability of the Finite Element Method for Calculating Free Edge Stresses in Composite Laminates", *Computers and Structures*, Vol 15., 1982, pp. 23-37.

39. Raju, I. S., Crews, J. H., Jr., "Interlaminar Stress Singularities at a Straight Free Edge in Composite Laminates", *Computers and Structures* , Vol. 14, 1981, pp. 21-28.

40. Reissner, E., "Note on the Theorem of the Symmetry of the Stress Tensor", *Journal of Mathematics and Physics*, Vol. 23, 1944, pp. 192-194.

41. Tang, S., "A Boundary Layer Theory - Part I: Laminated Composites in Plane Stress", *Journal of Composite Materials*, Vol. 7, 1975, pp. 33-41.

42. Tang, S. and Levy, A., "A Boundary Layer Theory - Part II: Extension of Laminated Finite Strip", *Journal of Composite Materials*, Vol. 9, 1975, pp. 42-52.

43. Reiss, E. L. and Locke, S., "On the Theory of Plane Stress", *Quarterly of Applied Mathematics*, Vol. 19, 1961, pp. 195-203.

44. Hsu, P. W. and Herakovich, C. T., "Edge Effects in Angle-Ply Composite Laminates", *Journal of Composite Materials*, Vol. 11, 1977, pp. 422- 428.

45. Wang, J. T. S. and Dickson, J. N., "Interlaminar Stresses in Symmetric Composite Laminates", *Journal of Composite Materials*, Vol. 12, 1978, pp. 390-402.

46. Bar-Yoseph, P. and Pian, T. H. H., "Calculation of Interlaminar Stress Concentration in Composite Laminates", *Journal of Composite Materials* , Vol. 15, 1981, pp. 225-239.

47. Bar-Yoseph, P. and Avrashi, J., "New Variational-Asymptotic Formulations for Interlaminar Stress Analysis in Laminated Plates", *Journal of Applied Mathematics and Physics*, Vol. 37, 1986, pp. 305-321.

48. Bar-Yoseph, P. and Siton, G., "The Effect of Material Non-Linearity on the Interlaminar Stress Field in Composite Laminates", *Computers and Structures*, Vol. 21, 1985, pp. 1105-1118.

49. Pagano, N. J., "Stress Fields in Composite Laminates", *International Journal of Solids and Structures*, Vol. 14, 1978, pp. 385-400.

50. Reissner, E., "On a Variational Theorem in Elasticity", *Journal of Mathematical Physics*, Vol. 29, 1950, pp. 90-95.

51. Pagano, N. J., "Free Edge Stress Fields in Composite Laminates", *International Journal of Solids and Structures*, Vol. 14, 1978, pp. 401-406.

52. Pagano, N. J. and Soni, S. R., "Global-Local Laminate Variational Model", *International Journal of Solids and Structures*, Vol. 19, No. 3, 1983, pp. 207-228.

53. Whitney, J. M. and Sun, C. T., "A Higher Order Theory for Extensional Motion of Laminated Composites", *Journal of Sound and Vibration*, Vol. 30, 1973, pp. 85-97.

54. Rehfield, L. W., Armanios, E. A., and Valisetty, R. R., "Simplified Sublaminate Analysis of Composites and Applications", *Computers and Structures*, Vol. 20, 1985, pp. 401-411.

55. Valisetty, R. R. and Rehfield, L. W., "A New Ply Model For Interlaminar Stress Analysis", *Delamination and Debonding of Materials*, ASTM Technical Publication 876, W. S. Johnson, Ed, 1985.

56. Rehfield, L. W. and Valisetty, R. R., "A Simple, Refined Theory for Bending and Stretching of Homogeneous Plates", *AIAA Journal*, Vol. 22, No. 1, 1976, pp. 90-95.

57. Rehfield, L. W. and Valisetty, R. R., "A Comprehensive Theory for Planar Bending of Composite Laminates", *Computers and Structures*, Vol. 16, No. 1-4, 1983, pp. 441-447.

58. Wang, S. S. and Choi, I. "Boundary-Layer Effects in Composite Laminates: Part 1 - Free Edge Stress Singularities", *Journal of Applied Mechanics* , Vol. 49, 1982, pp. 549-560.

59. Wang, S. S. and Choi, I., "Boundary Layer Effects in Composite Laminates: Part 2 - Free Edge Stress Solutions and Basic Characteristics", *Journal of Applied Mechanics*, Vol. 49, 1982, pp. 549-560.

60. Lekhnitskii, S. G., "Theory of Elasticity of an Anisotropic Elastic Body", Holden-Day, Inc., San Francisco, 1963.

61. Zwiers, R. I., Ting, T. C. T., and Spilker, R. L., "On the Logarithmic Singularity of Free-Edge Stress in Laminated Composites Under Uniform Extension", *Journal of Applied Mechanics*, Vol. 49, 1982, pp. 561-569.

62. Dempsey, J. P. and Sinclair, G. B., "On the Stress Singularities in the Plane Elasticity of the Composite Wedge", *Journal of Elasticity*, Vol. 9, No. 4, 1979, pp. 373-391.

63. Dempsey, J. P. and Sinclair, G. B., "On the Singular Behavior at the Vertex of a Bi-Material Wedge", *Journal of Elasticity*, Vol. 11 , No. 3, 1981, pp. 317-327.

64. Salamon, N. J., "Interlaminar Stresses in a Layered Composite Laminate in Bending", *Fibre Science and Technology*, Vol. 11, 1978, pp. 305-317.

65. Murthy, P. L. N. and Chamis, C. C., "Free-Edge Delamination: Laminate Width and Loading Condition Effects", NASA TM 100238, December 1987.

66. Chan, W. S., and Ochoa, O. O., "An Integrated Finite Element Model of Edge-Delamination Analysis for Laminates Due to Tension, Bending and Torsion Loads", AIAA Paper No. 87-0704, presented at the AIAA/ASME/ ASCE/AHS 28th SDM Conference, 1987.

67. Chan, W. S. and Ochoa, O. O., "Delamination Characterization of Laminates Under Tension, Bending and Torsion Loads", *Computational Mechanics*, Vol. 6, 1990, pp. 393-405.

68. Kassapoglou, C., "Determination of Interlaminar Stresses in Composite Laminates Under Combined Loads", *Journal of Reinforced Plastics and Composites*, Vol. 9, 1990, pp. 33-57.

69. Engrand, D., "A Boundary Layer Approach to the Calculation of Transverse Stresses Along the Free Edges of a Symmetric Laminate Plate of Arbitrary Width Under In-plane Loading", I. H. Marschall, ed., Composite Structures Appl.Sc. Rub. (1981), T.P. ONERA 1981-88.

70. Pagano, N. J., "On the Significance of Effective Modulus Solutions for Fibrous Composites", *Journal of Composite Materials*, Vol. 8, 1974, pp. 214-229.

71. Shames, Irving, and Dym, Clive, *Energy and Finite Element Methods in Structural Mechanics*, McGraw-Hill, NY, 1985.

72. Griffin, O.H., Jr., Kamat, M.P., and Herakovich, C.T., "Three Dimensional Inelastic Finite Element Analysis of Laminated Composites",VPI-E-80-28, November, 1980.

73. Press, W. H., Flannery, B. P., Teukolsky, S.A., and Vetterling, W.T., *Numerical Recipes*, Cambridge University Press, NY, 1989.

74. IMSL Problem-Solving Software Systems, IMSL, Inc., 1987.

75. Herakovich, C.T., Nagarkar, A., and O'Brien, D.A., "Failure Analysis of Composite Laminates with Free Edges", *Modern Developments in Composite Materials and Structures*, J.R. Vinson, ed., ASME, New York, 1979, pp. 53-66.

76. Norwood, D.S., An Analysis of Interlaminar Stresses in Unsymmetrically Laminated Plates, Ph.D. Dissertation, Virginia Polytechnic Institute, 1990.

77. Buczek, M.B., Gregory, M.A., and Herakovich, C.T., CLFE2D - A Generalized Plane Strain Finite Element Program for Laminated Composites Subjected to Mechanical and Hygrothermal Loading, VPI-E-83-40, Virginia Polytechnic Institute, 1983.

Appendix A: Energy Expression Expansion

In this appendix the energy expression presented in Chapter 3 is expanded. To facilitate the expansion contracted notation rather than tensor notation is used for the stresses. The assumed stresses are written in the form

$$\sigma_m = F_{m1}G_{m1} + F_{m2}G_{m2} + F_{m3}G_{m3} + F_{m4}G_{m4} + F_{m5}G_{m5}$$

where F_{mi} are functions of the decay parameters and y, and G_{mi} are functions of z. The functions G_{mi} can be taken directly from the stress expressions in equations (3.86)-(3.90) and are not repeated.

$$\begin{aligned}
&F_{m1} = 0 && m=2,3,4\\
&F_{51} = a_{51}e^{-\phi_1 y}\\
&F_{61} = (1 + a_{61}e1)\\
&\\
&F_{22} = (1 + a_{22}e^{-\phi_2 y} + a_{23}e^{-\lambda_1\phi_2 y})\\
&F_{m2} = (a_{m2}e^{-\phi_2 y} + a_{m3}e^{-\lambda_1\phi_2 y}) && m = 3,4\\
&F_{m2} = 0 && m = 5,6\\
&\\
&F_{m3} = 0 && m = 2,3,4\\
&F_{m3} = (a_{m4}e^{-\phi_3 y} + a_{m5}e^{-\phi_3\lambda_2 y}) && m = 5,6\\
&\\
&F_{m4} = (a_{m6}e^{-\phi_4 y} + a_{m7}e^{-\lambda_3\phi_4 y} + a_{m8}e^{-\lambda_4\phi_4 y}) && m = 2,3,4\\
&F_{m4} = 0 && m = 5,6\\
&\\
&F_{m5} = (a_{m9}e^{-\phi_5 y} + a_{m10}e^{-\lambda_5\phi_5 y} + a_{m11}e^{-\lambda_6\phi_5 y}) && m = 2,3,4\\
&F_{m5} = 0 && m = 5,6
\end{aligned}$$

where the a_{ij}'s are determined from inspection of equations (3.86)-(3.90).

The energy expression can be written as given below

$$\begin{aligned}
\Pi_c = {} & C_1 + A_1C_2 + A_2C_3 + A_3C_4 + A_1A_2C_5\\
& A_2A_3C_6 + A_1A_3C_7 + A_1^2C_8 + A_2^2C_9 + A_3^2C_{10}
\end{aligned}$$

where the terms C_i are defined below

$$C_1 = 1/2(f_{22}^2 g_{22}^2 + f_{23}^2 g_{23}^2 + f_{24}^2 g_{24}^2 + f_{61}^2 g_{61}^2 + f_{51}^2 g_{51}^2)$$
$$+ f_{22} f_{32} g_{22} g_{32} + f_{61} f_{32} g_{61} g_{32} + f_{42} f_{51} g_{42} g_{51} + f_{61} f_{22} g_{61} g_{22}$$
$$+ (a_{22}/\phi_2 + a_{23}/(\phi_2 \lambda_2))g_{22} + (a_{61}/\phi_1)g_{61}$$

$$C_2 = f_{51} f_{53} g_{51} g_{53} + f_{61} f_{63} g_{61} g_{63} + f_{63} f_{22} g_{63} g_{22} + f_{63} f_{32} g_{63} g_{32} + f_{53} f_{42} g_{53} g_{42}$$
$$+ [a_{64}/\phi_3 + a_{65}/(\lambda_2 \phi_3)]g_{63}$$

$$C_3 = f_{22} f_{24} g_{22} g_{24} + f_{32} f_{34} g_{32} g_{34} + f_{42} f_{44} g_{42} g_{44} + f_{22} f_{34} g_{22} g_{34}$$
$$+ f_{24} f_{32} g_{24} g_{32} + f_{61} f_{24} g_{61} g_{24} + f_{61} f_{34} g_{61} g_{34} + f_{51} f_{44} g_{51} g_{44}$$
$$+ [a_{26}/\phi_4 + a_{27}/(\lambda_3 \phi_4) + a_{28}/(\lambda_4 \phi_4)]\, g_{24}$$

$$C_4 = f_{22} f_{25} g_{22} g_{25} + f_{32} f_{35} g_{32} g_{35} + f_{42} f_{45} g_{42} g_{45} + f_{22} f_{35} g_{22} g_{35}$$
$$+ f_{25} f_{32} g_{25} g_{32} + f_{61} f_{25} g_{61} g_{25} + f_{61} f_{35} g_{61} g_{35} + f_{51} f_{45} g_{51} g_{45}$$
$$+ [a_{29}/\phi_5 + a_{210}/(\lambda_5 \phi_5) + a_{211}/(\lambda_6 \phi_5)]\, g_{25}$$

$$C_5 = f_{63} f_{24} g_{63} g_{24} + f_{63} f_{34} g_{63} g_{34} + f_{53} f_{44} g_{53} g_{44}$$

$$C_6 = f_{24} f_{35} g_{24} g_{35} + f_{34} f_{25} g_{34} g_{25} + f_{24} f_{25} g_{24} g_{25} + f_{34} f_{35} g_{34} g_{35} + f_{44} f_{45} g_{44} g_{45}$$

$$C_7 = f_{63} f_{25} g_{63} g_{25} + f_{63} f_{35} g_{63} g_{35} + f_{53} f_{45} g_{53} g_{45}$$

$$C_8 = 1/2[f_{63}^2 g_{63}^2 + f_{53}^2 g_{53}^2]$$

$$C_9 = 1/2[f_{24}^2 g_{24}^2 + f_{34}^2 g_{34}^2 + f_{44}^2 g_{44}^2] + f_{24} f_{34} g_{24} g_{34}$$

$$C_{10} = 1/2[f_{25}^2 g_{25}^2 + f_{35}^2 g_{35}^2 + f_{45}^2 g_{45}^2] + f_{25} f_{35} g_{25} g_{35}$$

The integrals required to evaluate the energy expression are expanded below. In these expressions lower case f_{mi} and g_{mi} are used to denote the integrated product of the F_{mi} and G_{mi}

functions.

for m = n = 2,3,5:

$$\iint R_{mn}\sigma_m\sigma_n dydz = \Big[f_{m2}^2 g_{m2}^2 + 2A_2 f_{m2} f_{m4} g_{m2} g_{m4} + 2A_3 f_{m2} f_{m5} g_{m2} g_{m5} + 2A_2 A_3 f_{m4} f_{m5} + A_2^2 f_{m4}^2 g_{m4}^2 + A_3^2 f_{m5}^2 g_{m5}^2 \Big] R_{mn}/2$$

for m=2, n=3:

$$\iint R_{mn}\sigma_m\sigma_n dydz = \Big[f_{22} f_{32} g_{22} g_{32} + A_2(f_{22} f_{34} g_{22} g_{34} + f_{24} f_{32} g_{24} g_{32}) + A_3(f_{22} f_{35} g_{22} g_{35} + f_{25} f_{32} g_{25} g_{32}) + A_2 A_3(f_{24} f_{35} g_{24} g_{35} + f_{25} f_{34} g_{25} g_{34}) + A_2^2(f_{24} f_{34} g_{24} g_{34}) + A_3^2(f_{25} f_{35} g_{25} g_{35}) \Big] R_{mn}$$

for m = n = 5,6:

$$\iint R_{mn}\sigma_m\sigma_n dydz = \Big[f_{m1}^2 g_{m1}^2 + 2A_1(f_{m1} f_{m3} g_{m1} g_{m3}) + A_1^2(f_{m3}^2 g_{m3}^2) \Big] R_{mn}/2$$

for (m = 6,n = 2,3),(m = 5,n = 4):

$$\iint R_{mn}\sigma_m\sigma_n dydz = \Big[f_{m1} f_{n_2} g_{m1} g_{n_2} + A_1(f_{m3} f_{n_2} g_{m3} g_{n_2}) + A_2(f_{m1} f_{n4} g_{m1} g_{n4}) + A_3(f_{m1} f_{n5} g_{m1} g_{n5}) + A_1 A_2(f_{m3} f_{n4} + g_{m3} g_{n4}) + A_1 A_3(f_{m3} f_{n5} g_{m3} g_{n5}) \Big] R_{mn}$$

where

$$f_{22}^2 = 2a_{21}/\phi_2 + 2a_{22}/(\lambda_1\phi_2) + a_{22}^2 e_{2,2} + 2a_{22}a_{23}e_{2,3} + a_{23}^2 e_{3,3}$$

for (m = n = 3,4), (m = 2,n = 3)

$$f_{m2} f_{n_2} = a_{m2}(a_{n_2} e_{2,2} + a_{n3} e_{3,2}) + a_{m3}(a_{n_2} e_{2,3} + a_{n3} e_{3,3})$$

$$f_{22} f_{24} = a_{26}/\phi_4 + a_{27}/(\lambda_3\phi_4) + a_{28}/(\lambda_4\phi_4) + a_{22}(a_{26}e_{2,6} + a_{27}e_{2,6} + a_{28}e_{2,8}) + a_{23}(a_{26}e_{3,6} + a_{27}e_{3,7} + a_{28}e_{3,8})$$

---

for (m = n = 3,4), (m = 2,n = 3)

$$f_{m2}f_{n4} = a_{m2}(a_{n_6}c_{2,6} + a_{n7}c_{2,6} + a_{n8}c_{2,8}) + a_{m3}(a_{n_6}c_{2,6} + a_{n7}c_{3,7} + a_{n8}c_{3,8})$$

- - - - -

$$f_{22}f_{25} = a_{29}/\phi_5 + a_{210}/(\lambda_5\phi_5) + a_{211}/(\lambda_6\phi_5) + a_{22}(a_{29}c_{2,9} + a_{210}c_{2,10} + a_{211}c_{2,11}) + a_{23}(a_{29}c_{3,9} + a_{210}c_{3,10} + a_{210}c_{3,10})$$

for (m = n = 3,4), (m = 2,n = 3)

$$f_{m2}f_{n5} = a_{m2}(a_{n9}c_{2,9} + a_{n10}c_{2,10} + a_{n11}c_{2,11}) + a_{m3}(a_{n9}c_{2,9} + a_{n10}c_{3,10} + a_{n11}c_{3,11})$$

- - - - -

for (m = n = 2,3,4), (m = 2,n = 3)

$$f_{m4}f_{n5} = a_{m6}(a_{n9}c_{6,9} + a_{n10}c_{6,10} + a_{n11}c_{6,11}) + a_{m7}(a_{n9}c_{7,9} + a_{n10}c_{6,10} + a_{n11}c_{7,11}) + a_{m8}(a_{n9}c_{8,9} + a_{n10}c_{8,10} + a_{n11}c_{8,11})$$

$$f_{m5}f_{n4} = a_{n_6}(a_{m9}c_{6,9} + a_{m10}c_{6,10} + a_{m11}c_{6,11}) + a_{n7}(a_{m9}c_{7,9} + a_{m10}c_{6,10} + a_{m11}c_{7,11}) + a_{n8}(a_{m9}c_{8,9} + a_{m10}c_{8,10} + a_{m11}c_{8,11})$$

- - - - -

for (m = n= 2,3,4)

$$f_{m4}f_{n4} = a_{m6}(a_{m6}c_{6,6} + a_{m7}c_{6,7} + a_{m8}c_{6,8}) + a_{m7}(a_{m6}c_{6,7} + a_{m7}c_{7,7} + a_{m8}c_{7,8}) + a_{m8}(a_{m6}c_{6,8} + a_{m7}c_{7,8} + a_{m8}c_{8,8})$$

- - - - -

for (m = n = 2,3,4)

$$f_{m5}f_{n5} = a_{m9}(a_{m9}c_{9,9} + a_{m10}c_{9,10} + a_{m9}c_{9,11}) + a_{m10}(a_{m9}c_{9,10} + a_{m10}c_{10,10} + a_{m11}c_{10,11}) + a_{m11}(a_{m9}c_{9,11} + a_{m10}c_{10,11} + a_{m11}c_{11,11})$$

- - - - -

$$f_{61}^2 = 2a_{61}/\phi_1 + a_{61}^2 e_{1,1}$$
$$f_{51}^2 = a_{51}^2 e_{1,1}$$

$$f_{61} f_{63} = a_{64}/\phi_3 + a_{65}/\lambda_2\phi_3 + a_{61}(a_{64}e_{1,4} + a_{65}e_{1,5})$$
$$f_{51} f_{63} = a_{51}(a_{54}e_{1,4} + a_{55}e_{1,5})$$

---

for (m = 5,6)

$$f_{m3}^2 = a_{m4}^2 e_{4,4} + 2a_{m4}a_{m5}e_{4,5} + a_{m5}^2 e_{5,5}$$

$$f_{61} f_{22} = a_{22}/\phi_2 + a_{23}/(\lambda_1\phi_2) + a_{61}/\phi_1 + a_{61}(a_{22}e_{1,2} + a_{23}e13)$$
$$f_{63} f_{22} = a_{64}/\phi_3 + a_{65}/(\lambda_2\phi_3) + a_{64}(a_{22}e_{2,4} + a_{23}e_{3,4}) + a_{65}(a_{22}e_{2,5} + a_{23}e_{3,5})$$
$$f_{61} f_{24} = a_{26}/\phi_4 + a_{27}/(\lambda_3\phi_4) + a_{28}/(\lambda_4\phi_4) + a_{61}(a_{26}e_{1,6} + a_{27}e_{1,7} + a_{28}e_{1,8})$$
$$f_{61} f_{25} = a_{29}/\phi_5 + a_{210}/(\lambda_5\phi_5) + a_{211}/(\lambda_6\phi_5) + a_{61}(a_{29}e_{1,9} + a_{210}e_{1,10} + a_{211}e_{1,11})$$

---

for (m = 6,n = 3), (m = 5,n = 4)

$$f_{m1} f_{m2} = a_{m1}(a_{n_2}e_{1,2} + a_{n3}e_{1,3})$$
$$f_{m3} f_{n_2} = a_{m6}(a_{n_2}e_{2,4} + a_{n3}e_{3,4})$$
$$f_{m1} f_{n4} = a_{m6}(a_{n_6}e_{1,6} + a_{n7}e_{1,7} + a_{n8}e_{1,8})$$
$$f_{m1} f_{n5} = a_{m6}(a_{n9}e_{1,9} + a_{n10}e_{1,10} + a_{n11}e_{1,11})$$

---

for (m = 6,n = 2,3) , (m = 5,n = 4)

$$f_{m3} f_{n4} = a_{m4}(a_{n_6}e_{46} + a_{n7}e_{47} + a_{n8}e_{48}) + a_{m5}(a_{n_6}e_{5,6} + a_{n7}e_{5,7} + a_{n8}e_{5,8})$$

where the $e_{i,j}$'s are given by

$$e_{ij} = \frac{1}{q_i + q_j}$$

and

$$q_1 = \phi_1 \quad q_2 = \phi_2 \quad q_3 = \phi_2\lambda_1$$
$$q_4 = \phi_3 \quad q_5 = \phi_3\lambda_2 \quad q_6 = \phi_4$$
$$q_7 = \lambda_3\phi_4 \quad q_8 = \lambda_4\phi_4 \quad q_9 = \phi_5$$
$$q_{10} = \lambda_5\phi_5 \quad q_{11} = \lambda_6\phi_5$$

The through-thickness integration terms are given by:

$$g_{22}^2 = R_{22}\,[\,B_3^2t^3 + 3B_3B_4t^2 + 3B_4^2t\,]/3.$$

$$g_{32}^2 = R_{33}/1260\Big[\,5B_3^2t^7 + 35B_3B_4t^6 + 84B_3B_6t^5 + 63B_4^2t^5 + (\,105B_3B_7 + 315B_4B_6\,)\,t^4 + 420\,(\,B_4B_7 + B_6^2\,)\,t^3 + 1260\,(\,B_6B_7t^2 + B_7^2t\,)\Big]$$

$$g_{61}^2 = R_{66}/3\Big[\,B_1^2t^3 + 3B_1B_2t^2 + 3B_2^2t\Big]$$

$$g_{22}g_{32} = R_{23}/30\Big[\,B_3^2t^5 + 5B_3B_4t^4 + (\,10B_3B_6 + 5B_4^2\,)\,t^3 + 15\,(\,B_3B_7 + B_4B_6\,)\,t^2 + 30B_4B_7t\Big]$$

$$g_{22}g_{61} = R_{26}/6\Big[\,2B_1B_3t^3 + 3\,(\,B_1B_4 + B_2B_3\,)\,t^2 + 6B_2B_4t\Big]$$

$$g_{32}g_{61} = R_{36}/120\Big[\,4B_1B_3t^5 + (\,15B_1B_4 + 5B_2B_3\,)\,t^4 + (\,40B_1B_6 + 20B_2B_4\,)\,t^3 + 60\,(\,B_1B_7 + B_2B_6\,)\,t^2 + 120B_2B_7t\,)\Big]$$

$$g_{51}g_{42} = R_{45}/120\Big[\,6B_1B_3t^5 + 15\,(\,B_1B_4 + B_2B_3\,)\,t^4 + 20\,(\,B_1B_6 + B_3B_5 + 2B_2B_4\,)\,t^3 + 60\,(\,B_2B_6 + B_4B_5\,)\,t^2 + 120B_5B_6t\Big]$$

$$g_{42}^2 = R_{44}/60\Big[\,3B_3^2t^5 + 15B_3B_4t^4 + 20\,(\,B_3B_6 + B_4^2\,)\,t^3 + 60B_4B_6t^2 + 60B_6^2t\Big]$$

$$g_{51}^2 = R_{55/60}\Big[\,3B_1^2t^5 + 15B_1B_2t^4 + 20\,(\,B_1B_5 + B_2^2\,)\,t^3 + 60\,(\,B_2B_5t^2 + B_5^2t\,)\Big]$$

$$g_{22} = \bar{S}_{12}/\bar{S}_{11}\,(\,6B_4CSIG1\;t + 3CSIG2\;t^2 + 2CSIG3\;t^3\,)/6$$

$$g_{61} = \bar{S}_{16}/\bar{S}_{11}\,(\,6B_2CSIG1\;t + 3CSIG4\;t^2 + 2CSIG5\;t^3\,)/6$$

$$g_{22}g_{24} = R_{22}\,[\,B_3t\delta v(1)\varepsilon_t + B_4\,(\,DIFNU\,)\,]$$

$$g_{24}^2 = R_{22}\left[4 / t\,(QUANU) \right]$$

$$g_{32}g_{34} = R_{33} / 2520\Big[2B_3t^5\,(DIFNU3) + 21B_4t^4\,DIFNU2 + 42B_6t^3\,DIFNU4 + 210B_7t^2\,(DIFNU) \Big]$$

$$g_{34}^2 = R_{33}t^3 / 210\,(QUANU2)$$

$$g_{61}g_{63} = R_{66} / 3\,[\, B_1t\,(DIFMI2) + 3B_2\,(DIFMI1)\,]$$

$$g_{63}^2 = 4R_{66} / 3t\,(QUAMI1)$$

$$g_{61}g_{34} = -R_{23} / 60\,[\, B_3t^3\,(DIFNU4) + 5B_4t^2\,(DIFNU)\,]$$

$$g_{24}g_{32} = R_{23} / 60\Big[B_3t^3\,(SUMNU3) + 5B_4t^2\,(SUMNU4) + 60B_6t\delta\nu(1)\varepsilon_t + 60B_7\,(DIFNU) \Big]$$

$$g_{24}g_{34} = -R_{23}t / 15\,(QUANU3)$$

$$g_{22}g_{63} = R_{26} / 3\,[\, B_3t\,(DIFMI2) + 3B_4\,(DIFMI1)\,]$$

$$g_{22}g_{61} = R_{26}\,[\, B_1t\delta\nu(1)\varepsilon_t + B_2\,(DIFNU)\,]$$

$$g_{24}g_{63} = 2R_{26} / t\,[\, \delta\nu(1)\delta\eta(1)\varepsilon_t^2 + \delta\nu(2)\delta\eta(2)\varepsilon_b^2\,]$$

$$g_{32}g_{63} = R_{36} / 60\left[B_3t^3\,(DIFMI4) + 5B_4t^2\,(DIFMI3) + 20B_6t\,(DIFMI2) + 60B_7\,(DIFMI1) \right]$$

$$g_{34}g_{61} = -R_{36} / 60\,[\, B_1t^3\,(DIFNU4) + 5B_2t^2\,(DIFNU)\,]$$

$$g_{34}g_{63} = -R_{36}t / 30\,[\, \delta\eta(1)\varepsilon_t\,(DIFNU4) - \delta\eta(2)\varepsilon_b\,(DIFNU5)\,]$$

$$g_{42}g_{53} = R_{45} / 60 \left[B_3 t^3 \left(SUMMI3 \right) + 5B_4 t^2 \left(SUMMI2 \right) + 20B_6 t \left(SUMMI1 \right) \right]$$

$$g_{44}g_{51} = R_{45} / 60 \left[B_1 t^3 \left(DIFNU4 \right) + 5B_2 t^2 \left(DIFNU \right) \right]$$

$$g_{44}g_{53} = R_{45} / 30 \left[\delta\eta(1)\varepsilon_t \left(DIFNU4 \right) - \delta\eta(2)\varepsilon_b \left(DIFNU5 \right) \right]$$

$$g_{42}g_{44} = R_{44} / 60 \left[B_3 t^3 \left(DIFNU4 \right) + 5B_4 t^2 \left(DIFNU \right) \right]$$

$$g_{42}^2 = R_{44} t / 15 \left(QUANU3 \right)$$

$$g_{51}g53 = R_{55} / 60 \left[B_1 t^3 \left(SUMMI3 \right) + 5B_2 t^2 \left(SUMMI2 \right) + 20B_5 t \left(SUMMI1 \right) \right]$$

$$g_{53}^2 = R_{55} t / 15 \left(QUAMI2 \right)$$

$$g_{24} = S_{12} / S_{11} \left[\delta\nu(1)\varepsilon_t t \left(B_9\bar{S}_{11} + B_3\bar{S}_{12} + B_1\bar{S}_{16} \right) + \left(DIFNU \right) \left(CSIG1 \right) \right]$$

$$g_{53} = S_{16} / \left(3S_{11} \right) \left[t \left(DIFMI2 \right) \left(B_9\bar{S}_{11} + B_3\bar{S}_{12} + B_1\bar{S}_{16} \right) + 3 \left(DIFMI1 \right) \left(CSIG1 \right) \right]$$

$$g_{22}g_{25} = S_{22} \left[- B_3 DIFNUB \right]$$

$$g_{24}g_{25} = S_{22} \left[- 6 / t^2 \left(DIFNUB\ SUMNU \right) \right]$$

$$g_{25}^2 = S_{22} \left[12 / t^3 \left(DIFNU \right)^2 \right]$$

$$g_{32}g_{35} = S_{33}h / 840 \left[5t^3 B_3 SUMNU5 + 28B_4 t^2 \left(SUMNU6 \right) + 42B_6 t \left(SUMNU7 \right) + 420B_7 \left(SUMNU \right) \right]$$

$$g_{34}g_{35} = - 11S_{33}t^2 / 210 \left[\left(DIFNU \right) \left(SUMNU \right) \right]$$

$$g_{35}^2 = S_{33} t / 35 \left[QUANU \right]$$

$$g_{22}g_{35} = S_{23}t / 20 \left[B_3 t \left(SUMNU7 \right) + 10B_4 \left(SUMNU \right) \right]$$

$$g_{32}g_{25} = -S_{23} / 20 \left(DIFNU \right) \left(3B_3 t^2 + 10B_4 t + 20B_6 \right)$$

$$g_{24}g_{35} = 11S_{23} / 10 \left(DIFNU \right) \left(SUMNU \right)$$

$$g_{32}g_{25} = S_{23} / 10 \left(DIFNU \right) \left(SUMNU \right)$$

$$g_{25}g_{35} = -6S_{23} / \left(5t \right) \left(DIFNU \right)^2$$

$$g_{61}g_{25} = -S_{26}B_1 \left(DIFNU \right)$$

$$g_{61}g_{25} - 2S_{26} / t^2 \left(DIFNU \right) \left(SUMMI1 \right)$$

$$g_{61}g_{35} = S_{36}t / 20 \left[B_1 t \left(SUMNU7 \right) + 10B_2 \left(SUMNU \right) \right]$$

$$g_{63}g_{35} = -S_{36} / 10 \left[\varepsilon_b \delta\eta(2) \left(SUMNU8 \right) - \varepsilon_t \delta\eta(1) \left(SUMNU7 \right) \right]$$

$$g_{51}g_{45} = S_{45} / 20 \left[\left(DIFNU \right) \left(3b1h2 + 10B_2 t + 20B_5 \right) \right]$$

$$g_{53}g_{45} = 3S_{45} / 10 \left[\left(DIFNU \right) \left(SUMMI1 \right) \right]$$

$$g_{42}g_{45} = S_{44} / 20 \left[\left(DIFNU \right) \left(3B_3 t^2 + 10B_4 t + 20B_6 \right) \right]$$

$$g_{45}g_{44} = -S_{44} / 10 \left[\left(DIFNU \right) \left(SUMNU \right) \right]$$

$$g_{45}^2 = 6S_{44} / \left(5t \right) \left[\left(DIFNU \right)^2 \right]$$

where

$$SUMNU = \left[\delta v(1)\varepsilon_t + \delta v(2)\varepsilon_b \right]$$

$$SUMNUB = [\ \delta\nu(1)_n\varepsilon_t + \delta\nu(2)_n\varepsilon_b\ ]$$

$$SUMNU2 = [\ \delta\nu(1)\varepsilon_t + 2\delta\nu(2)\varepsilon_b\ ]$$

$$SUMNU3 = [\ 7\delta\nu(1)\varepsilon_t + 2\delta\nu(2)\varepsilon_b\ ]$$

$$SUMNU4 = [\ 5\delta\nu(1)\varepsilon_t + \delta\nu(2)\varepsilon_b\ ]$$

$$SUMNU5 = [\ 6\delta\nu(1)_n\varepsilon_t + \delta\nu(2)_n\varepsilon_b\ ]$$

$$SUMNU6 = [\ 4\delta\nu(1)_n\varepsilon_t + \delta\nu(2)_n\varepsilon_b\ ]$$

$$SUMNU7 = [\ 7\delta\nu(1)_n\varepsilon_t + 3\delta\nu(2)_n\varepsilon_b\ ]$$

$$SUMNU8 = [\ 3\delta\nu(1)_n\varepsilon_t + 7\delta\nu(2)_n\varepsilon_b\ ]$$

$$DIFNU = [\ \delta\nu(1)\varepsilon_t - \delta\nu(2)\varepsilon_b\ ]$$

$$DIFNUB = [\ \delta\nu(1)_n\varepsilon_t - \delta\nu(2)_n\varepsilon_b\ ]$$

$$DIFNU2 = [\ 2\delta\nu(1)\varepsilon_t - \delta\nu(2)\varepsilon_b\ ]$$

$$DIFNU3 = [\ 5\delta\nu(1)\varepsilon_t - 2\delta\nu(2)\varepsilon_b\ ]$$

$$DIFNU4 = [\ 3\delta\nu(1)\varepsilon_t - 3\delta\nu(2)\varepsilon_b\ ]$$

$$DIFNU5 = [\ 2\delta\nu(1)\varepsilon_t - 3\delta\nu(2)\varepsilon_b\ ]$$

$$QUANU = [\ \delta\nu^2(1)\varepsilon_t^2 + \delta\nu(1)\delta\nu(2)\varepsilon_b\varepsilon_t + \delta\nu^2(2)\varepsilon_b^2\ ]$$

$$QUANU2 = [\ 2\delta\nu^2(1)\varepsilon_t^2 - 3\delta\nu(1)\delta\nu(2)\varepsilon_b\varepsilon_t + 2\delta\nu^2(2)\varepsilon_b^2\ ]$$

$$QUANU3 = [\, 2\delta\nu^2(1)\varepsilon_t^2 - \delta\nu(1)\delta\nu(2)\varepsilon_b\varepsilon_t + 2\delta\nu^2(2)\varepsilon_b^2 \,]$$

$$QUANU4 = [\, 13\delta\nu^2(1)_n\varepsilon_t^2 + 9\delta\nu(1)_n\delta\nu(2)_n\varepsilon_b\varepsilon_t + 13\delta\nu^2(2)_n\varepsilon_b^2 \,]$$

$$DIFMI1 = [\, \delta\eta(1)\varepsilon_t - \delta\eta(2)\varepsilon_b \,]$$

$$DIFMI2 = [\, 2\delta\eta(1)\varepsilon_t - \delta\eta(2)\varepsilon_b \,]$$

$$DIFMI3 = [\, 3\delta\eta(1)\varepsilon_t - \delta\eta(2)\varepsilon_b \,]$$

$$DIFMI4 = [\, 4\delta\eta(1)\varepsilon_t - \delta\eta(2)\varepsilon_b \,]$$

$$SUMMI1 = [\, \delta\eta(1)\varepsilon_t + \delta\eta(2)\varepsilon_b \,]$$

$$SUMMI2 = [\, 3\delta\eta(1)\varepsilon_t + \delta\eta(2)\varepsilon_b \,]$$

$$SUMMI3 = [\, 6\delta\eta(1)\varepsilon_t + \delta\eta(2)\varepsilon_b \,]$$

$$QUAMI1 = [\, \delta\eta^2(1)\varepsilon_t^2 - \varepsilon_b\varepsilon_t\delta\eta(1)\delta\eta(2) + \varepsilon_b^2\delta\eta^2(2) \,]$$

$$QUAMI2 = [\, 3\delta\eta^2(1)\varepsilon_t^2 + \delta\eta(1)\delta\eta(2)\varepsilon_b\varepsilon_t + 3\delta\eta^2(2)\varepsilon_b^2 \,]$$

Appendix B: Two-term Solution

The expressions for the two term solution are presented below. In these expressions G is the shear modulus of the resin layer and is taken to be 0.25 msi.

$$\sigma_{12}^{(k)} = \left(1 - e^{-\phi y}\right)\left[B_1^{(k)} z + B_2^{(k)}\right] \tag{B.1}$$

$$- \frac{G}{\phi}\left(\lambda e^{-\lambda\phi y} - e^{-\phi y}\right)\left[\frac{2z}{[t^{(k)}]^2}\left(\delta\eta_{12,1}(k,1)\varepsilon_t^{(k)} + \delta\eta_{12,1}(k,2)\varepsilon_b^{(k)}\right) - \frac{2}{t^{(k)}}\delta\eta_{12,1}(k,2)\varepsilon_b^{(k)}\right]$$

$$\sigma_{13}^{(k)} = \phi\, e^{-\phi y}\left[B_1^{(k)} z^2/2 + B_2^{(k)} z + B_5^{(k)}\right] \tag{B.2}$$

$$+ G\left(\lambda e^{-\lambda\phi y} - e^{-\phi y}\right)\left[\delta\eta_{12,1}(k,1)\varepsilon_t^{(k)} z^2/(t^{(k)})^2 + \delta\eta_{12,1}(k,2)\varepsilon_b^{(k)}(1 - z/(t^{(k)})^2)\right]$$

$$\sigma_{22}^{(k)} = \left[1 - \frac{\lambda}{\lambda - 1}\left(e^{-\phi y} - \frac{1}{\lambda}e^{-\lambda\phi y}\right)\right]\left[B_3^{(k)} z + B_4^{(k)}\right] \tag{B.3}$$

$$- G\phi\left[\frac{1}{\lambda}e^{-\lambda\phi y} - \frac{1}{\lambda\phi}(1 - \lambda)(\phi y + 1)e^{-\phi y} - \frac{1}{\phi}e^{-\phi y}\right]\left[\delta\nu_{12}(k,1)\varepsilon_t^{(k)}\left(6z/(t^{(k)})^2 - 2/t^{(k)}\right)\right.$$

$$\left. + \delta\nu_{12}(k,2)\varepsilon_b^{(k)}\left(6z/(t^{(k)})^2 - 4/t^{(k)}\right)\right]$$

$$\sigma_{23}^{(k)} = \phi\frac{\lambda}{\lambda - 1}\left[e^{-\lambda\phi y} - e^{-\lambda\phi y}\right]\left[B_3^{(k)} z^2/2 + B_4^{(k)} z + B_6^{(k)}\right] \tag{B.4}$$

$$+ G\left[e^{-\phi y} + \frac{\phi}{\lambda}(1 - \lambda)y e^{-\phi y} - e^{-\lambda\phi y}\right]\left[\delta\nu_{12}(k,1)\varepsilon_t^{(k)}\left(3z^2/(t^{(k)})^2 - 2z/t^{(k)}\right)\right.$$

$$\left. + \delta\nu_{12}(k,2)\varepsilon_b^{(k)}\left(3z^2/(t^{(k)})^2 - 4z/t^{(k)} + 1\right)\right]$$

$$\sigma_{33}^{(k)} = \phi^2\frac{\lambda}{\lambda - 1}\left[\lambda e^{-\lambda\phi y} - e^{-\phi y}\right]\left[B_3^{(k)} z^3/6 + B_4^{(k)} z^2/2 + B_6^{(k)} z + B_7^{(k)}\right] \tag{B.5}$$

$$- G\left[-\phi e^{-\phi y} + \frac{\phi}{\lambda}(1 - \lambda)(e^{-\phi y} - y\phi e1) + \lambda\phi e^{-\lambda\phi y}\right]\left[\delta\nu_{12}(k,1)\varepsilon_t^{(k)}\left(z^3/(t^{(k)})^2 - z^2/t^{(k)}\right)\right.$$

$$\left. + \delta\nu_{12}(k,2)\varepsilon_b^{(k)}\left(z^3/(t^{(k)})^2 - 2z^2/t^{(k)} + z\right)\right]$$

Appendix C: Cross-Ply and Angle-Ply Laminates

TABLE C.1. CLT Stresses for Symmetric Cross-Ply Laminates

Uniform Extension $\varepsilon_{11} = 0.1\%$							
$[0_4/90_4]_s$				$[90_4/0_4]_s$			
Ply	σ_{11} (ksi)	σ_{22} (ksi)	σ_{12} (ksi)	Ply	σ_{11} (ksi)	σ_{22} (ksi)	σ_{12} (ksi)
0°	192.8	3.196	0.000	90°	192.8	3.196	0.000
90°	15.54	-3.196	0.000	0°	15.54	-3.196	0.000
Uniform Bending $\kappa_{11} = 0.1$							
$[0_4/90_4]_s$				$[90_4/0_4]_s$			
Ply	σ_{11} (ksi)	σ_{22} (ksi)	σ_{12} (ksi)	Ply	σ_{11} (ksi)	σ_{22} (ksi)	σ_{12} (ksi)
0°	-57.76	-0.661	0.000	90°	-4.677	0.146	0.000
90°	-1.530	1.542	0.000	0°	-19.28	-0.3416	0.000

TABLE C.2. CLT Stresses for Unsymmetric Cross-Ply Laminates

Uniform Extension N_{11} = 1000 lb/in			
Ply	σ_{11} (ksi)	σ_{22} (ksi)	σ_{12} (ksi)
0°	36.62	0.418	0.000
90°	13.38	0.419	0.000
Uniform Bending M_{11} = 1 lb–in/in			
Ply	σ_{11} (ksi)	σ_{22} (ksi)	σ_{12} (ksi)
0°	-1.135	0.000	0.000
90°	1.135	0.000	0.000

TABLE C.3. CLT Stresses for Angle-Ply Laminates

$[(\pm 10)_2]_s$ and $[+10_2/-10_2]_s$ Laminates $\varepsilon_{11} = 0.1\%$			
Ply	σ_{11} (ksi)	σ_{22} (ksi)	σ_{12} (ksi)
10°	17.80	0.000	2.779
-10°	17.80	0.000	2.779

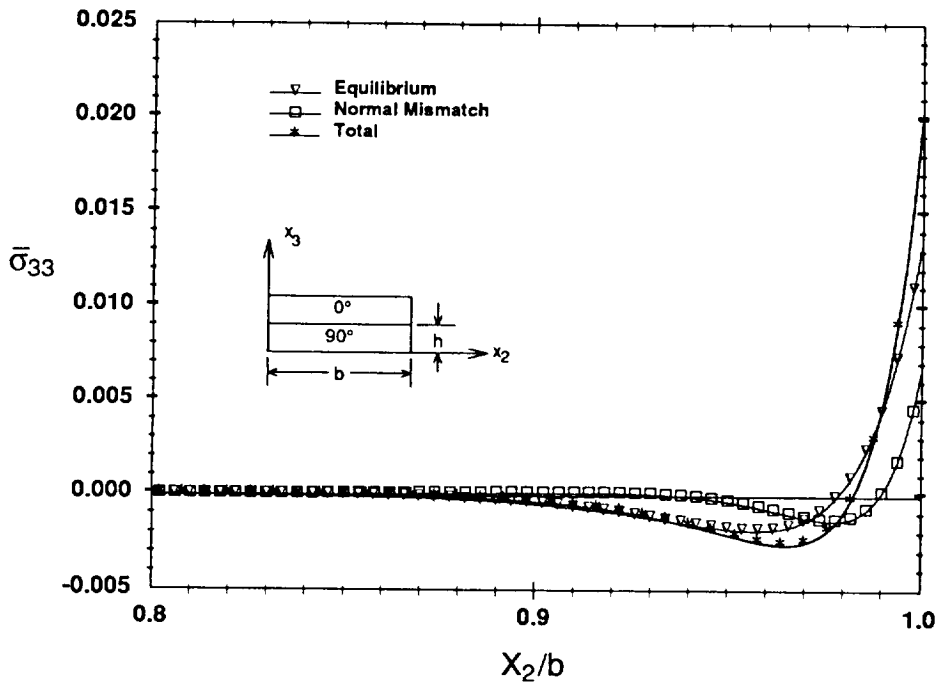

Figure C.1. σ_{33} Stress at 0/90 Interface for $[0_4/90_4]_s$ Laminate - Extension

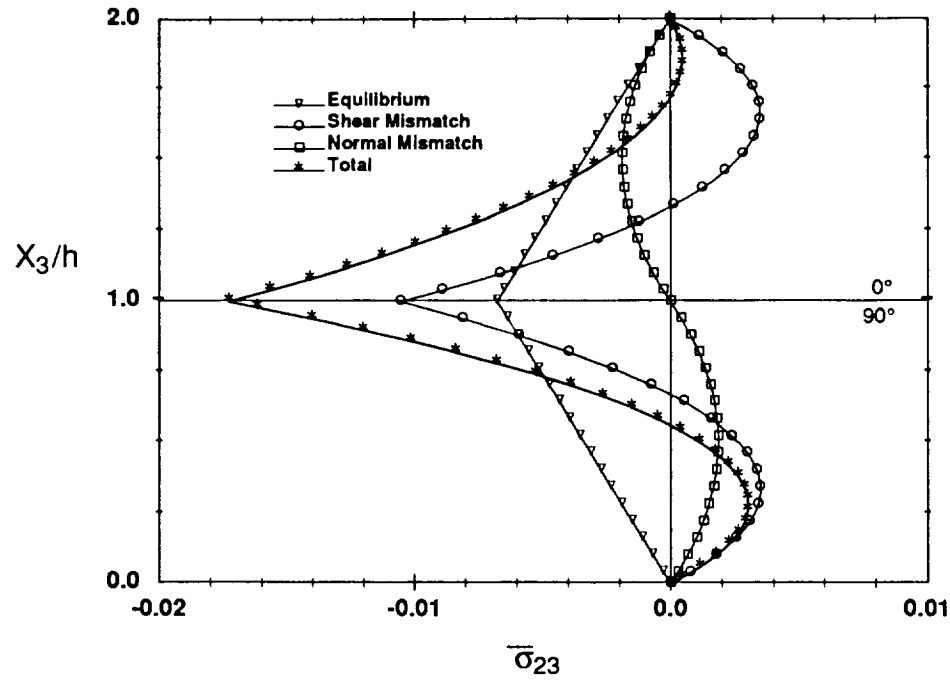

(a) $[0_4/90_4]_s$ Laminate

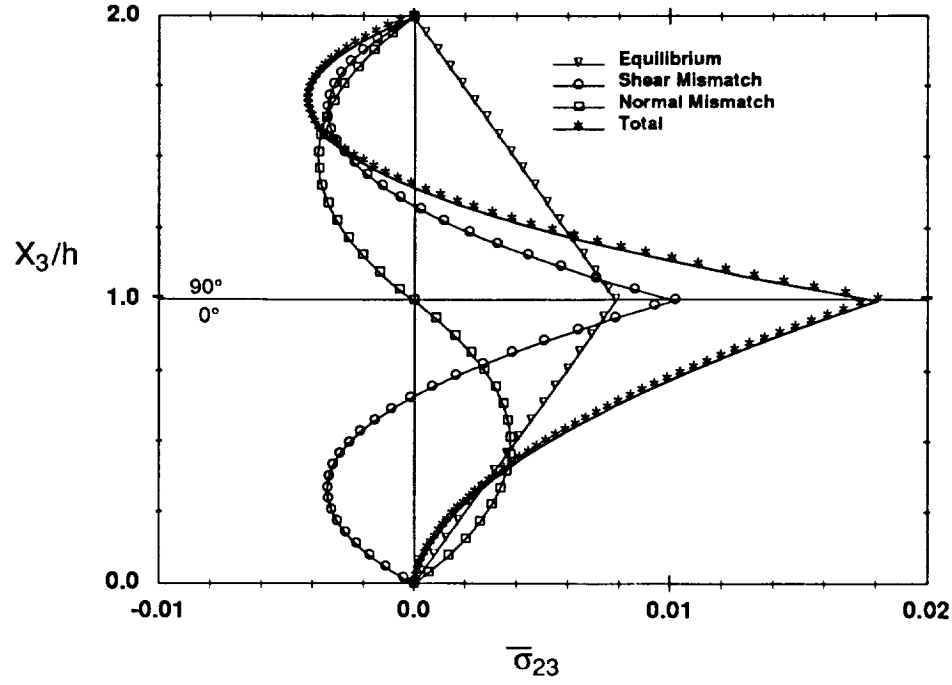

(b) $[90_4/0_4]_s$ Laminate

Figure C.2. Contributions to σ_{33} - Extension Load

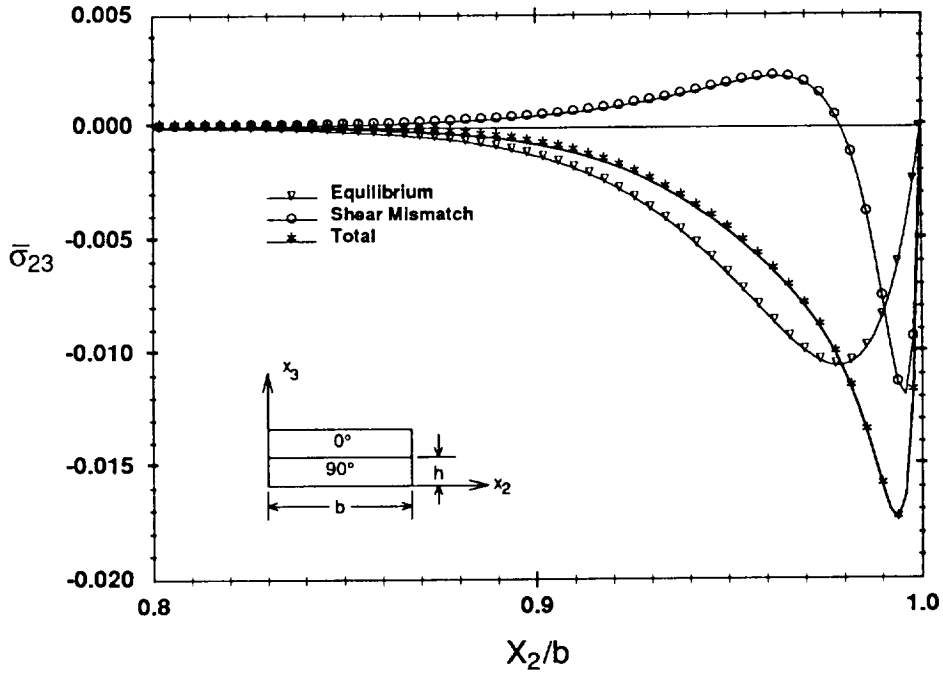

(a) $[0_4/90_4]_s$ Laminate

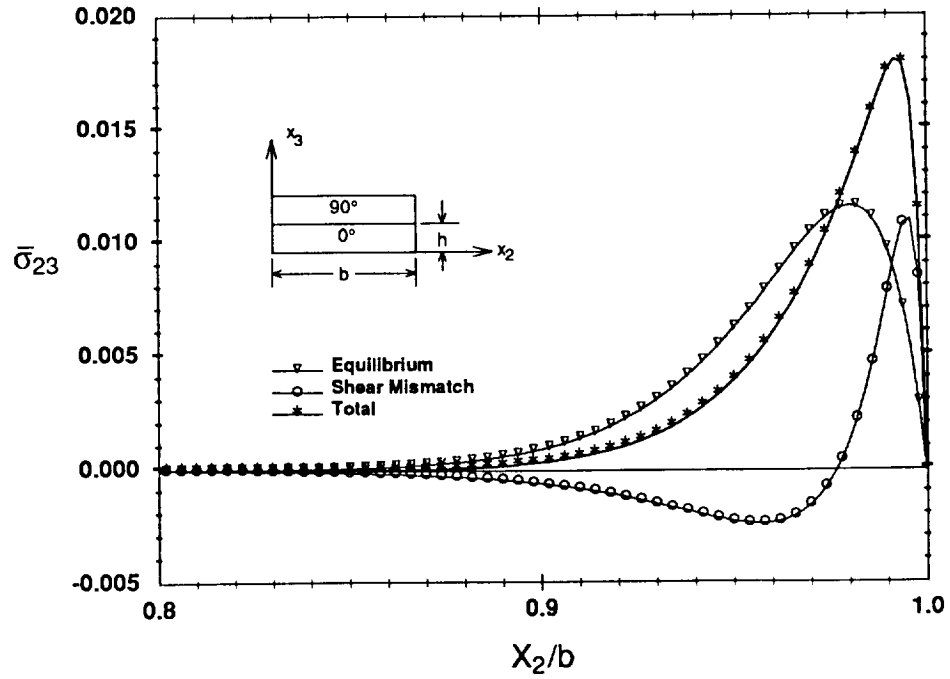

(b) $[90_4/0_4]_s$ Laminate

Figure C.3. Contributions to σ_{23} Stress at 0/90 Interface for $[0_4/90_4]_s$ and $[90_4/0_4]_s$ Laminates - Extension

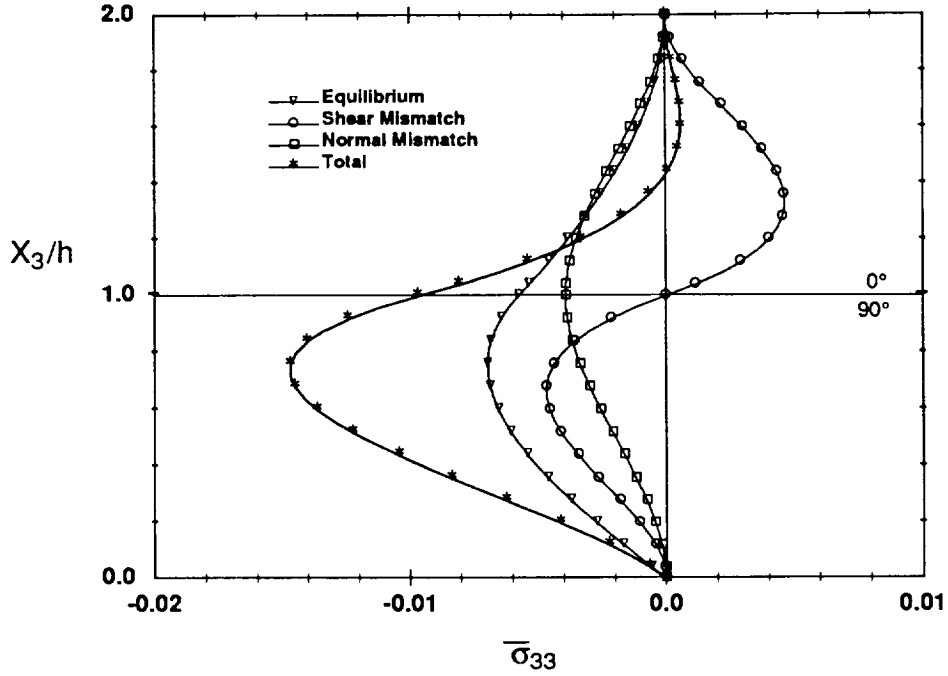

(a) $[0_4/90_4]_s$ Laminate

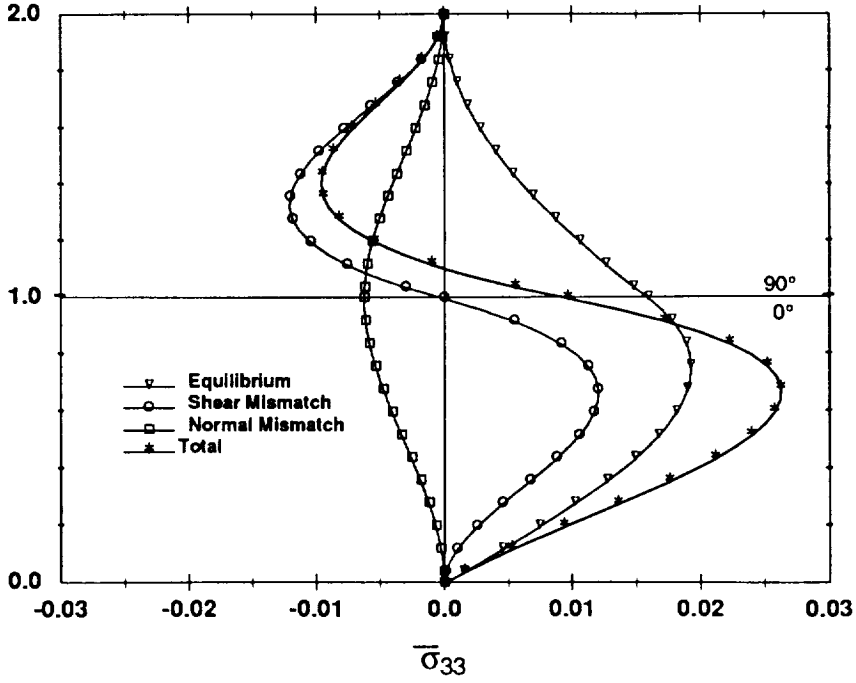

(b) $[90_4/0_4]_s$ Laminate

Figure C.4. Contributions to σ_{33} Stress at $X_2/b = 0.999$ for $[0_4/90_4]_s$ and $[90_4/0_4]_s$ Laminates - Bending

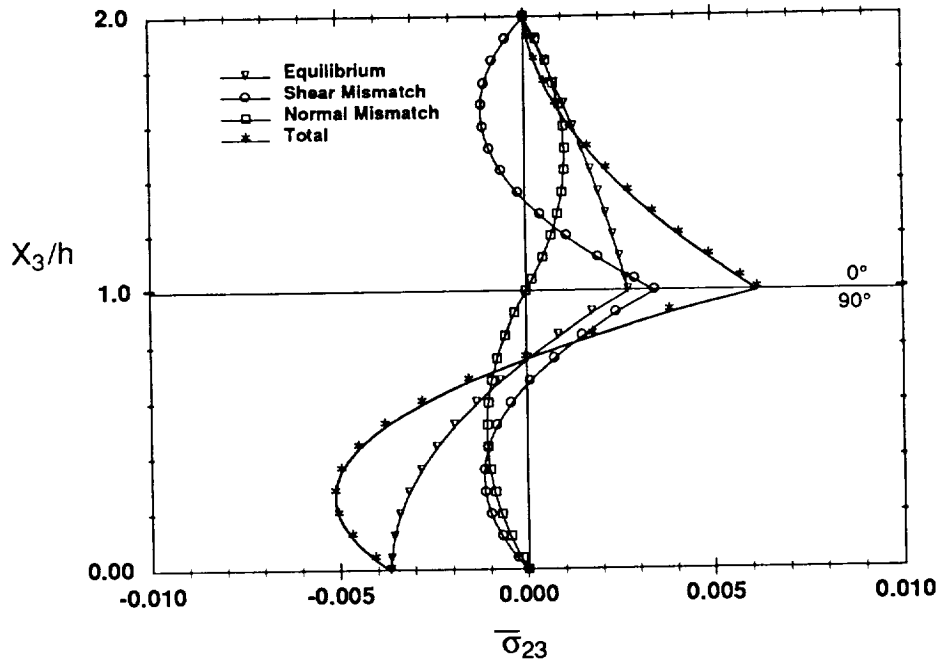

(a) $[0_4/90_4]_s$ Laminate

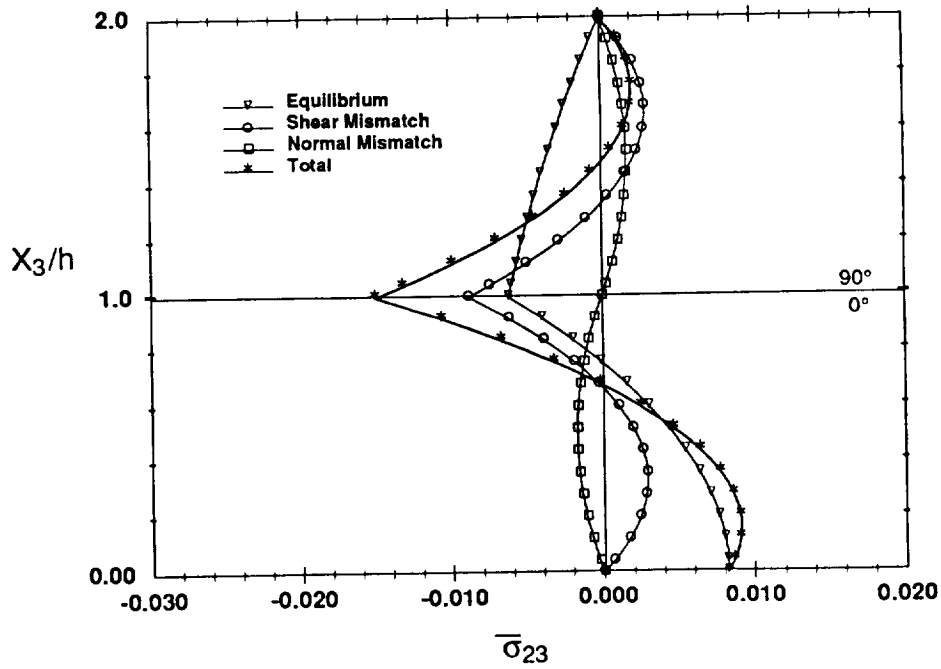

(b) $[90_4/0_4]_s$ Laminate

Figure C.5. Contributions to σ_{23} Stress at $X_2/b = 0.993$ for $[0_4/90_4]_s$ and $[90_4/0_4]_s$ Laminates - Bending

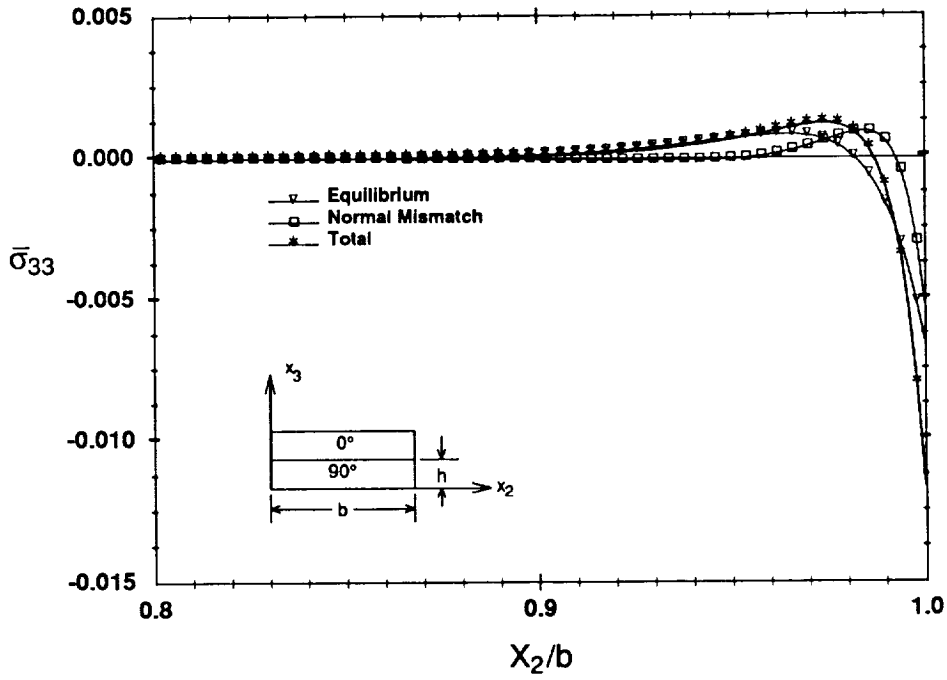

(a) $[0_4/90_4]_s$ Laminate

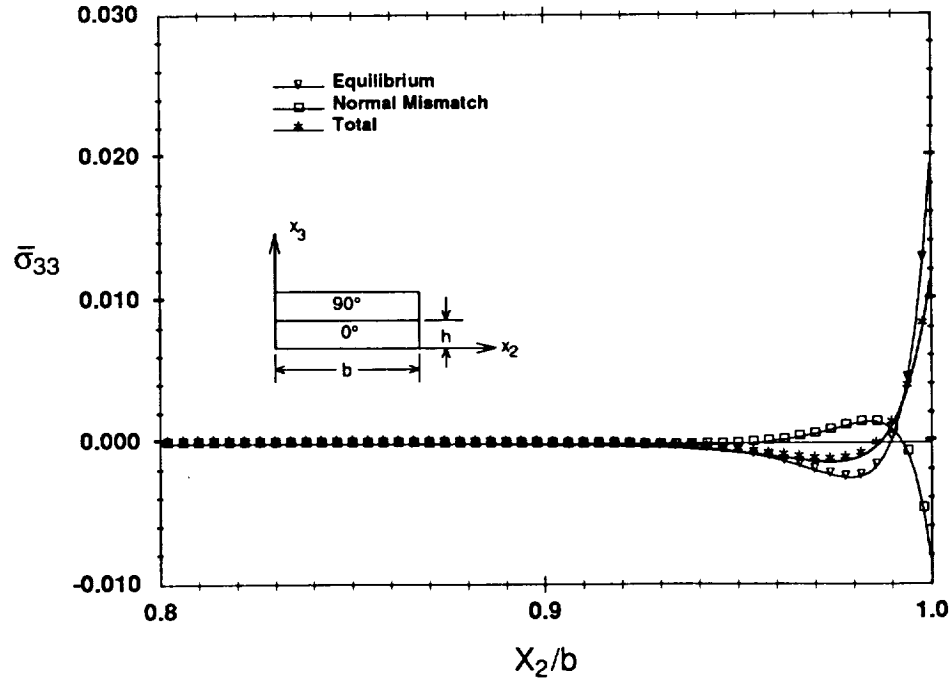

(b) $[90_4/0_4]_s$ Laminate

Figure C.6. Contributions to σ_{33} Stress at 0/90 Interface for $[0_4/90_4]_s$ and $[90_4/0_4]_s$ Laminates - Extension

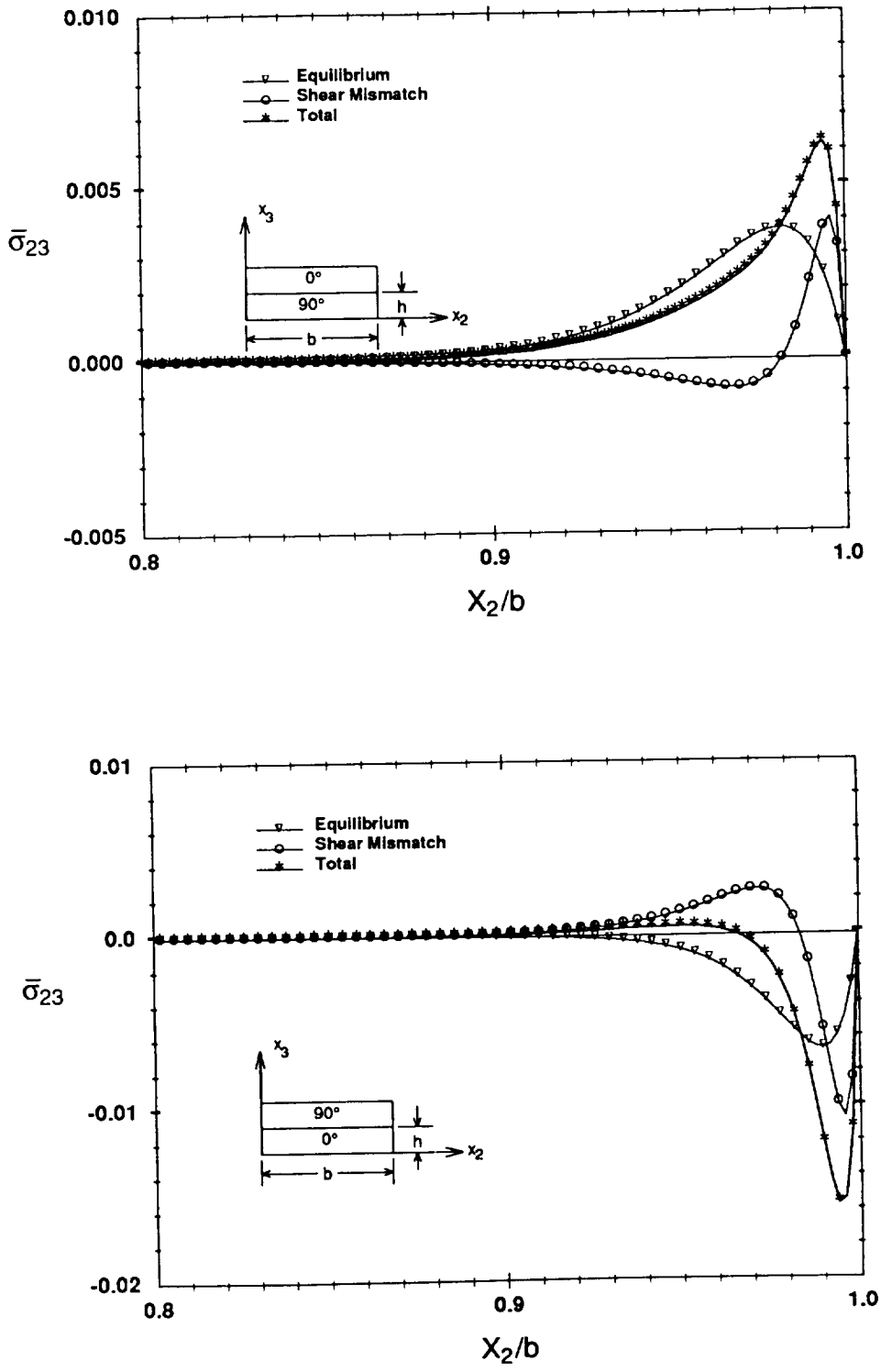

Figure C.7. Contributions to σ_{23} Stress at 0/90 Interface for $[0_4/90_4]_s$ and $[90_4/0_4]_s$ Laminates - Extension

Appendix D: Quasi-Isotropic Laminates

TABLE D.1. CLT Stresses for Quasi-Isotropic Laminates

All quasi-isotropic $\varepsilon_{11} = 0.1\%$			
Ply	σ_{11} (ksi)	σ_{22} (ksi)	σ_{12} (ksi)
0°	19.18	-0.096	0.000
90°	1.455	-5.368	0.000
45°	4.858	2.730	-3.111
-45°	4.858	2.730	-3.111

TABLE D.2. Solution Parameters for Quasi-Isotropic Laminates - Group 1

Solution Parameters For Quasi-Isotropic Laminates $\varepsilon_{11} = 0.1\%$			
Constant	$[0/-45/90/-45]_s$	$[90/45/0/-45]_s$	$[45/90/0/-45]_s$
ϕ_1 (1/in)	66.93	50.02	54.86
ϕ_2 (1/in)	81.68	61.75	59.83
ϕ_3 (1/in)	57.73	99.81	47.06
ϕ_4 (1/in)	128.4	56.23	70.08
ϕ_5 (1/in)	59.99	174.5	95.28
λ_1	5.698	1.386	6.725
λ_2	4.223	3.189	7.801
λ_3	3.394	3.661	12.32
λ_4	8.207	21.11	11.90
λ_5	6.748	5.047	1.490
λ_6	18.68	0.352	1.572
$A_1 X10^{-5}$ (psi)	1.242	3.703	6.204
$A_2 X10^{-5}$ (psi)	-4.318	-3.801	-1.057
$A_3 X10^{-5}$ (psi)	-0.009	-1.002	-0.386
h (in)	.020	.020	.020

TABLE D.3. Solution Parameters for Quasi-Isotropic Laminates - Group 2

Solution Parameters For Quasi-Isotropic Laminates $\varepsilon_{11} = 0.1\%$			
Constant	$[45/90/-45/0]_s$	$[45/0/90/-45]_s$	$[45/0/-45/90]_s$
ϕ_1 (1/in)	66.66	53.10	52.32
ϕ_2 (1/in)	82.13	61.39	47.25
ϕ_3 (1/in)	57.31	41.75	67.31
ϕ_4 (1/in)	130.4	77.69	43.01
ϕ_5 (1/in)	72.33	128.1	41.81
λ_1	5.048	3.609	3.227
λ_2	4.178	7.492	4.040
λ_3	3.320	14.18	25.14
λ_4	7.882	7.074	6.388
λ_5	7.223	1.856	8.910
λ_6	12.59	3.578	5.618
$A_1 X10^{-5}$ (psi)	1.234	0.504	1.564
$A_2 X10^{-5}$ (psi)	-4.843	-1.834	-1.935
$A_3 X10^{-5}$ (psi)	0.178	0.978	-0.025
h (in)	.020	.020	.020

TABLE D.4. Solution Parameters for Quasi-Isotropic Laminates - Group 3

Solution Parameters For Quasi-Isotropic Laminates $\varepsilon_{11} = 0.1\%$			
Constant	$[90/\pm45/0]_s$	$[90/0/\pm45]_s$	$[0/90/\pm45]_s$
ϕ_1 (1/in)	k54.75	-	56.90
ϕ_2 (1/in)	69.58	-	64.27
ϕ_3 (1/in)	158.6	-	154.6
ϕ_4 (1/in)	65.94	-	68.45
ϕ_5 (1/in)	81.06	-	71.07
λ_1	1.473	-	2.134
λ_2	2.469	-	2.191
λ_3	5.048	-	3.545
λ_4	11.73	-	17.73
λ_5	3.293	-	4.382
λ_6	5.739	-	6.984
$A_1 X10^{-5}$ (psi)	5.838	-	6.984
$A_2 X10^{-5}$ (psi)	-2.084	-	-4.332
$A_3 X10^{-5}$ (psi)	4.212	-	0.432
h (in)	.020	.020	.020

TABLE D.5. Solution Parameters for Quasi-Isotropic Laminates - Group 4

Solution Parameters For Quasi-Isotropic Laminates $\varepsilon_{11} = 0.1\%$			
Constant	$[\pm 45/0/90]_s$	$[\pm 45/90/0]_s$	$[0/\pm 45/90]_s$
ϕ_1 (1/in)	-	56.94	61.75
ϕ_2 (1/in)	-	61.75	58.81
ϕ_3 (1/in)	-	99.81	97.46
ϕ_4 (1/in)	-	56.23	56.04
ϕ_5 (1/in)	-	90.95	62.39
λ_1	-	1.996	3.530
λ_2	-	4.203	4.302
λ_3	-	5.488	8.821
λ_4	-	15.96	19.86
λ_5	-	1.722	5.189
λ_6	-	6.155	5.082
$A_1 X 10^{-5}$ (psi)	-	1.682	1.565
$A_2 X 10^{-5}$ (psi)	-	-3.639	-1.505
$A_3 X 10^{-5}$ (psi)	-	-1.352	-1.068
h (in)	.020	.020	.020